



# THE UNIVERSITY *of* EDINBURGH

This thesis has been submitted in fulfilment of the requirements for a postgraduate degree (e.g. PhD, MPhil, DClinPsychol) at the University of Edinburgh. Please note the following terms and conditions of use:

This work is protected by copyright and other intellectual property rights, which are retained by the thesis author, unless otherwise stated.

A copy can be downloaded for personal non-commercial research or study, without prior permission or charge.

This thesis cannot be reproduced or quoted extensively from without first obtaining permission in writing from the author.

The content must not be changed in any way or sold commercially in any format or medium without the formal permission of the author.

When referring to this work, full bibliographic details including the author, title, awarding institution and date of the thesis must be given.

**INVESTIGATING THE ROLE OF OPTINEURIN IN BONE  
BIOLOGY AND PAGET'S DISEASE OF BONE**

**Rami A. Obaid (MSc)**

**A thesis submitted for the degree of Doctor of Philosophy**

**University of Edinburgh**

**2016**

# Contents

1. Introduction.....	2
1.1 Bone.....	2
1.2 Bone Remodelling .....	6
1.2.1 Activation Phase.....	6
1.2.2 Resorption Phase .....	7
1.2.3 Reversal phase.....	7
1.2.4 Formation phase .....	7
1.2.5 Quiescence phase .....	8
1.3 Basic Multicellular Unit (BMU) Compartments .....	9
1.3.1 Osteoclasts .....	9
1.3.2 Osteoblasts .....	15
1.3.3 Osteocytes .....	18
1.3.4 Other BMUs compartments .....	19
1.4 Osteoblast-Osteoclast Crosstalk .....	19
1.5 Diseases Arising from Abnormal Bone Remodelling .....	20
1.6 Paget's Disease of Bone .....	21
1.6.1 Clinical features .....	21
1.6.2 Osteoclast and osteoblast phenotype.....	23
1.6.3 Cytokines and growth factors.....	24
1.6.4 Treatment .....	27
1.6.5 Epidemiology .....	27
1.6.6 Genetic architecture of PDB .....	28
1.6.7 PDB-like syndromes .....	28
1.6.8 Linkage studies.....	30
1.6.9 Candidate-gene association studies.....	32
1.6.10 Genome-wide association studies (GWAS).....	32
1.6.11 Somatic mutations .....	33
1.6.12 Environmental factors and PDB .....	35
1.6.13 Molecular genetics .....	38

1.7	Optineurin.....	47
1.7.1	Molecular structure .....	47
1.7.2	Protein characteristics .....	50
1.7.3	Optineurin-binding partners .....	51
1.7.4	Animal models .....	58
1.7.5	OPTN and bone metabolism - is there a link? .....	59
1.8	Project Aims .....	66
2	Materials and Methods.....	68
2.1	Materials .....	68
2.2	Methods .....	68
2.2.1	Study Subjects .....	68
2.2.2	Mutation screening of OPTN gene .....	68
2.2.3	TISSUE CULTURE.....	73
2.2.4	Animal Work.....	88
2.2.5	Western Blot.....	102
2.2.6	Immunoprecipitation (IP).....	105
2.2.7	Gene Expression using Quantitative Real-Time PCR (qPCR) .....	106
2.2.8	Data Analysis .....	110
3	The rs1561570 variant in <i>OPTN</i> is associated with Paget's disease severity and with OPTN gene expression but no disease-specific coding variants were detected in PDB patients .....	113
3.1	Summary .....	113
3.2	Introduction .....	115
3.3	Results .....	116
3.3.1	Genetic Variants in the Optineurin Gene are Associated with Disease Severity in Paget's disease of Bone .....	116
3.3.2	Reduced Expression of OPTN Predisposes to PDB .....	119
3.3.3	Mutation screening of OPTN by DNA sequencing .....	120
3.3.4	Determination of the CA repeat polymorphism of the OPTN gene... ..	126
3.4	Discussion .....	131
4	<i>Optn</i> Depletion in Mouse BMDMs Enhances Osteoclast Formation, Fusion, and Survival .....	136
4.1	Summary .....	136

4.2	Introduction .....	137
4.3	Results .....	137
4.3.1	Optimization of western blot assay to detect OPTN protein.....	137
4.3.2	Expression of OPTN during osteoclast development .....	138
4.3.3	Generation of lentiviral particles for Optn knockdown .....	139
4.3.4	Effect of Optn depletion on RAW 264.7 cell line.....	141
4.3.5	Effect of Optn depletion on osteoclast differentiation from primary BMDMs .....	147
4.4	Discussion .....	153
5	The Effect of Loss of Function Mutation in <i>Optn</i> on Osteoclast and Osteoblast Differentiation .....	160
5.1	Summary .....	160
5.2	Introduction .....	161
5.3	Results .....	163
5.3.1	Effect of Optn <sup>D477N</sup> mutation on osteoclast formation in Optn <sup>D477N/D477N</sup> mice .....	163
5.3.2	Expression of Optn during osteoclast (OC) development in Wild Type (WT) and Optn <sup>D477N/D477N</sup> mice .....	164
5.3.3	Effect of OPTN <sup>D477N</sup> mutation on NFκB signalling pathway.....	166
5.3.4	Optn interaction with the negative regulator of NFκB signalling pathway; the Cyld enzyme .....	168
5.3.5	OPTN expression during osteoblast differentiation .....	171
5.4	Discussion .....	174
6	The D477N Mutation In <i>Optn</i> Leads To Increased Bone Turnover And Enhanced Osteoclast Formation In Optn <sup>D477N/D477N</sup> Mice.....	181
6.1	Summary .....	181
6.2	Introduction .....	182
6.3	Results .....	183
6.3.1	Bone histomorphometry of Optn <sup>D477N/D477N</sup> mice .....	183
6.3.2	The D477N mutation in Optn increased bone resorption parameter in Optn <sup>D477N/D477N</sup> mice .....	183
6.3.3	Bone formation parameters in Optn <sup>D477N/D477N</sup> compared to WT .....	184
6.3.4	Analysis of dynamic bone formation indices in Optn <sup>D477N/D477N</sup> mice.....	185
6.3.5	Analysis of serum bone turnover markers in Optn <sup>D477N/D477N</sup> mice ...	188

6.3.6	μCT analysis showed no significant difference in bone structure between the WT and mutant mice.....	189
6.3.7	Analysis of PDB-like bone lesions in Optn <sup>D477N/D477N</sup> mice .....	192
6.4	Discussion .....	195
7	Discussion and conclusions .....	199
7.1	Suggested mechanisms of OPTN effect on osteoclastogenesis .....	204
7.1.1	Suggested role of OPTN through deubiquitinating enzymes for regulating RANKL-induced NFκB activity .....	204
7.1.2	Suggested role of OPTN through TBK1/IKKε.....	206
7.1.3	Suggested role of OPTN through IFNβ signalling.....	207
7.1.4	Suggested role of OPTN in MVNP mouse model for PDB.....	209
7.2	Future Work .....	210
7.3	General conclusions .....	212

## **DECLARATION**

I hereby declare that this thesis has been composed by myself and the work described within, except where specifically acknowledged, has been carried out entirely by myself and it has not been accepted in any previous application for a degree. The information obtained from sources other than this study is acknowledged in the text or included in the references.

Rami A. Obaid

## ACKNOWLEDGMENT

Foremost, I would like to express my special appreciation and sincere gratitude to my supervisor Dr. Omar Albagha for the continuous support of my PhD study, for his patience, motivation, and sharing his knowledge with me. I have been extremely lucky to have a supervisor who responded to my questions and queries so promptly and I could not have imagined a better supervisor.

My sincere thanks also goes to Dr. Sachin Wani, who as a good friend, was always willing to help me in all aspects of experimental work and for his contribution in reviewing my thesis. I wish to also extend my sincere thanks to my co-supervisor Prof. Stuart Ralston for his advice and for his inspiring enthusiasm for science. I must express my gratitude to Dr. Antonia Sophocleous for her continued support and for her quick response to any question or request I had regarding my work. Also, I am very grateful to Dr. Rob van't Hof for his excellent technical assistance in  $\mu$ -CT and histomorphometric analysis. I would also like to thank Dr. Nerea Alonso, Dr. Asim Azfer and Dr. Micaela Rios Visconti for their help, feedback and suggestions which they offered without any hesitation. A special thank you goes to Belinda Stephens for her administrative support. Warm thanks go to my friends Asim Khogeer, Ghassan Tashkandi and Dr. Nayef Alyamani for all the good times spent together and for their help and support.

In addition to all past and present members of the bone group, I would also like to thank the Saudi Government and Umm Al-Qura University for sponsoring my tuition fee and living expenses. Without them, this project would have been impossible.

I also owe a special thank you to my wife, Hadeel for her patience and all the sacrifices she has made on my behalf.

Last but not the least, I dedicate this thesis to my dear parents and my two daughters whose love and prayers have always encouraged me to strive towards my goal.



## Abstracts and Publications

### Abstracts

Rami A. Obaid, W. D. Fraser, P. L. Selby, S. H. Ralston, O. M.E. Albagha (2010). **Genetic variants in the Optineurin gene are associated with disease severity in Paget's disease of bone.** Presented at the ECTS/IBMS 3rd joint Meeting, Athens, Greece, May 7-11, 2010.

Rami A. Obaid, S. Wani, S. H. Ralston, O.M.E. Albagha (2011). **Optineurin Negatively Regulates Osteoclast Formation *in vitro*.** Presented at the 39th Annual Congress of the European-Calcified-Tissue-Society (ECTS), Stockholm, Sweden, May 19-23, 2012.

Rami A. Obaid, S. Wani, S. H. Ralston, O.M.E. Albagha (2012). **Depletion of the autophagy adaptor OPTN leads to increased osteoclast formation, fusion and survival as well as increased NF- $\kappa$ B activation *in vitro*.** Presented at the Annual Congress of the European-Calcified-Tissue-Society (ECTS), Lisbon, Portugal, May 18-21, 2013.

### Publications

Obaid, R., Wani, S.E., Azfer, A., Hurd, T., Jones, R., Cohen, P., Ralston, S.H., Albagha, O.M.E., 2015. **Optineurin Negatively Regulates Osteoclast Differentiation by Modulating NF- $\kappa$ B and Interferon Signaling: Implications for Paget's Disease.** Cell Rep. doi:10.1016/j.celrep.2015.09.071

## ABBREVIATIONS

<b>1,25-(OH)<sub>2</sub> vitamin D3</b>	1,25-dihydroxyvitamin D3
<b>ABIN1</b>	A20-binding inhibitor of NFκB 1
<b>ACP5</b>	Acid Phosphatase 5, encoding TRAcP
<b>Akt</b>	Protein kinase B
<b>ALFY</b>	Autophagy-linked FYVE domain-containing protein
<b>ALP</b>	Alkaline phosphatase
<b>ANOVA</b>	Analysis of variance
<b>AP-1</b>	Activator protein-1
<b>Atg5</b>	Autophagy 5
<b>Atp6v0d2</b>	A subunit of V-ATPase
<b>Bcl-2</b>	Anti-apoptotic molecule
<b>BFR</b>	Bone formation rate
<b>BMDMs</b>	Bone marrow derived macrophages
<b>BMPs</b>	Bone morphogenetic proteins
<b>BMUs</b>	Basic multicellular units
<b>bp</b>	Base pair
<b>BV/TV</b>	Trabecular bone volume to total volume
<b>C57BL/6 (BL6)</b>	An inbred mouse strain
<b>CA</b>	Carbonic anhydrase
<b>Ca<sup>2+</sup></b>	Calcium ions
<b>CAII</b>	Encode carbonic anhydrase
<b>cAMP</b>	Cyclic AMP
<b>Casp3</b>	encoding caspase
<b>CaSR</b>	Calcium-sensing receptor
<b>CD9</b>	Member of the transmembrane 4 superfamily
<b>cDNA</b>	Complementary DNA
<b>CDV</b>	Canine distemper virus
<b>c-Fms</b>	Receptor of M-CSF
<b>CFU-GM</b>	Colony forming unit granulocyte-macrophage
<b>Cl<sup>-</sup></b>	Chloride ions
<b>CLC-7</b>	Chloride channel 7
<b>c-myc</b>	Proto-Oncogene Protein (transcription factor)
<b>CNOT4</b>	Ccr4-not transcription complex subunit
<b>COL1A1</b>	Type I collagen
<b>CREB</b>	Cyclic AMP response element-binding protein
<b>CSF1</b>	Gene coding for M-CSF
<b>Ct.Th</b>	Cortical thickness
<b>C-terminus</b>	Carboxyl-terminus
<b>CTSK</b>	Encoding cathepsin K
<b>CTX</b>	C-terminal telopeptides of type I collagen
<b>CYLD</b>	Cylindromatosis gene
<b>DC-STAMP</b>	Dendritic cell-specific transmembrane protein
<b>dH<sub>2</sub>O</b>	Distilled water
<b>DISC</b>	death-inducing signalling complex
<b>DMEM</b>	Dulbecco's modified eagle's medium
<b>DMSO</b>	Dimethyl sulfoxide
<b>DRs</b>	Death receptors
<b>ECM</b>	Extracellular matrix
<b>EDTA</b>	Ethylenediaminetetraacetic acid
<b>ePDB</b>	Early onset PDB
<b>ERK</b>	Extracellular regulated kinase
<b>ESH</b>	Expansile skeletal hyperphosphatasia
<b>ESR1</b>	Oestrogen receptor 1
<b>FCS</b>	Fetal calf serum
<b>FEO</b>	Familial expansile osteolysis
<b>FGF</b>	Fibroblast growth factors

<b>FIP2</b>	14.7K-interacting protein-2 (synonym to OPTN)
<b>FSD</b>	Functional secretory domain
<b>FUS/TLS</b>	Fused in Sarcoma/Translocated in Sarcoma
<b>g, mg, µg, ng</b>	Gram, milligram, microgram, nanogram
<b>GABARAP</b>	γ-Aminobutyric acid receptor-associated protein
<b>GFP</b>	green fluorescent protein
<b>GM-CSF</b>	Granulocyte-macrophage colony stimulating factor
<b>GOLGA6A</b>	Golgin Subfamily A, member 6
<b>GWAS</b>	Genome-wide association studies
<b>H<sup>+</sup></b>	Hydrogen ions
<b>HBSS</b>	Hank's balanced salt solution
<b>HCO<sub>3</sub><sup>-</sup></b>	Bicarbonate ions
<b>Hi Di</b>	De ionised Formamide
<b>Hi-DMEM</b>	Dulbecco's Modified Eagle's Medium with high glucose and pyruvate
<b>HIP7</b>	Huntingtin-interacting protein 7
<b>HLA</b>	Human leukocyte antigen
<b>HSF1</b>	Heat shock factors
<b>HTLV-1</b> Page 20	TAX1 of the human T-cell leukemia virus type 1
<b>Htt</b>	Huntingtin
<b>IBMPFD</b>	Inclusion body myopathy, Paget's disease, and frontotemporal dementia
<b>ID</b>	Identification number
<b>IFNγ</b>	Interferon gamma
<b>IGF</b>	Insulin growth factor
<b>IKK</b>	Iκb kinase
<b>IL (R)</b>	Interleukin (receptor)
<b>IRF-1</b>	Interferon regulatory factor 1
<b>IRF3</b>	Interferon regulatory factor 3
<b>ITAM</b>	immunoreceptor tyrosine-based activation motif
<b>IκB</b>	Inhibitor of NFκB
<b>JNK</b>	C-Jun N-terminal kinase
<b>JPD</b>	Juvenile Paget's disease
<b>K<sup>+</sup></b>	Potassium ions
<b>kb</b>	Kilobase
<b>kg</b>	Kilogram
<b>kV</b>	Kilovolt
<b>l, ml, µl</b>	Litre, millilitre, microlitre
<b>LC3</b>	Light chain 3
<b>LD</b>	Linkage disequilibrium
<b>LIR</b>	LC3-interacting motif
<b>LRP5</b>	Low-density lipoprotein receptor-related protein 5
<b>LZ</b>	Leucine zipper
<b>M, mM, µM, nM</b>	Molar, millimolar, micromolar, nanomolar
<b>mA</b>	Milliampere
<b>MAPK</b>	Mitogen Activated Protein kinase
<b>MAR</b>	Mineral apposition rate
<b>M-CSF</b>	Macrophage colony stimulating factor
<b>MEA</b>	2-Methoxyethyl acetate
<b>mGluR1 and mGluR5</b>	Metabotropic glutamate receptors 1 and 5
<b>MITF</b>	Microphthalmia-induced transcription factor
<b>Mm, nm</b>	Millimetre, nanometre
<b>MMA</b>	Methyl methacrylate
<b>MMP9</b>	Matrix metalloproteinase 9
<b>MMPs</b>	Metalloproteases
<b>MOI</b>	Multiplicity of infection
<b>MSCs</b>	Mesenchymal stem cells
<b>MVNP</b>	Measles virus nucleocapsid
<b>Na<sup>+</sup></b>	Sodium ions
<b>NAP1</b>	NAK-associated protein 1
<b>NDP52</b>	Identifies ubiquitin-coated Salmonella
<b>NFATc1</b>	Nuclear factor of activated T-cells, cytoplasmic 1

<b>NF-κB</b>	Nuclear factor κb
<b>NRP</b>	NEMO-related protein (synonym to OPTN)
<b>NRSF</b>	Myod, neuron-restrictive silencing factor
<b>N-terminus</b>	Amino-terminus
<b>NUP205</b>	Nucleoporin 205
<b>Ob.N/BS</b>	Osteoblast number per bone surface
<b>Oc.N/BS</b>	Osteoclast umber per Bone Surface
<b>Oc.S/BS</b>	Active resorption area per bone surface
<b>OCPs</b>	Osteoclasts precursors
<b>OC-STAMP</b>	Osteoclast stimulatory transmembrane protein
<b>OPG</b>	Osteoprotegerin
<b>OPTN</b>	Optineurin
<b>Osx</b>	Osterix
<b>PBS</b>	Phosphate-buffered saline
<b>PCR</b>	Polymerase chain reaction
<b>PDB</b>	Paget's disease of bone
<b>PGE2</b>	Prostaglandin E2
<b>pGIPZ</b>	GIPZ Lentiviral shrna
<b>PI3</b>	Inositol triphosphate
<b>PI3K</b>	Phosphatidylinositol-3-kinase
<b>PINP</b>	N-terminal propeptide of type I procollagen
<b>PIP2</b>	Phosphatidylinositol bisphosphate
<b>PLC</b>	Phospholipase C
<b>PML</b>	Inducer of promyelocytic leukemia
<b>POAG</b>	Primary open-angle glaucoma
<b>PRISM</b>	Randomised Trial of Intensive versus Symptomatic Management
<b>PTH</b>	Parathyroid hormone
<b>PTHrP</b>	Parathyroid hormone-related protein
<b>PVDF</b>	Polyvinylidene difluoride
<b>qPCR</b>	Real time quantitative PCR
<b>Rab8</b>	A member of large families of guanosine triphosphatases (gtpases)
<b>RANK(L)</b>	Receptor activator of nuclear factor κB (ligand)
<b>RB</b>	Ruffled border
<b>RelA/p50</b>	Transcription factor p65
<b>RelB/p52</b>	Transcription Factor NFκB2
<b>RIN3</b>	Ras Rab interactor 3
<b>RIP1</b>	Serine/threonine kinase receptor-interacting protein 1
<b>RNA</b>	Ribonucleic acid
<b>RNAi</b>	RNA interference
<b>ROI</b>	Region of interest
<b>Ror2</b>	Wnt5a co-receptor tyrosine kinase-like orphan receptor 2
<b>RSV</b>	Respiratory syncytial virus
<b>RT/PCR</b>	Reverse transcription polymerase chain reaction
<b>Runx2</b>	Runt-related transcription factor
<b>S1P</b>	Sphingosine 1-phosphate
<b>SD</b>	Standard deviation
<b>SEM</b>	Standard error of mean
<b>Sema3A</b>	Member of the semaphorin family (3A)
<b>sFRP-1</b>	Frizzled- related protein 1
<b>shRNA</b>	Short hairpin RNA
<b>SINTBAD</b>	Similar to NAP1 TBK1 adaptor
<b>SLC13A4</b>	Solute Carrier Family 13, member 4
<b>SNPs</b>	Single nucleotide polymorphisms
<b>Sp1 page33</b>	Specificity protein 1 (Transcription factor)
<b>Sp7</b>	Osterix gene
<b>SQSTM1</b>	Sequestosome 1
<b>Src</b>	Tyrosine-protein kinase
<b>STAT1</b>	Signal transducer and activator of transcription 1
<b>SZ</b>	Sealing zone
<b>TAB2</b>	TAK1 binding protein 2

<b>TAFII-17</b>	VDR binding protein
<b>TAK1</b>	Transforming growth factor $\beta$ activated kinase-1
<b>TANK</b>	TRAF-associated NF- $\kappa$ B activator
<b>TAX1BP1</b>	Tax1-binding protein 1
<b>Tb.N</b>	Trabecular number
<b>Tb.Th</b>	Trabecular thickness
<b>TBK1</b>	TANK binding kinase 1
<b>TCIRG1</b>	Encode $\alpha 3$ subunit of V-ATPase
<b>TFIIIA-INTP</b>	Transcription factor IIIA- interacting protein
<b>TGF-<math>\beta</math></b>	Transforming growth factor- $\beta$
<b>TM7SF4</b>	Encode DC-STAMP
<b>TNF (R)</b>	Tumour necrosis factor (receptor)
<b>TNFAIP3</b>	The zinc finger protein A20
<b>TNFRSF10A</b>	Trail receptor
<b>TNFRSF11A</b>	TNF receptor superfamily 11A
<b>TNFRSF11B</b>	Encode osteoprotegerin
<b>TRAcP</b>	Tartrate-resistant acid phosphatase
<b>TRAF</b>	TNF receptor-associated factor
<b>TRAIL</b>	TNF-related apoptosis-inducing ligand
<b>TRC1-pLKO.1-puro</b>	Plasmid plko.1 with Puromycin resistance gene
<b>UBD</b>	Ubiquitin-binding domain
<b>UPS</b>	Ubiquitin-proteasome system
<b>UTR</b>	Untranslated region
<b>UV</b>	Ultraviolet
<b>UXT</b>	Ubiquitously expressed transcript
<b>V</b>	Volt
<b>v/v</b>	Volume to volume
<b>V-ATPase</b>	Vacuolar-type proton ATPase
<b>VCP</b>	Valosin-containing protein (CDC48)
<b>VDR</b>	Vitamin D receptor
<b>w/v</b>	Weight to volume
<b>WB</b>	Western blot
<b>Wnt signaling</b>	Wingless
<b>ZF</b>	Zinc finger
<b><math>\alpha</math>MEM</b>	Alpha-minimum essential medium
<b><math>\alpha</math>V<math>\beta</math>3</b>	The integrin vitronectin receptor
<b><math>\beta</math>GP</b>	Betaglycerophosphate
<b><math>\mu</math>CT</b>	Micro computed tomography

# INVESTIGATING THE ROLE OF OPTINEURIN IN BONE BIOLOGY AND PAGET’S DISEASE OF BONE

Rami Obaid

School of Molecular, Genetic and Population Health Sciences

University of Edinburgh

## ABSTRACT

Paget’s disease of bone (PDB) is a common disease with a strong genetic component. Approaches such as linkage analysis and candidate gene studies have shown that mutations in Sequestosome 1 (*SQSTM1*) explain up to 40% of familial cases and 10% of sporadic cases, however the majority of PDB patients have no mutations in this gene. Genome-wide association studies (GWAS) have recently identified new susceptibility loci for PDB including variants at *CSF1*, *TNFRSF11A*, *OPTN*, *TM7SF4*, *PML*, *NUP205* and *RIN3* loci. These loci were confirmed to be associated with PDB in various European populations. *OPTN* encodes optineurin, a widely expressed protein involved in many cellular processes but its role in bone metabolism is yet unknown. The aim of this PhD thesis was to investigate the role of *OPTN* in bone metabolism and PDB using *in vitro* and *in vivo* studies. In chapter 3, the *OPTN* rs1561570 identified by previous GWAS was examined for its association with the severity and clinical outcome of PDB in patients without *SQSTM1* mutations. The results showed that rs1561570 was significantly associated with total disease severity score so that carriers of the risk allele “T” had higher severity score compared to non-carriers ( $P < 0.05$ ). A trend for reduced quality of life physical scores (SF36) was also associated with the rs1561570 risk allele, but the relationship was not statistically significant. In order to identify functional variants within *OPTN*, the coding regions as well as the exon-intron boundaries were sequenced in 24 familial PDB cases and 19 controls. No mutation was found that could be predicted as pathogenic suggesting that disease susceptibility could be mediated by regulatory polymorphisms that influence gene expression. In chapter 4, the role of *OPTN* was

investigated in osteoclast development using *in vitro* knockdown experiments. *Optn* was expressed in mouse bone marrow derived macrophages (BMDMs) as well as all stages of osteoclast development and it was significantly increased three days post RANKL treatment. *Optn* expression was knocked down in BMDMs and cells were induced to form osteoclast in the presence of RANKL and M-CSF. Compared to non-targeted cells, *Optn* depleted cells formed significantly more and larger osteoclasts ( $P < 0.05$ ). *Optn* knockdown was also found to enhance osteoclast survival as well as RANKL-induced NF $\kappa$ B activation. In chapter 5, the role of *OPTN* was investigated *in vitro* from cells obtained from knock in mice with a loss-of-function mutation in *Optn* (*Optn*<sup>D477N/D477N</sup>). In agreement with the *in vitro* knockdown experiments, osteoclasts were significantly higher and larger in mutant mice compared to WT and the NF- $\kappa$ B activity measured by luciferase reporter assay was significantly higher in cells from *Optn*<sup>D477N/D477N</sup> compared to WT during most stages of osteoclast development. *OPTN* from mutant and WT mice was co-precipitated with its *CYLD* binding-partner, which acts as a negative regulator to RANK signalling by inhibiting the TRAF6 downstream signalling. The data from this immunoprecipitation (IP) experiment revealed that defective *OPTN* interacted less with *CYLD* from mutant mice compared to WT. This study also showed that *OPTN* was expressed in osteoblasts and the expression rate did not change during osteoblast development. The data obtained from the mineralization assay revealed no significant difference between *Optn*<sup>D477N/D477N</sup> and WT. In chapter 6, I investigated the effect of the D477N loss of function mutation in *Optn* on bone metabolism. Bone Histomorphometrical analysis of *Optn*<sup>D477N/D477N</sup> mice showed higher bone resorption parameters (Oc.N/BS and Oc.S/BS) compared to wild type (WT). Osteoid analysis showed evidence of increased bone formation parameters (OS/BS and OV/BV) in mutant mice compared to WT. Calcein labelling showed a significant difference in mineral apposition rate (MAR) from mutant mice compared to WT. Analysis of serum biomarkers of bone turnover showed evidence of enhanced bone turnover in mutant mice compared to WT. Micro computed tomography ( $\mu$ CT) analysis of 4 and 14 months old mice showed no significant differences in bone morphology between WT and *Optn*<sup>D477N/D477N</sup> mice of both sexes.

In conclusion, this study has shown for the first time that OPTN plays a role in regulating bone turnover by acting as a negative regulator of osteoclast differentiation. The data obtained from this study strongly suggest the crucial role of OPTN in RANK signalling. The effect of OPTN on osteoblast activity may be direct or indirect compensation for increased osteoclast activity. Further detailed studies will be required to explore the underlying mechanism of OPTN including downstream RANK signalling and a complete knockout model to corroborate these findings.



# **CHAPTER ONE**

## **INTRODUCTION**

# 1. Introduction

## 1.1 Bone

Bone together with cartilage makes up the skeletal system (Post et al., 2010). Bone is a dynamic multifunctional connective tissue, which consists of an organic matrix and inorganic elements. It plays a role in mechanical support, hematopoiesis, mineral homeostasis, protection of the internal organs, and is considered part of the endocrine system (Burr and Akkus, 2014; Kular et al., 2012).

During embryogenesis and after birth, skeletal development occurs through two different processes, namely, intramembranous ossification and endochondral ossification. The intramembranous ossification involves a condensation of mesenchymal stem cells that differentiate directly into bone cells. Flat bones, such as the clavicle and scapula, and most of the skull bones are formed through this process (Allen and Burr, 2014a). The endochondral ossification is a process whereby a hyaline cartilage template is produced by chondrocytes and replaced by bone over time. This process leads to the formation of long bones such as the tibia, femur, humerus and radius (Allen and Burr, 2014a).

At macroscopic level, bone can be divided into cortical (compact) bone and trabecular (cancellous, spongy) bone. These two categories of bone are distinguished from each other by their porosity, location and function. Cortical bone constitutes 80% of the skeleton and is the primary structure of the diaphysis (shaft) of short and long bones, surrounding the marrow cavity (Burr and Akkus, 2014; Post et al., 2010). Due to its high density and low surface area, this type of bone provides protection to the vital organs as well as playing a major role in mechanical strength and body movements (Post et al., 2010). The cortical bone is composed of secondary structures called Haversian systems (osteons), which represent units of bone remodelling. The osteons comprise concentric lamellae of bone tissue surrounding a central canal which houses the blood vessel, nerve and lymphatics (Burr and Akkus, 2014). The second category of bone, the trabecular bone, constitutes 20% of the skeletal mass but

represents 80% of the bone surface of the skeleton (Post et al., 2010). Trabecular bone is found in the metaphyses of long bones, flat bones and vertebrae. It is composed of interconnected trabeculae, separated by spaces and filled with bone marrow. Like cortical bone, trabecular bone is lamellar, but its structure runs parallel to the trabecular surface (Burr and Akkus, 2014). In contrast to cortical bone, trabecular bone has a large surface area, lower density and higher remodelling rate. These structural differences therefore make the trabecular bone metabolically more active and loss of bone due to any reason will be more obvious in these areas under high bone turnover conditions (Ralston, 2013a) (Figure 1-1).

Bone is composed of an organic matrix, water, and minerals. The bone mineral, which accounts for 65% of the weight of bone, is composed of calcium and phosphate bound together to form crystals of hydroxyapatite. Water makes up 10% of the bone and the remaining 25% is the organic part of the bone. The organic part of the bone matrix consists of type I collagen in a proportion of 90%, while the remaining 10% contains non-collagenous proteins such as versican, alkaline phosphatase, vitronectin, bone sialoprotein, osteopontin, osteocalcin and osteonectin. Of these, 85% are extracellular and the rest are found within bone cells. Non-collagenous proteins play an important role in regulating collagen formation, mineralization and cell adhesion to the matrix (Burr and Akkus, 2014).

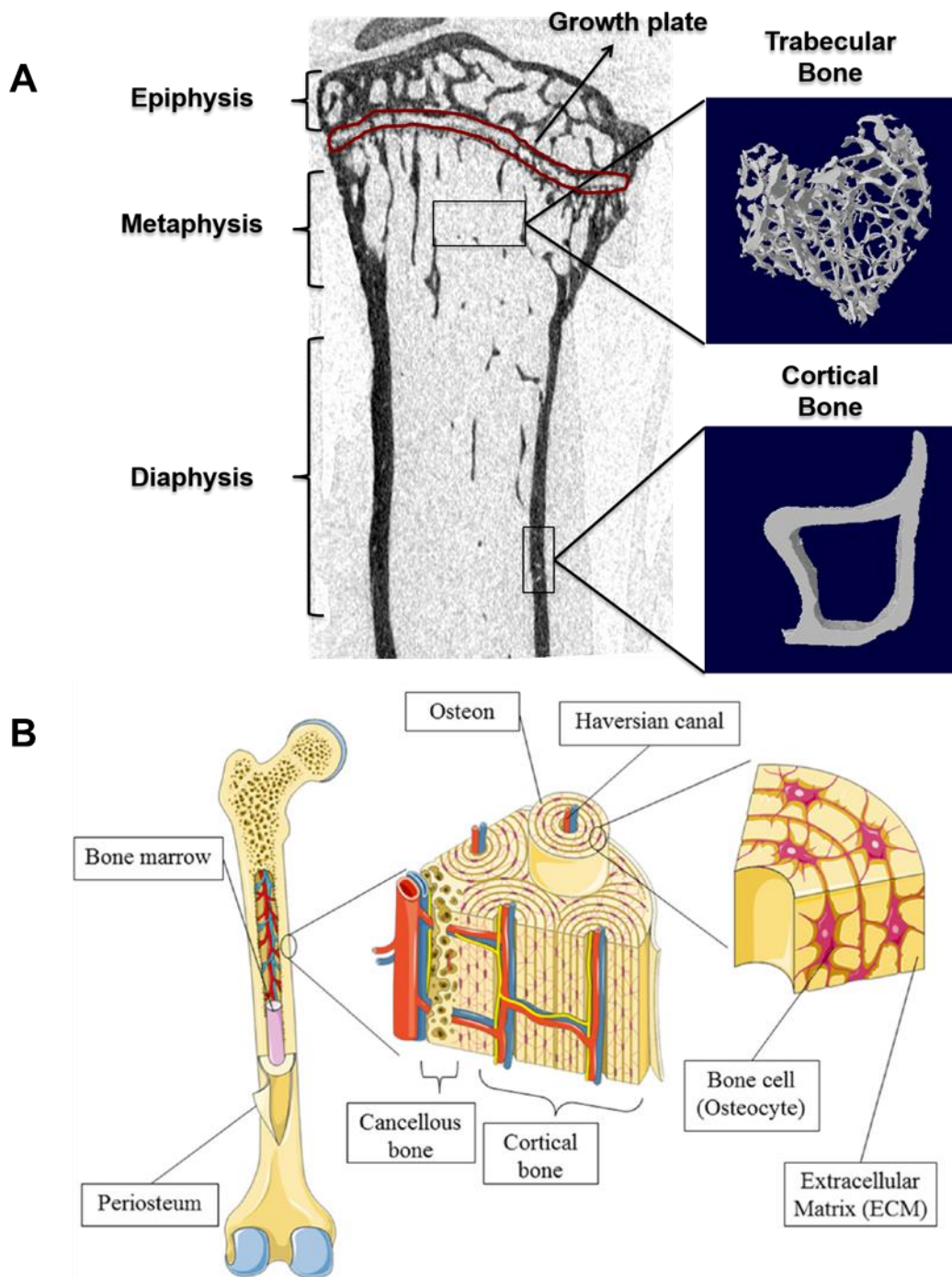


Figure 1-1: **(A)** Representative image of micro computed tomography ( $\mu$ CT) obtained from a WT male BL6 showing a coronal cross-section of tibia and illustrating 3D reconstructed images of the cortical and trabecular bone structure. **(B)** Schematic overview of bone tissue at microscopic level . See text for description. The original image in panel B was taken from (Meng Bao et al., 2013).

## 1.2 Bone Remodelling

Due to its dynamic nature and its role in preserving skeletal size, shape, and structural integrity, bone undergoes modelling and remodelling in order to maintain the skeletal system. Bone remodelling is a complex, tightly regulated process that combines bone resorption with bone formation in order to maintain skeletal integrity during adult life (Kular et al., 2012; Post et al., 2010). Bone remodelling occurs at basic multicellular units (BMUs), whereby a series of distinct types of cells, including osteoblasts, osteoclasts, osteocytes, bone-lining cells, osteomacs and endothelial cells, collaborate together to accomplish this task (Figure 1-2). The remodelling cycle consists of five sequential phases: activation, resorption, reversal, formation and termination [reviewed in (Y. et al., 2013) and (Kular et al., 2012)] (Figure 1-3).

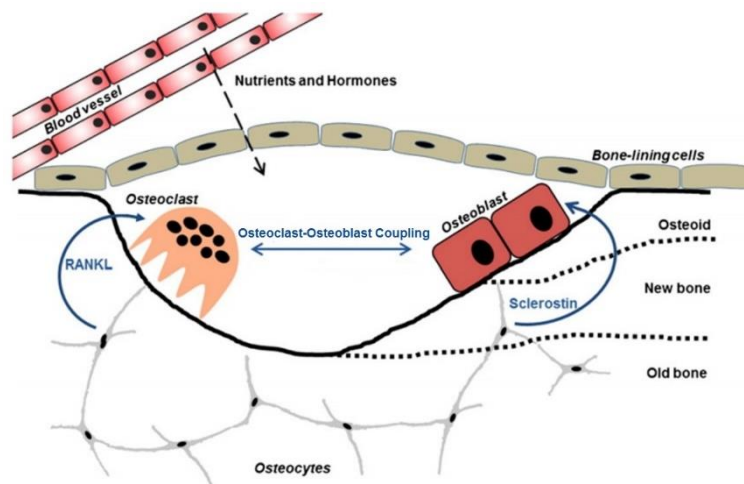


Figure 1-2: The basic multicellular unit compartments. The BMU compartments consist of osteoblasts, osteoclasts, osteocytes, bone-lining cells and endothelial cells, which cooperate with each other to maintain bone remodelling (adapted from (Kular et al., 2012)).

### 1.2.1 Activation Phase

This phase of bone remodelling is initiated by detecting signals, which may be activated by several events, including micro-damage, mechanical stress or osteocyte apoptosis. Such signals have been described as key signals for the remodelling process. Studies on rodents showed that micro-damage results in disruption of the osteocyte network where the affected osteocytes undergo apoptosis. Prior to dying, the

osteocytes start producing cytokines that recruit the osteoblast lineage and the osteoclast precursors to the remodelling site (Kular et al., 2012; Y. et al., 2013).

### *1.2.2 Resorption Phase*

In this phase, the osteoblast lineage controls the formation and activity of mature osteoclasts by producing the main osteoclastogenesis cytokines, namely, macrophage colony stimulating factor (M-CSF), receptor activator of nuclear factor  $\kappa$ B ligand (RANKL) and osteoprotegerin (OPG). When mature osteoclasts are formed, bone-lining cells retract allowing osteoclasts to attach to the bone surface and become polarized. Following the polarization, osteoclasts tightly seal the remodelling site and start acidifying the area by releasing protons ( $H^+$  ions) and proteolytic enzymes (e.g. cathepsin K), which degrade mineral bone and release collagen fragments. These collagen fragments are used as biomarkers to assess the bone remodelling by measuring them in blood and urine. Throughout this phase, the recruitment of new osteoclasts at the resorption site to replace dead ones is ongoing. The duration of the resorption phase at a given BMU is estimated to be around 20 to 40 days (Y. et al., 2013).

### *1.2.3 Reversal phase*

After the resorption phase reaches the maximum eroded depth, the reversal phase starts and lasts for nearly 9 days. In this phase, osteoclasts prepare the resorbed area for osteoblasts by undergoing apoptosis. In the meantime, the bone-lining cells enter the eroded lacuna and start cleaning the residual bone matrix. In addition, these cells deposit the initial collagenous layer and form a cement line that facilitates the attachment of osteoblasts (Y. et al., 2013).

### *1.2.4 Formation phase*

The formation phase is the longest stage of bone remodelling. During this phase, osteoblasts differentiate and proliferate, laying down an un-mineralized organic matrix (osteoid). Osteoid formation is followed by mineralisation, during which the composition and organisation of the extracellular matrix go through a series of

modifications. Mineralisation is a long process, which lasts for more than a year. The early stage of mineralization lasts for 2-3 weeks and starts when calcium and phosphate ions become incorporated into the collagen matrix, accounting for 70% of the final mineral content. The later stage of mineralization starts when hydroxyapatite crystal deposition turns osteoid into mature mineralised matrix and gives bone its rigidity and stiffness. The formation stage is completed when an equal quantity of resorbed bone has been replaced by new bone (Y. et al., 2013).

### 1.2.5 Quiescence phase

The last stage of the remodelling cycle is the quiescence phase, in which bone-lining cells cover the bone surface, entering the state of quiescence (resting) (Y. et al., 2013).

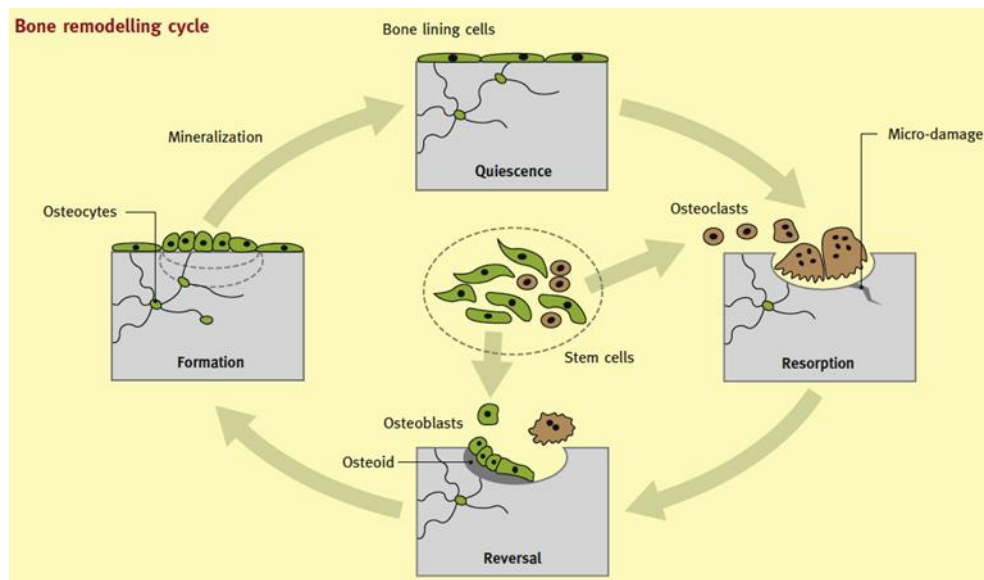


Figure 1-3: Bone remodelling cycle. Micro-damage or mechanical stress initiates the remodelling cycle by recruiting mature osteoclasts to the affected site and the resorption phase take place. Resorption is followed by recruitment of osteoblasts, which proliferate and differentiate into mature osteoblasts. Osteoblasts then fill the resorption cavity with osteoid, thereby initiating the bone formation phase. The new osteoid subsequently mineralizes to generate new bone, which is covered by bone-lining cells. Bone enters the resting phase and this completes the remodelling cycle (adapted from (Ralston, 2013a).

## 1.3 Basic Multicellular Unit (BMU) Compartments

### 1.3.1 *Osteoclasts*

Osteoclasts are the primary cells of hematopoietic origin which are involved in bone resorption. Osteoclast activity is crucial for bone modelling and remodelling. Therefore, any disruption of this activity can result in reduced or increased bone mass, depending on whether osteoclast activity is increased or decreased (Bellido et al., 2014). However, as part of the growing field of osteoimmunology, recent research has shown that osteoclasts have a regulatory role in autoimmune and inflammatory diseases affecting the skeleton (Boyce et al., 2012). Several overlapping signalling pathways control the osteoclastogenesis and malfunction of the key components of such pathways leads to bone diseases.

The osteoclasts derived from the hematopoietic monocyte-macrophage lineage and the earliest nonspecific osteoclast precursors (OCPs) are colony-forming units of granulocyte-macrophages (CFU-GM), which require specific cytokines, transcription factors and signalling molecules to stimulate them to form osteoclasts. Haematopoietic precursors in the bone marrow or circulation proliferate to early OCPs that already express receptor activator of nuclear factor  $\kappa$ B (RANK) (Boyce and Xing, 2008). The differentiation of these precursors into committed osteoclasts occurs when they enter the bone marrow and are exposed to RANKL. Subsequently, committed osteoclasts are recruited to the bone modelling/remodelling sites under the control of quiescent osteoblasts (bone-lining cells) and other factors, including osteocyte/osteoblast-derived cytokines, calcium gradients and matrix metalloproteinases. The committed OCPs then fuse into mature multinucleated cells. Cellular polarization takes place when these multinucleated cells attach to the bone-forming specialized functional structures as part of the resorption process (Bellido et al., 2014) (Figure 1-4).



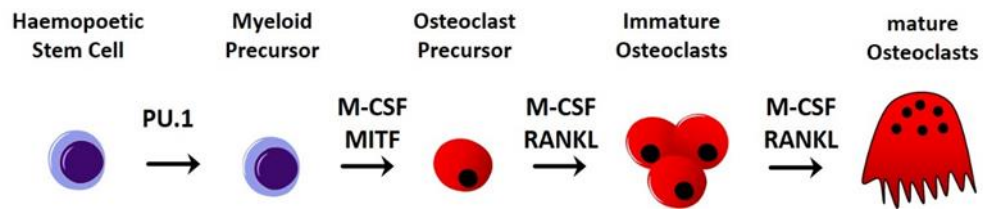


Figure 1-4: Regulation of osteoclast formation and differentiation. PU.1 and MITF are the earlier transcriptions that drive the common myeloid precursors toward osteoclast formation. The expression of PU.1 and MITF regulate the expression of c-fms, the receptors for M-CSF and RANK in OCPs, thus priming them for further differentiation when they encounter RANKL. The committed osteoclasts then fuse to form multinucleated polarized osteoclasts that are capable of resorbing bone.

The earliest identifiable non-specific transcription factors of the differentiation process toward osteoclast/macrophage lineage are PU.1 and Pax5. Research has shown that PU.1<sup>-/-</sup> and Pax5<sup>-/-</sup> mice have severe osteopetrosis without osteoclast formation. PU.1 and microphthalmia-induced transcription factor (MITF) regulate the expression of c-fms (M-CSF receptor) in the osteoclast precursors (Boyce et al., 2012). M-CSF is a macrophage proliferation and survival cytokine which, alongside RANKL, is considered to be an important cytokine for osteoclast formation. M-CSF is expressed by a number of cells, including osteoblasts, bone marrow stromal cells and osteocytes. M-CSF attachment to its receptor c-fms in osteoclasts leads to the activation of several signalling cascades that are required for survival and proliferation; additionally, by activating the c-fos transcription factor, this process also induces the expression of RANK. These signalling cascades include phosphatidylinositol-3-kinase/protein kinase B (PI3K-Akt) and extracellular regulated kinase (ERK) signalling pathways (Bellido et al., 2014). Animal models with naturally occurring mutations in M-CSF, such as the osteopetrotic op/op mouse or the toothless tl/tl rat, have been observed to develop osteopetrosis due to decreased osteoclast numbers. The same osteopetrotic phenotype is exhibited by the CSF1 (gene coding for M-CSF) knockdown model. However, compensatory cytokines enabled these osteopetrotic mice to recover with age.

The RANK/RANKL signalling pathway was discovered in the late 1990s and since then it has been considered the key element in bone remodelling as it mediates multiple aspects of osteoclast function including osteoclast differentiation from mononucleated precursors to multinucleated cells, resorption and survival (Kong et al., 1999; Yasuda et al., 1998). RANK is expressed in OCPs, mature osteoclasts, dendritic cells, and breast epithelial cells as well as in some cancers such as breast and prostate (Boyce et al., 2012). RANK gene mutations are associated with several PDB-like syndromes, which will be discussed later on. RANKL is expressed by several cells, including osteoblasts, bone marrow stromal cells, osteocytes, and T and B cells. The expression of RANKL is induced by parathyroid hormone (PTH), vitamin D, IL-1, IL-6 and IL-11. RANK<sup>-/-</sup> and RANKL<sup>-/-</sup> mice develop severe osteopetrosis due to the lack of osteoclast formation (Kong et al., 1999; Yasuda et al., 1998). Ubiquitination is a complex biochemical process, where attachment of ubiquitin regulates cellular processes through non-proteasomal modifications, such as protein–protein interactions or subcellular localization, or through termination of target proteins by proteasomal degradation. Ubiquitin harbours seven lysine residues, but only one ubiquitin molecule is linked by covalent binding of the C-terminal glycine of another ubiquitin to form ubiquitin chains (polyubiquitin) (Davis and Gack, 2015). Among them are K48-linked ubiquitination, which targets proteins for proteasomal degradation, and K63-linked polyubiquitination, which is involved in other cellular processes such as vesicular trafficking and inflammation. Deubiquitinating (DUB) enzymes, such as cylindromatosis (CYLD) and the NFκB negative regulator A20 (TNFAIP3), counteract the NFκB signalling activity by removing K63-linked polyubiquitin chains (Davis and Gack, 2015). The downstream targets to RANK/RANKL signalling include NFκB, the three components of mitogen activated protein kinase (MAPK), namely, c-jun N-terminal kinase (JNK), proto-oncogene protein (c-myc) and tyrosine-protein kinase (Src). NFκB remains inactive in the cytoplasm as long as it is attached to the inhibitory protein IκBα. RANK is activated when it interacts with RANKL, which in turn recruits TNF receptor-associated factor 6 (TRAF6) to the cytoplasmic domain of RANK. TRAF6 becomes ubiquitinated and then recruited to the transforming growth factor β activated kinase-1-TAK1-binding protein 2 (TAK1–

TAB2) complex, which facilitates TAK1 phosphorylation and activation. This results in K63-polyubiquitination of NEMO and subsequent phosphorylation of IKK $\alpha$ , which in turn phosphorylates the inhibitory protein I $\kappa$ B $\alpha$ , targeting it for proteasomal degradation (Mellis et al., 2011). Activated TRAF6 also stimulates NF $\kappa$ B activity by activation of the I $\kappa$ -B kinase (IKK) complex through atypical protein kinase c (aPKC), which phosphorylates IKK $\beta$  that in turn triggers the phosphorylation of the inhibitory protein I $\kappa$ B $\alpha$ , targeting it for proteasomal degradation (Li et al., 2014). Subsequently, the degradation of I $\kappa$ B $\alpha$  liberates the NF $\kappa$ B to enter the nucleus in order to activate the expression of its target genes. NF $\kappa$ B has two signalling pathways (Mellis et al., 2011), namely, the RelA/p50 canonical pathway and the RelB/p52 non-canonical (alternative) pathway. RANKL stimulates both pathways, as well as activating the three members of MAPK in osteoclasts or osteoclast precursors, including ERK, C-Jun N-terminal kinase (JNK), and p38. Activator protein-1 (AP-1) transcription factors are activated by phosphorylation of ERK and JNK, while MITF is activated by phosphorylation of p38. The nuclear factor of activated T-cells, cytoplasmic 1 (NFATc1), is considered one of the main targets of RANK/RANKL signalling pathway and is up-regulated by NF $\kappa$ B, AP-1 complex and elevated level of cytosolic calcium. The activated NF $\kappa$ B, AP-1 complex and MITF transcription factors in conjunction with NFATc1 then enter the nucleus to promote the expression of genes that are involved in osteoclast differentiation, resorption and survival, including tartrate resistant acid phosphatase (TRAcP), cathepsin K, matrix metalloproteinase 9 (MMP9), dendritic cell-specific transmembrane protein (DC-STAMP), calcitonin receptor, osteoclast-associated receptor (OSCAR), chloride channel 7 (CLC-7), and  $\beta$ 3 integrins (Abu-Amer, 2013; Mellis et al., 2011) (Figure 1-5). OPG is another crucial element in osteoclast function due to its role as a decoy receptor that prevents RANKL from interacting with RANK. OPG<sup>-/-</sup> mice were shown to have osteopenia due to increased osteoclastogenesis and mutation in this gene was reported to cause a PDB-like syndrome called juvenile Paget's disease (Boyce et al., 2012).

Mature osteoclasts are characterized by several important structures which are essential for the resorption process. An earlier feature displayed by the mature

osteoclast is multinucleation, which is determined by the fusion of osteoclast precursors (Bellido et al., 2014). Numerous proteins, such as DC-STAMP, OC-STAMP, Atp6v0d2 (a subunit of V-ATPase), and CD9 (member of the transmembrane 4 superfamily) are implicated in the fusion process (Boyce et al., 2012). Mature osteoclasts become activated when they attach to  $\alpha V\beta 3$  (the integrin vitronectin receptor) at the exposed bone surface after the bone-lining cells that cover quiescent bone surfaces retract their cytoplasm. As a result, several Src signalling pathways become activated (Boyce et al., 2012). The osteoclast becomes polarized and forms a tight seal, where protons and proteases are secreted to demineralise and degrade the bone matrix. At this stage, the osteoclast membrane exhibits three distinct regions, which are the sealing zone (SZ), the ruffled border (RB), and the functional secretory domain (FSD). During polarization, the osteoclast's actin cytoskeleton is rearranged to form the F-actin ring (SZ). The SZ contains podosomes that facilitate the osteoclast attachment to and detachment from the bone surface. The second region is the RB, where the protons and proteolytic enzymes are released. Carbonic anhydrase (CA) produces the ( $H^+$ ) protons, which are transported to RB through the vacuolar-type proton ATPase (V-ATPase). Chloride ions ( $Cl^-$ ) are also secreted at the RB and are controlled by the H/Cl exchange transporter 7 (CIC-7) (Mellis et al., 2011). A coupled activity of bicarbonate  $HCO_3^-$  /  $Cl^-$  exchanger maintains intracellular electron neutrality at the basolateral membrane. The formation of HCl in the resorption lacuna acidifies the area and dissolves the bone matrix. Subsequently, the organic matrix (mainly type 1 collagen) of the dissolved bone is enzymatically digested by the action of secreted cathepsin K (Cat K) and matrix metalloproteases (MMPs) (Mellis et al., 2011). TRAcP is also secreted but its role is still unclear. It is thought that TRAcP facilitates the dephosphorylation of osteopontin and bone sialoprotein, which are essential for normal endochondral bone formation and play a role in matrix degradation. Studies have reported that TRAcP knockout mice developed normally but adults showed mild osteopetrosis, deformity of the long bones and increased mineral density and bone tissue, which revealed its role in skeleton. Furthermore, TRAcP is used in histology as a cellular marker of osteoclasts (Hayman and Cox, 2003; Hayman et al., 2001). After bone is degraded, the resorbed products are removed and degraded by lysosomes or

by transcytosis to be secreted across FSD towards the basolateral membrane (Mellis et al., 2011) (Figure 1-6).

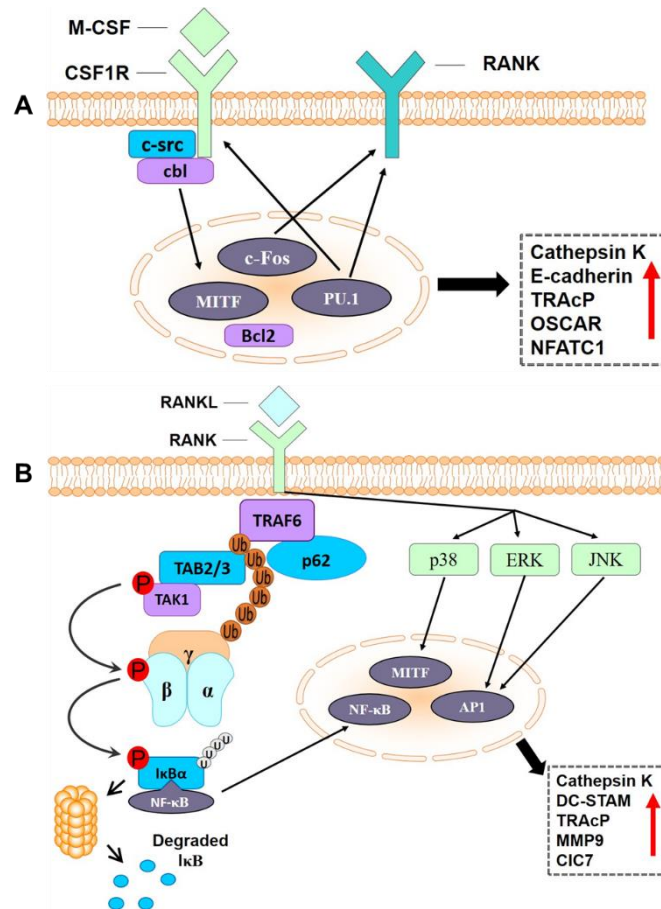


Figure 1-5: RANKL and M-CSF are the main signalling cytokines in osteoclasts, regulating their proliferation, differentiation, and survival. **(A)** PU.1 is the earliest transcription factor in the osteoclast lineage and stimulates the expression of the CSF1R receptor in the osteoclast precursors. Once M-CSF binds to its receptor, M-CSF signalling starts promoting macrophage proliferation and survival by stimulation of several signalling proteins. MITF expression is enhanced by M-CSF and through the stimulation of Bcl2 stimulates macrophage survival. M-CSF and PU.1 also induce the expression of the receptor RANK. **(B)** RANKL binds its receptor RANK, resulting in the recruitment of TRAF6 and p62, which together create a platform for the assembly of the TAB2/3-TAK1 complex. Once TAK1 becomes phosphorylated, the NF $\kappa$ B inhibitory protein I $\kappa$ B $\alpha$  subsequently undergoes phosphorylation as well, targeting it for degradation. Additionally, RANKL activates MAPKs, leading to the phosphorylation of p38 that activates MITF, ERK and JNK, which in turn activate AP-1 transcription factors. Following activation, these transcription factors (NF $\kappa$ B, MITF, AP-1) enter the nucleus and promote the expression of genes required for osteoclast survival and differentiation. (Mellis et al., 2011).

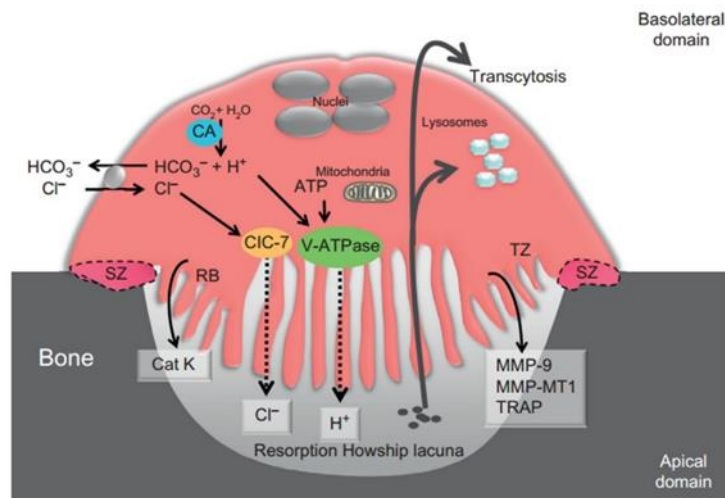


Figure 1-6: Schematic illustration of a resorbing osteoclast. Following contact with bone, the osteoclast becomes polarised and forms several regions including the sealing zone (SZ), ruffled border (RB), transition zone (TZ), nuclei, resorption lacuna, and apical domain directed toward the bone surface. Hydrogen and chloride ions ( $H^+$  and  $Cl^-$ ) are secreted across the ruffled membrane into the Howship's lacuna by means of vacuolar proton pumps (V-ATPases) and chloride channels (ClC7), respectively. Furthermore, Cathepsin K, TRAcP and MMP-9 are also secreted across the ruffled membrane into the Howship's lacuna by secretory transport. Bone degradation products are endocytosed through the ruffled border into the cytoplasm toward the basolateral membrane or degraded via the lysosomes. Adapted from (Bellido et al., 2014).

### 1.3.2 Osteoblasts

Osteoblasts are the bone formation cells that are responsible for bone matrix secretion and bone mineralization. Osteoblasts lie on the surface of bone and secrete osteoid, which consists of type 1 collagen as well as other specialized matrix proteins. Osteoblasts also secrete a great amount of osteocalcin and alkaline phosphatase and their levels in circulation reflect the bone formation rate. Osteocalcin regulates bone formation, while alkaline phosphatase is essential in bone mineralization (Bellido et al., 2014). In addition to their role in bone homeostasis, osteoblasts have other roles in haematopoiesis, bone metastasis, phosphate and glucose metabolism (Boyce et al., 2012). Furthermore, osteoblasts are involved in bone modelling and remodelling tasks, which is regulated by interaction with osteoclasts. Osteoblasts originate from the mesenchymal stem cells (MSCs), which also differentiate into other cells including chondrocytes, myocytes, and adipocytes. Osteoblasts have different fates upon

completion of bone matrix formation; some cover the bone surface as bone-lining cells, others get entrapped into the bone as osteocytes and the remaining die by apoptosis. Histologically, osteoblasts, osteocytes and bone-lining cells are stained positively for alkaline phosphatase, but only mature osteoblasts have a cuboidal shape with large nuclei located near the basal membrane, Golgi apparatus on the apical surface, and large endoplasmic reticulum (Bellido et al., 2014).

The commitment of mesenchymal progenitors to osteoblast precursors and osteoblast differentiation and function is controlled by an array of factors including Runx2, osterix, Wnt signalling and Notch, in addition to growth factors, cytokines, and the endocrine system. Runx2 is a member of the Runt-related transcription factor and one of the earliest transcription factors that is responsible for establishing the osteoblastic lineage. Research has demonstrated that lack of osteoblasts and bone mineralisation results in the prenatal death of Runx2 knockout mice. The second earlier transcription factor downstream to Runx2 is the Sp7/osterix. Conditional deletion of osterix in postnatal mice revealed its multiple role in bone growth and homeostasis. In addition, conditional deletion of osterix in mature osteoblasts leads to decreased osteoblast activity with mild bone phenotype in adult mice suggesting its role in bone formation. Both Runx2 and osterix are responsible for the expression of genes that control bone formation and remodelling, including osteocalcin, osteopontin, collagenase 3, OPG, and RANKL (Boyce et al., 2012).

A crucial role in osteoblast differentiation is played by bone morphogenetic proteins (BMPs) which regulate the Runx2 expression through their canonical and non-canonical pathways. Multiple BMPs have been identified, but only five have been involved in bone formation (BMPs 2, 4, 5, 6, and 7). Experiments showed that BMP2, 4 and 7 regulate limb development and single knockout of BMP4 or 7 did not affect normal limb development. On the other hand, BMP2-deficient mice showed osteoporosis with spontaneous fracture and inability to start fracture repair (Boyce et al., 2012).

Similar to BMPs, Wingless (Wnts) is a key signalling molecule that stimulates not only the commitment of MSCs towards the osteoblastic lineage, but also preosteoblast differentiation. Moreover, Wnt ligands prevent apoptosis in osteoblastic cells through their  $\beta$ -catenin canonical and non-canonical pathways. In addition, Wnt signalling inhibits osteoclast development by increasing the expression of OPG. Low-density lipoprotein receptor-related protein 5 (LRP5) and frizzled proteins are receptors for Wnt ligands. Activating mutations of LRP5 leads to high bone mass phenotype in humans and mice. These mutations also reduce the ability of LRP5 to bind to the Wnt antagonist sclerostin, which is secreted by osteocytes and induces osteoblast apoptosis. Conversely, mice lacking the Wnt antagonist frizzled-related protein 1 (sFRP-1) showed increased bone formation and decreased osteoblast and osteocyte apoptosis (Bellido et al., 2014).

Notch is a family of four transmembrane receptors, which are activated by five different ligands. Notch signalling is critical for maintaining a pool of mesenchymal progenitors and inhibiting osteoblastic differentiation. It has been found that *in vivo* depletion of Notch in genetically modified mice resulted in increased bone mass in young mice followed by development of osteopenia as they aged (Boyce et al., 2012). Furthermore, Notch was found to inhibit the osteoclastogenesis because Notch-depleted mice showed increased osteoclastogenesis as a result of low production of OPG. Dysregulation of Notch signalling has been reported to lead to several diseases, including Alagille syndrome and spondylocostal dysostosis (Boyce et al., 2012).

The transforming growth factor- $\beta$  (TGF- $\beta$ ) was observed to have an effect on both osteoblasts and osteoclasts, and therefore it is considered to play a crucial role in bone remodelling. It was found to stimulate the early differentiation of osteoblasts and inhibit them at a later stage. PTH stimulates TGF- $\beta$  production in osteoblasts, which means that it cross-talks with TGF- $\beta$ . During resorption, osteoclasts release and activate the latent TGF- $\beta$  in the bone matrix, which in turn stimulates osteoblast formation. The insulin-like growth factor-I (IGF-I) pathway stimulates osteoblast proliferation, function, and survival. IGF-I-depleted mice showed severe reduction in bone mineral density. Fibroblast growth factors (FGFs) regulate bone osteoblast



differentiation and survival. Studies also showed that FGFs interact with Wnt and BMPs in regulation of bone formation (Plotkin and Bivi, 2013).

The endocrine system is involved in osteoblastogenesis due to the participation of several hormones, including parathyroid hormone (PTH), oestrogen, glucocorticoid, calcitonin and 1,25-dihydroxyvitamin D3 (1,25-(OH)<sub>2</sub> vitamin D3) (Boyce et al., 2012). PTH stimulates osteoblast differentiation by activating the Runx2. In addition, PTH increases osteoblast proliferation and survival by activating the MAPK and PI3K signalling. The induction of IGF-I by PTH enhances osteoblast proliferation, differentiation and activity. Similar to PTH, 1,25-(OH)<sub>2</sub> vitamin D3 stimulates osteoblast differentiation by up-regulating Runx2. Furthermore, as a calcium-regulating hormone, 1,25-(OH)<sub>2</sub> vitamin D3 acts on intestinal calcium and phosphate absorption. Glucocorticoids display a dual effect, stimulating osteoblast differentiation during development and increasing bone resorption by promoting calcium absorption and sex hormone production. Oestrogen is an important systemic hormone involved in the regulation of normal bone turnover. Oestrogen deficiency was found to increase bone resorption and decrease bone mass, which indicates a defect in bone formation. Calcitonin is a potent inhibitor of osteoclast activity and used clinically for treating bone diseases (Y. et al., 2013).

### *1.3.3 Osteocytes*

One of the fates of osteoblasts is to become osteocytes, which are entrapped in the newly formed bone matrix. The smaller size and lack of several cytoplasmic organelles is what differentiates osteocytes from osteoblasts. Osteocytes are the most abundant cells distributed through the matrix and they have been recently shown to regulate osteoblast and osteoclast functions in response to micro-damage or mechanical stress. Subsequently, osteocytes undergo apoptosis and activate osteoclasts by enhancing the production of RANKL. Recently, osteocytes were found to produce RANKL, M-CSF and OPG, which in turn regulate bone remodelling (Bonewald, 2011). In addition to their role in osteoclasts, osteocytes were also noted to regulate the osteoblasts through the production of sclerostin, which inhibits bone formation and enhances osteoclast

function. Osteocyte numbers reduce with aging as a result of apoptosis, which may alter remodelling and thereby contribute to the low bone mass in old people (Kular et al., 2012; Onal et al., 2013).

#### *1.3.4 Other BMUs compartments*

Additional BMU components that participate in bone remodelling include bone-lining cells, osteomacs, and vascular endothelial cells. The bone-lining cells have been proposed to attract the osteoclast precursors via the action of collagenase, which digests the non-mineralised thin layer of bone exposed underneath the mineralised matrix. Osteomacs are macrophages found near the periosteal and endosteal surfaces of bones and are often associated with bone-lining cells. These macrophages have been suggested to regulate osteoblast mineralization and thus play a role in bone homeostasis. Another BMU compartment is made up of vascular endothelial cells which constitute a source of oxygen and nutrients, playing a vital role in bone formation, remodelling and healing, as well as being involved in the removal of resorption waste products (Kular et al., 2012).

### **1.4 Osteoblast-Osteoclast Crosstalk**

As previously mentioned, osteoblasts play a major role in the regulation of osteoclasts. Osteoblasts produce the main cytokines for osteoclast differentiation, namely, M-CSF and RANKL. RANKL is also produced in response to bone resorption factors such as PTH, 1,25-(OH)<sub>2</sub> vitamin D<sub>3</sub>, interleukin 11 (IL-11), IL-6 and prostaglandin E<sub>2</sub> (PGE<sub>2</sub>). At the same time, osteoblasts express OPG as well, which blocks the RANK/RANKL interaction and thus inhibits osteoclastogenesis. In addition, osteoblasts also express Sema3A, which hinders OCPs from turning into osteoclasts through the inhibition of immunoreceptor tyrosine-based activation motif (ITAM) co-stimulatory signalling. Furthermore, osteoblasts produce Wnt5a, while osteoclast precursors express the Wnt5a co-receptor tyrosine kinase-like orphan receptor 2 (Ror2). Through Wnt5a-Ror2 signalling, osteoblasts stimulate RANK expression in osteoclasts (Yamashita, 2012).

Osteoclasts, on the other hand, have been suggested to regulate osteoblasts in different ways. Osteoclasts secrete Sphingosine 1-phosphate (S1P), which binds to its receptor in osteoblasts, enhancing the survival and migration of osteoblasts as well as increasing the production of RANKL. Another ligand which is expressed by osteoclasts and binds to its receptor EphB4 on osteoblasts is Ephrin B2. On the one hand, this interaction results in bi-directional signalling by promoting the osteoblast differentiation and bone formation and on the other hand, it suppresses osteoclast differentiation. Semaphorin 4D has been identified recently as a coupling factor expressed by osteoclasts which suppresses bone formation through interaction with its receptor on osteoblasts (Kular et al., 2012).

## 1.5 Diseases Arising from Abnormal Bone Remodelling

The maintenance of skeletal integrity during adult life is dependent on the balance of bone resorption and bone formation during bone remodelling. A number of bone diseases occur due to the imbalance of cellular activities of bone remodelling. For instance, osteoporosis arises as a result of the net loss of bone with age, which leads to a reduction in bone mass with a consequent increase in bone fragility and susceptibility to fractures. This disease is most prevalent among postmenopausal women due to deficiency in oestrogen, which causes increased bone turnover due to increased levels of circulating cytokines such as IL-1, IL-6, TNF $\alpha$ , and granulocyte macrophage colony stimulating factor (GM-CSF) (Kular et al., 2012; Ralston, 2013a). Another example of disease related to bone remodelling is osteopetrosis, which occurs as a result of mutations in genes responsible for osteoclast differentiation and function. Mutations in RANKL and RANK genes give rise to osteoclast poor forms of osteopetrosis. On the other hand, osteoclast-rich forms of osteopetrosis occur as a result of mutations in genes responsible for the acidification machinery of osteoclasts, such as *TCIRG1* (encode  $\alpha 3$  subunit of V-ATPase), *CAII* (encode carbonic anhydrase type II), and *CLC-7* (Kular et al., 2012; Ralston, 2013a). Paget's disease of bone (PDB) is a condition associated with dysfunctional bone remodelling. This disease is discussed in more detail in the next section.

## 1.6 Paget's Disease of Bone

PDB was first described in 1877 when Sir James Paget noticed progressive skeletal deformities upon post-mortem examination of a patient he had followed for over 20 years. In a related paper, Paget named this condition osteitis deformans, which was later renamed Paget's disease of bone (Paget, 1877).

### 1.6.1 *Clinical features*

PDB is a late-onset disease (classical form) characterized by abnormal bone remodelling with increased bone resorption and disorganized bone formation in the resorbed focal areas (Ralston, 2013b). This disease affects primarily the axial skeleton including the skull, pelvis, femur, tibia and the lumbar spine. The histological findings from PDB cases showed increased bone resorption, with the activated osteoclasts at the lesion sites exhibiting a larger size and a greater number of nuclei than normal osteoclasts. This is accompanied by other abnormalities such as marrow fibrosis, increased vascularity of bone and excessive bone formation with disorganized pattern. As a result, bone production takes on a mosaic appearance, consisting of a mixture of woven and lamellar bone. Bone with such disorganized structure has impaired mechanical strength, which in turn increases the risk of developing bone deformities and fractures (Ralston et al., 2008). The other histological finding is the intranuclear inclusion bodies that resemble the paramyxovirus nucleocapsids. This finding suggests that viral infection may be involved in the aetiology of this disease (Harvey et al., 1982). However, these inclusion bodies have been recently suggested to occur as a result of abnormal protein aggregates (Daroszewska et al., 2011). PDB has a variety of complications ranging from asymptomatic conditions to more severe complications including deafness, osteosclerosis, high-output cardiac failure, vascular calcification, and osteosarcoma (rarely). Excessive bone formation also results in bone expansion, which may lead to complications such as spinal stenosis, osteoarthritis, or pseudo-fracture (Ralston et al., 2008) (Figure 1-7).

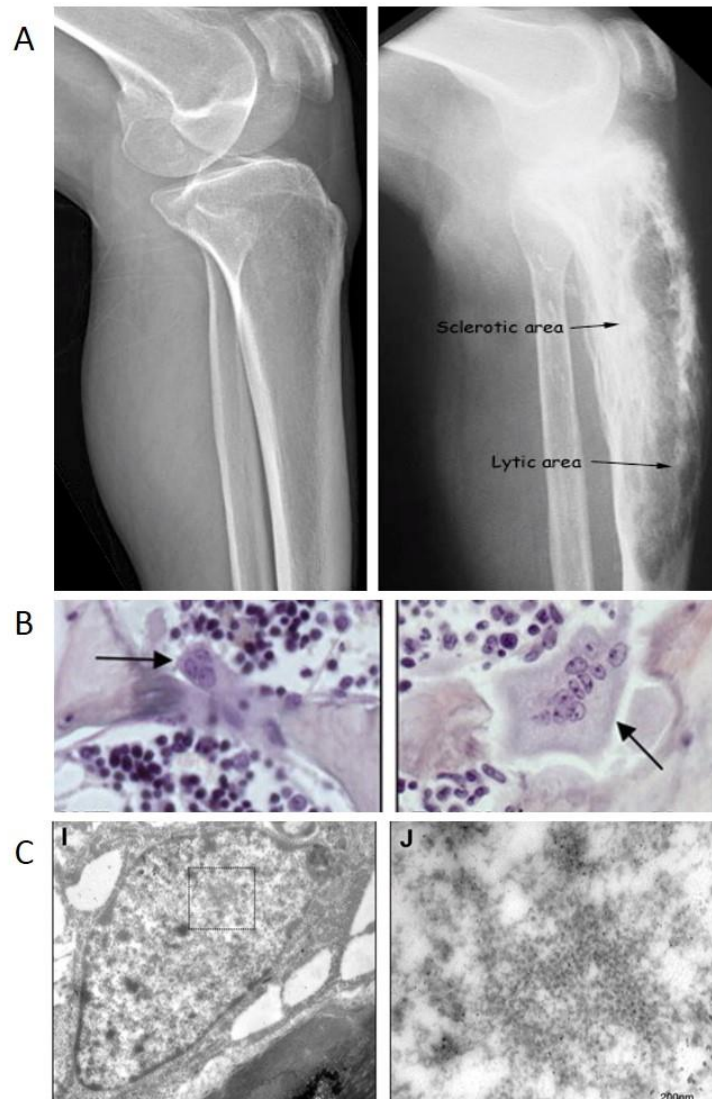


Figure 1-7: **(A)** The x-ray picture displays the difference between normal bone (left) and Pagetic bone (right). Pagetic bone shows two distinct areas, namely, sclerotic area (dense with too much bone) and lytic area (with thin and little bone). **(B)** The left image is a normal osteoclast containing three nuclei from a WT mouse, while the right image is a large osteoclast within a lesion, containing 10 nuclei, from a P394<sup>+/+</sup> mouse. **(C)** The left image is a transmission electron micrograph (TEM) image showing nuclear inclusions of osteoclast nucleus from a focal bone lesion in a P394<sup>+/+</sup>. The right image is a high-power transmission electron microscopy (TEM) image of the nuclear inclusion.

**(A)** Reproduced from

<http://depts.washington.edu/bonebio/ASBMRed/diseases/Pagets/Pagets2.html>.

**(B)** and **(C)** reproduced from (Daroszewska et al., 2011).

### 1.6.2 Osteoclast and osteoblast phenotype

Previous studies showed that Pagetic osteoclasts are hypersensitive to RANKL and 1,25-(OH)<sub>2</sub> vitamin D<sub>3</sub> (Cheikh Menaa et al., 2000a, 2000b). The transcription activating factor 12 (TAF12; formerly known as TAFII-17) protein is a member of the transcription factor IID (TFIID) transcription initiation complex. TAF12 was found to interact with vitamin D receptor (VDR) when osteoclast precursors derived from Pagetic patients and MVNP-transduced osteoclast precursors were incubated with a GST-VDR chimeric protein, and thus TAF12 was implicated in PDB. In this study, the hypersensitivity to 1,25-(OH)<sub>2</sub> vitamin D<sub>3</sub> was associated with MVNP expression in osteoclast precursors from PDB patients carrying P392L mutation, and when MVNP was knocked down, the hypersensitivity to 1,25-(OH)<sub>2</sub>D<sub>3</sub> was lost (Kurihara et al., 2004). It has also been observed that osteoclast precursors from Paget's patients carrying the P394L mutation of Sequestosome 1 (*SQSTM1*) did not show elevated levels of TAF12 expression (Kurihara et al., 2007). These findings suggest that elevated TAF12 levels in osteoclast precursors may be specific to the over-expression of MVNP in osteoclast precursors. Comparison of gene expression profile between osteoclast cultures from PDB patients and healthy controls in one study showed that Pagetic osteoclasts exhibited down-regulation in *TNFRSF11A*, which encodes RANK (Michou et al., 2010). Michou et al. also noted that genes such as *CTSK* (encoding cathepsin K) and *ACP5* (encoding TRAcP), which are involved in the bone resorbing function of osteoclasts, had decreased expression. These findings were surprising as osteoclasts are characteristically overactive in PDB and suggest that the hyperactivity of Pagetic osteoclasts may be caused by additional factors. In the same study, genes involved in apoptosis such as *CASP3* (encoding caspase) and *TNFRSF10A* (encoding TRAIL), also exhibited decreased expression (Michou et al., 2010). Another study found enhanced expression of anti-apoptotic Bcl2 gene in Pagetic osteoclasts (Brandwood et al., 2003). Collectively, these findings implicate apoptosis in the pathogenesis of PDB. What is more, by comparison to healthy controls, the gene expression profile of peripheral blood monocytes and lymphocytes derived from Pagetic cases revealed higher expression of IFN $\alpha$ , IFN $\beta$  and IFN $\gamma$  (Nagy et al., 2007).

It has been reported that, compared to non-Paget osteoclasts, Pagetic osteoclasts manifested upregulation of c-fos expression (Hoyland and Sharpe, 1994).

The excessive bone formation in PDB at lesion sites may occur not only due to the impaired osteoclast function but also due to the impaired function of osteoblasts. It has been found that Pagetic osteoblasts from bone lesions express higher osteoclastogenic cytokines such as, IL-1, IL-6, and Dickkopf1 (Naot et al., 2006). These findings led the authors to speculate that overexpression of these cytokines would result in stimulation of osteoclast activity, which in turn would lead to the formation of lytic bone lesions. When osteoblast activity is enhanced, Dickkopf1 and IL-6 may also stimulate bone formation, leading to the conversion of lytic lesions to sclerotic lesions. Naot et al. further observed that alkaline phosphatase (ALP) was upregulated while bone sialoprotein and osteocalcin were downregulated in Pagetic osteoblasts. These findings are consistent with their circulating levels in Pagetic patients (Naot et al., 2006).

### *1.6.3 Cytokines and growth factors*

Interleukin-6 (IL-6) has been implicated in PDB as a result of studies which showed Paget's patients have elevated IL-6 levels in their bone marrow plasma and blood samples (Roodman et al., 1992). Based on *in situ* hybridisation, Hoyland et al. reported that, by comparison to control samples, PDB bone samples had increased expression of IL-6, IL-6 receptor and nuclear factor IL-6 (Hoyland et al., 1994). However, another study did not find evidence of increased expression of IL-6 using RT-PCR in PDB bone samples versus control (Ralston et al., 1994). In addition, genetic variation of the IL-6 gene or variation of other genes that encode other components of the IL-6 signalling pathway have not been reported to be involved in the pathogenesis of PDB (Vallet and Ralston, 2015). Several results have been reported concerning the effects of IL-6 on osteoclastogenesis and bone. One result indicated that IL-6 blocking antibodies inhibited osteoclastogenesis in bone marrow cultures from PDB patients but not control cultures, whereas addition of IL-6 to normal marrow enhanced RANKL induced osteoclastogenesis (C Menaa et al., 2000). Indeed, several studies

demonstrated that the stimulatory effects of IL-6 on osteoclastogenesis are indirect and mediated by the production of RANKL by osteoblasts (Palmqvist et al., 2002; Tamura et al., 1993). Another study found that addition of IL-6 may act to directly inhibit RANKL-induced osteoclastogenesis in several cell types, including RAW 264.7 cells, mouse bone marrow, and human blood monocytes (Duplomb et al., 2008). The role of IL-6 on osteoclastogenesis has also been reported in a study using measles virus nucleocapsid protein (MVNP) mouse model of PDB (Kurihara et al., 2011). The findings of this study revealed that mice with MVNP overexpression had high levels of IL-6 and the crossing of these mice with IL-6 deficient mice resulted in the inhibition of Pagetic osteoclast development both *in vivo* and *in vitro*. However, in the same study, osteoclasts from knock-in mice of the P394L mutation did not express high levels of IL-6, suggesting that elevated IL-6 levels induced by MVNP in osteoclast precursors may be specific to this mouse model (Kurihara et al., 2011). Indeed, a very recent study used over-expressed IL-6 mice crossed with P394L knock-in mice and found that elevated IL-6 levels in osteoclasts from knock-in mice was not sufficient to induce Paget's-like osteoclasts or bone lesions *in vivo* (Teramachi et al., 2014).

Peripheral blood monocytes and lymphocytes derived from Pagetic patients also displayed overexpression of IFN $\gamma$ , which was present in high amounts in Pagetic serum as well (Nagy et al., 2007). Controversial studies have been reported concerning the effect of IFN $\gamma$  on osteoclastogenesis, but it seems that IFN $\gamma$  may act directly to suppress osteoclast activity and indirectly by promoting osteoclastogenesis *in vivo* and *in vitro* (Gao et al., 2007). Moreover, IFN $\gamma$  has been shown to suppress osteoclastogenesis *in vitro* (Takayanagi et al., 2000). Other studies revealed that IFN $\gamma$  decreases serum calcium and bone resorption in nude mice (Sato et al., 1992). In addition, IFN $\gamma$  has been shown to directly inhibit osteoclastogenesis by degradation of TRAF6 and by antagonizing RANKL-stimulated cathepsin K (Pang et al., 2005). Furthermore, IFN $\gamma$  has been reported to inhibit bone resorption by inducing apoptosis of osteoclast progenitors and suppressing osteoclast activity (van't Hof and Ralston, 1997). In contrast to previous studies, IFN $\gamma$  has been found to enhance the formation



of osteoclasts in cultures of peripheral blood from osteopetrotic patients (Madyastha et al., 2000). Additional studies revealed that IFN $\gamma$ -producing human T cells enhance the differentiation of human monocytes into osteoclasts via the expression of RANKL (Kotake et al., 2005). Vermeire et al. documented accelerated collagen-induced arthritis and bone resorption in mice with IFN $\gamma$  receptor deficiency (Vermeire et al., 1997). Furthermore, IFN $\gamma$  was found to enhance bone resorption in oestrogen-deficient mice by inducing T cells to secrete osteoclastogenic factors RANKL and TNF- $\alpha$  (Cenci et al., 2003).

Circulating levels of M-CSF were increased in Paget's patients compared to controls (Neale et al., 2002). Variable results of serum levels of RANKL and OPG have been obtained from different studies. In one, elevated levels of RANKL and OPG were found in PDB cases compared with those in controls (Martini et al., 2007). Other studies reported increased level of OPG, whereas RANKL levels were normal (Alvarez et al., 2003; Mossetti et al., 2005). Furthermore, levels of OPG have been shown to increase or decrease following antiresorptive therapy but RANKL levels remained unchanged (Alvarez et al., 2003; Martini et al., 2007). Further details concerning these osteoclastogenic cytokines (M-CSF, RANKL and OPG) see sections 1.3.1 and 1.6.13. Circulating levels of FGF-2 were also found to be elevated in PDB cases compared to controls. Mouse model with deleted Fgf-2 gene showed a significant decrease in trabecular bone volume, mineral apposition, bone formation rates and decreased mineralization of bone marrow stromal cultures. These findings suggested that FGF-2 is an important regulator of bone formation (Montero et al., 2000). Interestingly, studies also found that heat-shock factor-2 (HSF-2) and signal transducer and activator of transcription 1 (STAT1) are downstream targets of FGF-2 signalling and that elevated levels of FGF-2 stimulate RANKL expression in PDB (Sundaram et al., 2009).

#### *1.6.4 Treatment*

Bisphosphonates is the first treatment choice for PDB. Bisphosphonates act as anti-remodelling drugs that suppress the increased bone turnover in Paget's disease and eventually induce osteoclast apoptosis. In cases where bisphosphonates are contraindicated, calcitonin can be used instead. Calcitonin is also known to inhibit bone turnover and can relieve bone pain in PDB patients. Other drugs, along with antiresorptive therapy, are also used in clinical practice to control the pain suffered by Paget's patients, including analgesic agents, anti-inflammatory drugs, and anti-neuropathic agents. What is more, patients with Paget's disease may benefit from non-pharmacologic therapy such as physiotherapy, acupuncture, transcutaneous electrical nerve stimulation and hydrotherapy (Ralston, 2013b).

#### *1.6.5 Epidemiology*

There are marked ethnic differences and unusual geographical distribution in the prevalence of PDB. Caucasians have the highest susceptibility to the disease and the highest prevalence of PDB was recorded in the UK, where 1-2% of white adults over 55 years of age develop the disease. The incidence increases with age to affect 5% of women and 8% of men at 80 years of age. PDB is also common in France, the Netherlands, Italy, Australia, New Zealand, and North America, but is rare in Scandinavia, Africa, and Asia (Ralston, 2008). Archaeological studies show that cases that meet modern PDB diagnostic criteria were restricted to Western Europe, with the greatest concentration being located in England, suggesting that PDB originated in the UK and that the prevalence of this disease has not changed over the past 500 years (Mays, 2010). In the last 25 years, the prevalence of PDB in the UK and New Zealand appears to have declined, while in other countries it has either remained unchanged (e.g. the USA) or has increased (e.g. Italy) (Ralston, 2008).

### *1.6.6 Genetic architecture of PDB*

Familial aggregation of PDB has been reported in several studies and the risk of the patients' first degree relatives to develop Paget's disease was 6-10 times greater than the rest of the population (Siris et al., 1991; Sofaer et al., 1983). The familial clustering varies from 5% as in Holland to about 50% in French-Canadian population. These differences in familial clustering possibly reflect a founder effect of high penetrance variants in some populations, other environmental factors that trigger the disease incidence or variations between countries in determining the disease (Ralston and Albagha, 2013). The involvement of genetic factors in susceptibility to this disease is also supported by the documented variation in geographical prevalence of PDB among different ethnicities (Ralston and Albagha, 2011). In addition, the disease was found to be prevalent among migrants from high prevalence regions like Europe to regions where PDB is rare in their original population such as Australia and New Zealand (Barker, 1984). Further evidence is the mode of inheritance of classical PDB, which is autosomal dominant with a penetrance of about 80% and 90% by the seventh decade (Ralston and Albagha, 2011). However, recessive inheritance in some families has been reported, with only siblings developing the disease. In this regard, the most likely reason for disease development is the fact that a parent had an asymptomatic form of Paget's disease (Ralston and Albagha, 2013).

### *1.6.7 PDB-like syndromes*

There are several rare familial forms of disorders that share the main clinical features with the classical PDB but with some phenotypic variations such as the age of onset and the type of affected bone. These PDB-like syndromes are inherited in a Mendelian manner and are caused by mutations in genes involved in the RANKL-RANK-NF $\kappa$ B signalling pathway. These genes are considered candidate genes for PDB due to their involvement in the NF $\kappa$ B signalling and their mutant form causes syndromes to manifest some common clinical signs with Paget's disease (Ralston and Albagha, 2011). Mutations in the TNF receptor superfamily 11A (*TNFRSF11A*) gene, which encodes RANK, causes familial expansile osteolysis (FEO) (Hughes et al., 2000), expansile skeletal hyperphosphatasia (ESH) (Whyte et al., 2000), and early

onset PDB (ePDB) (Nakatsuka et al., 2003). These syndromes are inherited in an autosomal dominant manner and the onset starts during childhood or early adulthood, being associated with tooth loss, deafness, and osteolytic expansile bone lesions. Other mutations in *TNFRSF11B*, which encodes OPG, lead to juvenile Paget's disease (JPD) (Whyte et al., 2002). This syndrome is inherited in an autosomal recessive manner, which is characterized by bone pain, enlargement, deformity with mixed lytic and sclerotic lesions and fractures during childhood, in addition to a generalized increase in bone turnover (Ralston and Albagha, 2011). Mutations of valosin-containing protein (*VCP*), which codes for p97, cause a rare syndrome known as inclusion body myopathy, Paget's disease, and frontotemporal dementia (IBMPFD) (Watts et al., 2004). The causal locus for this disease was identified by genome-wide linkage analysis to be located on chromosome 9p21. Afterward, positional cloning linked this locus to *VCP* and several missense mutations at the CDC48 domain have been identified as the cause of the disease. IBMPFD is an autosomal dominant progressive disease, characterised by the gradual occurrence of symptoms over time. Myopathy is highly penetrant, displays a bone phenotype similar to PDB and the age on onset is 40-50 years old. Meanwhile, in 40% of cases, dementia develops around 50-60 years of age (Ralston and Albagha, 2013). Most recently, unique 12 bp duplication in the signal peptide region of *TNFRSF11A* was reported in a patient with a severe panostotic expansile bone disease associated with multiple bone deformities and a massive jaw tumour (Schafer et al., 2014). Histopathology revealed that the tumour consisted of woven bone and fibrous tissue. Furthermore, activating duplication of *TNFRSF11A* was recently reported in a patient with JPD, being known to develop due to mutations of *TNFRSF11B* (Whyte et al., 2014). These findings expand the range and overlap of phenotypes among conditions with known constitutive activation of RANK signalling and highlight the significance of mutation analysis to improve diagnosis. Recently, cases of osteoclast-poor autosomal recessive osteopetrosis (ARO) have been identified with a total of 12 novel mutations in *TNFRSF11A*, including missense and nonsense mutations, and a single-nucleotide insertion (Guerrini et al., 2008; Pangrazio et al., 2012). Some of these mutations cause amino acid substitutions in the extracellular domain or intracellular domain and these mutations are likely to affect the binding to

RANKL. Other mutations including nonsense mutations and the insertion cause stop mutations/frameshift mutation within the intracellular domain, which may lead to the production of truncated forms of RANK protein (Guerrini et al., 2008; Pangrazio et al., 2012). The patients with these mutations display from a very young age clinical features such as osteopetrotic bone phenotype, bone fractures, skull deformities and other clinical features including impairment of immunoglobulin-production, hypocalcaemia, gastroesophageal reflux and blindness.

### *1.6.8 Linkage studies*

The documentation of familial aggregation of PDB prompted the undertaking of linkage studies with the purpose of identifying the common genetic factors shared by families. Linkage analysis was developed to detect the segregation of genes and genetic markers, which are inherited together because of their proximity on the same chromosome in certain pedigrees (Xavier and Rioux, 2008). Studies aimed at establishing linkage between a genetic marker and disease locus usually resulted in the identification of a large genomic region with poor genetic resolution. Following the identification of the linked loci in a pedigree, different approaches are used to identify the underlying genes behind the disease, such as candidate gene linkage studies and positional cloning (Bailey-Wilson and Wilson, 2011). For PDB, seven potential susceptibility loci (PDB1-7) that predispose to late onset PDB have been identified using the linkage approach (Table 1-1). The first locus PDB1 was identified by candidate gene linkage studies and has been linked to the human leukocyte antigen (HLA) region on chromosome 6. So far, PDB1 is considered a false positive since none of the replicated studies have confirmed its candidacy to PDB. The other loci (PDB2-7) were identified by genome wide linkage studies (Ralston and Albagha, 2013). PDB2 locus was first identified by positional cloning, being linked to the *TNFRSF11A* gene in patients with FEO (Hughes et al., 2000). Two different subsequent studies linked this locus to familial PDB (Ralston and Albagha, 2013). Furthermore, the locus has been recently confirmed with genome wide association studies (Albagha et al., 2010). Following the identification of PDB3, two independent genome wide linkage studies applied the positional cloning strategy and successfully

identified the Sequestosome 1 gene (*SQSTM1*) as a causative gene for PDB (Hocking et al., 2001; Laurin, 2002; Laurin et al., 2001). Mutations in *SQSTM1* have been confirmed in different populations and are responsible for about 40% of familial cases and 10% of sporadic cases (Ralston and Albagha, 2011). PDB4 was strongly linked to PDB in French-Canadian families with low probability of linkage to *SQSTM1*. However, this locus did not emerge as a significant linkage to PDB in a British cohort or in genome-wide association studies. PDB5 was described in British families with PDB, while PDB7 was identified in PDB cases among an Australian cohort (Good et al., 2004; Hocking et al., 2001). However, it is now likely that these loci constituted false positives because subsequent genome wide scan in the same British families without *SQSTM1* mutations found no evidence of linkage to PDB5 or PDB7 (Lucas et al., 2007). The other possibility is that PDB5/7 loci may contain modifier genes that cooperate with *SQSTM1* to cause the disease. Interestingly, this study found strong evidence in support of the linkage to the PDB6 locus that was subsequently identified by GWAS to harbour the optineurin (*OPTN*) gene, which will be described later (Albagha et al., 2010; Lucas et al., 2007).

Table 1-1: Linkage studies in PDB showing the chromosomal position and the gene directly involved.

Locus	Chromosome	Gene
PDB1	6p21.3	HLA
PDB2	18q21	TNFRSF11A
PDB3	5q35	SQSTM1
PDB4	5q31	???
PDB5	2q36	???
PDB6	10p13	???
PDB7	18q23	???

### 1.6.9 Candidate-gene association studies

Candidate gene approaches have been applied in several studies in order to identify PDB susceptibility genetic variants in selected genes based on their function in bone metabolism or relationship with bone diseases (Chung and Van Hul, 2012). The first PDB-associated candidate gene was *SQSTM1*. Three single nucleotide polymorphisms (SNPs) were screened for the association with PDB in Belgian PDB patients without *SQSTM1* mutations and none of these SNPs was associated with PDB (Beyens et al., 2004). No correlation with PDB in a Belgian population was found in the case of SNPs associated with IL6 and TNFSF11 (RANKL) either (Chung et al., 2011). Another PDB-associated candidate gene was *VCP*. The *VCP* variants were reported to be associated with PDB in a Belgian cohort (Chung et al., 2011), whereas the association was not found in a British population (Lucas et al., 2006). Donath et al. screened a Hungarian population for PDB-associated variants of vitamin D receptor (*VDR*) gene, calcium-sensing receptor (*CaSR*) gene and oestrogen receptor 1 (*ESR1*) gene. The *VDR* polymorphisms did not show association with PDB, while the other two genes, *CaSR* and *ESR1*, appeared to be associated with PDB in the same cohort (Donath et al., 2004). Variants of the *TNFRSF11B* gene were reported to be a PDB-associated candidate gene in several populations including British and Belgian cohorts. Among these variants, some polymorphisms in *TNFRSF11B* revealed a female-specific effect (Beyens et al., 2007; Daroszewska et al., 2004; WUYTS et al., 2001). For the *TNFRSF11A*, variants were found to be significantly associated in different populations including Belgian, British and Dutch cohorts, with a major effect among females (Chung et al., 2010b, 2009).

### 1.6.10 Genome-wide association studies (GWAS)

GWAS are “studies in which a dense array of genetic markers (SNPs), which captures a substantial proportion of common variation in genome sequence, is typed in a set of DNA samples that are informative for a trait of interest” (McCarthy et al., 2008). Although genotyping the marker SNPs might not directly detect the disease-causing SNP at a specific locus, it would be possible to detect the associations between genotype frequency and trait status by using the linkage disequilibrium (LD) between

these marker SNPs and by fine mapping with their associated SNPs (Duncan and Brown, 2013). Hence, GWAS represent an impartial approach to the identification of common genetic variants that may be involved in the disease in populations sharing the same ethnicity. In addition, GWAS also identify novel pathways not previously implicated in the disease and are hypothesis free, without dependence on knowledge of disease pathology (Kitsios and Zintzaras, 2009). Nevertheless, GWAS are not without limitations. Firstly, the loci identified by GWAS have weak predictive power for a specific phenotype, which limit these findings to be used in clinical field. Secondly, the difficulty to conduct a functional analysis of the non-coding loci findings is another limitation, especially if they are located far from genes. The third limitation is the lack of power of GWAS to identify rare variants that may predispose to the disease. In addition, not all GWAS findings can be replicated. Furthermore, the majority of the GWAS findings are statistical signals either to known genes with known implications or to novel genes that have not been related to a particular disease before, which need further analysis to confirm the functional association with the disease (Ward and Kellis, 2012).

Recently, GWAS conducted on people of European descent identified 5 candidate genes (*CSF1*, *TNFRSF11A*, *OPTN*, *TM7SF4* and *RIN3*) and 2 loci 7q33 and 15q24 (Table 1-2). These findings have been replicated in other European populations (Albagha et al., 2011a, 2010; Chung et al., 2010a). *CSF1* is the gene coding for M-CSF, *TNFRSF11A* encodes RANK and *TM7SF4* is the gene coding for DC-STAMP. These three genes have a known role in osteoclast function. By contrast, the function of the other loci in bone biology remains unknown so far.

#### 1.6.11 Somatic mutations

One of the characteristics of PDB is the resorbed focal area, which cannot be explained by germline mutations. This gave rise to the possibility that these focal areas are caused by somatic mutations. Recent studies which have investigated the occurrence of somatic mutations have produced conflicting results. One of these studies detected the P392L mutation of *SQSTM1* in the Pagetic bone tissue from some



sporadic cases of PDB, but not in their blood samples. In addition, the P392L *SQSTM1* mutation was found in some tissues from PDB patients with osteosarcoma while the adjacent tissues were normal (Merchant et al., 2009). In contrast, another study has sequenced cDNA samples from osteoblasts and bone marrow culture derived from PDB patients with P392L mutation and found no evidence for somatic mutations (Matthews et al., 2009). Therefore, further studies are required to confirm the implication of somatic mutation in the incidence of PDB.

Table 1-2: Summary of the PDB findings of genome-wide association studies

<i>Locus</i>	<i>Nearest gene(s)</i>	<i>SNPs</i>	<i>Candidate protein</i>
<b>1p13</b>	<b><i>CSF1</i></b>	<b>rs10494112</b>	<b>M-CSF</b>
<b>10p13</b>	<b><i>OPTN</i></b>	<b>rs4294134</b>	<b>Optineurin</b>
<b>18q21</b>	<b><i>TNFRSF11A</i></b>	<b>rs2458413</b>	<b>RANK</b>
<b>8q22</b>	<b><i>TM7SF4</i></b>	<b>rs1561570</b>	<b>DC-STAMP</b>
<b>15q24</b>	<b><i>PML</i></b>	<b>rs10498635</b>	<b>Inducer of promyelocytic leukemia</b>
	<b><i>GOLGA6A</i></b>		<b>Golgin Subfamily A, member 6</b>
<b>14q32</b>	<b><i>RIN3</i></b>	<b>rs5742915</b>	<b>Ras Rab interactor 3</b>
<b>7q33</b>	<b><i>CNOT4</i></b>	<b>rs3018362</b>	<b>CCR4-NOT Transcription Complex Subunit</b>
	<b><i>NUP205</i></b>		<b>Nucleoporin 205</b>
	<b><i>SLC13A4</i></b>		<b>Solute Carrier Family 13, member 4</b>

### 1.6.12 Environmental factors and PDB

Based on the findings of several studies, it has been proposed that environmental factors may act side by side with genetic factors in the development of PDB. The role of environmental factors in disease aetiology is strongly supported by a change in disease prevalence in certain populations (see section 1.6.5) (Ralston, 2008).

Viral infection was suggested as a factor implicated in PDB due to the presence of nuclear inclusion in Pagetic osteoclasts, which are similar to the paramyxovirus nucleocapsids (Mills & Singer 1976). Earlier studies identified the measles virus (MV) and the respiratory syncytial virus (RSV) in Pagetic osteoclasts using immunohistochemistry directed against their antibodies (Mills et al., 1994, 1981). Further studies using *in situ* hybridisation were positive for MV in Pagetic bone and in peripheral blood cells from Paget's patients (Baslé et al., 1986; Reddy et al., 1999). Studies have also detected the canine distemper virus (CDV) in bone samples from British PDB patients using *in situ* hybridization, reverse-transcription/PCR-*in situ* hybridisation (RT/PCR-ISH) and RT/PCR (Gordon et al., 1992, 1991; Mee et al., 1998). On the other hand, comprehensive studies undertaken by other researchers have failed to detect paramyxovirus expression in bone, bone marrow cells, or peripheral blood cells from PDB cases using RT-PCR-based methods (Birch et al., 2009; Ooi et al., 2000). A possible explanation for this conflict could be differences in the sensitivity of RT-PCR methods for virus detection. In an attempt to resolve this conflict, Ralston et al. sent bone and blood samples derived from PDB patients blindly to different laboratories in order to compare the sensitivity of different RT-PCR-based techniques for detecting MV and CDV. In this study they found no evidence to support the fact that laboratories that failed to detect viral transcripts in PDB samples had less sensitive RT-PCR assays than those which successfully detected viral transcripts. In addition, this study failed to detect paramyxovirus transcripts in Paget's samples using the most sensitive assays evaluated (Ralston et al., 2007). Irrespective of this conflict, the role of viral proteins in modulating osteoclast differentiation and function cannot be neglected. In one study, osteoclast formation was increased *in vitro* when canine bone marrow cells were infected with CDV (Mee et al., 1995). Another study also

noticed an increase in osteoclast formation and activity *in vitro* when they infected the bone marrow of the hCD46 transgenic mice that overexpressed the cellular receptors for MV (Reddy et al., 2001). In the same context, increased bone turnover was found in the histological analysis of the vertebrae derived from mice with overexpression of the measles virus nucleocapsid (MVNP). It was found that the osteoclasts derived from those mice not only had greater sensitivity to 1,25(OH)<sub>2</sub> vitamin D<sub>3</sub>, but were also hyper-nucleated and produced higher amounts of interleukin-6 (IL-6) *in vitro* compared to WT. When the cells were treated with IL-6 antibody, osteoclast formation was inhibited. This suggests that increased osteoclast formation and activity is mostly due to MVNP-induced IL-6 overproduction (Kurihara et al., 2011). However, all these data do not necessarily imply that viral infection is a direct cause to PDB since other viral proteins HTLV-Tax are also capable of stimulating bone turnover (Ruddle et al., 1993). In addition, recent studies have suggested that the formation of inclusion bodies is due to autophagical malfunction (Hocking et al., 2012).

Mechanical loading has been suggested as a triggering factor that may determine the affected bone in Paget's disease. For instance, it has been reported that the main reason why a billiards player developed Paget's disease in his hands was the pressure associated with the use of the cue (Solomon, 1979). Similarly, Gasper (1979) proposed a direct correlation between the development of Paget's disease in the right leg of an elderly woman and her occupation as wristband maker (Gasper, 1979). However, these findings need to be confirmed experimentally.

Additional environmental factors which have been suggested to be involved in PDB include vitamin D deficiency, dietary calcium deficiency, and the association of the disease with rural life and exposure to toxins. An important epidemiological finding regarding Paget's disease was related to calcium intake. By evaluating milk consumption during childhood and adolescence, it was found that milk consumption was lower in patients than in controls (Siris, 1994). On the basis of distribution similarities between Paget's disease and rickets, another epidemiological study suggested that vitamin D deficiency in childhood was a predisposing factor of PDB (Barker and Gardner, 1974). Studies from Spain and Italy have emphasized the

correlation between the risk of developing PDB and the rural lifestyle involving frequent contact with animals such as pigs and cattle or their products (Merlotti et al., 2005). Exposure to toxins such as arsenic-based pesticides has also been proposed as a factor that predisposed to PDB, since workers in cotton mills were exposed to high level of these pesticides (LEVER, 2002). However, to confirm the correlation of these factors with PDB, further investigation is required.

The next section will describe the possible molecular implication of the up-to-date candidate genes for PDB which have been identified by various studies.

### *1.6.13 Molecular genetics*

#### **1.6.13.1 CSF1**

CSF1 is the gene coding for the cytokine M-CSF, which has an important role in macrophage and osteoclast differentiation and survival (see the osteoclast section (1.3.1) for the role of M-CSF). The strongest association identified by GWAS was rs484959 SNP, which is situated 87kb upstream of *CSF1*. *CSF1* is a strong candidate to PDB as PDB patients showed increased level of serum M-CSF compared to controls. However, the mechanism through which the genetic variants at the *CSF1* locus contribute to the disease is still unknown (Ralston & Albagha 2013).

#### **1.6.13.2 TNFRSF11A**

*TNFRSF11A* encodes RANK, the receptor activator of NK- $\kappa$ B ligand (RANKL). RANK/RANKL signalling plays an important role in osteoclast differentiation, resorption and survival, as described previously. Linkage analysis first identified this gene as being implicated in the PDB-like syndrome FEO (Hughes et al., 2000, 1994). Mutations causing syndromes are heterozygous tandem duplication of a certain number of base pairs (84dup18bp as in FEO, 84dup27bp as in ePDB and 84dup15bp as in ESH). The overexpression of these mutations was shown to cause a constitutive activation of NF $\kappa$ B signalling *in vitro* and this finding was interpreted as the reason behind the presence of focal osteolytic lesions *in vivo* (Hughes et al., 2000). However, other studies showed that these mutations in RANK prevent the normal cleavage of RANK signal peptide, which leads to the accumulation of RANK in the endoplasmic reticulum, thereby preventing the cells from being directly activated by RANKL. Homozygote mice for these mutations developed osteopetrotic phenotype, while heterozygote mice developed severe osteolytic lesions similar to those observed in ePDB patients (Crockett et al., 2011). However, mutations in RANK have not been detected in late onset PDB patients, although *TNFRSF11A* locus was identified as a strong candidate gene for PDB by GWAS. In addition, polymorphisms at the *TNFRSF11A* locus have been associated with PDB by a candidate gene study of Dutch, Belgian and British cases. Therefore, further investigations are required to determine

how variants at the *TNFRSF11A* locus are implicated in classical PDB (Ralston and Albagha, 2013).

#### **1.6.13.3 TNFRSF11B**

*TNFRSF11B* encodes the OPG protein, which is a cytokine that acts as a decoy receptor for RANKL. OPG-deficient mice were observed to develop severe osteoporosis with increased bone turnover. Several mutations for *TNFRSF11B* have been reported in JPD (Cundy et al., 2002; Middleton-Hardie et al., 2005; Whyte et al., 2002). The first mutation was a homozygous deletion of 100bp of *TNFRSF11B* gene that resulted in the absence of OPG in the circulation of patients with increased bone turnover. The second mutation was found in an Iraqi family which displayed a homozygous 3bp deletion that affected the aspartate residue. Functional studies showed that deletion of aspartate in OPG led to a loss of function mutation that impaired the binding to RANKL. The other mutations were missense mutations affecting the binding of OPG to RANKL. However, mutations of *TNFRSF11B* have not been detected in classical PDB and this gene did not emerge as a candidate gene in recent GWAS (Ralston and Albagha, 2013).

#### **1.6.13.4 VCP**

As mentioned before, mutations of the *VCP* gene (p97) cause IBMPFD (Watts et al., 2004). *VCP* is a member of the type II AAA-ATPase family with a high level of expression. From an evolutionary perspective, this protein is highly conserved and plays an essential role in a variety of cellular processes, such as cell cycle, membrane fusion, DNA damage repair, and organelle biogenesis. It also has a role in protein degradation through the ubiquitin-proteasome system (UPS), endoplasmic reticulum-associated degradation (ERAD) and autophagy. However, it remains unclear through which mechanisms *VCP* causes IBMPFD. However, the role of *VCP* in I $\kappa$ B turnover links this protein to the NF $\kappa$ B pathway, a crucial signalling pathway in osteoclasts. Furthermore, mutations of *VCP* impair its role in autophagy, which leads to accumulation of non-degradative autophagosome and vacuolation. Mutations of *VCP* have not been reported in classical PDB, although a study on a Belgian cohort showed an association between *VCP* polymorphism and PDB (Chung et al., 2011). In contrast

to this finding, a study on a British cohort showed no evidence in support of the association of VCP variants and PDB. Since the other feature of the IBMPFD syndrome is absent in PDB cases, it is unlikely that common variants of VCP are involved in the pathogenesis of PDB (Ralston and Albagha, 2013).

#### **1.6.13.5 TM7SF4**

The transmembrane 7 superfamily member (*TM7SF4*) polymorphisms associated with PDB were identified recently by GWAS. This gene encodes a transmembrane protein known as dendritic cell-specific transmembrane protein (DC-STAMP), which plays an essential role in the fusion of the osteoclast precursors and macrophages. Furthermore, DC-STAMP is stimulated by RANKL to enhance the formation of mature osteoclasts. Therefore, this gene is a strong candidate gene for PDB since the osteoclasts from the PDB cases are hypernucleated and larger compared to the osteoclasts from controls but further analysis is required to confirm this hypothesis (Ralston and Albagha, 2013).

#### **1.6.13.6 RIN3**

*RIN3* is a member of the RIN family of Ras interaction-interference proteins, which are binding partners to the RAB5 small GTPases. This gene was identified recently by GWAS but its role in bone metabolism is unknown (Albagha et al., 2011a). However, *RIN3* might be involved in bone resorption since small GTPases have a role in osteoclast function through effects on vesicular trafficking (Taylor et al., 2011). Most recently, genetic analysis has identified 13 rare missense variants, which were over-represented among PDB cases (Vallet et al., 2015). In this research, *in silico* studies have identified two groups of variants; those found in structured domains of the protein (SH2 and VPS9) and those situated within the proline-rich domain. Most of these were rare variants but one common missense variant (R279C) located within the proline-rich domain was strongly associated with PDB. Furthermore, the expression of *RIN3* was detected in bone tissue and it was higher in osteoclasts compared with osteoblasts (Vallet et al., 2015). Collectively, these findings suggest that genetic variants in *RIN3* may predispose to PDB by affecting osteoclast function.

#### **1.6.13.7 7q33 Locus**

Recent GWAS indicated the 7q33 locus as a genetic determinant of PDB. This locus contains three genes (*CNOT4*, *NUP205*, and *SLC13A4*) and two predicted coding transcripts (PL-5283 and FAM180A). *CNOT4* encodes the CCR4 subunit of the CCR4-NOT complex, which is implicated in transcriptional regulation of RNA deadenylation. Furthermore, this protein was reported to have E3 ubiquitin ligase activity (Mersman et al., 2009). The *NUP205* gene encodes the protein nucleoporin 205, which plays a role in the regulation of cellular trafficking between the cytoplasm and nucleus (Albagha et al., 2011a). *SLC13A4* (Solute Carrier Family 13 (Sodium/Sulfate Symporter), Member 4) is a protein-coding gene and may play a major role in sulfate incorporation in high endothelial venules (Girard et al., 1999). None of these genes have been implicated in bone biology and any one of them could be responsible for the development of PDB (Ralston and Albagha, 2013).

#### **1.6.13.8 15q24 Locus**

Two candidate genes within the 15q24 locus were identified by GWAS. The strongest association SNP is located within *PML* and causes a phenylalanine to leucine change at amino acid 645. Previous studies have shown that *PML* plays a role in regulating cell growth, apoptosis, senescence, and TGF- $\beta$  signalling. *PML* has unknown function in bone metabolism and might be involved in the pathogenesis of PDB because of its role in regulating TGF- $\beta$  and, thus, bone turnover. The role of this gene in apoptosis also strengthens its association with PDB since cultured osteoclasts from PDB patients survived longer than the osteoclasts from controls. The second gene in this locus is *GOLGA6A* which encodes a member of the golgin family of proteins that are associated with the structure of the Golgi apparatus. Like *PML*, *GOLGA6A* has unknown function in bone biology and any one of these two candidate genes could be involved in the development of PDB (Ralston and Albagha, 2013).



### 1.6.13.9 SQSTM1

As previously mentioned, the interaction between RANKL and RANK stimulates downstream molecules to express osteoclast-specific genes, thus promoting osteoclastogenesis. Experiments on mice showed that absence of different components of this process caused the onset of osteopetrosis. SQSTM1 has multiple binding partners and acts as scaffold for multiprotein complexes in response to different types of stimuli (Figure 1-8). SQSTM1 is a TRAF6 binding partner and regulates the RANK signalling downstream of TRAF6. PDB patients have been found to have more than 20 *SQSTM1* mutations. The most common mutation was P392L, which caused a proline to leucine change at position 392 of the gene product. Other mutations were found clustering in the UBA domain of *SQSTM1* protein while a few mutations were reported outside this region (Rea et al., 2013).

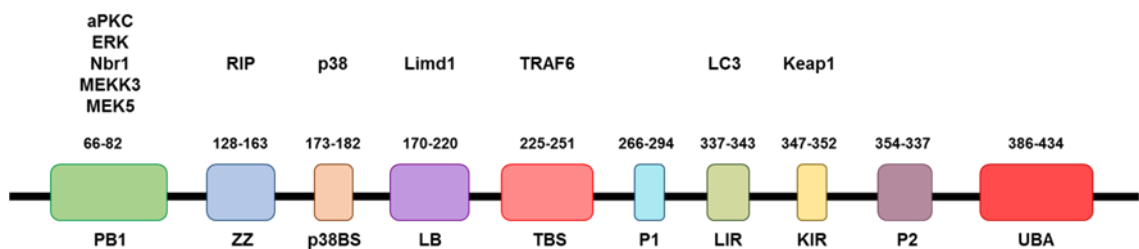


Figure 1-8: Domain structure of SQSTM1/p62 and its interacting partners. p62 is a scaffolding protein with multiple interaction domains necessary for its interaction with specific proteins and regulation of downstream signaling pathways. The N-terminal Phox and Bem1p (PB1) domain that interacts with aPKC, ERK, Nbr1 (neighbour of BRCA1), MEKK3 (mitogen-activated kinase kinase 3) and MEK5 (mitogen-activated protein kinase 5), whereas zinc finger (ZZ) binds to RIP, the TRAF6-binding sequence (TBS) interacts with TRAF6, p38 binding sequence (p38BS) binds p38, LC3-interacting region (LIR) interacts with LC3, and the Keap-interacting region (KIR) interacts with Keap1, two PEST sequences (P1 and P2), Lim protein binding region (LB) and a carboxy-terminal UBA domain. p62-binding partners are indicated above the appropriate domain. The numbers represent the numbers of amino acid residues. Adapted from (Rea et al., 2013).

Several mouse models for *SQSTM1*-induced PDB were generated in order to examine the effect of the *SQSTM1* mutations on the bone phenotype of these mice. The first model was generated by overexpressing the P392L mutation in mice (Kurihara et al., 2007). The osteoclast precursors from these mice were hypersensitive to RANKL and TNF $\alpha$  and were larger and hypernucleated compared to control

osteoclasts. In addition, it was found that P392L mutant animals showed reduced bone volume in older mice compared to WT without evidence of developing skeletal phenotype of PDB. Subsequently, two models with germline knock-in of P394L, which is the mouse equivalent of the human P392L mutation, were generated. Based on radiological and histological findings, Daroszewska et al. concluded that *SQSTM1* mutations were sufficient to cause PDB (Daroszewska et al., 2011). They found that *Sqstm1* P394L knock-in mice developed focal bone lesions mainly targeting the lower limbs. The bone lesions from mutant mice contained larger and more multinucleated osteoclasts than normal and some of these osteoclasts were seen to contain nuclear inclusion bodies. Histological examination also showed increased bone turnover with increased bone resorption and bone formation and accumulation of woven bone. On the other hand, using the same germline mutation (*Sqstm1*<sup>P394L</sup>), Hiruma et al. argued that *SQSTM1* mutations were not enough to develop the disease alone *in vivo*, despite predisposing to PDB (Hiruma et al., 2008). In this study they found that osteoclasts from mutant mice were hyper-responsive to RANKL and TNF $\alpha$  but not 1,25(OH)<sub>2</sub> vitamin D<sub>3</sub>. Co-culture of *Sqstm1*<sup>P394L</sup> stromal cells formed more osteoclasts than the co-culture of WT cells. However, histological examination of the lumbar spine from mutant mice showed normal bone. The reasons behind the difference in skeletal phenotype between the two studies may be explained by the different techniques used (Ralston and Albagha, 2013). Kurihara et al. conducted experiments on double knock-in mice with *Sqstm1*<sup>P394L</sup> and overexpression of MNVP (Kurihara et al., 2011). These mice developed focal lesions in the spine similar to PDB. The osteoclasts precursors obtained from this model were hyper-responsive to both RANKL and 1,25(OH)<sub>2</sub> vitamin D<sub>3</sub>, with increased numbers of formed osteoclasts which were larger than either *Sqstm1*<sup>P394L</sup> knock-in mice or WT mice. The expression of IL-6 production was also found to be significantly increased. This finding was in agreement with previous studies where IL-6 was increased in MVNP-overexpressing mice in addition to the high level of IL-6 reported in PDB. They also found that when *Sqstm1*<sup>P394L</sup> mice bred with mice with overexpressed MNVP, the hypersensitivity to 1,25(OH)<sub>2</sub> vitamin D<sub>3</sub> *in vitro* was abolished. These results suggest that the IL-6 is a crucial contributor to the Pagetic osteoclast phenotype. *Sqstm1*-deficient mice also had impaired

osteoclastogenesis *in vitro* and *in vivo*. Histological analysis of these mice was similar to the WT, suggesting that loss of *Sqstm1* does not affect basal osteoclastogenesis. However, when *Sqstm1*-deficient mice were treated with parathyroid hormone-related protein (PTHrP) to induce osteoclastogenesis, they showed mild alteration in the bone histological analysis (Durán et al., 2004). Collectively, these findings emphasise the role of *SQSTM1* in the pathogenesis of PDB.

#### 1.6.13.9.1 Role of *SQSTM1* in NFκB signalling pathway

Among the major factors implicated in osteoclastogenesis is NFκB signalling, including both NFκB canonical and non-canonical pathways. Overexpression of *SQSTM1* was found to inhibit NFκB activity. At the same time, overexpression of mutant *SQSTM1* enhanced the activity of the NFκB pathway (Rea et al., 2013). These findings revealed the role of *SQSTM1* in NFκB signalling. The deubiquitinating enzyme CYLD was identified to inhibit NFκB signalling and it has been observed to interact with the UBA domain of *SQSTM1*, which in turn promoted the binding of CYLD with TRAF6. When the UBA domain was removed, *SQSTM1* failed to form a complex with TRAF6 and CYLD, and NFκB signalling was enhanced (Jin et al., 2008). Furthermore, *SQSTM1* and TRAF6 were upregulated and formed a ternary complex together with aPKC in response to RANKL stimulation, while genetic inactivation of *Sqstm1* in mice led to impaired osteoclastogenesis (Durán et al., 2004).

#### 1.6.13.9.2 Role of *SQSTM1* in protein degradation

The main components of the protein degradation system are autophagy and UPS, which cooperate to maintain cellular homeostasis by clearing damaged organelles, intracellular pathogens and protein aggregates. Abnormal or overexpressed protein aggregates are sequestered within the cells and form what are called inclusion bodies. A hallmark of neurodegenerative diseases, inclusion bodies are also one of the clinical features that characterise Pagetic osteoclasts. *SQSTM1* was found to accumulate in these inclusion bodies, suggesting its implication in the protein degradation system (Rea et al. 2013). Studies investigating the causative effect of *SQSTM1* mutations on Paget's disease have reported impaired autophagic flux. Furthermore, the expression

of ubiquitin-proteasome system (UPS) and autophagy-related proteins was found to be high in osteoclasts from Pagetic bone biopsies (Hocking et al., 2012). Several studies have explored the role of *SQSTM1* in UPS. *SQSTM1* was reported to shuttle the ubiquitinated substrates to the UPS for degradation. The PB1 domain of *SQSTM1* was noted to be essential for interaction with the proteasome. At the same time, *SQSTM1* was found to be degraded by both the UPS and autophagy. Another study reported that clearance of ubiquitinated proteins by UPS was suppressed due to accumulation of *SQSTM1* after autophagy inhibition. This suggests the implication of *SQSTM1* in the UPS as well as crosstalk between autophagy and UPS (Rea et al., 2013).

The role of *SQSTM1* in autophagy was highlighted by several studies. Komatsu et al. showed that inhibition of *SQSTM1* by RNA interference (RNAi) led to suppression of inclusion body formation (Komatsu et al., 2007). In another study, *SQSTM1* was found to interact with ALFY (autophagy-linked FYVE domain-containing protein) and this interaction was obvious as a result of nutrient deprivation, which induced autophagy. This interaction organised misfolded, ubiquitinated proteins into aggregates to be degraded by autophagy (Hocking et al., 2010). Recently, *SQSTM1* was also found to interact with light chain 3 (LC3) during the autophagy process and LC3 was observed to be localize at the ruffled border in osteoclasts, alongside Atg5 and Atg7 (DeSelm et al., 2011; Rea et al., 2013). Collectively, these findings point to the critical role of *SQSTM1* in autophagy.

#### 1.6.13.9.3 Role of *SQSTM1* in apoptosis

Beside its function in the protein degradation system, *SQSTM1* is also involved in apoptosis through the regulation of the apoptotic upstream protease, caspase-8. TNF-related apoptosis-inducing ligand (TRAIL) signals the apoptosis process through the cell-surface death receptors (DRs), which in turn stimulate the formation of a death-inducing signalling complex (DISC) (Rea et al., 2013). These signals require caspase-8 aggregation and activation, which is facilitated by *SQSTM1*. Inhibition of *SQSTM1* by RNAi was found to attenuate the TRAIL and decrease the activity of caspase-8 as well as downstream caspase-3 and 7 (Rea et al., 2013).

1.6.13.9.4 Role of *SQSTM1* in pathogen infection

Thanks to its multiple protein domains, *SQSTM1* can act as a scaffold for the formation of multi-protein complexes in response to viral infection. In this context, levels of *SQSTM1* were found higher in Epstein-Barr virus lymphocytes from PDB cases either with or without *SQSTM1* mutations compared with healthy controls. In addition, overexpression of the viral protein significantly reduced NFκB signalling in WT compared to PDB cases with mutant *SQSTM1*. Based on such observations, it was concluded that *SQSTM1* is involved in viral infection (Rea et al., 2013). The ubiquitin system has been found to play a crucial role in the recognition of bacterial pathogens in the cells' cytoplasm. The cytosolic receptor NDP52 identifies ubiquitin-coated Salmonella and recruits TBK1 and LC3 targeting the bacteria to autophagic clearance. The role of *SQSTM1* in bacterial infection has been established by the fact that its ubiquitin-binding domain (UBD) targets bacteria to autophagy by interacting with LC3 (Shaïd et al., 2012).

## 1.7 Optineurin

### 1.7.1 Molecular structure

Optineurin (OPTN), a 67 kDa protein, was first isolated as a binding partner of the adenoviral protein E3-14.7K in a yeast two hybrid screening and was given the name 14.7K-interacting protein-2 (FIP2). Furthermore, due to its strong homology with the NF $\kappa$ B essential molecule (NEMO), OPTN is also known as the NEMO-related protein (NRP). In addition, according to the binding partners with which it interacts, OPTN is referred to as transcription factor IIIA-interacting protein (TFIIIA-INTP) and Huntingtin-interacting protein 7 (HIP7). The name Optineurin was derived from “optic neuropathy-inducing” based on the link with primary open-angle glaucoma (POAG) (Kachaner et al., 2012).

In humans, the OPTN gene spans the 37kb genomic region on chromosome 10p13 (10:13142082-13180276, gene ID: 10133). The human *OPTN* contains 3 noncoding exons in the 5'-UTR region and 13 exons that encode for a 577 amino acid protein. Alternative splicing at the 5'UTR generates four different transcripts (NM\_001008211.1, NM\_001008212.1, NM\_001008213.1, and NM\_001008214.1), but all share the same open reading frame (Figure 1-9) (<http://www.ncbi.nlm.nih.gov/nucore/?term=optn>).

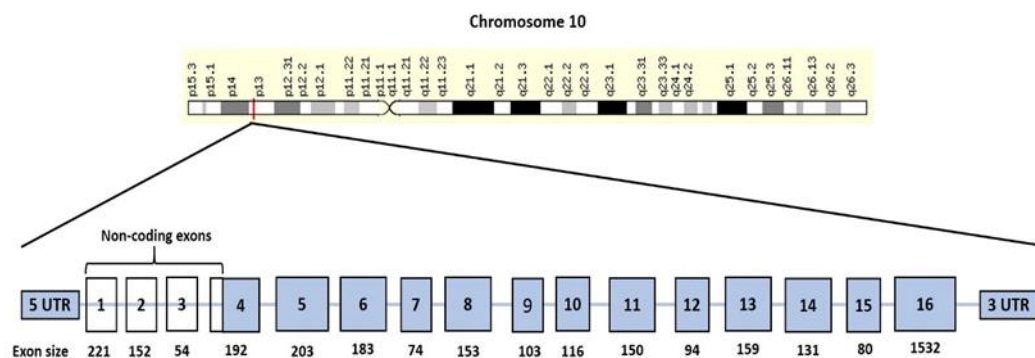


Figure 1-9: A schematic representation of the genomic structure of *OPTN*. *OPTN* is located on chromosome 10p13 and consists of 3 non-coding exons and 13 coding exons.

The detailed promoter structure regulating *OPTN* expression is so far unknown. However, one of the studies that discovered the relationship between *OPTN* and NFκB has cloned 1077 bp of DNA fragment upstream of the human *OPTN* cDNA sequence (Sudhakar et al., 2009). This putative promoter includes 221bp of exon 1, which is present in all *OPTN* transcripts. Analysis of this promoter revealed several putative Sp1 sites and one NFκB site located immediately upstream of the transcription start site. No TATA box or initiator element is present in this promoter. Other putative binding sites were also identified, including the heat shock factors, HSF1 and HSF2, MyoD, neuron-restrictive silencing factor (NRSF), and cyclic AMP response element-binding protein (CREB). This promoter was activated in HeLa and A549 cells upon treatment with TNFα. A smaller promoter size (360bp) was also made in the same study, which included the putative Sp1 sites and NFκB site, and found to be activated in HeLa and A549 cells by TNFα as well. Interestingly, the smaller promoter size showed more basal activity than the larger promoter size, suggesting that a negative regulatory element exists upstream of the smaller promoter (Sudhakar et al., 2009). IFNγ was reported to enhance the *OPTN* protein and mRNA through a mechanism which is as yet unknown (Schwamborn et al., 2000). IFNγ activates the expression of several genes through the interferon regulatory factor 1 (IRF-1) and STAT1 transcription factors. A very recent study identified a mechanism of regulation of *OPTN* expression by IFNγ through the induction of IRF-1, which in turn bound to its responsive sites in the first intron of *OPTN*. The study revealed that IRF-1 was a strong activator of *OPTN* promoter activity and mutational analysis of *OPTN* promoter caused a loss of activation of the promoter by IRF-1 or IFNγ. They also found that TNFα cooperated with IFNγ to activate the two transcription factors IRF-1 and NFκB, which synergistically induced the *OPTN* promoter (Sudhakar et al., 2013).

### 1.7.2 Protein characteristics

OPTN is ubiquitously expressed in several tissues including the brain, heart, placenta, skeletal muscle, pancreas, liver, kidney, adrenal cortex, and the eye (Kachaner et al., 2012). A high amino acid sequence homology in optineurin protein has been identified in other species, including chimpanzee, cow, dog, rat, mouse, chicken, and zebrafish. The structural domain of OPTN includes NEMO-like domain, N-terminal region containing a putative leucine zipper (LZ), 2 coiled-coil motifs, an UBD, LC3-interacting motif (LIR) and a carboxyl (C)-terminal ubiquitin-binding zinc finger (ZF) (Kachaner et al., 2012) (Figure 1-10). Studies showed that endogenous OPTN was neither a membrane nor a secreted protein but rather it was found localized in the cytoplasm with a diffuse distribution pattern (Kroeber et al., 2006; Park et al., 2006). Post-translational modification studies demonstrated that OPTN was neither N- nor O-glycosylated protein (Schwamborn et al., 2000; Ying et al., 2010). Most recently, it was reported that endogenous or ectopically-expressed OPTN interacts with itself and exists as oligomers in cultured cells under physiological conditions (Gao et al., 2014). In addition, most OPTN was found to be present in protein complexes with a high molecular weight and H<sub>2</sub>O<sub>2</sub> stimulation induced it to form nondisulfide-linked covalent trimer (Gao et al., 2014). Furthermore, endogenous OPTN was found phosphorylated by TRAF family member-associated NFκB activator (TANK) binding kinase 1 (TBK1) at Ser177, which enhances LC3 binding affinity and selective autophagy (Wild et al., 2011). Overexpression after transfection causes OPTN to take the form of dots known as foci. A subsequent study further investigated the effect of phosphorylation on crystal structures of the autophagy modifier LC3B in the complex LIR domain of OPTN. The results demonstrated that LC3B recognised phosphorylated OPTN, which in turn enhanced the affinity for OPTN-based selective autophagy, while mutational analysis weakened its interaction with LC3B (Rogov et al., 2013). Turnover experiments revealed that the endogenous OPTN was a short-lived protein, with a half-life of approximately 8 hours (Ying et al., 2010). The UPS was identified to be the major pathway for endogenous optineurin processing in neuronal cells, while autophagy and lysosomes were found to have a minor role (Shen et al., 2011).



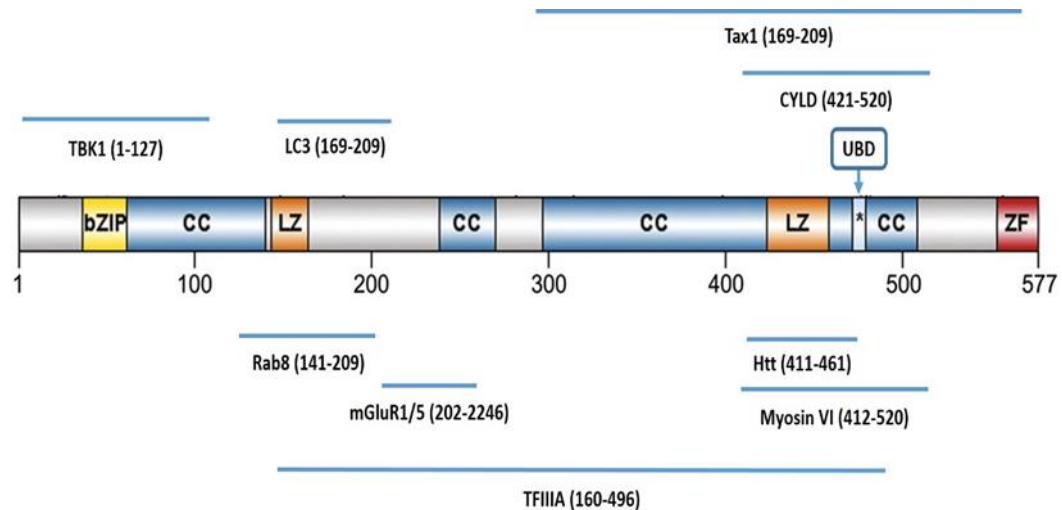


Figure 1-10: The structural domain of OPTN and its binding partners (adapted from (Rezaie, 2002)).

### 1.7.3 Optineurin-binding partners

#### 1.7.3.1 Rab8

The RAB8 (MEL) gene, which encodes Rab8, was isolated as a transforming gene following transfection of NIH3T3 mouse fibroblasts with DNA from a human melanoma cell line (Nimmo et al., 1991). Rab8 is a member of large families of guanosine triphosphatases (GTPases) that participate in and regulate vesicular trafficking between the trans-Golgi network and the plasma membrane. In addition, Rab8 promotes changes in cell shape by reorganizing actin and microtubules in fibroblast (Peränen et al., 1996). Rab8 interacts with N-terminal region of OPTN that contain a LZ at the amino acids numbers 141–209 (Hattula and Peränen, 2000). Furthermore, the Rab8-mediated endocytic trafficking of transferrin receptor was observed to be inhibited by a Rab GTPase-activating protein known as TBC1 Domain Family, Member 17 (TBC1D17). Interestingly, OPTN is a binding-partner of TBC1D17 and acts as an adaptor that mediates the interaction of TBC1D17 with Rab8 (Chalasani et al., 2009; Vaibhava et al., 2012).

### **1.7.3.2 Huntingtin (Htt)**

The gene locus of the human Huntingtin (Htt), which is associated with Huntington disease, was discovered near the tip of the short arm of chromosome 4 in 1983 and ten years later, in 1993, the gene was cloned for the first time (Cheng et al., 1989; The Huntington's Disease Collaborative Research Group, 1993). Htt is expressed throughout the body but at varying levels depending on cell type. It is implicated in many cellular processes, including development of the nervous system, immunity, transcription and intracellular signalling, intracellular transport, the secretory pathway, endocytic recycling, mitochondrial impairment, cell adhesion, and its ability to influence brain-derived neurotrophic factor (BDNF) production and transport (Zuccato and Cattaneo, 2014). It has been shown that Htt interacts with OPTN at the C-terminal region at the amino acid numbers 411–461. In addition, OPTN colocalizes with Htt in the Golgi apparatus, linking Htt to Rab8. Furthermore, co-expression of OPTN and Htt enhances the interaction of Htt to Rab8- positive vesicular structures, while cells expressing mutant Htt have impaired post-Golgi trafficking to lysosomes by delocalizing the OPTN/Rab8 complex from the Golgi apparatus (del Toro et al., 2009).

### **1.7.3.3 Myosin VI**

In humans, the proximal tubule cells of the kidney represented the location where Myosin VI was first identified (Hasson and Mooseker, 1994). Myosin VI is a multifunctional motor protein that attaches to the actin and has been found in a number of intracellular compartments including endocytic vesicles, membrane ruffles, Golgi complex, and secretory vesicles (Hasson and Mooseker, 1994; Rock et al., 2001). Furthermore, Myosin VI was observed to interact with the OPTN C-terminal between amino acid numbers 412 and 520. Myosin VI and OPTN work together in organising the Golgi apparatus while also taking part in the fusion of secretory vesicles at the plasma membrane (Sahlender et al., 2005).

#### **1.7.3.4 Transferrin receptor**

The recognition by monoclonal antibody (OKT9) of an antigen on the cell surface of human leukemic cells led to the discovery of the transferrin receptor (TFRC), which is a membrane carrier protein for transferrin. Subsequently, the OKT-9 antigen was immunoprecipitated in the presence of radio-labelled transferrin, resulting in specific precipitation of transferrin. The OKT9 antibody did not bind transferrin itself, which indicated that the antigenic structure recognized by this antibody was presumably the transferrin receptor (Sutherland et al., 1981). OPTN is required for transport of transferrin receptor from the recycling endosome to plasma membrane (Nagabhushana et al., 2010). Although the binding site for OPTN is yet to be determined, the transferrin receptor displays interaction with OPTN, prompting assumptions about its role in endocytic recycling (Park et al., 2010).

#### **1.7.3.5 Metabotropic glutamate receptors 1 and 5 (mGluR1 and mGluR5)**

Glutamate is the primary neurotransmitter that mediates the postsynaptic excitation of neural cells and is important for higher brain functions such as memory and learning, sensory pathways and cytotoxicity and neuronal death (Romano et al., 1996). Glutamate receptors are classified into two classes: the ionotropic glutamate receptors (iGluRs) and the metabotropic glutamate receptors (mGluRs) (Masu et al., 1991). The latter are classified into different groups. Among them are mGluR1 and mGluR5, which belong to group 1 of the subfamily of G-protein-coupled receptors (Conn and Pin, 1997) and are linked to the inhibition of phospholipase C (PLC) and inositol 1,4,5-triphosphate (IP3), which regulate the release of  $\text{Ca}^{2+}$  stores inside the cells (Conn and Pin, 1997). OPTN has been found to be a group 1 mGluR-interacting protein (Anborgh et al., 2005), antagonising the agonist-stimulated mGluR1a signalling when it is expressed in HEK 293 cells (Anborgh et al., 2005).

#### **1.7.3.6 Transcription factor IIIA (TFIIIA)**

TFIIIA was first isolated in eukaryotes from *Xenopus laevis* using ion exchange chromatography (Engelke et al., 1980). Its main function is the activation of 5S ribosomal RNA gene transcription in eukaryotes by RNA polymerase III. OPTN was identified using yeast two-hybrid systems to screen for TFIIIA-interacting proteins of

Xenopus. The interaction of OPTN with TFIIB was verified by chromatography and by coimmunoprecipitation *in vitro*, results showing that the location of this interaction was the central leucine domain (Moreland et al., 2000). However, the role of OPTN in the 5S ribosomal RNA gene transcription is yet to be identified (Moreland et al., 2000).

#### **1.7.3.7 Serine/threonine kinase receptor-interacting protein 1 (RIP1)**

RIP1 was partially isolated after screening the cytoplasmic domain of surface cytokine receptors (FAS) using a yeast two-hybrid system (Stanger et al., 1995). In a subsequent study, a full-length RIP cDNA was isolated by screening human umbilical vein endothelial cell cDNA library (Hsu et al., 1996). RIP1 is part of the TNF $\alpha$ -induced NF $\kappa$ B pathway. Binding of TNF $\alpha$  to its receptor (TNFR) results in recruitment of signal transducers that activate TNF receptor-associated factor 2 (TRAF2), TNF receptor-associated death domain (TRADD) and RIP1 (Hsu et al., 1996; Zhu et al., 2007). RIP1 becomes ubiquitinated with K63-linked polyubiquitin chains and binds the UBD of IKK $\gamma$  (NEMO). This leads to phosphorylation of IKK $\alpha$  which in turn phosphorylates the inhibitory protein I $\kappa$ B $\alpha$ , targeting it for proteasomal degradation and subsequent translocation of NF $\kappa$ B to nucleus in order to activate the expression of its target genes. OPTN has been found to compete with NEMO to bind with ubiquitinated RIP, which in turn inhibits the NF $\kappa$ B activation induced by TNF $\alpha$  (Zhu et al., 2007).

#### **1.7.3.8 Cyldromatosis (CYLD) gene**

The gene responsible for familial Cyldromatosis was identified by positional cloning (Bignell et al., 2000). *CYLD* encodes for a cytoplasmic protein, which acts as a deubiquitinating enzyme that negatively regulates the NF $\kappa$ B signalling pathway (Jin et al., 2008; Trompouki et al., 2003). Empirical evidence highlighted the interaction of CYLD with the UBA domain of SQSTM1. This binding facilitates the recruitment of CYLD to bind with TRAF6. On the other hand, this latter binding of CYLD to TRAF6 has a negative effect on the regulation of RANK signalling by inhibiting TRAF6 ubiquitination and, implicitly, the downstream signalling events (Jin et al., 2008). CYLD was reported to be a OPTN-interacting protein due to its interaction with the C-terminal region of OPTN that contains an UBD domain between the amino acids

424–509 (Nagabhushana et al., 2011). Furthermore, OPTN was suggested to recruit the CYLD to facilitate deubiquitination of ubiquitinated RIP, which in turn inhibits the TNF $\alpha$ -induced NF $\kappa$ B signalling (Nagabhushana et al., 2011).

#### **1.7.3.9 A20**

The zinc finger protein A20 (TNFAIP3) was one of six genes that have been identified after analysing the genes which respond to the exposure of endothelial cells to TNF $\alpha$  (Dixit et al., 1990). A20 is involved in regulation of inflammation by inhibiting NF $\kappa$ B signalling in response to several proinflammatory cytokines (Shembade et al., 2010). Sustained NF $\kappa$ B activation and increased serum levels of inflammatory cytokines have been reported in myeloid A20-deficient mice which developed erosive polyarthritis resembling rheumatoid arthritis (Matmati et al., 2011). A20 is also one of the OPTN-binding partners and future studies are required to evaluate the role of this interaction in different signalling pathways (Chalasani et al., 2009).

#### **1.7.3.10 TRAF-associated NF $\kappa$ B activator binding kinase 1 (TBK1)**

Degenerate primers based on sequences shared by IKK $\alpha$  and IKK $\beta$  together with screening of foetal brain cDNA library were used to isolate TBK1 (Tojima et al., 2000). TBK1 is a member of the IKK subfamily of protein kinases. TBK1 is triggered in response to lipopolysaccharide or viral double-stranded DNA and subsequently it activates the transcription factor interferon regulatory factor 3 (IRF3) and IFN $\beta$  in order to stimulate the downstream antiviral signalling (Gleason et al., 2011). The involvement of TBK1 in the NF $\kappa$ B pathway has also been suggested (Sun et al., 2013). TBK1 was found to interact with the N-terminal region of OPTN between residues 1-127 of OPTN. In addition, TBK1-binding domain located between residues 78-121 of OPTN was found to be homologous to the TBK1-binding domain present in three other binding partners for TBK1, namely, TANK, NAP1 (NAK-associated protein 1) and SINTBAD (similar to NAP1 TBK1 adaptor) (Morton et al., 2008). OPTN has also been shown to bind to the C-terminal region of TBK1 and therefore deletion of the C-terminal residues of TBK1 abolishes the interaction with OPTN and TANK (Morton et al., 2008).

#### **1.7.3.11 TAX1, TAX2 and TAX1BP1**

TAX1 of the human T-cell leukaemia virus type 1 (HTLV-1) is a transcriptional activator for viral gene expression (TAX2 is the equivalent of HTLV-2). Both TAX1 and TAX2 act at the same time as a transforming protein by inducing the expression of several cellular genes. In addition, TAX1 has been reported to activate NF $\kappa$ B signalling through its binding to NEMO (Harhaj and Sun, 1999). OPTN has been reported to coprecipitate with both transcription factors and the UBD of OPTN is necessary for the interaction with TAX1 (Journo et al., 2009). Tax1-binding protein 1 (TAX1BP1) is a binding partner of TAX1. Two different studies using a yeast two-hybrid screen have isolated TAX1BP1 cDNA by screening of a HeLa cell cDNA library (De Valck et al., 1999; Ling and Goeddel, 2000). The first study used a mouse fibrosarcoma library with A20 as bait and the second study used TRAF6 as bait. It has been shown that overexpression of TAX1BP1 led to apoptosis of NIH 3T3 cell lines and apoptosis induced by TNF led to TAX1BP1 degradation (De Valck et al., 1999). A different study observed that TAX1BP1 was responsible for downstream signalling activation by binding TRAF6 after stimulation of the cells with Interleukin-1 (IL-1) and TRAF6, but not with TAX1BP1 (Ling and Goeddel, 2000). Furthermore, A20 was found to interact with TAX1BP1 and together they triggered their ubiquitination and proteasomal degradation, leading to the inhibition of inflammatory signaling pathways (Shembade and Harhaj, 2010). Interestingly, interaction between TAX1BP1 and OPTN has also been observed (Journo et al., 2009). The mechanism by which OPTN exerts its effect on such signalling is complex but it appears to induce NF $\kappa$ B activation when OPTN interacts with TAX1 and to inhibit the inflammatory signalling pathways when present with A20 and TAX1BP1.

#### **1.7.3.12 LC3/GABARAP**

Microtubule-associated protein 1 light chain 3 (LC3) was identified as one of three light chains (LC1, LC2, and LC3) associated with purified neuronal microtubule-associated proteins MAP1A and MAP1B (Mann and Hammarback, 1994). LC3 is an autophagy protein required in the formation of autophagosomal membrane (Kabeya et al., 2000).  $\gamma$ -Aminobutyric acid receptor-associated protein (GABARAP) is also an autophagy protein which was identified by yeast two-hybrid screening (Wang et al.,

1999). GABRAP has been shown to play a role in neuronal cells by linking GABAA receptors and cytoskeleton. This interaction is important for clustering of GABAA receptors on neuronal cell surfaces. In addition, GABRAP was reported to be involved in apoptosis as well as playing an essential role at a later stage in the autophagosome maturation (Lee et al., 2005). Recently, OPTN was identified to be a LC3/GABARAP binding partner through its LIR motif, which is located among the coiled-coil domains of OPTN between amino acids 169-209 (Wild et al., 2011). This study provided evidence that during bacterial infection OPTN acted as an autophagy receptor.

#### **1.7.3.13 TNF receptor-associated factor 3 (TRAF3)**

TRAF3 was identified by performing a yeast two-hybrid screen on a CD40 cytoplasmic domain cDNA library and it was given the name of CD40-binding protein (Hu et al., 1994). TRAF3 is a critical signalling molecule for regulating the IFN $\beta$  production in response to virus infection. It links the TLR and downstream regulatory kinases important for interferon regulatory factor 3 and 7 (IRF3/7), which regulate IFN $\beta$  activity (Oganesyan et al., 2005). Furthermore, it has been observed that TRAF3 negatively regulates both MAPK activation and non-canonical NF $\kappa$ B signalling (Hu et al., 2013; Matsuzawa et al., 2008). TRAF3 is a binding-partner for TANK and TBK1 while, interestingly, it also interacts with OPTN. Moreover, TRAF3 may be involved in the polyubiquitylation of OPTN-binding partners in the antiviral signalling pathway (Mankouri et al., 2010).

#### **1.7.3.14 Others**

Other OPTN-binding partners displayed weaker interaction with OPTN including ubiquitously expressed transcript (UXT), zinc finger and BTB domain containing 33 (ZBTB33) and GPANK1 (G Patch Domain and Ankyrin Repeats 1) or BAT4 (Chalasani et al., 2009). Future investigations will be required to reveal the physiological significance of the interaction of these proteins with OPTN.

#### 1.7.4 Animal models

1.  $\beta$ B1-crystallin-OPTN mice and  $\beta$ B1-crystallin-TGF $\beta$ 1/  $\beta$ B1-crystallin-OPTN double transgenic mice: These mice were developed to study the overexpression of OPTN in mice lens and to assess the effect of transgenic OPTN on apoptosis *in vivo*. This model did not support the anti-apoptotic effect of OPTN, which was previously suggested by other experiments (Kroeber et al., 2006).
2. Human OPTN (E50K) transgenic mice: This model was designed by overexpression of WT and mutated human OPTN (E50K) with the purpose of evaluating the impact of this overexpression on the phenotypic characteristics in the retina. They found that the introduction of E50K mutation disrupted the OPTN interaction with Rab8, which in turn led to retinal degeneration in mice (Shen et al., 2011).
3. *Optn*<sup>D477N/D477N</sup> knock-in mice: The creation of these mice involved the use of C57/B16 background mice which were inoculated with a polyubiquitin binding-defective point mutation corresponding to an Asp-477 to Asn mutation in exon 12 of the human OPTN. This model was generated in order to assess the involvement of the ubiquitin-binding of OPTN in regulating TBK1 and IFN $\beta$  production. It was found that TBK1 production was reduced in knock-in mice compared to WT, which in turn impaired the production of IFN $\beta$  (Gleason et al., 2011). In the present project, this model has been used to evaluate the role of OPTN in PDB and bone metabolism.
4. *Optn*<sup>470T</sup> knock-in mice: This model was recently generated by removing the entire UBD thereby resembling OPTN mutations found in certain neurodegenerative disorders. This is the first model showing OPTN insufficiency as well as lack of ubiquitin-binding to assess the role of OPTN *in vivo*. This model was used to evaluate the major immune cell types including macrophages, dendritic cells, B-cells and T-cells in response to optineurin insufficiency. Munitic et al. found that *Optn*<sup>470T</sup> knock-in mice did not affect the NF $\kappa$ B activity in immune cells when compared to WT but instead it impaired the interferon regulatory factor 3 (IRF3) in these cells (Munitic et al., 2013).



### *1.7.5 OPTN and bone metabolism - is there a link?*

The role of *OPTN* in PDB or bone metabolism is unknown. However, the findings of previous studies suggest that *OPTN* may play a critical role in the pathogenesis of PDB and in regulation of bone metabolism. As mentioned before, *OPTN* is located on chromosome 10p13 region, which was previously linked to PDB but the causative gene has not been identified despite positional cloning efforts. In addition, locus rs1561570 was the top GWAS hit and is located within *OPTN*, finding which was replicated in different populations. Furthermore, *OPTN* has been implicated in different signalling pathways and aetiological factors which were suggested for PDB, such as NF $\kappa$ B signalling pathway, viral infection and autophagy. In the following part, arguments are provided in support of the idea that *OPTN* is a highly plausible candidate gene for PDB on the basis of the related data and information from the available literature.

#### **1.7.5.1 Role of OPTN in NF $\kappa$ B signalling**

One major signalling pathway involved in skeletal development is the transcription factor NF $\kappa$ B. Following a number of activator signals including RANKL, TNF $\alpha$ , interleukin- 1 (IL-1), CD40L, bacterial endotoxins, Toll-like receptor (TLR) ligands, and oxygen radicals, NF $\kappa$ B kinase complexes (IKK $\alpha$ , IKK $\beta$ , IKK $\gamma$ /NEMO, TAK1 and NIK) become activated and phosphorylate the NF $\kappa$ B inhibitory protein, I $\kappa$ B $\alpha$ . The latter undergoes proteasomal degradation allowing the NF $\kappa$ B dimers to translocate to the nucleus and activate their target genes (Abu-Amer, 2013). Ubiquitination is a posttranslational modification that plays a central role in NF $\kappa$ B signalling pathway. Polyubiquitin chains can be linked through several internal lysine (K) residues, most commonly K63 and K48. K63-linked polyubiquitination mediate activation of the NF $\kappa$ B IKKs and TAK1. K48-linked polyubiquitination targets substrates (e.g. I $\kappa$ B $\alpha$ ) for proteasomal degradation (Abu-Amer, 2013).

The role of *OPTN* as a negative regulator of NF $\kappa$ B signalling has been proposed by several studies. Firstly, *OPTN* has been found to have an UBD similar to that present in IKK $\gamma$  (NEMO), which enables the *OPTN* to compete with NEMO's binding

for ubiquitinated RIP1 following TNF $\alpha$  stimulation. Furthermore, it was found that knockdown of OPTN increased the NF $\kappa$ B basal activity in non-stimulated cells (Zhu et al., 2007). In a different study, Sudhakar et al. recognised NF $\kappa$ B binding sites in the *OPTN* promoter (Sudhakar et al., 2009). They also noticed a negative feedback loop in which TNF $\alpha$ -induced NF $\kappa$ B activity mediated the expression of OPTN, which in turn negatively regulated NF $\kappa$ B signalling. Overexpression of OPTN in the previous two studies was found to inhibit the TNF $\alpha$ -induced NF $\kappa$ B activity. Furthermore, Nagabhushana et al. also found that OPTN mediated the interaction of CYLD with RIP1 and this interaction was essential for deubiquitination of RIP1 by CYLD (Nagabhushana et al., 2011). The consistent increase in the NF $\kappa$ B basal activity was an additional important observation of this study. *OPTN* depletion in this study resulted in the accumulation of higher levels of ubiquitinated RIP1. These findings led the authors to suggest that, due to the accumulation of higher levels of ubiquitinated RIP1 in *OPTN*-depleted cells, CYLD was unable to associate with ubiquitinated RIP1 and thus enhancing the NF $\kappa$ B activity. They also proposed this model as explanation for the elevated NF $\kappa$ B basal activity in non-stimulating *OPTN*-depleted cells (Nagabhushana et al., 2011). Another study showed that OPTN is an adaptor protein that interacts with TAX1BP1 and TAX1 leading to sustained NF $\kappa$ B activation by increasing the polyubiquitination of TAX1 (Journo et al., 2009). OPTN also interacts with A20, a deubiquitinating enzyme that downregulates the NF $\kappa$ B signalling by inhibiting the TRAF6 and RIP1 ubiquitination (Chalasani et al., 2009; Harhaj and Dixit, 2010). In addition to the previous findings, OPTN was also found to interact with the co-activator of NF $\kappa$ B FUS, also known as translocated in liposarcoma (TLS) (Ito et al., 2011). FUS binds NF $\kappa$ B p65 through its C-terminal domain and mediates the NF $\kappa$ B activity (Uranishi, 2001). TBK1 is another OPTN-binding partner which has been observed to be recruited to the TNF receptor complex in response to TNF $\alpha$ , thus enhancing the NF $\kappa$ B signalling. Interestingly, E50K OPTN has been found to facilitate the binding of OPTN to TBK1 (Morton et al., 2008). All these findings strongly suggest that OPTN is a regulatory factor for NF $\kappa$ B signalling. However, very recent studies have found that OPTN is dispensable for NF $\kappa$ B activation in

macrophages in response to TLR or TNF $\alpha$  but necessary for the activation of IRF3 and IFN $\beta$  production (Gleason et al., 2011; Munitic et al., 2013). The reason for these conflicting findings may be due to the type of cells or stimulants used. This calls for further analysis to confirm these findings.

#### **1.7.5.2 Role of OPTN in vesicular trafficking**

As previously mentioned, VCP is implicated in vesicular trafficking. In light of the fact that VCP mutations are involved in the PDB-associated disease IPMPFD, vesicular trafficking has been proposed to contribute to the molecular pathology of PDB. IPMPFD has phenotypic appearances similar to PDB, which make it a useful model to explore the aetiology of PDB (Badadani et al., 2010). In addition, vesicular trafficking pathways that are regulated by Rab GTPases play a crucial role in bone-resorbing osteoclasts (Coxon and Taylor, 2008). Interestingly, OPTN was found to interact with several structures that are involved in vesicular trafficking, including myosin VI, Rab8, huntingtin and transferrin receptor (Figure 1-11). Further studies are required to explore the physiological and pathological interaction of OPTN with these vesicular trafficking proteins in bone biology (Nagabhushana et al., 2010; Sahlender et al., 2005).

#### **1.7.5.3 Role of OPTN in apoptosis**

The findings regarding the involvement of OPTN in apoptosis are contradictory. OPTN was shown to increase cell survival by protecting the transfected 3T3 cells against hydrogen peroxide-induced apoptosis (Kachaner et al., 2012). On the other hand, Park et al. reported that overexpression of WT and E50K OPTN in ocular cells increased apoptosis (Park et al., 2006). Another study found that the overexpression of OPTN did not prevent cell loss induced by transforming growth factor- $\beta$  (TGF $\beta$ ) in double transgenic mice  $\beta$ B1-crystallin-OPTN/ $\beta$ B1-crystallin-TGF $\beta$ 1 (Kroeber et al., 2006). Overexpression of optineurin E50K also enhanced the apoptosis in retinal ganglion cells (Chi et al., 2010). A very recent study revealed that, by knocking down OPTN in neuron cells, sustained NF $\kappa$ B activity resulted in neuronal cell death (Akizuki et al., 2013). These variations may be due to the cell type that has been used and future work is needed to address the OPTN role in bone cell apoptosis.

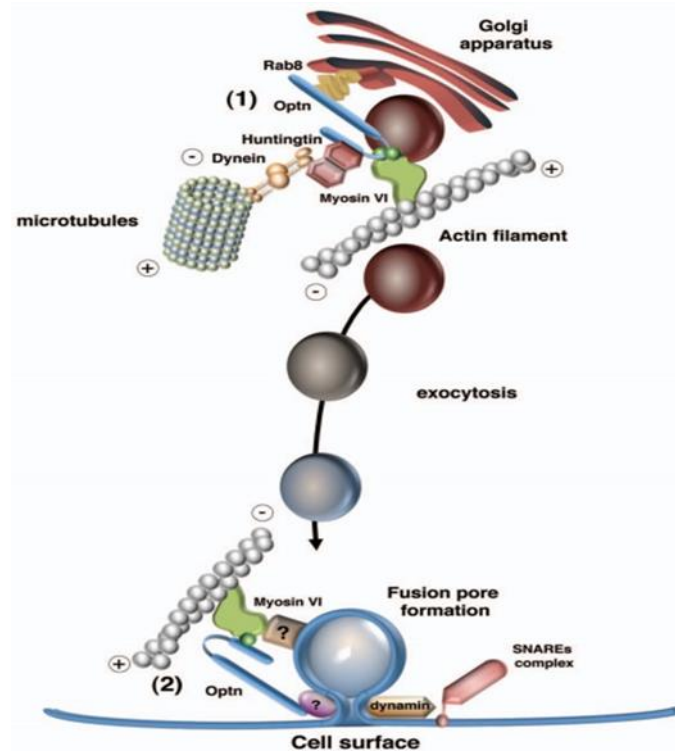


Figure 1-11: The role of OPTN in membrane trafficking. OPTN is associated with the Golgi network through interaction with Rab8, myosin VI and Htt and therefore OPTN may coordinate actin cytoskeleton and microtubule system for maintaining Golgi morphology. Derived from (Kachaner et al., 2012).

#### 1.7.5.4 Role of OPTN in the protein degradation system

Investigations of OPTN processing in neuronal cells revealed that the major system of OPTN processing is UPS and, to a lesser extent, autophagy. Treatment of neuronal cells with proteasomal inhibitors was observed to increase OPTN, whereas treatment with autophagy inhibitors had no effect. When cells overexpressed WT and E50K OPTN, the UPS activity was decreased and the turnover of overexpressed WT or E50K OPTN was slowed down compared to the endogenous OPTN. At the same time, the LC3 was induced, which represents the autophagy. These results suggest that the UPS function is compromised when OPTN is mutated or overexpressed, while autophagy is induced in order to degrade the mutated or overexpressed OPTN (Shen et al., 2011). Furthermore, it has been found that overexpression of WT and E50K OPTN led to the formation of foci, similar to the inclusion bodies found in the neurodegenerative diseases and PDB (Ying et al., 2010). The role of OPTN in the formation of inclusion

bodies has been proven when OPTN was shown to colocalize with TDP-43, FUS/TLS and SQSTM1 in cells from cases of inclusion body myositis (Yamashita et al., 2013). Interestingly, LC3 is an OPTN binding-partner and OPTN has been recently shown to act as an autophagy receptor during bacterial infection (Wild et al., 2011). In addition, OPTN was involved in autophagic clearance of protein aggregates via its C-terminal coiled-coil domain in an ubiquitin-independent manner. Korac et al. found that OPTN depletion in HeLa cells resulted in the increase of protein aggregates. Furthermore, they noticed that TBK1 was colocalized with OPTN in protein aggregates, which indicated the importance of TBK1 and OPTN in autophagy (Korac et al., 2013).

#### **1.7.5.5 Role of OPTN in bacterial and viral infection**

After viral infection, signals were found to induce the innate immunity by triggering the TBK1, which subsequently activates IRF3, IRF7 and NF $\kappa$ B to regulate the induction of type I interferons, IFN $\alpha/\beta$  (Richards and Macdonald, 2011) (Figure 1-12). Loss of type I interferons leads to severe inhibition of the immune response towards viral infection (Müller et al., 1994). Previous studies reported contradictory data on the function of OPTN in viral infection. In one study, OPTN overexpression in HEK cells followed by infection with RNA virus inhibited virus induced-IFN $\beta$ , whereas knockdown of *OPTN* in these cells stimulated virus-induced-IFN $\beta$  production and reduced viral replication (Mankouri et al., 2010). On the other hand, OPTN was reported to have an antiviral role through the interaction with TAX1BP1 after cells were infected with HTLV-1. This in turn modulated the TAX1-induced NF $\kappa$ B pathway (Journé et al., 2009).

A recent study provided proof that OPTN is involved in bacterial clearance due to its effect on cytosolic pathogens, linking them to autophagic elimination. Furthermore, OPTN was found to interact with autophagy modifiers LC3/GABARAP proteins, both of which are members of the autophagosomal membrane (Wild et al., 2011). Depletion of *OPTN* abolished the LC3-GABARAP binding and thus the autophagy. Upon infection with salmonella, cytosolic Salmonella was rapidly coated with ubiquitin and OPTN bound to these ubiquitinated Salmonella through its UBD. Subsequently, TBK1

phosphorylated OPTN, which enhanced the LC3-binding affinity, triggering the autophagic clearance of cytosolic Salmonella (Wild et al., 2011).

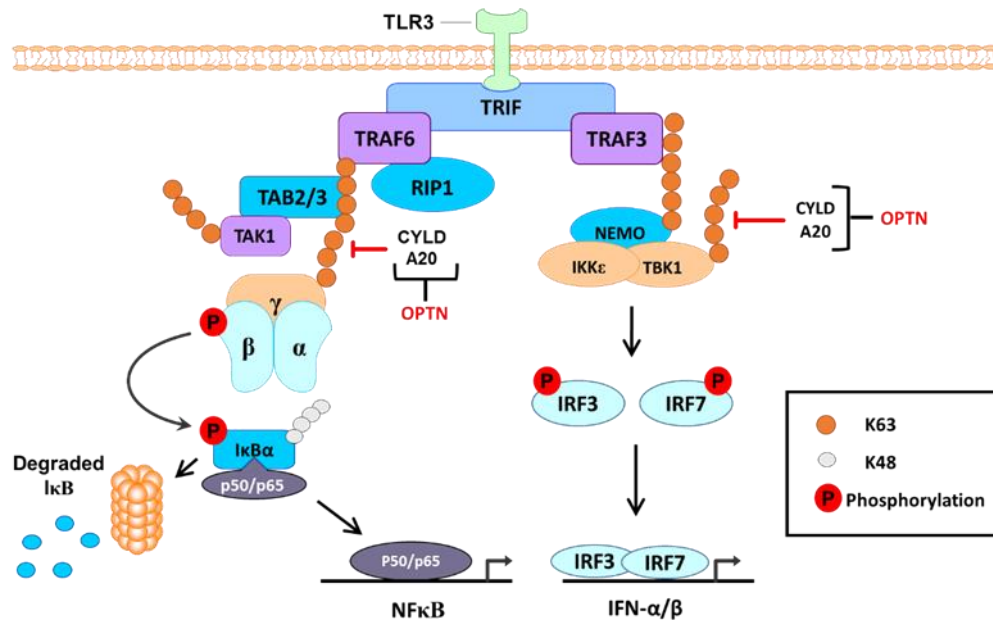


Figure 1-12: Suggested role of OPTN in viral infection. Recognition of viral dsRNA by TLR3 initiates signaling cascades by binding to the adaptor protein TRIF. TRIF then signals to TRAF6, which is induced by interaction with K63-linked polyubiquitin and leads to the recruitment of the TAK1/TAB2/3 complex. Subsequently, the IKKα/β/γ complex is recruited and activated, which leads to phosphorylation and K48-ubiquitination of IκBα, targeting it for proteasomal degradation. The degradation of IκBα liberates the NFκB to enter the nucleus in order to activate the expression of its target genes. TRIF also signals downstream through TRAF3, which becomes activated by K63-linked ubiquitination. TRAF3 then recruits the TBK1/IKKε complex, which triggers IRF3/7-mediated IFN-α/β induction. Deubiquitinase enzymes, such as CYLD and A20, are responsible for the removal of polyubiquitin. OPTN is a binding partner to these enzymes and may have a regulatory role downstream of TRAF6 and TRAF3 signalling in response to viral infection

#### 1.7.5.6 Other possible roles

Since glutamate regulates osteoblast and osteoclast differentiation and activity, it has been deduced that glutamate plays a physiological role in bone homeostasis (Brakspear and Mason, 2012). It is important to note that OPTN is a binding partner to both mGluR1 and mGluR5 and further studies will be required to explore the effect of OPTN on these proteins (Anborgh et al., 2005).

#### **1.7.5.7 Conclusion**

It is obvious from the preceding evidence that OPTN may have a crucial role in bone biology. Previous studies have demonstrated that OPTN is involved in various mechanisms and processes, including NF $\kappa$ B signalling, autophagy, apoptosis, vesicular trafficking, and pathogen infection, all of which were proposed to contribute to the molecular pathology of PDB. Interestingly, most of these roles have been assigned to SQSTM1 as well. Collectively, these findings strongly suggest that OPTN is a candidate gene involved in PDB pathology.

## 1.8 Project Aims

The main aim of my project is to explore the role of OPTN in bone metabolism and development of Paget's disease of bone. Specifically, the following will be investigated:

1. To investigate the association between *OPTN* genetic variants with the severity and clinical outcome of PDB.
2. Mutation screening of *OPTN* gene in Paget's disease patients to identify disease associated polymorphisms/mutations.
3. To study the role of OPTN in bone metabolism by
  - *in vitro*: to investigate the effect of *Optn* knockdown on osteoclasts differentiation and survival.
  - *in vivo*: to analyse the skeletal phenotype of a mouse model with a loss of function mutation in optineurin (*Optn*<sup>D477N/D477N</sup>) and to investigate the molecular mechanism leading to osteoclast activation in this mouse model.



# **CHAPTER TWO**

## **MATERIALS AND METHODS**

## 2 Materials and Methods

### 2.1 Materials

Materials used in this study are listed in Appendix 1.

### 2.2 Methods

#### 2.2.1 *Study Subjects*

##### 2.2.1.1 **Study subjects used for sequencing of *OPTN***

DNA samples were selected from clinically confirmed cases of PDB and controls who participated in the Paget's disease Randomised Trial of Intensive versus Symptomatic Management (PRISM) study (Langston et al., 2009). Most samples were cases selected from chromosome 10-linked families. The working stock was prepared at a concentration of 10 ng/μl, and stored at -20°C. Some of these samples belonged to familial cases as well as controls. The total number of subjects screened for *OPTN* mutation was 43 (16 controls and 27 cases).

##### 2.2.1.2 **Study subjects used for investigating the association between *OPTN* variants and disease severity**

The study subjects comprised 635 PDB patients without *SQSTM1* mutations who were recruited for the PRISM study (Langston et al., 2009). Gender and rs1561570 allele distribution for the study subjects are shown in Chapter 3, Table 3-1.

#### 2.2.2 *Mutation screening of *OPTN* gene*

##### 2.2.2.1 **Primer design**

All primers were designed using Primer3+ software. The primer pairs were designed to amplify the coding region and the exon-intron boundaries of the *OPTN* gene. A list of all primers used for mutation screening and can be found in Table 2-3.

##### 2.2.2.2 **Polymerase Chain Reaction (PCR)**

PCR was used to amplify the selected exons from DNA samples using the previously designed primer pairs. All reaction conditions were optimised using two

different kits, Invitrogen and Qiagen (see Tables 2-1, 2-2 and 2-3). Gel electrophoresis was performed after the PCR to confirm successful amplification of the product size using a ladder scale.

#### **2.2.2.3 Sequencing of PCR products**

After successfully confirming the PCR product size using gel electrophoresis, the PCR product was then sent to the sequencing department. Sequencing was performed using the BigDye Terminator Chemistry kit to remove excess salts and run on an ABI 3730 DNA analyser. The minimum amount needed for PCR products to be sequenced was 20 µl and the concentration of the primers was 20 µM. Sequencing data was received as ABI files. These files were then analysed using the ChromasPro software. This software manually analyses the polymorphic variation in each sequence compared to reference sequence.

#### **2.2.2.4 Microsatellite genotyping.**

I have noticed the presence of a microsatellite during the analysis of sequences amplified from exon 2 and 3 of *OPTN*. A PCR-based assay was designed to genotype this microsatellite. One of the primers was labelled with the fluorescent dye FAM in order to determine the actual size of PCR products using the DNA sequencing machine (Figure 2-1). PCR product (1 µl) was added to 0.5 µl of 500 LIZ size markers and 10 µl of Hi-Di Formamide from Applied Biosystems. The reaction mix was then heated to 95°C for 5 minutes. Samples were sent for analysis on an ABI 3730 DNA analyser. The software used for microsatellite analysis was GeneMarker.

>[chr10:13150842+13150980](#) 139bp GGCCCTCATTGTACCCTTTT  
 TGGACATTTTTTGATTCTTCCTTTT

**Forward Primer  
(FAM)**

↓

**GGCCCTCATTGTACCCTTTT**atacacccatacacacacacgcacacacacacatgca  
 cacatgcgcggtgcacacacacacacacttttctgaagctacatatacctttttgtt  
 t**AAAAGGAAGAATCAAAAATGTCCA**

↑  
**Reverse Primer**

Figure 2-1: The primer sequences for PCR amplification of *OPTN* microsatellites using the UCSC genome browser.

Table 2-1: PCR reaction conditions

Invitrogen Kit		Qiagen Kit	
Reagent	Per well (μl)	Reagent	Per well (μl)
Buffer (10x)	2.5	Buffer (10x)	2.50
dNTP (10 mM)	0.5	dNTP (10 mM)	2.00
MgCl <sub>2</sub> (50 mM)	0.75	Q solution (5x)	5.00
Primers(F) 10 μM	2.5	Primers (F) 10 μM	1.00
Primers (R) 10 μM	2.5	Primers (R) 10 μM	1.00
dH <sub>2</sub> O	14.05	dH <sub>2</sub> O	8.38
<i>Taq</i> U/μl	0.2	Qiagen <i>Taq</i> U/μl	0.13
DNA 10 ng/μl	2	DNA ng/μl	5.00
Total volume/Reaction	25	Total volume/Reaction	25

Table 2-2: The thermal cycling protocol

Thermocycling conditions		
Step	Temperature (°C)	Duration (Min)
Denature	94	03:10
Denature	94	00:50
Annealing	vary according to the primer used (See table 2.3)	01:00
Extension	72	01:30
No. of cycles	35	
Extension	72	10:00
Store	4	Forever

Table 2-3: A list of primers used for *OPTN* sequencing.

Amplified region	Sequence (5' – 3')	Primer name	Kit used	Annealing Temp (°C)	Amplification size
Exon1	GTGACGCCTTAGAGCAGTCC	OPTN_X3_F	Qiagen	58	623
	ACCCTCTCCCACCAGGTC	OPTN_X3_R			
Exon2	TCTATGTCCACATGGATGCC	OPTN_X4_F	Invitrogen	60	459
	TGCAAATCTTCAAATTCAAATCTC	OPTN_X4_R			
Exon3 and Exon4	TCCTGACCTCATGATCTGTCC	OPTN_X5_6_F	Invitrogen	64.8	414
	TAAATCCTGTGCTTCCCCAC	OPTN_X5_6_R			
Exon5	TTCAGAGCCATGTGGTCAAG	OPTN_X7_F	Invitrogen	60	654
	TCCAGACTGAACCATGAAAGG	OPTN_X7_R			
Exon6	AGAGCTCTGCGATTAAGGG	OPTN_X8_F	Invitrogen	60	369
	TCAATCCTTGGCTTGTGTTG	OPTN_X8_R			
Exon7	CTTCCTTGGGTTGCATGTC	OPTN_X9_F	Qiagen	58	269
	AACATTTGACCTCCGGTGAC	OPTN_X9_R			
Exon8	ACCTTCCCTAGGAAGCATGG	OPTN_X10_F	Invitrogen	60	538
	GACAGTGAGTGCTGTTTGGG	OPTN_X10_R			
Exon9	AACCCCTGATCCTTTATCCC	OPTN_X11_F	Invitrogen	60	290
	TTTGAATTCAGTGGCTGGAC	OPTN_X11_R			
Exon10	TGGTTCAGCCTGTTTTCTCC	OPTN_X12_F	Invitrogen	53.6	373
	TTCATGCTCACACATTAAGTGG	OPTN_X12_R			
Exon11	AAACCCTACAGCCCTAAAATTC	OPTN_X13_F	Invitrogen	60	394
	TGCTAGGACTCCTTCAGATAAGTG	OPTN_X13_R			

Amplified region	Sequence (5' – 3')	Primer name	Kit used	Annealing Temp (°C)	Amplification size
Exon12	AGAAGGTTGGGAGGCAAGAC	OPTN_X14_F	Invitrogen	60	283
	CAACCTTTGAAACCAGATTTAGTG	OPTN_X14_R			
Exon13	CCACCTCAGCCTCTCAATTC	OPTN_X15_F	Invitrogen	60	369
	TGCTTTCCAATGCGAGAATAC	OPTN_X15_R			
Exon14	CAGCACTACCTCCTCATCGC	OPTN_X16_F	Invitrogen	64.8	295
	CAGGAACGTCTTTGGACAGG	OPTN_X16_R			
Exon15	TGGACTGTCTGCTCAGTGTTG	OPTN_X17_F	Invitrogen	60	249
	GAATCCATTGTAGAGAATGAAGTGG	OPTN_X17_R			
Exon16 Part 1	TGTGCTCATGTCCCACTACG	OPTN_X18_1_F	Invitrogen	60	725
	CAGGTACCTTTTCTTCTCCTTCC	OPTN_X18_1_R			
Exon16 Part 2	GAAGTGGCAGTTGCAGTGAG	OPTN_X18_2_F	Invitrogen	60	643
	AGGTACAATGAAAGCATGAAGG	OPTN_X18_2_R			
Exon16 Part 3	TTGCAGCCACAATAATTTTACC	OPTN_X18_3_F	Invitrogen	60	729
	TGTGTTCTCTTGGCATGAAG	OPTN_X18_3_R			

### 2.2.3 TISSUE CULTURE

#### 2.2.3.1 Tissue culture conditions and medium

All tissue culture work and media preparation was carried out in either a laminar flow hood or a Class II Biological Safety Cabinet. Standard  $\alpha$ MEM was used for bone marrow macrophage and calvarial osteoblast cultures. RAW 264.7 cells were cultured in DMEM. Hi-DMEM was used for culturing HEK293T cells. Osteogenic media was used with osteoblast cultures. Table 2-4 summarises the components of each medium. All cultures were kept in incubators with standard conditions of 5% CO<sub>2</sub> and 37°C in a humidified atmosphere. A water bath was used to warm all the solutions to 37°C prior to use. Plasticware and instruments used inside the hood were either bought pre-sterilized or autoclaved before use. Cells were counted using a hemocytometer device. A phase-contrast microscope was used to assess the cultures' situation.

Table 2-4: Media preparation for cell culture work

Media Type	Description
<b>Standard <math>\alpha</math>MEM</b>	Minimum Essential Medium (MEM) supplemented with 10% foetal calf serum (FCS), 2 mM L-glutamine, 100 U/ml penicillin and 100 $\mu$ g/ml streptomycin.
<b>DMEM</b>	Dulbecco's Modified Eagle's Medium (DMEM) supplemented with 10% foetal calf serum (FCS), 2 mM L-glutamine, 100 U/ml penicillin and 100 $\mu$ g/ml streptomycin.
<b>Hi-DMEM</b>	Dulbecco's Modified Eagle's Medium with high glucose and pyruvate supplemented with 10% foetal calf serum (FCS), 2 mM L-glutamine, 100 U/ml penicillin and 100 $\mu$ g/ml streptomycin.
<b>Osteogenic media</b>	Minimum Essential Medium (MEM) supplemented with 10% foetal calf serum (FCS), 2 mM L-glutamine, 100 U/ml penicillin, 100 $\mu$ g/ml streptomycin, 50 $\mu$ g/ml Vitamin C and 3 mM betaglycerophosphate ( $\beta$ GP).

#### 2.2.3.2 Viability assay

This assay was used to quantitatively measure the cells' viability using the Alamar Blue reagent. The assay is based on the oxidation/reduction (redox) power of the cell. Alamar Blue is a non-toxic, cell permeable, non-fluorescent blue compound. When entering cells, resazurin (the active ingredient of Alamar Blue) is reduced to the

highly fluorescent red compound resorufin; thus, the amount of this redox indicator is directly proportional to the number of viable cells. Briefly, Alamar Blue was added as 10% of the sample volume for each well and left for 2 hours at 37°C. The resulting fluorescence was then measured using the plate reader (BIO-Tek Synergy HT) with the following settings: an excitation wavelength of 540 nm and an emission wavelength of 590 nm. Control wells were used to correct the data for background fluorescence by adding 10% of the Alamar Blue to wells containing only the media.

### **2.2.3.3 Rodent Osteoclast Culture**

#### ***2.2.3.3.1 Bone Marrow Macrophage Culture***

Wild-type CD1 mice or C57 black 6 (BL6) mice between 2-5 months of age were culled by cervical dislocation according to Schedule 1 of the Animal (Scientific Procedures) Act. The cadavers were sprayed with 70% ethanol and then skinned. The lower limbs (tibia and femur) were carefully extracted without affecting the bones. The bones were placed in sterile phosphate-buffered saline (PBS) to be processed in a laminar flow hood with sterilised equipment. The limbs were placed in a Petri dish and cut off at the knee joint using a scalpel to separate the tibia from the femur. The bones were cleaned by removing the soft tissue and then cutting the bones' epiphyses. The bone marrow was flushed out in a sterile plastic Petri dish with serum-free  $\alpha$ MEM by using a syringe with a 25-gauge needle. The flushed bone marrow was homogenised with a 21-gauge needle. The homogenised marrow was then transferred to a centrifuge tube to pellet the cells by spinning at 300g for 3 minutes at room temperature. Following centrifugation, the supernatant was discarded and cells' pellets were resuspended in standard  $\alpha$ MEM containing 100 ng/ml of M-CSF and then plated in a 10 cm tissue culture Petri dish and incubated under standard conditions for 48 hours. The adherent cells at this stage were macrophages (Figure 2-2). To scrape off these cells, a culture medium was removed, followed by the addition of a 5 ml cell dissociation buffer for 5 minutes at 37°C. The cells were scraped off using a rubber scraper and topped with 5 ml of complete media. Cell suspension was then centrifuged



at 300g for 3 minutes and the pellet was resuspended with 1 ml of full media to be counted and plated according to the downstream experiment.

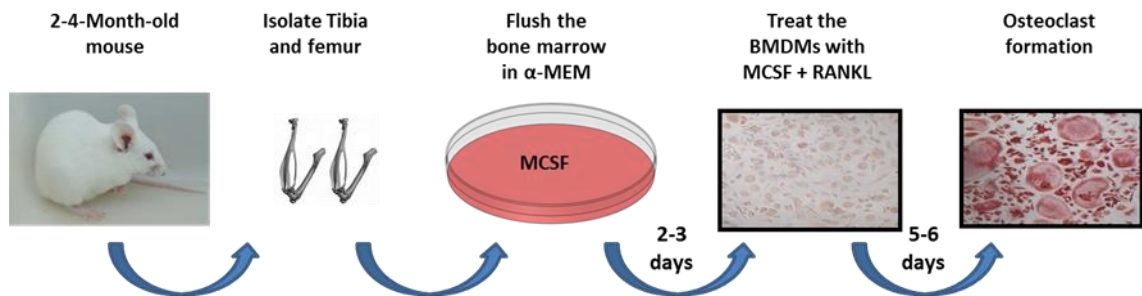


Figure 2-2: Schematic illustration of osteoclast culture assay.

#### 2.2.3.3.2 *RANKL Signalling Assay*

Bone marrow macrophages (generated as described in Section 2.2.3.3.1) were seeded in multiple 12-well plates at  $3 \times 10^5$  cells/well and incubated under standard conditions for 24 hours. The culture medium was then removed, and the cells serum-starved for 1 hour, followed by a stimulation of the cells with 100 ng/ml RANKL, with the exception of one plate that remained without RANKL stimulation to measure the cells' basal activity. The cells were lysed at different time points post-RANKL stimulation, including the plate without RANKL stimulation (0, 10, 15 and 60 minutes). Cell lysates were stored at  $-20^\circ\text{C}$  for further investigations.

#### 2.2.3.3.3 *Osteoclast Formation Assay*

Bone marrow macrophages (generated as mentioned in 2.2.3.3.1) were counted and then plated in 96-well plates at  $1.2 \times 10^4$  cells/well in standard  $\alpha$ MEM supplemented with 25 ng/ml of M-CSF and different RANKL concentrations (25, 50 and 100 ng/ml) for 5 days until osteoclasts were formed. The cultured medium was replaced every two days until multinucleated osteoclasts were formed.

#### 2.2.3.3.4 *Osteoclast Survival Assay*

Osteoclasts were formed in multiple 96-well plates as described above. RANKL was then removed from the osteoclast culture media but the M-CSF 25 ng/ml was retained, and the plates were fixed and stained with TRAcP at different time points post-RANKL withdrawal (0, 12h, 24h, 48h and 72h).

#### 2.2.3.3.5 *Osteoclast Staining Using Tartrate-Resistant Acid Phosphatase (TRAcP)*

The principle of TRAcP staining is based on the fact that the TRAcP enzyme was found to be highly expressed in osteoclasts. Accordingly, staining this enzyme makes the visualisation of osteoclasts an easy task. After osteoclasts were formed, culture media were removed and the cells rinsed with warm PBS. The cells were then fixed with 150  $\mu$ l/well of 4% (v/v) formaldehyde in PBS for 15 minutes at room temperature, followed by 2 further rinsings with PBS. At this stage, the cells were stored in 70% ethanol for future staining with TRAcP. Cells post-PBS rinsing were stained with a TRAcP solution (See Appendix 2.1) and kept at 37°C for 30 to 45 minutes (osteoclasts were checked frequently for red colour every 20 minutes to prevent overstaining). The cells were rinsed twice with PBS and then stored in 70% ethanol at 4°C. TRAcP-positive multinucleated osteoclasts (> 3 nuclei) were counted using a Zeiss Axiovert light microscope with a 10x objective lens (See Figure 2-3).

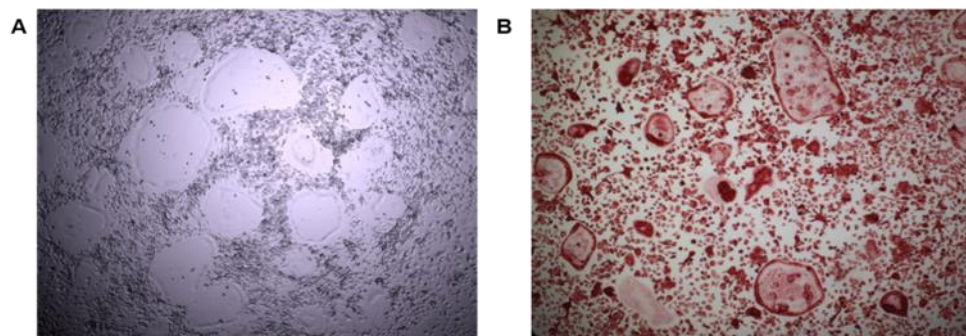


Figure 2-3: Phase-contrast microscopy of osteoclast formation at Day 5 post-RANKL treatment. (A) The osteoclasts' appearance before TRAcP staining. (B) The osteoclasts after TRAcP staining.

### 2.2.3.3.6 *OPTN Knockdown Experiment in Bone Marrow Macrophages Using Lentiviral Particles*

Gene knockdown can be identified as an experimental technique using RNAi to repress a targeted gene with high specificity and selectivity. Figure 2-4 briefly describes the knockdown steps.

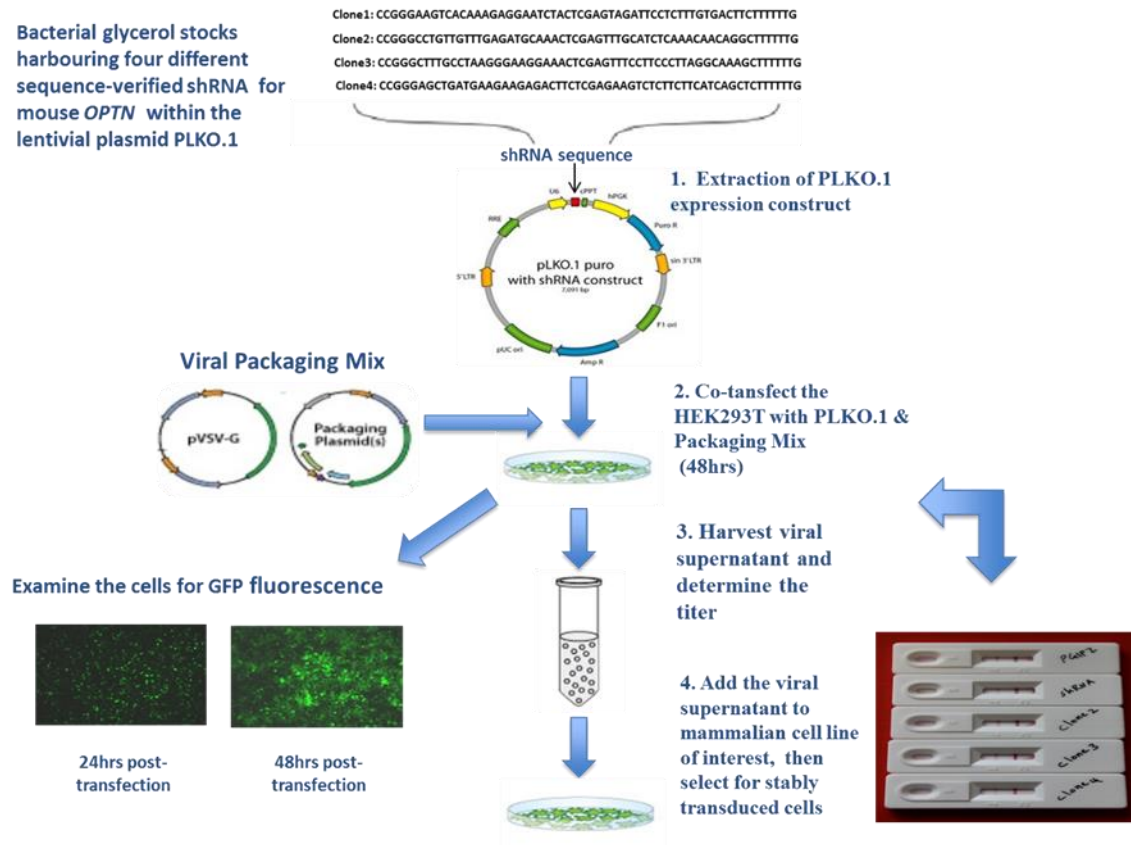


Figure 2-4: Schematic illustration summarises the steps that have been followed to knockdown the expression of *Optn*.

The knockdown experiment can be divided into 3 steps:

#### *Step 1: shRNA Plasmid Preparation and Isolation*

Four different shRNA clones (see Table 2-5) targeting the *Optn* gene were ordered from Sigma Aldrich. Each clone was constructed within the plasmid vector TRC1-pLKO.1-puro and provided in a frozen bacterial glycerol stock containing Terrific Broth, carbenicillin at 100 µg/ml, and 15% glycerol. A non-targeting shRNA vector was also ordered as a negative control. This non-targeting shRNA vector is a useful

negative control that activates the RISC and the RNAi pathways, but does not target any human or mouse genes and used for comparison to the *Optn*-targeting vectors. A positive control, pGIPZ, was used to microscopically examine the transfection efficiency through the green fluorescent protein (GFP) expression. Tubes that contain frozen bacterial glycerol stock were gently spun down and 10  $\mu$ l from each tube was placed into a separate sterile tube containing 100  $\mu$ l of Terrific Broth without antibiotics, kept at 37°C, and shaken for 15-30 minutes. A freshly prepared plate containing LB agar and 100  $\mu$ g/ml of carbenicillin was streaked with a sterile loop using 10-20  $\mu$ l from the culture and then incubated overnight for 16-19 hours. Five isolated colonies from each clone were sub-cultured in 2X LB broth with low salt (see Appendix 2.3) containing 100  $\mu$ g/ml of carbenicillin overnight for 16-19 hours. A plasmid extraction midiprep kit (Invitrogen, HiPure Plasmid Midiprep Kit) was used to purify the plasmid DNA following the manufacturer's instructions.

The concentration of plasmid DNA was subsequently measured using a Nanodrop 1000 spectrophotometer (ThermoScientific) followed by a restriction digest (Table 2-6) in order to verify the pLKO.1 vector orientation, as viral vectors have a tendency to recombine. A restriction enzyme map was generated for each plasmid based on the verified sequence using the NEB cutter software (Figure 2-5). Additionally, the plasmid DNA was sequenced in order to confirm the plasmids' orientation using the primers listed in Table 2-7. For the plasmids to be sequenced, a primer concentration of 20  $\mu$ M was used, with a DNA concentration of 100-1000 ng/ $\mu$ l.

Table 2-5: Sequence-verified shRNA lentiviral plasmid vectors for mouse *Optn* cloned into the pLKO.1-puro vector

TRC Number	Clone ID	Clone number	Sequence
TRCN0000182388	NM_181848.3-766s1c1	Clone 1	CCGGGCTTTGCCTAAGGGAAGGAACTCGAGTTTCCTTCCCTTAGGCAAAGCTTTTTTG
TRCN0000177380	NM_181848.3-1851s1c1	Clone 2	CCGGGAAGTCACAAAGAGGAATCTACTCGAGTAGATTCTCTTTGTGACTTCTTTTTTG
TRCN0000178154	NM_181848.3-291s1c1	Clone 3	CCGGGCCTGTTGTTTGAGATGCAAACTCGAGTTTGCATCTCAAACAACAGGCTTTTTTG
TRCN0000178374	NM_181848.3-1022s1c1	Clone 4	CCGGGAGCTGATGAAGAAGAGACTTCTCGAGAAGTCTCTTCTTCATCAGCTCTTTTTTG

Table 2-6: Restriction digest conditions

Reaction	<i>OPTN</i> -targeting Clones (μl)	non-targeting shRNA (-ve control) (μl)	pGIPZ (+ve control) (μl)
H <sub>2</sub> O	12.55	13.8	13.3
Buffer (10x)	2 (Neb 2)	2 (Neb4)	2 (Neb3)
BSA (100x)	0.2	0.2	0.2
DNA (40-100 ng/μl)	3	3	1.5
ENZ1 (20000 U/ml)	1 (XhoI)	1 (SacII)	3 (SalI)
ENZ2 (10000 U/ml)	1.25 (KpnI)		
Reaction volume	20	20	20
Incubation	37°C for 8h, 65°C for 20min		
Product size (kb)	5.6, 1.4	6.2, 0.75	2.2, 4.3, 5.1

Table 2-7: Primers used to verify the plasmid vector orientation

Primer name	Sequence (5' – 3')
U6-F	acgatacaaggctgttagagagata
PGK-R	aaaccagggtgccttggaag
5'LTR-F	tgtggaattgtgagcggata
3'LTR-R	cgggatagctagagccagac

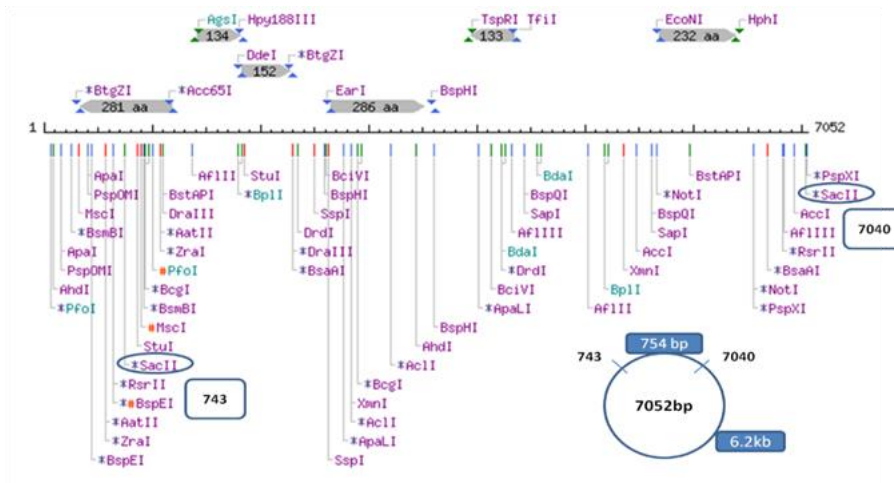


Figure 2-5: Schematic illustration of NEB cutter software used to determine the restriction enzyme (SacII) and the expected product size for the non-targeting shRNA.

*Step 2: Producing Lentiviral Particles in HEK293T Cells*

**HEK293T preparation**

The HEK293T packaging cell line was ordered from ThermoScientific. Once the cell line was removed from liquid nitrogen, it was placed in a water bath at 37°C for 2 minutes. Subsequently, the cells were slowly transferred to conical tube containing pre-warmed HEK293T culture media (Hi-DMEM), and then centrifuged at room temperature for 3 minutes at 300g. The supernatant was then discarded and the cells suspended in 12 ml of Hi-DMEM before being transferred to a T25 flask and incubated under standard conditions for 2 days. When the cells were ready (80% confluent) for passage the culture media were removed and the cells were rinsed with pre-warmed PBS. Subsequently, the cells were trypsinised with 2 ml of trypsin for the T25 flask or 4 ml for the T75 flask and kept at 37°C for 2-3 minutes. The flasks were gently tapped and the cells suspended with the appropriate amount of pre-warmed media to deactivate the trypsin. The cells were passaged at a ratio of 1:20 for general maintenance.

**Transfection**

The day before transfection, the HEK293T cells were trypsinised and counted using the hemocytometer before being placed in a 10 cm Petri dish at a seeding density of  $5.5 \times 10^6$  cells with 14 ml of Hi-DMEM and kept overnight under standard conditions.

On the day of transfection, the  $\text{CaCl}_2$  and 2X HBSS were thawed briefly at 37°C using a water bath and all the transfection steps were carried out in a Class II Biological Safety Cabinet. The tubes used were sterile polystyrene tubes. Table 2-8 describes the steps that were followed according to manufacturer protocols to generate the lentiviral particles.

Table 2-8: Suggested amount of DNA, medium and transfection reagent for virus production

<b>lentiviral vector DNA</b>	<b>Packaging mix</b>	<b>Total volume (with sterile water)</b>
<b>42 µg</b>	<b>30 µl</b>	<b>945 µl</b>
<b>Add 105 µl of CaCl<sub>2</sub></b>		
<b>Vortex the tube carefully without spillover and while vortexing, add drop-wise 1050 µl of 2X HBSS.</b>		
<b>Add the transfection mix to the cells without removing the culture media and incubate for 16 hours under standard conditions.</b>		
<b>Check the positive control pGIPZ vector for green cells under a fluorescent microscope.</b>		
<b>Replace the media with a serum-reduced medium and incubate for 48 hours under standard conditions.</b>		
<b>Harvest the medium and concentrate the lentiviral particles as described in the next section.</b>		

### **Lentiviral particles' harvesting and concentration**

A Lenti-X Concentrator kit from ClonTech was used to concentrate the lentiviral particles and all the steps were carried out on ice. The lentivirus-containing supernatant from the transfection step was harvested on ice and then centrifuged at 4°C for 10 minutes at 500g. The clarified supernatant was then transferred to a 50 ml tube containing Lenti-X Concentrator at a ratio of 1 volume to 3 volumes of supernatant. The mixture was incubated at 4°C for 2-4 hours followed by centrifugation at 4°C for 45 minutes at 1500g. The supernatant was removed carefully and the pellet resuspended with 1200 µl of complete DMEM followed by aliquoting into smaller volumes and stored at -70°C.

### **Lentiviral detection**

The presence of lentiviral particles was confirmed using Lenti-X GoStix strips from ClonTech. The occurrence of the test band (T) and control band (C) indicates the presence of the viral particles, and the intensity indicates the higher concentration of lentivirus (see Figures 2-4, 4-6, 4-8).

### **Puromycin kill curve**

The shRNA plasmid vector (PLKO.1) has been engineered to harbour a puromycin-resistant gene for selecting the transduced or transfected cells, and to generate a fully transduced population of cells as well. This can be achieved by

generating a killing curve to determine the minimum amount of puromycin required to eliminate untransduced cells in 48-72 hours. The target cells for transduction (RAW 264.7 or bone marrow-derived macrophages) were plated at  $5 \times 10^4$  in multiple 24-well plates with their corresponding culture media the day before starting the puromycin treatment and kept under standard conditions. The following day, the media were replaced with media containing a range of antibiotic concentrations, from 0-5  $\mu\text{g/ml}$ . The cell viability was measured every 24 hours using the Alamar Blue method (see Section 4.3.3.2). The minimum puromycin concentration used was 5  $\mu\text{g/ml}$ , wherein 100% of the cells were killed in 48 hours.

### **Viral titering**

This procedure was done to determine the lentiviral titer needed to transduce the macrophage cells. The cells were seeded the day before transduction in 24-well plates and kept overnight under standard conditions. The following day, viral stock was diluted to 5-fold dilution in 96-well plates. The media from the 24-well plates was then removed and replaced with 225  $\mu\text{l}$  of serum-free media. The cells were transduced by adding 25  $\mu\text{l}$  of undiluted pGIPZ (+ve control) stock as well as the other dilutions per well. Polybrene (hexadimethrine bromide) was also added to enhance the efficiency of transduction. Two concentrations of polybrene, 5 and 8  $\mu\text{g/ml}$ , were examined with the viral titering. The best transduction efficiency obtained from using the undiluted viral stock was with 5  $\mu\text{g/ml}$  of polybrene. After 48 hours, multi-cell colonies were counted as 1 transduced cell (see Figure 2-6) and the Transducing Units per ml (TU/ml) were determined using the following formula:

<b>Number of TurboGFP positive colonies counted x dilution factor x 40 = (TU/ml)</b>
--

### *Step 3: Transduction*

Two cell types were transduced: the osteoclast-like RAW 264.7 cells and the mouse bone marrow macrophages. After the RAW 264.7 cells were passaged, they were left until they reached 70% confluence. Bone marrow cells from wild-type CD1 mice were isolated and cultured for 48 hours in the presence of M-CSF (100 ng/ml).



Both cells – the RAW 264.7 cells and the adherent bone marrow-derived macrophages (BMDMs) – were then treated for 2 days with lentiviral particles that expressed shRNA targeting the *Optn* gene. Non-targeting shRNA lentiviral particles were also used as a negative control. Cells were subjected to 48-hour selection using puromycin (5 µg/ml) in order to reduce background expression of *Optn* from untransfected cells. After the 2-day selection period, the transduced cells were used for downstream experiments. Western Blot (WB) was used to confirm the knockdown of *Optn* in these cells (see sections 4.3.4 and 4.3.5).

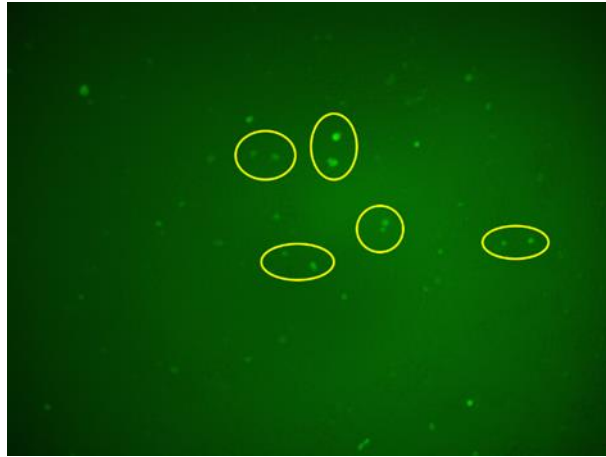


Figure 2-6: Examples of individual colonies of macrophages after 48-hour post-transduction with undiluted pGIPZ viral stock and 5 µg/ml of polybrene.

### **Lentiviral NFκB luciferase reporter assay**

The lentiviral NFκB luciferase reporter is engineered to express firefly luciferase genes according to changes in the activity of the NFκB signalling pathway. A Signal Lenti Luciferase Reporter kit was ordered from SABiosciences and used to assess the NFκB activity for 2 different experiments, as discussed below. The Multiplicity of Infection (MOI) used in this experiment was measured using the following formula:

$$\text{Total mL of lentiviral particles to add to T25 flask} = \frac{\text{Total number of cells} \times \text{Desired MOI}}{\text{TU/mL reported on kit}}$$

$$= \frac{(1 \times 10^6) \times 3}{2.1 \times 10^7} \cong 150 \mu\text{l/flask}$$

2.2.3.3.7 *NFκB Luciferase Reporter Assay Post-Optn Knockdown*

BMDMs were transfected with the lentiviral particles expressing shRNA targeted against the *Optn* gene for 2 days, followed by a 48-hour selection using puromycin (5 µg/ml). One million of the transduced cells were then plated in a T25 flask and transduced with a lentiviral NFκB luciferase reporter with a MOI of 3 (150 µl) in 3 ml of serum-free αMEM media for 5 hours. An additional 3 ml of standard αMEM was added to the cells and left under standard conditions for 2 days. The cells were then plated in 96 wells for 24 hours, after which the luciferase activity was measured with a SteadyGlo-Luciferase Reporter Assay System at the basal level. This procedure was followed by RANKL stimulation (100 ng/ml) and the luciferase activity was measured with a SteadyGlo-Luciferase Reporter Assay at indicated time points (24, 72 hours, and on the 5th day) using a Bio-Tek Synergy HT plate reader.

2.2.3.3.8 *NFκB Luciferase Reporter Assay for *Optn*<sup>D477N/D477N</sup> Knock-in Mice Compared to WT*

BMDMs were generated as described in Section 2.2.3.3.1. BMDMs from WT and *Optn*<sup>D477N/D477N</sup> mice were scraped and 1 X 10<sup>6</sup> cells were plated and cultured in a T25 flask for 24 hours. These cells were transduced with a lentiviral NFκB luciferase reporter with a MOI of 3 (150 µl) in 3 ml of serum-free αMEM media for 5 hours. An additional 3 ml of standard αMEM was added to the cells and left under standard conditions for 2 days followed by selection for 48 hours using puromycin (5 µg/ml). The cells were then plated in 96 wells for 24 hours, and luciferase activity was measured with a SteadyGlo-Luciferase Reporter Assay System at the basal level. This procedure was followed by RANKL stimulation (100 ng/ml) at 24 and 72 hours, and on Days 4, 5, and 7 using a Bio-Tek Synergy HT plate reader.

#### **2.2.3.4 Rodent Osteoblast Culture**

##### **2.2.3.4.1 Calvarial Osteoblast Culture**

Primary osteoblasts were isolated from the calvaria of 2-3-day-old mice. The calvaria were washed thoroughly in HBSS and then transferred to a 50 ml tube containing 3 ml of Type 1 collagenase (1 mg/ml) in HBSS, where they were incubated for 10 minutes at 37°C in a shaking water bath. The supernatant was discarded and the calvarial tissue was resuspended with 3-4 ml of Type 1 collagenase in HBSS for 30 minutes at 37°C in a shaking water bath. The cell suspension (fraction 1) was collected and transferred to another 50 ml tube (Tube A) containing 6 ml of full  $\alpha$ -MEM media. The remaining calvaria were washed with 2 ml of PBS and the supernatant was collected with the cell suspension in Tube A. Four ml of pre-heated EDTA in PBS (1:100) was added to the remaining calvarial tissue and left for 10 minutes at 37°C in a shaking water bath. The cell suspension (fraction 2) was collected with previous fraction in Tube A, followed by adding additional 6 ml of standard  $\alpha$ -MEM to the same tube. The remaining calvaria were also washed with 2 ml of PBS and the supernatant was grouped with the same tube containing the cell suspension (Tube A). This step is followed by the incubation of the remaining calvaria with 4 ml of Type 1 collagenase in HBSS for 30 minutes at 37°C in a shaking water bath. The cell suspension (fraction 3) and extra 6 ml of standard  $\alpha$ -MEM were added to the same tube containing the cell suspension (Tube A). The 50 ml tube containing the cell suspension from the previous 3 steps was then centrifuged at 300g at room temperature. The supernatant was discarded and the pellets were suspended in 12 ml of standard  $\alpha$ -MEM and then cultured in a T75 flask under standard conditions. The media was changed after a 24-hour incubation period in order to remove non-adherent cells, and the osteoblasts were left for 48 hours until they became confluent.

##### **2.2.3.4.2 Mineralisation Assay**

The cultured media were removed and the osteoblast cells washed with pre-heated (37°C) sterile PBS. The osteoblast cells were then incubated with 4 ml of trypsin for 3 minutes in order to detach the cells, after which 6 ml of standard  $\alpha$ -MEM was added to deactivate the trypsin. The cells were then centrifuged at 300g and the pellet

resuspended with 1 ml of standard  $\alpha$ -MEM to be counted using a hemocytometer. The cells were plated in 12-well plates at  $1 \times 10^5$  cells/well with standard  $\alpha$ -MEM and incubated for 48 hours under standard conditions. The media were replaced and refreshed every 2 days with standard  $\alpha$ -MEM supplemented with 50  $\mu$ g/ml of Vitamin C and 3 mM of betaglycerophosphate ( $\beta$ GP) (osteogenic media, see Table 2-4) and kept under these conditions for 21 days. Protein was extracted in order to check the Optn expression at different time points (0, 5, 9, and 21 days) post-Vitamin C supplementation (see Figure 2-7).

Mineralisation nodules that formed after 21 days were stained for calcium deposits with Alizarin Red. Alizarin Red was prepared by dissolving it in  $\text{DH}_2\text{O}$  to a final concentration of 40 mM with a pH adjusted to 4.1-4.3 using 10% (v/v) ammonium hydroxide. The Alizarin Red solution was mixed and filtered with a 0.45 $\mu$ m filter. Cells' layer was carefully washed with pre-warmed PBS, followed by fixation in 70% pre-chilled ethanol; it was then either kept on ice for 1 hour or stored at 4°C. The cells were rinsed multiple times with  $\text{dH}_2\text{O}$  to remove traces of ethanol and stained with the Alizarin Red solution for 20 minutes on a rocking table. The stained cells were then washed 4 times (5 minutes for each wash on a rocking table) and the plate was then left to air-dry overnight. The stained plate was photographed using a standard scanner (Epson Perfection 4990 photo/slide scanner). A destaining procedure was subsequently performed to quantify the mineralised nodules using 10% (w/v) cetylpyridinium chloride in 10 mmol/l of sodium phosphate (pH 7.0). One ml/well of destaining solution was incubated on a rocking table overnight at room temperature. Absorbance of the extracted Alizarin Red stain was measured at 562 nm using a Bio-Tek Synergy HT plate reader and compared to the Alizarin Red standard curve (0, 0.05, 0.1, 0.25, 0.5, 1.0, 1.5, 2.5, 5, 7.5, and 10 mM).

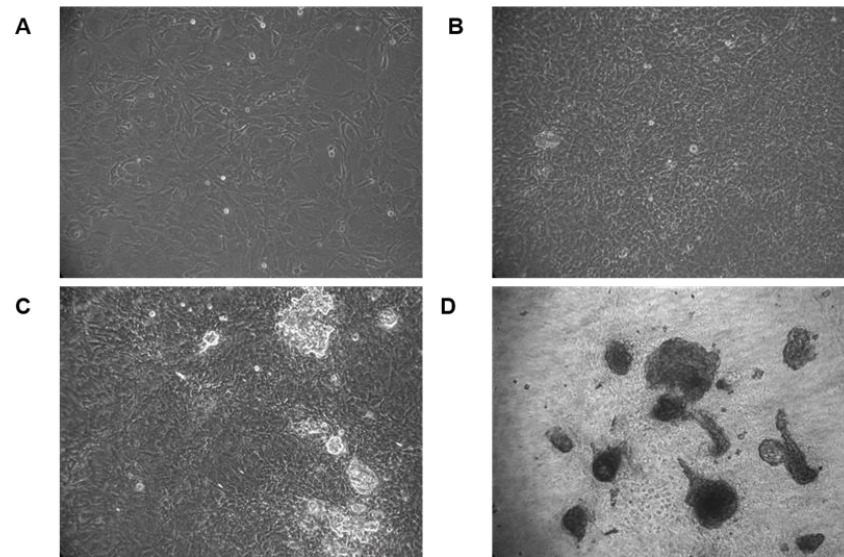


Figure 2-7: Phase-contrast microscopy of primary osteoblast cultures. Representative image of an unstained cell before adding Vitamin C (**A**); by Day 5, post-Vitamin C cells became more confluent (**B**); By Day 9, cells became more compacted and an organic matrix began to be deposited (**C**); after 21 days of culture, there was widespread formation of bone nodules (**D**).

#### 2.2.4 Animal Work

All animal protocols were approved by the Ethics Committee at the University of Edinburgh and were conducted in accordance with UK Home Office regulations (Personal Licence Number 60/13163; Project Licence Number 60/3981).

##### 2.2.4.1 Animals

*Optn* knock-in mice (*Optn*<sup>D477N/D477N</sup>) were obtained from Professor Philip Cohen at the University of Dundee. Briefly, these mice (C57/BL6 background) were generated by introducing a loss-of-function point mutation corresponding to an Asp-477 to Asn in exon 12 of the *Optn* gene. This polyubiquitin-binding defective mutation corresponds to the D474N mutation in humans. Wild-type (WT) C57/B16 mice were used as a control (Gleason et al., 2011).

##### 2.2.4.2 Mice genotyping for *Optn*

Genomic DNA was extracted from mouse ear snips by following the Qiagen DNeasy Blood and Tissue Kit manufacturer's manual (Spin-column protocol). The extracted DNA was used for genotyping the mice by PCR. The PCR was carried out

using the primers listed below and the Qiagen *Taq* DNA polymerase. The following Tables (2-9 and 2-10) summarise the PCR reaction and thermocycler conditions that were used. Afterward, gel electrophoresis (2.5%) was used to view the PCR products. The samples, alongside the low molecular weight and/or 100 bp ladder, were run for approximately 90-100 minutes at 75V. The *Optn* genotype of mice was determined according to the yielded band size and the number of bands per lane in the gel picture (see Figure 2-8):

***OPTN* Forward primer:** 5'-GATCCGGAGGAGAGCAATGCATG-3'

***OPTN* Reverse primer:** 5'-CTGTAATCTTAGTGTTCACAGGCAG-3'

Table 2-9: PCR conditions used for *OPTN* genotype

PCR Reaction		Thermocycler conditions		
Reagents	Volume (µl)	Step	Temp (°C)	Duration
dH <sub>2</sub> O	8.375	1. Denature Template	94	4min
Buffer (10x)	2.5	2. Denature Template	94	30sec
dNTPs (10 mM)	2	3. Anneal primers	60	1min
Q solution (5x)	5	4. Extend primers	72	1min
Forward primer (20 µM)	1	5. Repeat steps 2 to 4		35 cycles
Reverse primer (20 µM)	1	6. Extend primers	72	10min
Qiagen <i>Taq</i> U/µl	0.125	7. Hold	4	Forever
DNA 10 ng/µl	5			
Total Vol	25			

Table 2-10: *Optn* genotype

Band size /Lane	<i>OPTN</i> genotype
350 bp	WT
450bp	Knock-in (KI)
350 bp and 450 bp	WT/KI Heterozygous

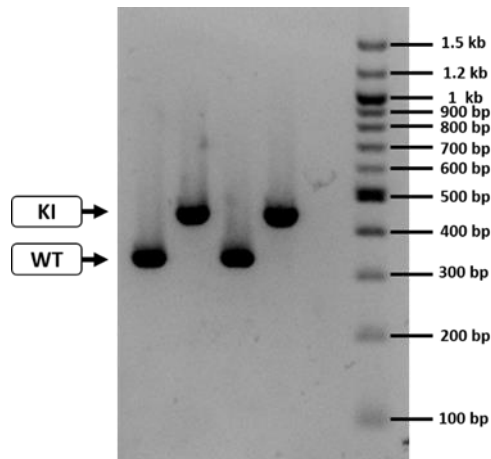


Figure 2-8: Photograph of a 2.5% agarose gel showing PCR products of *Optn*<sup>D477N</sup> genotype

#### 2.2.4.3 CTX and PINP serum assay

CTX (a marker of bone resorption) was measured in serum samples using an enzyme-linked immunosorbent assay. The principle behind this assay is that Type 1 collagen (the major organic matrix of bone) is synthesised in bone and released in circulation during the resorption process. The CTX assay quantitatively determines the C-terminal telopeptides of Type 1 collagen, which in turn reflects the level of osteoclast activity. The assay was carried out according to manufacturer protocols.

PINP (a marker for bone formation) was measured in serum samples using a competitive enzyme immunoassay. This assay is also based on Type 1 collagen, but measures the N-terminal peptide of Type I procollagen released in circulation during collagen synthesis. The assay was carried out according to manufacturer protocols.

The serum used for these assays was collected from the blood of mice. The mice were culled by CO<sub>2</sub> asphyxiation and their blood was collected in Eppendorf tubes from the posterior vena cava. Blood samples were first left to clot, then the sera were separated by a bench top centrifuge for 10 minutes. The serum was collected and stored at -20°C.

#### 2.2.4.4 Micro-computed tomography ( $\mu$ CT)

##### 2.2.4.4.1 *In Vivo* $\mu$ CT

A SkyScan  $\mu$ CT 1076 was used to scan the mice *in vivo*. WT and *Optn*<sup>D477N/D477N</sup> mice were scanned at different stages of their lives (at 4, 8 and 12 months old). On the day of scanning, the O<sub>2</sub> and isofluorane level was checked before proceeding to scan the mice. The mice were brought in with a filter lid on their cage. They were prepared for scanning using isofluorane-induced inhalation anaesthesia. They were then placed in the bed with their noses remaining in the cone and their legs fixed to a semi-circular polystyrene holder; their legs were then stretched out gently. A small polystyrene block was also placed on their abdomens to monitor their breathing, and the scanner door was closed. A scout scan was done to select the area to be scanned. The  $\mu$ CT was set at 50 KV and 201  $\mu$ A. The pixel size was set at 18  $\mu$ m and the scanning width at 35 mm. The filter used was 0.5 mm of aluminium with a 0.6 rotation step and an averaging number of 1. The animals were given an appropriate amount of recovery time before being returned to their cage. The NRecon software from SkyScan was used to reconstruct the 3D image stacks and the file was saved as a bmp. Reconstruction parameters were set as shown in Table 2-11.

##### 2.2.4.4.2 *Ex Vivo* $\mu$ CT

*Ex vivo* scanning was performed by using the SkyScan  $\mu$ CT 1172. The mice were euthanised by CO<sub>2</sub> inhalation according Schedule 1 of the Animal Act, and their blood was subsequently collected from the posterior vena cava. The blood was transferred to Eppendorf tubes, left to coagulate, and then centrifuged for 10 minutes in order to separate the serum. The serum was stored at -20°C for future experimentation. Mouse tissues, including the lower extremities, skull, liver, kidney and spleen, were collected and fixed in 4% formaldehyde in PBS for 24 hours. These tissues were then stored in 70% ethanol at 4°C.

The left tibiae were detached and collected in ethanol for scanning. To detach the tibiae from the lower extremities, most of the surrounding muscle tissue and fibulae were gently removed. The ligaments were cut using a scalpel, and the tibiae gently detached from the femora. Three tibiae were scanned per run in which bones were



wrapped using a parafilm, then placed in a 1 ml syringe with the proximal end facing up and the distal end facing down. The 1 ml syringe containing the tibiae was placed vertically inside the SkyScan 1172 (see Figure 2-9). The  $\mu$ CT was set at 60 KV and 167  $\mu$ A. A medium camera with a pixel size set at 4.9  $\mu$ m was used. The 0.5 mm aluminium filter was added with a rotation of the specimen of 180 degrees and a rotation step of 0.6 degree. An oversize scan was selected to scout scan the samples. The proximal metaphysis and diaphysis were selected for each tibia and then scanned. The NRecon software from SkyScan was used to reconstruct the 3D image stacks and the file was saved as a bmp. Reconstruction parameters were set as shown in Table 2-12.

Table 2-11: Reconstruction parameters for *in vivo*  $\mu$ CT scanning using NRecon software

Parameter	Description	Setting
<b>Smoothing</b>	Applied to the projections in order to smooth the images and reduce noise.	Width: 1 pixel
<b>Beam hardening factor</b>	Corrects the x-ray attenuation of the outside layer of a sample.	10%
<b>Ring artefact reduction</b>	Corrects for artefacts resulting from the rotation of the sample.	10

Table 2-12: Reconstruction parameters for *ex vivo*  $\mu$ CT scanning using NRecon software

Parameter	Description	Setting
<b>Smoothing</b>	Applied to the projections in order to smooth the images and reduce noise.	Width: 1 pixel
<b>Beam hardening factor</b>	Corrects the x-ray attenuation of the outside layer of a sample.	18%
<b>Ring artefact reduction</b>	Corrects for artefacts resulting from the rotation of the sample.	12

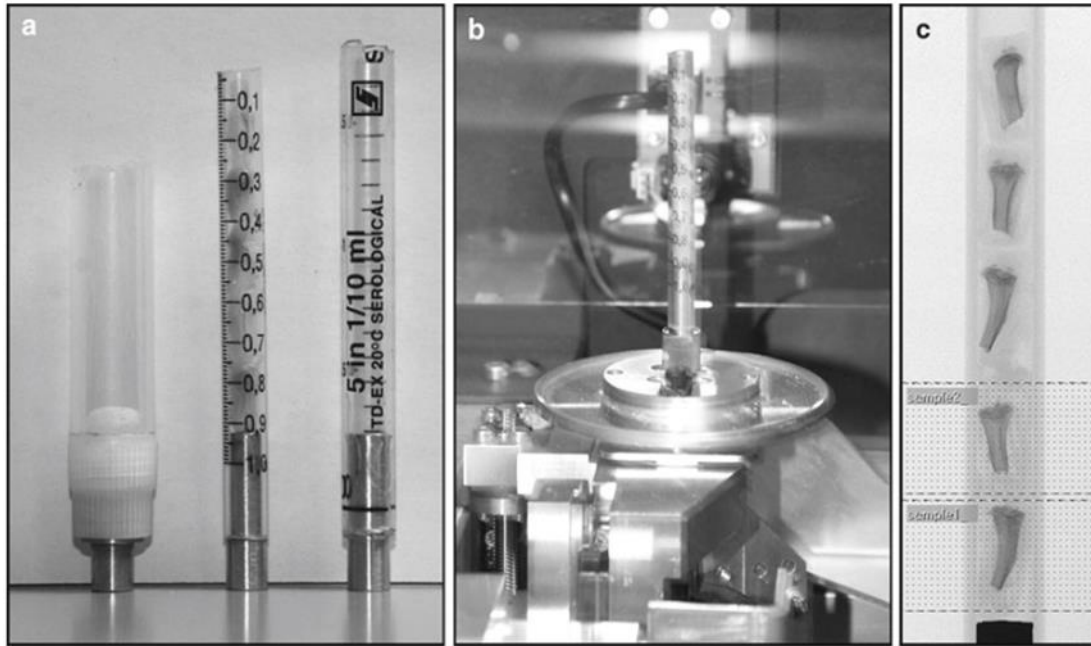


Figure 2-9: Sample holders and batch scan of multiple samples: **(a)** Shows different types of sample holders, **(b)** Shows the sample holder fitted to the sample stage, **(c)** Shows a scout view of the sample holder with multiple samples. This picture was obtained from (van 't Hof, 2011) .

#### 2.2.4.4.3 $\mu$ CT Analysis

After the images were reconstructed, the SkyScan Dataviewer software was used to rotate the image stack along all three major axes. This is an important factor that allowed for the fixing of the orientation of all scanned bones and their regions of interest (ROI) (van 't Hof, 2011). The landmark used in this study was the growth plate in the proximal tibia, and the reference point was where the mineralised cartilage breaks. For trabecular analysis, the ROI was 200 slices started at 20 slices proximal from the reference level. For cortical analysis, the ROI was 100 slices started at a distance of 600 slices from the reference level (see Figure 2-10). The trabecular and cortical analyses for these slices were then analysed using the SkyScan CTan software. This software separates the trabecular from the cortical bone by manually drawing a number of layers (usually from 6 to 10) distributed throughout the selected region. The software then interpolates to create a separation for the layers in-between. The parameters used for separating the soft tissues from the bone tissues, and those used for trabecular and cortical analysis, were determined as described in Tables 2-13 and

2.14. These parameters were applied to all the samples. The CTAn software generated an Excel spreadsheet that included all the analyses' results. The software also generated a 3D model picture for the trabecula and the cortex, which can be viewed by the SkyScan CTVol software (see Figure 2-10).

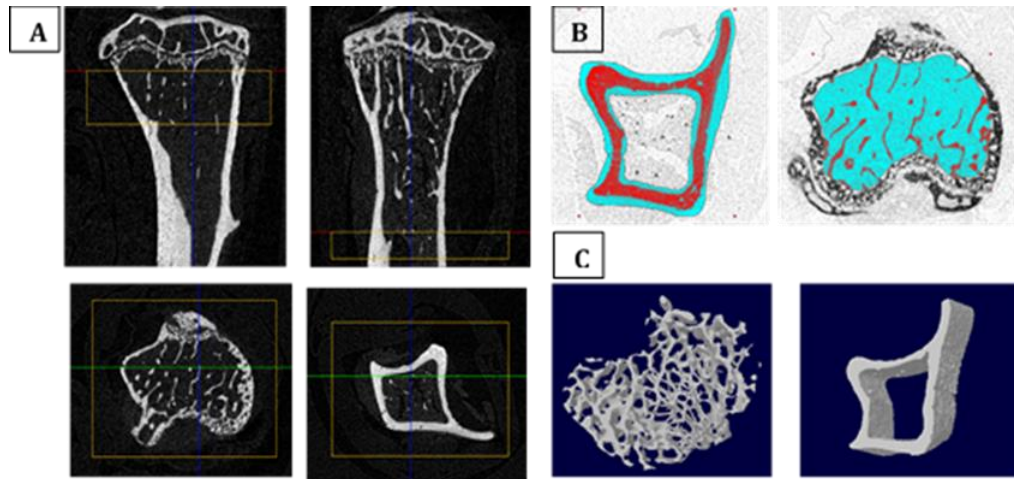


Figure 2-10: SkyScan  $\mu$ CT software used for selecting volumes for analysis: **(A)** Represented pictures from SkyScan Dataviewer, which were used to select the ROI (proximal tibial metaphysis [left] and proximal diaphysis [right]; **(B)** Manual selection of ROI using SkyScan CTAn software; **(C)** 3D model pictures of the trabecular bone (left) and cortical bone (right) viewed by SkyScan CTVol software.

Table 2-13: Trabecular analysing parameters used by CTAn software

Parameter	Description	Setting
<b>Filtering</b>	Smoothing, noise reduction, and unsharpening of images. The result is a grayscale image.	Type: Median (2D space) Radius: 1
<b>Thresholding</b>	Segments the foreground from the background to binary image.	Mode: Global Lower grey threshold: 100 Upper grey threshold: 255
<b>Despeckle</b>	Removes speckles from images.	Type: Remove white speckles (3D space) Volume: less than 150 voxels Apply to: Image
<b>3D-Analysis</b>	Calculates the 3D parameters of binary images.	Trabecular Thickness Trabecular Number Trabecular Separation
<b>3D-Mode</b>	Calculates the 3D surface from binary images.	Model creation algorithm: Adaptive rendering Apply to: Image inside ROI Smoothing = Off Locality = 1 Tolerance = 0.250000 File saved as: <i>p3g</i>

Table 2-14: Cortical analysing parameters by CTAn software

Parameter	Description	Setting
<b>Filtering</b>	Smoothing, noise reduction, and unsharpening of images. The result is a grayscale image.	Type: Median (2D space) Radius: 1
<b>Thresholding</b>	Segments the foreground from the background to binary image.	Mode: Global Lower grey threshold: 100 Upper grey threshold: 255
<b>Despeckle</b>	Removes speckles from images.	Type: Sweep (2D space) Remove: all except the largest object Apply to: Image
<b>Despeckle</b>	Removes speckles from images.	Type: Remove Black speckles (2D space) Volume: less than 80 voxels Apply to: Image
<b>Morphological operation</b>	Morphology-based operations.	Type: Opening (2D space) Kernel: Square Radius: 2 Apply to: Image
<b>Morphological operation</b>	Morphology-based operations.	Type: Closing (2D space) Kernel: Square Radius: 2 Apply to: Image
<b>Bitwise operation</b>	Operations based on binary arithmetic.	Region of Interest = <Region of Interest> AND <Image>
<b>Bitwise operation</b>	Operations based on binary arithmetic.	Region of Interest = COPY<Region of Interest>
<b>3D-Mode</b>	Calculates 3D surface from binary images	Model creation algorithm: Marching Cubes 33 Apply to: Image inside ROI File saved as: <i>p3g</i>
<b>Despeckle</b>	Removes speckles from images.	Type: Remove pores (2D space) Detected by: image borders Apply to: Image
<b>Bitwise operation</b>	Operations based on binary arithmetic.	Image = <Image> X OR <Region of Interest>
<b>3D-Analysis</b>	Calculates the 3D parameters of binary images.	Cortical Thickness

The parameters that were obtained from each scan of the tibiae are listed in Table 2-15.

Table 2-15: Parameters calculated by  $\mu$ CT

Parameter	Abbreviation (unit)
Trabecular Bone Volume	BV/TV (%)
Trabecular Thickness	Tb.Th (m)
Trabecular Separation	Tb.Sp (m)
Trabecular Number	Tb.N (1/mm)
Cortical Thickness	Ct.Th (mm)

#### 2.2.4.5 Bone histomorphometry

Left tibiae that were scanned were cut at the tibial crest using a Dremel rotary tool. The tibiae were fitted in embedding baskets and kept moist with 70% ethanol. The tibiae were then transferred to a Leica automatic tissue processor for 24 hours at room temperature. These tibiae were subjected to 8 stages, including dehydration with ethanol dilutions and defatting with xylene as shown in Table 2-16. Following this step, the tibiae were infiltrated using a freshly prepared methyl methacrylate (MMA) solution (Appendix 2.2) for two weeks at 4°C in airtight vacuum desiccators. The rest of the MMA solution was stored at 4°C for use after the infiltration step. The infiltrated samples were polymerised by transferring them into moulds and covering them with the stored MMA; each mould was then tightly covered with a lid smeared with a very thin layer of Vaseline (petroleum jelly) and placed in a water bath for 24-48 hours at 30°C. The resin blocks that were formed were then tightly covered with plastic embedding rings and mounted with a fresh and fast-hardening medium made by adding together two thirds dibenzoylperoxide and one third N,N-dimethyl-p-toluidine. The blocks were left overnight and then ripped from the moulds with a pair of mole grip pliers.

A low speed microtome using a steel knife was used to trim the blocks. The blocks were rinsed with 30% ethanol while they were being trimmed and sectioned. They were trimmed until the sagittal plane of each tibia was reached. To check that the sagittal plane had been reached, each section was stained with toluidine blue for quick evaluation under a light microscope. The blocks were cut into multiple 5  $\mu$ m-thick sections. These sections were then placed onto silane coated slides containing 96% ethanol, which is used to smooth and straighten the section on the slide. The sections

were then covered with Kisol-foil coverslips and the excess ethanol was removed using a paper tissue; the slides were then left to dry under pressure using a slide press for 2 days at 37°C. At this stage, the slides were ready for staining and were stored in a slide box at room temperature.

Table 2-16: Stages for the Leica tissue processor programme

Stage	Reagent	Time (hr)
1	70% Ethanol	01.00
2	80% Ethanol	02.00
3	96% Ethanol	02.00
4	100% Ethanol	03.00
5	100% Ethanol	03.00
6	Xylene	01.00
7	Xylene	12.00

#### 2.2.4.5.1 *Staining bone sections with TRAcP*

This method was used to identify osteoclasts in bone sections, which had been embedded in MMA and sectioned as described in Section 2.2.4.5. Before staining, the coverslips were carefully removed, followed by the resin as described in Figure 2-11. The slides were then immersed in a TRAcP stain (Appendix 2.2) and incubated for 2 hours at a humidified temperature of 37°C. Subsequently, the slides were washed with distilled H<sub>2</sub>O four times in different containers, and then incubated with Aniline Blue (as a counter stain) for 20 to 45 minutes at room temperature. After the slides had been washed in 3 containers of water, they were mounted with Apath's aqueous mounting medium and stored in the dark; within 2 weeks, they were analysed with custom software based on the Aphelion image analysis tool kit (Adcis, Herouville-Saint-Clair, France) in combination with Fiji-Image J, developed by Dr. Rob J. van't Hof (Institute of Ageing and Chronic Disease, University of Liverpool). This software identifies bone (blue colour) and osteoclasts (red colour) by colour thresholding in combination with object filtering tools. After parameters had been optimised, they were applied to

all of the samples. The software captured multiple pictures from the target area. The pictures were then stitched together using Microsoft Ice software (see Figure 2-12). The software then applied the chosen setting to the stitched picture.

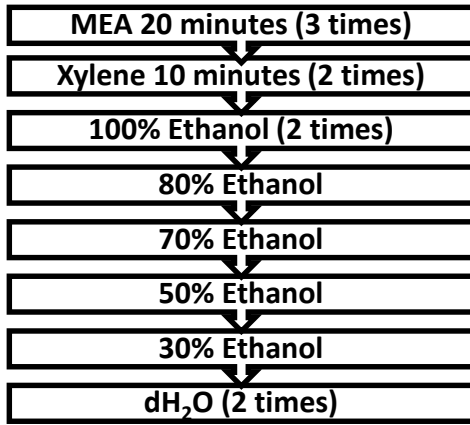


Figure 2-11: Stages for removing the resin from the bone sections

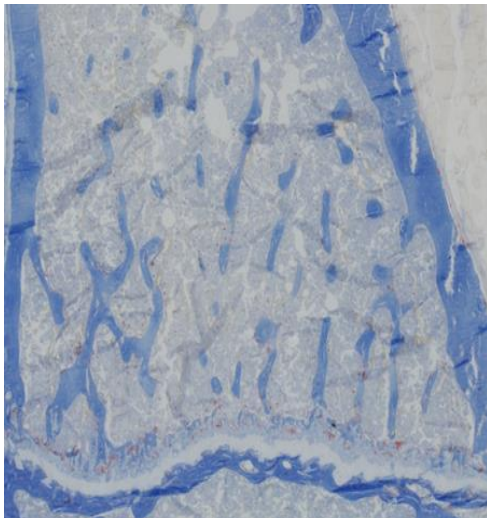


Figure 2-12: A stitched picture of a trabecular stained section at 10X magnification using a Zeiss Axio Imager microscope.

#### 2.2.4.5.2 Staining bone sections with VON KOSSA and Van Gieson Counterstain

To assess bone mineralisation and osteoid parameters in bone sections, a VON KOSSA/Van Gieson stain was used (Appendix 2.2). This stain provides a clear distinction between mineralised bone (black stain) and un-mineralised osteoid tissue (osteoid/collagen, red stain) as shown in Figure 2-14. The resin was removed carefully as described in Figure 2-13. Then, the sections were immersed in 1% silver nitrate for

3 minutes followed by 3 washes in different containers with distilled H<sub>2</sub>O. Thereafter, the sections were stained with freshly made hydroquinone for 1 minute followed by 3 washes with distilled H<sub>2</sub>O. The sections were then placed in Van Gieson's stain for 3 minutes and washed with water 3 more times. The sections were then cleaned in a series of ethanol concentrations: 50%, 70%, 80% and 100%. Once completed, the sections were dipped in xylene, mounted with DPEX, and covered with Kisol-foil coverslips. Custom software, based on a combination of the Aphelion image analysis tool kit (Adcis, Herouville-Saint-Clair, France), Fiji-Image J, and Microsoft Ice packages developed by Dr. Rob J. van't Hof was then used to analyse the histomorphometric osteoid parameters.

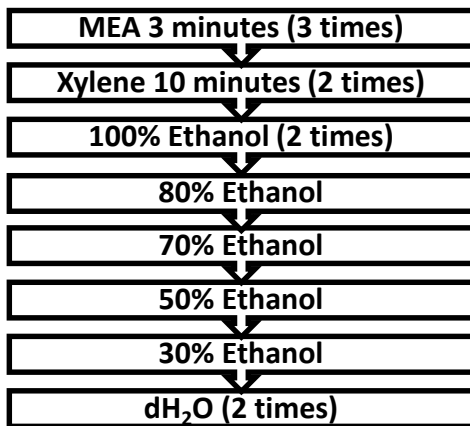


Figure 2-13: Stages for removing the resin from the bone sections.

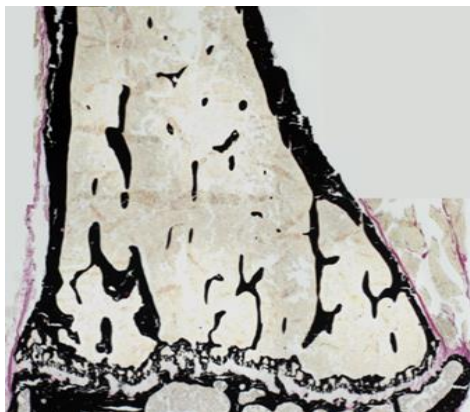


Figure 2-14: A stitched picture of a VON Kossa-Van Gieson stained section at 10X magnification using a Zeiss Axio Imager microscope.



#### 2.2.4.5.3 *Assessing dynamic bone histomorphometric parameters*

Mice received 2 injections of calcein (3 days apart) prior to culling to assess dynamic bone formation parameters. Bone sections were stained with this method in order to evaluate the rate of bone formation and mineralisation. The bone sections were immersed in Aniline Blue (0.1 g in 150 ml of DH<sub>2</sub>O) for 20 minutes after the resin was removed, as described in Figure 2-13. The sections were then washed in a series of ethanol concentrations (70%, 96% and 100%) and then immersed twice in xylene. The slides were subsequently mounted with DPEX after the excess xylene had been removed. The stained sections were then visualised on a Zeiss Axioimager fluorescence microscope fitted with a QImaging Retiga 4000R digital camera. Histomorphometry was performed using custom software based on the Aphelion image analysis tool kit (Adcis, Herouville-Saint-Clair, France) combined with Fiji-Image J and Microsoft Ice packages. This semi-automated software detects calcein double labelling (See Figure 2-15).

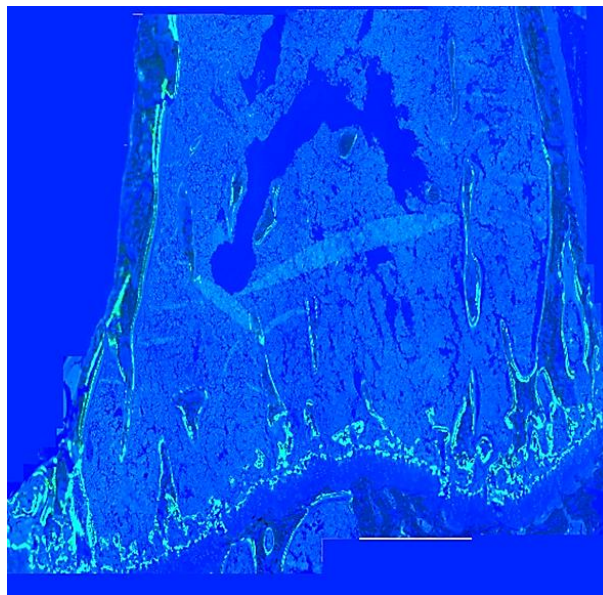


Figure 2-15: The stitched picture for calcein double labelling for the measurement of bone formation visualised by fluorescent microscope at 20X magnification.

The parameters defined by the previously mentioned custom software were calculated according to the ASBMR Histomorphometry Nomenclature Committee (Dempster et al., 2013) and are shown in Table 2-17.

Table 2-17: Bone histomorphometry parameters used in this study

Parameter	Abbreviation (unit)
Bone Volume per Total Volume	BV/TV (%)
Active Resorption area per Bone Surface	Oc.S/BS (%)
Osteoclast Number per Bone Surface	Oc.N/BS (# of cells/mm <sup>-1</sup> )
Osteoclast Surface per Bone Surface	Oc.S/BS (%)
Mean Osteoclast Size	( $\mu\text{m}^2$ )
Osteoid Surface per Bone Surface	Os.S/BS (%)
Osteoid Volume per Bone Volume	Os.V/BV (%)
Label Width	L.Wi ( $\mu\text{m}$ )
Mineral Apposition Rate	MAR ( $\mu\text{m}/\text{day}$ )
Mineralising Surface per Bone Surface	MS/BS (ratio)
Bone Formation Rate	BFR ( $\mu\text{m}^2/\mu\text{m}/\text{day}$ )

### 2.2.5 Western Blot

#### 2.2.5.1 Preparation of cell lysates

Prior to cell lysate, a RIPA lysis buffer (Table 2-18) was prepared on ice. The culture media were removed and plated cells washed with cold PBS. The PBS was then discarded and the ice-cold RIPA lysis buffer was added to the cells, which were left on ice for 10-15 minutes. The cells were then scraped with a syringe plunger and the lysate was collected in a 1.5 ml Eppendorf tube. Bone marrow cell lysate was prepared by collecting the bone marrow cells in standard  $\alpha$ MEM followed by a 3-minute centrifugation at 300g. The pellets were then washed twice with PBS, and another 3-minute centrifugation at 300g was performed. The pellets were subsequently resuspended in the RIPA lysis buffer and left for 10 minutes on ice, after which the lysate was transferred to a 1.5 ml Eppendorf tube. Both lysates were centrifuged at 12000g for 10 minutes at 4°C. Supernatants were collected and stored at -20°C.

Table 2-18: Solutions for cell Lysis

***RIPA Lysis buffer***

1% Triton 100X, 0.5% (w/v) Sodium Deoxycholate, 0.1% (w/v) Sodium Dodecyl Sulphate (SDS), 50 mM Tris-HCl (pH 7.4) and 150 mM Sodium Chloride were dissolved in dH<sub>2</sub>O.

On the day of extracting the cells Protease inhibitor, Phosphatase inhibitor, 0.5 M EDTA and 1 M NaF are added.

***IP Lysis buffer for Immunoprecipitation***

25 mM Tris-HCl pH 7.4, 150 mM NaCl, 1% NP-40, 1 mM EDTA, 5% glycerol. On the day of extracting the cells Protease inhibitor and Phosphatase inhibitor are added.

### 2.2.5.2 Measurement of protein concentration (Pierce protein assay)

The protein concentration was determined using the bicinchoninic acid (BCA) protein assay. In brief, the working solution was prepared by mixing 1 part copper (II) sulfate (4% (w/v)) with 50 parts bicinchoninic acid solution. Ready-to-use standard Bovin serum albumin (BSA) from ThermoScientific and duplicate protein samples were added to a 96-well plate (10 µl), followed by the addition of 200 µl of working solution. The plate was then sealed and incubated at 37°C for 15-20 minutes. The absorbance at 562 nm was then measured using the plate reader (BIO-Tek Synergy HT) and the protein concentration was measured according to the BSA standard curve.

### 2.2.5.3 Protein gel electrophoresis

Precast gels from BioRAD (12% Bis-Tris) were used to separate the protein lysate. The gel tank was filled with an electrophoresis running buffer (Appendix 2.4) and the gel's wells were washed. The loading samples were prepared by mixing 1 part of a 5X reducing sample buffer (Appendix 2.4) with 4 parts cell lysate and then heated at 95°C for 5 minutes using a heating block. The samples were then removed and left to cool at room temperature. The samples were loaded along with a Kaleidoscope marker (1 µl) mixed with Magic marker (1 µl) in order to identify the molecular weight. The gel was run for 40-50 minutes at a voltage of 200 V until the dye front reached the bottom of the gel.

#### 2.2.5.4 Electrophoretic transfer

This step was used to transfer the proteins from the polyacrylamide gel in order to be accessible to antibody detection on a solid membrane: polyvinylidene difluoride (PVDF). Prior to removing the gel from the tank, a PVDF membrane (Hybond TM-P from Amersham) was cut to the size of the polyacrylamide gel and immersed in 100% methanol for 5 minutes. The membrane was equilibrated with transfer buffer for 5 minutes. The gel was removed from the transfer buffer (Appendix 2.4). A blotting sandwich was assembled by placing the polyacrylamide gel on top of the PVDF membrane between 2 filter papers pre-soaked with transfer buffer (see Figure 2-16). The transfer was performed using a constant current of 60 mA/gel for 120 minutes.

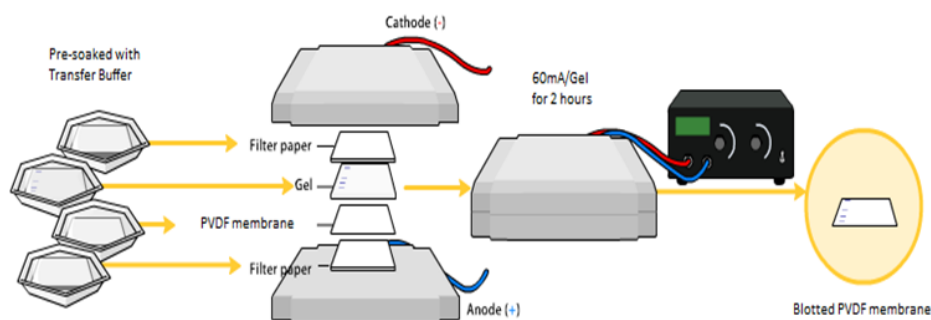


Figure 2-16: A gel transfer assembly diagram for western blotting.

Adapted from

[https://upload.wikimedia.org/wikipedia/commons/9/93/Western\\_blot\\_transfer.png](https://upload.wikimedia.org/wikipedia/commons/9/93/Western_blot_transfer.png)

#### 2.2.5.5 Immunostaining

The blotted PVDF membrane was removed from the blotter and transferred to a tray containing 5% skimmed milk in TBST (Appendix 2.4) for blocking all non-specific sites and left on a shaking platform for one hour. For probing the membrane

with an optineurin antibody, the membrane was blocked with 5% Bovin serum albumin for 1 hour. The membrane was then rinsed with TBST and probed for a primary antibody. The antibody was prepared in 3% BSA in TBST with a suitable dilution for the antibody (Table 2-19). The membrane was then soaked in the primary antibody and left shaking for 1 hour either at room temperature or overnight at 4°C, depending on the type of primary antibody used. The primary antibody was re-used by filtering it with a sterilised 0.2 µm filter and then stored at -20°C. The membrane was washed 3 times using TBST (15 minutes per wash), followed by membrane probing with a secondary antibody for 1 hour at room temperature. The anti-rabbit horseradish peroxidase-conjugated secondary antibody (Jackson ImmunoResearch) was prepared in 3% skimmed milk in TBST using a 1:5000 dilution. The membrane was then washed multiple times (~15 minutes/wash) for 90 minutes. During the final wash, the membrane was left on the rocker with TBS (Appendix 2.4) for 15 minutes.

#### **2.2.5.6 Band visualisation and quantification**

In order to detect the bands on the membrane, the membrane was transferred to a chemiluminescent detection system (Syngene Genegnome Bioimaging system) tray. One ml of freshly prepared SuperSignal substrate from ThermoScientific was spread over the membrane and the tray was then returned to the Syngene Genegnome Bioimaging system for detection of the bands. The bands' intensity was measured using a Syngene software package called GeneSnap to compare the protein expression among the samples.

#### **2.2.5.7 Membrane stripping**

In order to probe the membrane with another primary antibody, the membrane was soaked in a tray containing a stripping buffer (Appendix 2.4) supplemented with 50 µl of DTT. Subsequently, the tray was placed in a water bath at 55°C for 10 minutes. The membrane was checked for complete stripping by visualising it using SuperSignal, as mentioned in the previous section. After stripping, the membrane was blocked with 5% skimmed milk and the downstream steps were then continued as mentioned in the immunostaining section (2.2.5.5).

### 2.2.6 Immunoprecipitation (IP)

Bone marrow macrophages and osteoclasts were generated as described in Section 2.2.3.3.1. Protein from those cells was extracted using an IP lysis buffer (Table 2-18). To immunoprecipitate Optn, 50 µg of protein lysate was incubated in an Eppendorf tube overnight and rotated at 4°C with 4 µg of the sheep anti-mouse OPTN antibody (obtained from Dundee group). Protein G Sepharose beads (15 µl) were added to the OPTN antibody-protein lysate mixture and left for an additional overnight incubation at 4°C. The Sepharose beads were collected by centrifugation and then washed 3 times with the IP lysis buffer. The Sepharose beads were thereafter suspended in 25 µl of IP lysis Buffer with 6 µl of loading buffer added to each sample. The samples were heated to dissociate the protein attached to the beads, followed by a 1min centrifugation. The supernatant was loaded to a polyacrylamide gel, and the downstream steps were continued as detailed in the Western Blot section (2.2.5.5). The IP membrane was probed first with an OPTN antibody (1:200 dilution, from Cayman) and then CYLD (1:1000 dilution, Cell Signalling). The membrane was then re-probed with  $\beta$ -Actin (1:1000 dilution). An anti-rabbit antibody (Jackson ImmunoResearch) was used as a secondary antibody and the bands' re-visualisation and quantification was performed as described before in Section 2.2.5.6.

Table 2-19: List of antibodies used in this study: mAb (monoclonal antibody), pAb (polyclonal antibody), and IP (Immunoprecipitation).

Antibody (conc.)	Class/Host/Isotype	Source	Cat No.
<b>OPTN (1:250)</b>	pAb Rabbit/IgG	Cayman	100000
<b>OPTN (IP: 4 µg)</b>	pAb Sheep Anti-mouse/IgG (s308c)	Dundee group	
<b>OPTN (1:100)</b>	pAb Rabbit/IgG	Abcam	Ab23666
<b>CYLD (1:1000)</b>	mAb Rabbit/IgG	Cell Signaling	8462
<b>Phospho-I<math>\kappa</math>B<math>\alpha</math> (1:1000)</b>	mAb Rabbit/IgG	Cell Signaling	2859
<b>Actin (1:1000)</b>	mAb Rabbit/IgG	Sigma	A0483

### 2.2.7 Gene Expression using Quantitative Real-Time PCR (qPCR)

#### 2.2.7.1 RNA extraction

The RNA was extracted from the cultured cells using an RNA extraction kit (GenElute Mammalian Total RNA Purification Kit, from Sigma Aldrich). Briefly, the cells were lysed for 2 minutes using a lysis buffer after withdrawal of the media. The lysed samples were stored at this stage at  $-70^{\circ}\text{C}$  before proceeding to RNA isolation. The lysate was filtered from cellular debris and the RNA was bound to the provided columns (GeneElute Binding Columns). The columns were subsequently either washed and eluted for storage at  $-70^{\circ}\text{C}$  or proceeded to measurement.

#### 2.2.7.2 Measuring RNA concentration

Two methods were used to measure the RNA concentration:

##### 2.2.7.2.1 *Nanodrop 1000 Spectrophotometer*

This spectrometer (from ThermoScientific) was used to measure the RNA quantity at different absorbance levels (230, 260 and 280 nm). One  $\mu\text{l}$  of the RNA sample was added to the Nanodrop before the measurement was started. The absorbance at 260 nm was used to measure the RNA concentration in  $\text{ng}/\mu\text{l}$ . The 260/280 ratio was used to evaluate RNA purity, with a ratio of  $\sim 2$  generally considered acceptable for RNA purity. Lower readings of this ratio indicate the presence of protein or phenol contaminants, which are detected at 280 nm. A ratio of 260/230 is another parameter used for nucleic acid purity. The expected value for this ratio is equal to 2-2.2 nm and lower readings indicate the presence of contaminants, measured at 230 nm.

##### 2.2.7.2.2 *RiboGreen Kit*

The Quant-iT RiboGreen RNA reagent is a sensitive fluorescent nucleic acid stain used for measuring RNA concentration according to manufacturer protocols. The samples were measured first by the Nanodrop for a rough estimation of RNA concentration because the kit allows quantitation of 20  $\text{ng}/\text{ml}$ . Serial dilutions (0.3125–2  $\text{ng}/\mu\text{l}$ ) of the RNA standard provided by the kit were used to generate the standard curve. A black 96-well flat bottom plate was used to carry out the test. One hundred  $\mu\text{l}$  of 0.5 – 1  $\text{ng}/\mu\text{l}$  of the RNA samples measured by the Nanodrop in DEPECT water

were plated in duplicate and 100 µl of RiboGreen dye was added to each well. The fluorescence was then measured at an excitation/emission wavelength of 485/528 nm.

### **2.2.7.3 Reverse transcription**

The RNA samples were used to synthesize the cDNA by reverse transcription. The qScript cDNA SuperMix kit from QuantaBioscience was used according to manufacturer protocols. In brief, an equal amount of RNA concentration (10 pg – 1 µg) was added to DEPECT-treated water and 4 µl of qScript cDNA SuperMix (5X) for a total volume of 20 µl/reaction. After a brief centrifugation, the sample mix was incubated for 5 minutes at 25°C, 30 minutes at 42°C, 5 minutes at 85°C, and then held at 4°C.

### **2.2.7.4 qPCR amplification using a fluorescent probe**

Gene expression was measured from a cDNA using TaqMan probes and primers specific to the genes being studied. These probes were designed using the Roche Universal Probe Library (UPL) Assay Design Center (<https://lifescience.roche.com/shop/en/us/overviews/brand/universal-probe-library>).

Primers which have been obtained from UPL was used to study the expression of *Optn* (see Table 2-20). These primers amplify regions that present in all *Optn* isoforms. The TaqMan probes consist of two labels: the fluorescence fluorophore at the 5' end of the probe, and the quencher that quenches the fluorescence of the fluorophore at the 3' end of the probe. The quencher inhibits fluorophore fluorescence as long as it is attached to the probe. During the extension phase, the exonuclease activity of the Taq polymerase degrades the probe, causing a release of the fluorophore from the quencher and thereby inducing fluorescence. Fluorescence was quantified using a MJ Research Chromo4 cyclor and the data were analysed using the MJ OpticonMonitor 3.1 software (Figure 2-17).



Table 2-20: Mouse *Optn* qPCR primers and the universal probe library number.

UPL No.	Universal Probe Library (UPL) Forward and Reverse Primer	Amplicon Length (nt)	Length of intron spanned (nt)
<i>Optn</i> -91	F: caaaataccaacgaagcagtga	77	9190
	R: agaggttgatgggacatggt		
<i>Optn</i> -63	F: gctccgaaatcaagatggag	63	927
	R: gcagagtggctaacctggac		

To study gene expression, RNA was extracted from the samples using the GenElute Mammalian Total RNA Purification Kit and then measured using the Quant-iT RiboGreen kit. Fixed concentrations of RNA from all samples were used to create a cDNA using QuantaBioscience as described before. The amplification of all PCR products was performed in a MJ Research Chromo4 Real-Time PCR thermocycler. The PCR reaction was set up as follows:

Reagent	Volume (μl)	Final concentration
2X SensiFast Probe	10	1X
Universal ProbeLibrary Probe (10 μM)	0.2	100 nM
Forward Primer (10 μM)	0.8	400 nM
Reverse Primer (10 μM)	0.8	400 nM
RNase-free H <sub>2</sub> O	5	
Template	4	

The thermal cycling protocol consisted of an initial incubation for 3 minutes at 95°C, followed by 35 cycles of 50 seconds at 95°C, then 45 seconds at 55.1°C and 1 minute at 72°C.

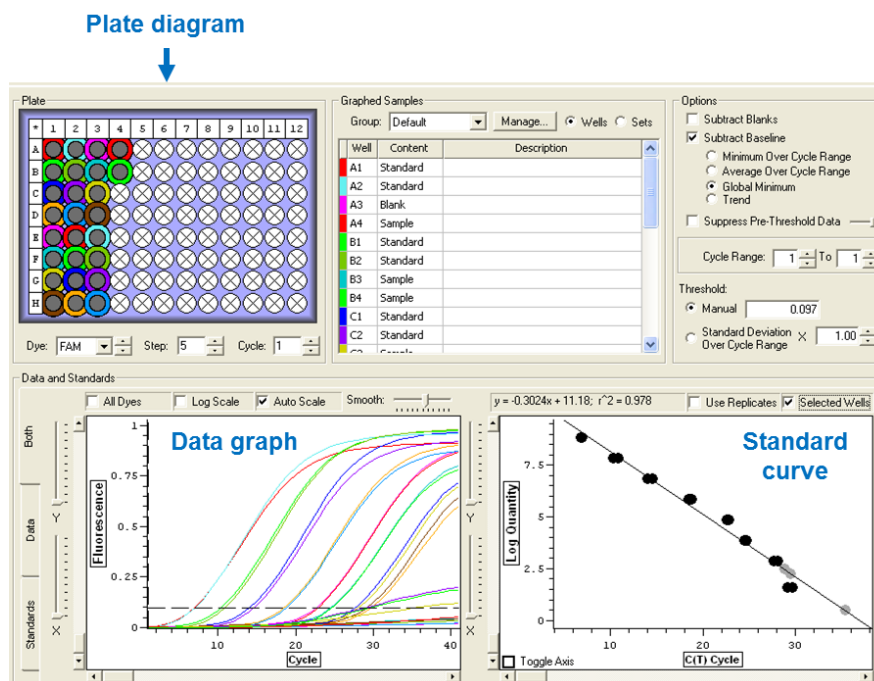


Figure 2-17: Schematic illustration of amplification plot and standard curve generated by Opticon Monitor 3. The Plate diagram is used for selecting wells to include in the Data graph. Each colour of a well in the Plate diagram correlates with the signal intensity of each sample measured in the well. Real-time amplification plot (Data graph) shows the standard dilutions from a 10-fold dilution series. The graph measures the fluorescence versus number of cycles. The Standards curve is automatically generated using the information (e.g. number of copies or molecules) that was provided by the user. It measures the logarithm of the amount of DNA against the C(T) cycle. The samples will appear as grey dots while the standards appear as black dots.

To generate standard curves, a test sample was used to create a cDNA standard of known concentration. The yielded qPCR product was then purified using the QIA quick PCR Purification Kit and loaded on a gel to verify the successful amplification of the cDNA into a clean amplicon of the expected size. The concentration of qPCR product was quantified by taking multiple measurements of the same sample using the Nanodrop 1000 spectrophotometer as described before. The average reading of the product concentration was used in the following formula in order to calculate the number of copies (molecules) in this product:

$$\text{no. of copies} = \frac{\text{template amount (ng)} \times 6.022 \times 10^{23}}{\text{amplicon size (bp)} \times 1 \times 10^9 \times 660}$$

Standard curves were generated by serial 10-fold dilutions of the quantified cDNA. qPCR was performed on samples alongside with standards and the copy number of each sample was measured according to fluorescence intensity using the MJ Opticon Monitor 3.1 analysis software. In addition to the fixed amount of starting RNA, the housekeeping gene 18S ribosomal RNA was also used as a reference gene for normalizing gene expression levels. For 18S ribosomal RNA, the PCR reaction was set up as follows:

Reagent	Volume (µl)	Final concentration
2X SensiFast Probe	10	1X
TaqMan Assay Mix for 18S ribosomal RNA	1	
RNase-free H <sub>2</sub> O	5	
Template	4	

### 2.2.8 Data Analysis

Statistical analysis was performed using either Excel 2007 or MINITAB version 16. Fisher's exact test was used for the analysis of microsatellite allele frequencies of chromosome 10-linked subjects. Differences between the *OPTN*-targeted shRNA and the non-targeted shRNA used for the *Optn* knockdown experiment, or the data obtained from the wild-type and *Optn*<sup>D477N/D477N</sup> knock-in mice, were analysed by a Student's *t* test. A one-way ANOVA was used to analyse the association between rs1561570 alleles and either disease severity or SF36 parameters. A general linear model ANOVA was used to analyse the association between rs1561570 alleles, and the total disease severity score was adjusted for age and gender. All data were presented as means  $\pm$  standard deviation (SD) or means  $\pm$  standard error of the mean (SEM). A *P* value below 0.05 was considered statistically significant.

## CHAPTER THREE

**The rs1561570 variant in *OPTN* is associated with Paget's disease severity and with *OPTN* gene expression but no disease-specific coding variants were detected in PDB patients**

### 3 The rs1561570 variant in *OPTN* is associated with Paget's disease severity and with *OPTN* gene expression but no disease-specific coding variants were detected in PDB patients

#### 3.1 Summary

Mutations in *SQSTM1* gene are known to cause about 40 % of familial cases and 10% of sporadic cases of PDB and previous studies have shown that these mutations are associated with disease severity (Ralston and Albagha, 2011). Recent GWAS have identified further susceptibility loci for PDB (Albagha et al., 2011a, 2010), including variants within the *OPTN* gene. All these variants are located in the intronic region of *OPTN*. Particularly, the risk allele T of the common variant rs1561570 in *OPTN* was one of the highest association signals in different populations loci ( $P = 4.37 \times 10^{-38}$ , OR = 1.67). In this chapter, the relationship between rs1561570 in *OPTN* and disease severity in 635 PDB patients without *SQSTM1* mutations was investigated. A disease severity score was devised based on several clinical features including: number of affected bones, clinical evidence for bone deformity, the presence of bone pain, bone fractures, requirements of orthopedic surgery and the use of hearing aid for deafness. The association between rs1561570 and disease severity score was investigated using general linear model ANOVA adjusting for age and gender. Also, *OPTN* was screened for genetic variation by direct sequencing of 43 samples obtained from PDB familial cases and controls. The direct sequencing covered the coding regions as well as the exon-intron boundaries.

Results showed significant association between rs1561570 and severity score. Carriers of the risk allele T had higher severity score ( $6.02 \pm 0.11$ ) compared to non-carriers ( $5.39 \pm 0.28$ ,  $P = 0.031$ ). Reduced quality of life (as assessed by SF36 physical summary score) was also noticed in patients who carried the risk allele ( $36.8 \pm 0.5$ ) compared to those who did not ( $39.3 \pm 1.4$ ;  $P = 0.091$ ) but this was not statistically significant. All variants identified from *OPTN* screening by direct sequencing are present in SNP databases. It seems that these variants did not have a direct effect on

the *OPTN* nor did they alter the splicing sites and therefore they are unlikely to be pathogenic.

To conclude, the results presented in this chapter showed that the *OPTN* rs1561570 variant is associated with disease severity and complications of PDB and could be of clinical value in identifying patients who are *SQSTM1* negative and at risk of developing a severe disease. In addition, the mutation screen did not identify variants in the coding region and further screening is required to cover the non-coding region as the unidentified variant(s) may have a regulatory effect at the gene expression level.

## 3.2 Introduction

The severity of PDB varies from one patient to another and it ranges from asymptomatic to various complications including osteoarthritic pain, nerve compression syndromes, deafness, bone deformity, fracture and tendency to develop osteosarcoma (Ralston, 2013b). Genetic risk factors are strong in PDB pathology but vary markedly between countries (5% - 50%), and a wide range of individuals have an affected first-degree relative (Ralston and Albagha, 2013). Mutations affecting the ubiquitin associated domain of *SQSTM1* (the only gene known to cause PDB) are found in 5 – 10% of sporadic cases and 40 – 50% of familial PDB cases (Ralston, 2013b), suggesting that other related genes remain to be identified. These mutations were found strongly associated with PDB severity and are implicated in the development of the disease phenotype in animal models (Daroszewska et al., 2011; Hiruma et al., 2008). Recent GWAS have identified seven new PDB susceptibility loci; near the *CSF1* gene, near the *TNFRSF11A* gene, the *OPTN* gene, the *TM7SF4* gene, the *NUP205* gene, the *RIN3* gene, and the *PML* gene. These loci were confirmed to be associated with the disease in various European populations (Albagha et al., 2011a, 2010; Chung et al., 2010a) and account for about 13% of the heritability when combined together (Albagha et al., 2013). However, their influence in the PDB severity is currently unknown. One of these loci is 10p13 with the highest association signal tagged by rs1561570 within *OPTN* ( $P = 4.37 \times 10^{-38}$ , risk allele OR = 1.67) (Albagha et al., 2010). Interestingly, *OPTN* is located in the 10p13 region and has been previously linked to PDB by linkage studies (Lucas et al., 2007). *SQSTM1* mutations are the only mutations that have been associated with disease severity and complications of PDB. *OPTN* was linked to glaucoma (Rezaie et al., 2002) and to amyotrophic lateral sclerosis (Maruyama et al., 2010). Several population and ethnicities were screened for mutations in the optineurin gene for patients affected with these diseases (Ayala-Lugo et al., 2007). However, the role of *OPTN* in bone metabolism is unknown but it is known to have a role in NF $\kappa$ B signaling and autophagy (Kachaner et al., 2012), both of which have been implicated in osteoclast biology. The *OPTN* gene in humans contains 3 non-coding exons in the 5' UTR region

and 13 coding exons that encode a 577 amino acid protein. Alternative splicing generates four different transcripts having the same open reading frame (Kachaner et al., 2012). In the first part of this chapter, I investigated if *OPTN* variants are associated with the severity and clinical outcome of PDB in patients without *SQSTM1* mutations. The second part discusses the results of *OPTN* screening for mutations by direct DNA sequencing of *OPTN* coding regions as well as the exon-intron boundaries in 24 samples obtained from chromosome 10-linked families and 19 samples from controls.

### 3.3 Results

#### 3.3.1 *Genetic Variants in the Optineurin Gene are Associated with Disease Severity in Paget's disease of Bone*

The study subjects comprised of 635 PDB patients without *SQSTM1* mutations who were recruited in PRISM study (Langston et al., 2009). All participants had a radioisotope bone scan at baseline to assess the extent of skeletal involvement. Deformity was assessed based on clinical evidence of bone deformity using a three-point scale (0 = no deformity, 1 = mild deformity, and 2 = severe deformity). Other disease-related information was recorded including: the presence of bone pain and whether pain was caused by PDB, previous bone fractures and if they had occurred in affected bones, use of hearing aid for deafness, previous bisphosphonate treatment, and requirement of orthopaedic surgical procedures. PDB severity was assessed as previously described (Visconti et al., 2010). Briefly, a total disease severity score was devised based on several clinical features including: number of affected bones, clinical evidence for bone deformity, the presence of bone pain, bone fractures, requirements of orthopaedic surgery and the use of hearing aid for deafness. Health-related quality of life within the PRISM study was assessed by the Short-form-36 (SF36) questionnaire (Ware John E and Gandek, 1998). General linear model ANOVA was used to analyse the association between rs1561570 alleles and the total disease severity score or SF36 parameters adjusting for age and gender. Gender and rs1561570 allele distribution for the study subjects are shown in Table 3-1.



Table 3-1: Gender and rs1561570 allele distribution for the study subjects. The distribution of geotype frequencies in this population follow the Hardy-Weinberg equation

Number of PDB cases	Gender		rs1561570 risk Allele (T)		
	Male	Female	Carrier		Non-Carrier
<b>635</b>	344	291	Homo (TT)	Het (CT)	CC
			n = 298	n = 260	n = 77

My results showed that carriers of the rs1561570 risk allele had a higher total disease severity score (mean  $\pm$  SEM;  $6.02 \pm 0.11$ ) compared to non-carriers ( $5.39 \pm 0.28$ ;  $P = 0.031$ ) after adjusting for age and gender (Figure 3-1). The analysis also showed that age ( $P = 0.005$ ) but not gender ( $P = 0.62$ ) was a significant predictor of total disease severity score. Analysis of rs1561570 in relation to SF36 parameters showed a trend for reduced SF36 physical score in patients who carried the risk allele T ( $36.8 \pm 0.5$ ) compared to those who did not ( $39.3 \pm 1.4$ ) but this was not statistically significant ( $P = 0.091$ ) (Figure 3-2). Analysis of rs1561570 in relation to other SF36 parameters showed no significant difference between carriers of the rs1561570 risk allele compared to non-carriers. Figure 3-3 shows the relation of the *OPTN* rs1561570 with Bodily Pain Score.

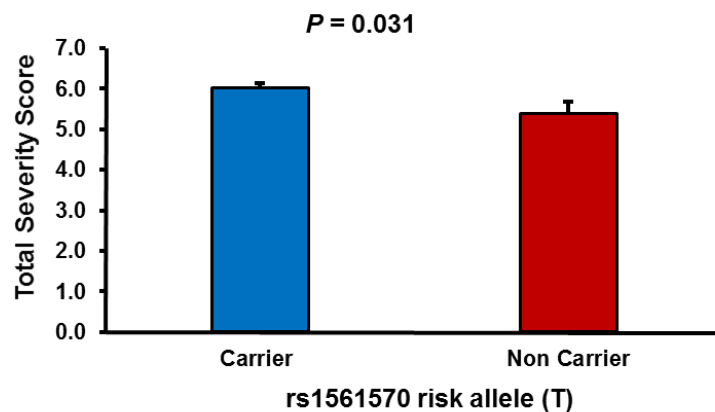


Figure 3-1: *OPTN* rs1561570 is associated with the disease severity score. Analysis using general linear model ANOVA showed a significant association between *OPTN* rs1561570 and total disease severity score. Error bars represent SEM.

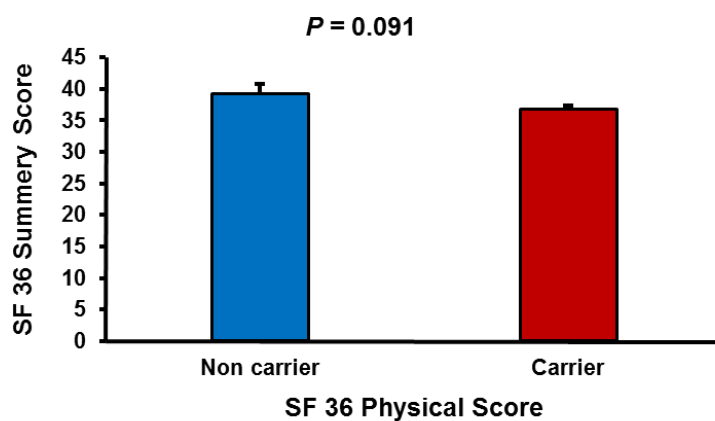


Figure 3-2: The association of *OPTN* rs1561570 with SF 36 Physical Score. A trend for reduced quality of life in patients who carried the risk allele T ( $36.8 \pm 0.5$ ) compared to those who did not ( $39.3 \pm 1.4$ ) was found but the relationship was not statistically different. Error bars represent SEM.

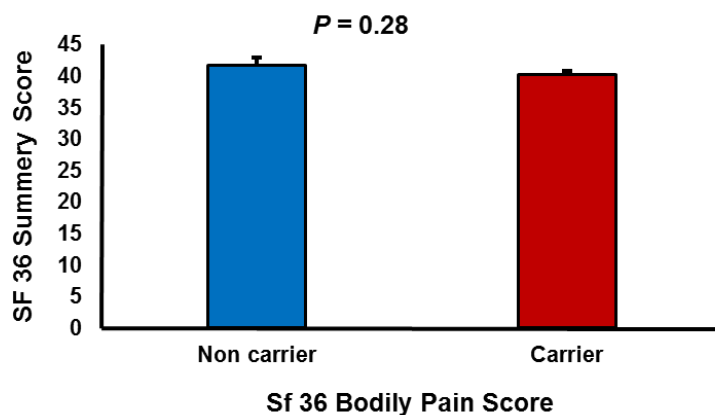


Figure 3-3: The association of *OPTN* rs1561570 with Bodily Pain Score. The relationship between *OPTN* rs1561570 and the SF36 bodily pain summary score was not significant. Error bars represent SEM.

### 3.3.2 Reduced Expression of *OPTN* Predisposes to PDB

The locus rs1561570 identified by the GWAS is located in non-coding region and therefore is likely to be involved in gene regulation. eQTL analysis becomes a useful tool to study how genetic variants could affect the gene expression levels measured in cells or tissues (Nica and Dermitzakis, 2013). Therefore, eQTL analysis was performed to address whether rs1561570 is associated with *OPTN* mRNA expression. The analysis involved human monocytes and peripheral blood mononuclear cells. The results revealed that the rs1561570 was a strong eQTL for *OPTN* in human monocytes (Zeller et al., 2010) and peripheral blood mononuclear cells (Westra et al., 2013), with reduced *OPTN* gene expression in carriers of the Paget's disease risk allele "T" (Figure 3-4). These data indicate that reduction in the *OPTN* expression is associated with increased PDB risk and suggest the interesting possibility that *OPTN* might play a role in regulating bone turnover by acting as a negative regulator of osteoclast differentiation. Based on these findings, the potential role of *OPTN* as a negative regulator to osteoclast differentiation and in bone metabolism has been extensively investigated in the coming chapters.

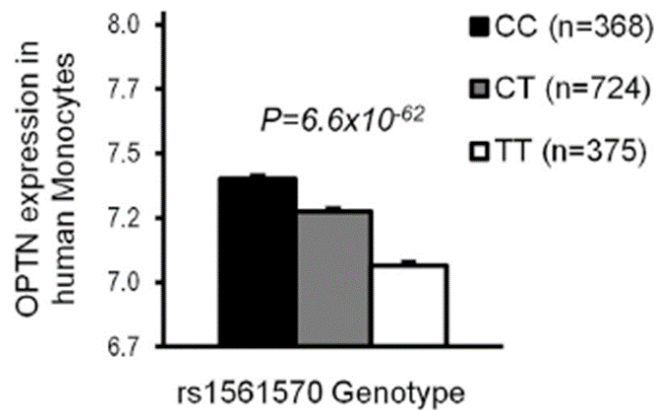


Figure 3-4: The top GWAS hit (rs1561570) is a Strong eQTL in Human Monocytes. *OPTN* mRNA expression levels are shown in relation to rs1561570 genotype in human monocytes. PDB-predisposing "T" allele is associated with reduced *OPTN* gene expression. n indicates the number of subjects in each genotype group (Obaid et al., 2015).

### 3.3.3 Mutation screening of *OPTN* by DNA sequencing

As shown in the previous section, the GWAS signal from chr10p13 was a strong eQTL suggesting that the association with PDB could be driven by a regulatory polymorphism influencing *OPTN* gene expression. However, the presence of rare pathogenic coding mutations cannot be excluded because the GWAS approach is not suited to identify disease-causing rare variants. Therefore, in this section, mutation screening of *OPTN* was performed in patients from 10p13-linked families. Genomic DNA was isolated from peripheral blood and the entire coding and non-coding exons as well as the exon-intron boundaries (including at least 50 bp of adjacent intronic sequences) were amplified by PCR. PCR products were examined by gel electrophoresis for the correct size of DNA bands (Figure 3-7) and sent for direct sequencing as discussed in section 2.2.2.3. Eighteen primer pairs have been designed using Primer3+ software (Figure 3-5 and 3-6). The sequencing data results were then analysed by using the Chromas Pro software (Figure 3-8).

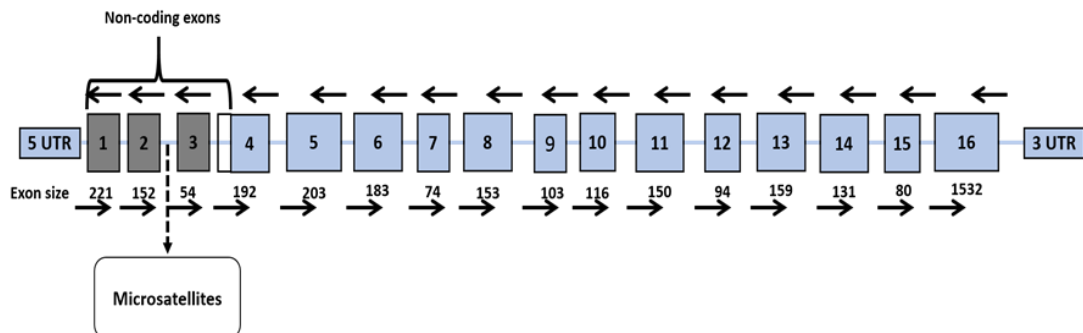


Figure 3-5: Schematic diagram of human *OPTN* gene. This diagram shows the primer pairs designed to cover the non-coding exons, coding exons and the intron/exon boundaries of each exon. Also it shows the location of the microsatellite repeats between the non-coding exons 2 and 3.

The data obtained from sequence alignment of samples in comparison with the reference sequence, produced by Chromas Pro, showed that some of the exons did not show any variation between the samples and the reference sequence including exon 5, 6, 8, 11, 12, 13, 14, 15, and 16. Seven SNPs located in the intronic region of the non-coding exons 1 and 2 and two SNPs from the intronic region of the coding exon 16

were identified as shown in Table 3-2. These SNPs were analysed using functional analysis and selection tool for single nucleotide polymorphisms (FASTSNP); a web server used for predicting the functional significance of identified SNPs (Table 3-3). It classifies and prioritizes high-risk SNPs in coding and non-coding region according to their phenotypic risks and putative functional effects (Yuan et al., 2006). In addition, this web server scores the SNPs' level of risk with a ranking of 0, 1, 2, 3, 4, or 5. These scores indicate the levels of no, very low, low, medium, high, and very high effect, respectively (Rajasekaran et al., 2007). For example, the SNP rs2304706 was identified by FASTSNP as intronic enhancer. The possible effect of this SNP was predicted by FASTSNP to alter the binding site of a transcription factor in an intronic region (Yuan et al., 2006). FASTSNP scores the risk level for these kind of SNPs to be very low to low (1 to 2). The difference in distribution of the allele and genotype frequencies of identified SNPs in cases compared to controls was not statistically significant ( $P > 0.05$ ); Table 3-2).

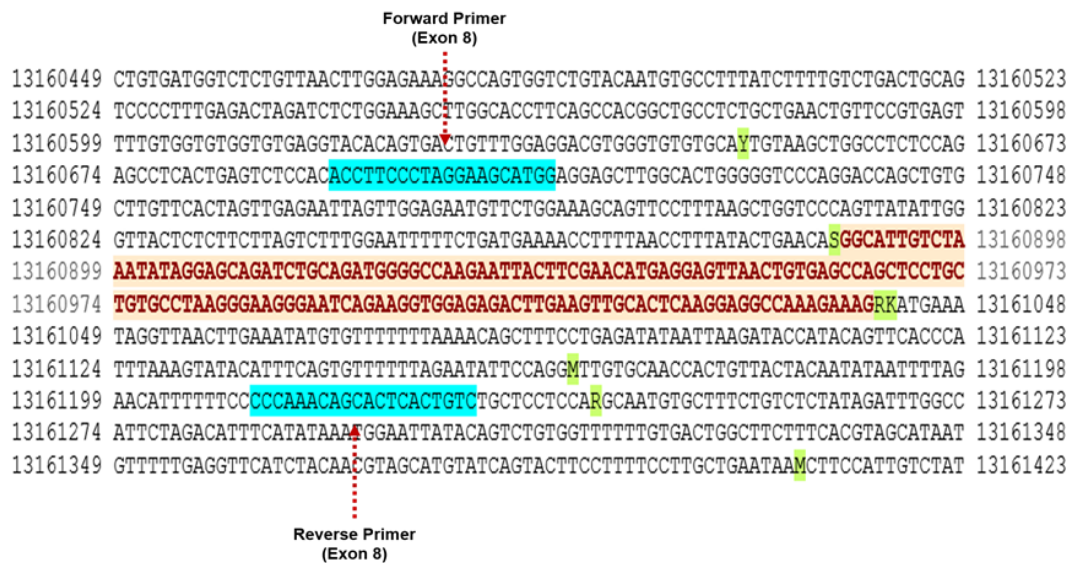


Figure 3-6: Part of the genomic sequence of *OPTN* for exon 8 obtained from Ensemble genome website. This diagram shows the primer sequences used for PCR amplification (highlighted with blue). The primers cover the coding sequence (red bold letters) as well as the intron/exon boundaries (black letters). Green boxes indicate the location of SNPs generated by Ensemble.

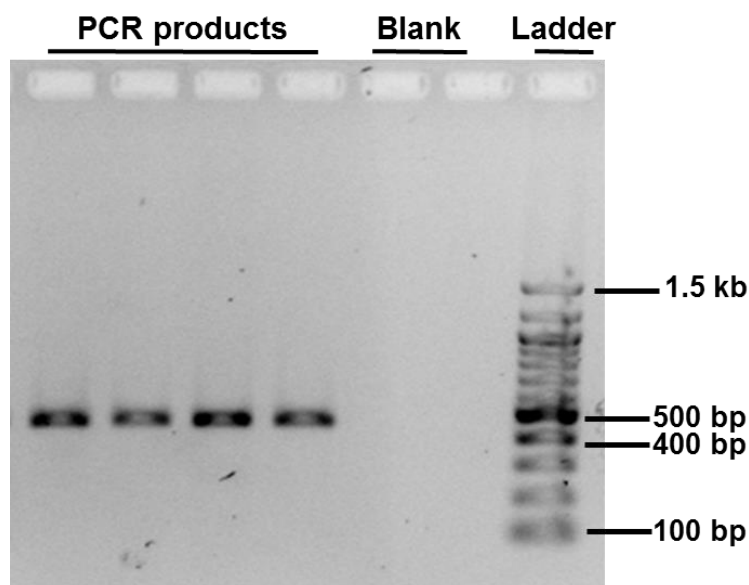


Figure 3-7: Gel electrophoresis analysis for the PCR products of Exon 2. Based on the primer design the expected size of the PCR product is 459 bp for Exon 2

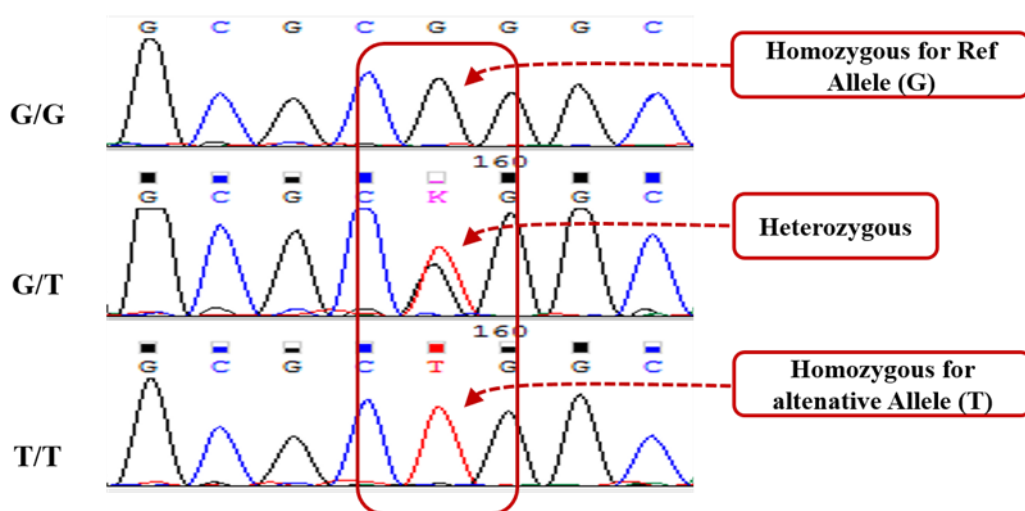


Figure 3-8: DNA sequencing results for exon 3 polymorphisms. This is an example of Chromatogram picture obtained from Chromas Pro software. This diagram shows the difference pattern between the homozygous for the reference allele, heterozygous and the homozygous for the alternative allele obtained from screening exon 3.

Table 3-2: Summary of the polymorphisms identified in the *OPTN* gene.

Exon	SNP ID	Possible functional effect Fast SNP	Allele	Genomic location	Homozygous of reference Allele (%)		Heterozygous		Homozygous of alternative Allele (%)	
					cases	controls	cases	controls	cases	controls
1	rs3814657	Intronic with no known function	G/T	10:13100087	66.67	33.33	66.67	33.33	33.33	66.67
	rs71492279	Intronic with no known function	T/C	10:13100153	90.00	10.00	42.86	57.14	62.50	37.50
	rs11548142	Intronic with no known function	G/A	10:13100251	53.85	46.15	64.71	35.29	100.00	0.00
	rs4748020	Intronic with no known function	C/G	10:13100327	65.38	34.62	57.14	42.86	0.00	0.00
2	rs2304706	Intronic enhancer	A/C	10:13108044	62.50	37.50	83.33	16.67	0.00	100.00
	rs41291307	Intronic with no known function	C/T	10:13108110	64.86	35.14	50.00	50.00	0.00	0.00
	rs41291309	Upstream with no known function (5UTR)	G/A	10:13108265	35.14	64.86	0.00	100.00	0.00	0.00
16-1	rs10906310	Intronic with no known function	C/A	10:13136697	63.33	36.67	50.00	50.00	66.67	33.33
16- 3	rs12415716	Downstream with no known function (3UTR)	T/G	10:13138287	70.59	29.41	55.56	44.44	83.33	16.67

### 3.3.4 Determination of the CA repeat polymorphism of the *OPTN* gene

A CA repeat microsatellite was detected during the analysis of sequences amplified from exon 2 and 3 of *OPTN*. A microsatellite is a region of DNA that consists of tandem repeats ranging in length from 2–5 base pair sequences located throughout the genome (Turnpenny and Ellard, 2007). This region is distinguished by having CA microsatellite. Upon examining the sequence data from exon 2 and 3, I have noticed that the sequence following CA repeats is noisy with overlapping peaks (see Figure 3.9) suggesting the presence of a polymorphic microsatellite in this region. This microsatellite is located approximately 200 bp upstream from the non-coding exon, between non-coding exons 2 and 3 (Figures 3-5 and 2-1). Therefore, a PCR-based assay was designed using unique primers flanking the repeating sequence in order to genotype this microsatellite as described in materials and methods section (2.2.2.4). These primers have been designed to sequence the intronic region between exons 2 and 3 from both directions. One of these primers is labelled with the fluorescent dye (FAM) in order to visualize and the PCR product on the DNA sequencer. However, analysis of PCR products has shown that single allele does not appears as a single peak on an electropherogram, but often as a group of peaks called stutter bands. Figure 3-10 shows an example of the peak pattern observed from a homozygous sample with the genotype 135/135. The peak with the highest intensity represents the true allele size and the peaks to the left are artefacts called stutter peaks. Stutter peaks are produced by the amplification of products one (s1-peak), two (s2-peak) or three (s3-peak) repeat units (CA) shorter than the actual amplicon due to the slippage of *Taq* polymerase on the repeated CA sequence (Hauge and Litt, 1993).



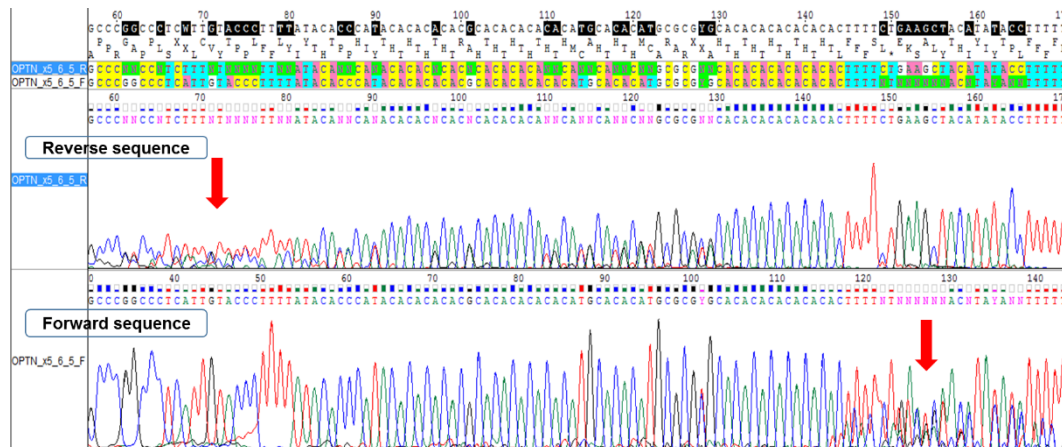


Figure 3-9: Analysis of DNA sequence traces of Exon 2-3 indicates the presence of a polymorphic microsatellite. An example of sequence chromatograms derived from one sample shows the effect of microsatellites on forward and a reverse sequence. The quality of sequence data follow the microsatellite repeats (red arrow) is often greatly reduced due to the noisy background caused by overlapping peaks indicating a heterozygous sample with different CA repeat allele length.

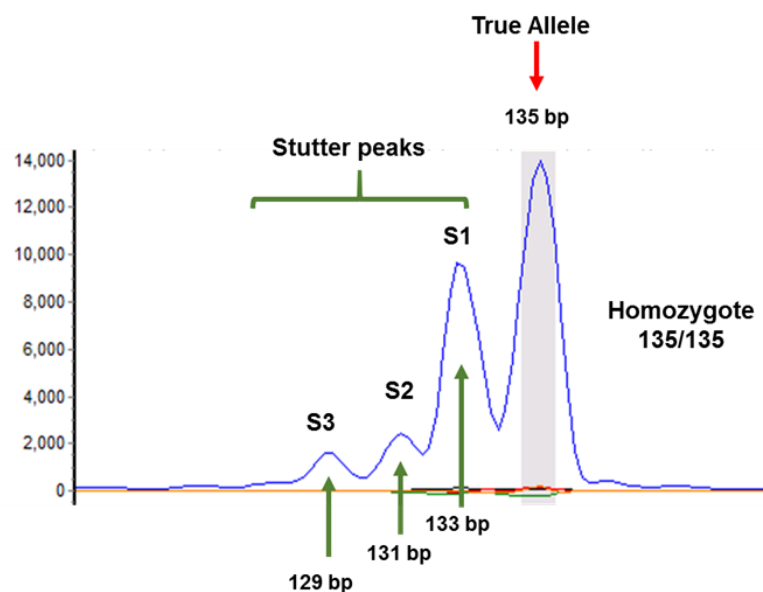


Figure 3-10: Electropherogram shows the peak pattern observed from a homozygous sample with the genotype 135/135. The red arrow indicates the true allele peak while green arrows indicate the stutter peaks (S1-S3). S1 differ in length from the main allele by 2 bp ( $135 - 2 \{CA\} = 133$ ), S2 is shorter by 4 bp ( $135 - 4 \{CA+CA\} = 131$ ) and S3 by 6 bp = 129.

The 43 subjects included in this study were genotyped for CA repeats polymorphism by PCR amplification followed by analysis of PCR products on an ABI 3730 DNA Analyser. The size of the PCR products was ~139 bp and all the samples passed the size call verification produced by the GeneMarker software (Figure 3-11). Four samples were excluded from the analysis because their peak pattern was unclear. Four alleles observed in this population (Figure 3-12) and the distribution of these alleles is listed in Table 3-3. To study the association of the CA repeat polymorphism with the disease trait, the allele frequencies were compared between cases and controls using Fisher's exact test. The data showed no statistically significant difference between the different genotype groups ( $P = 0.28$ ). Analysis of this CA repeat in a further 50 cases and 60 controls showed no association with PDB ( $P > 0.05$ ; Albagha *et al*, unpublished data).

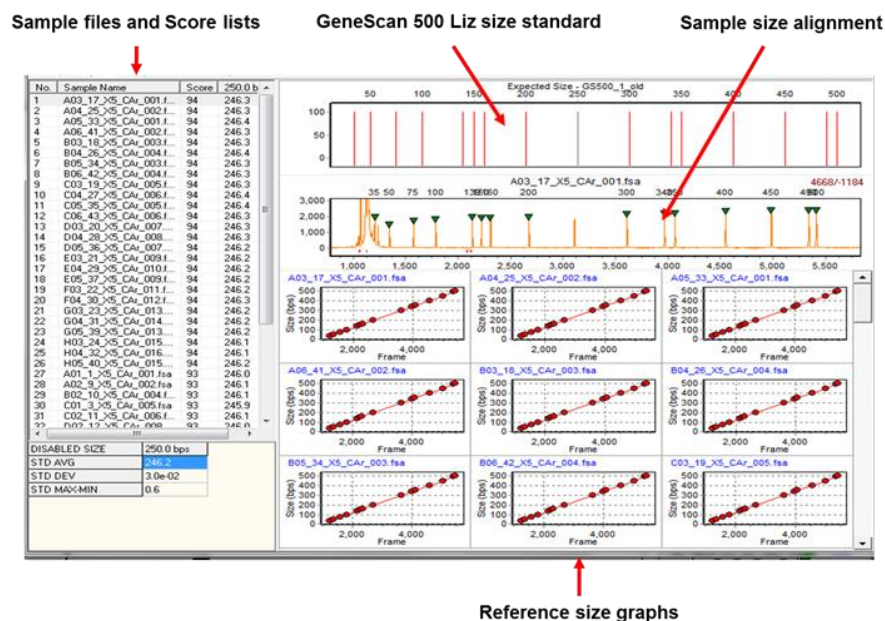


Figure 3-11: Size calibration charts from GeneMarker software. This chart is used to check the software's size calling accuracy and to review the sizing quality for samples. This example shows that the samples are in the linear range for accurate size calling with GeneScan 500-Liz standard (top section). The middle section shows the actual sized data from the selected sample file and green triangles indicate the size standard peaks called by GeneMarker. The bottom section shows the reference size graphs for the selected sample files. The left partition of the diagram shows the sample files and linearity scores.

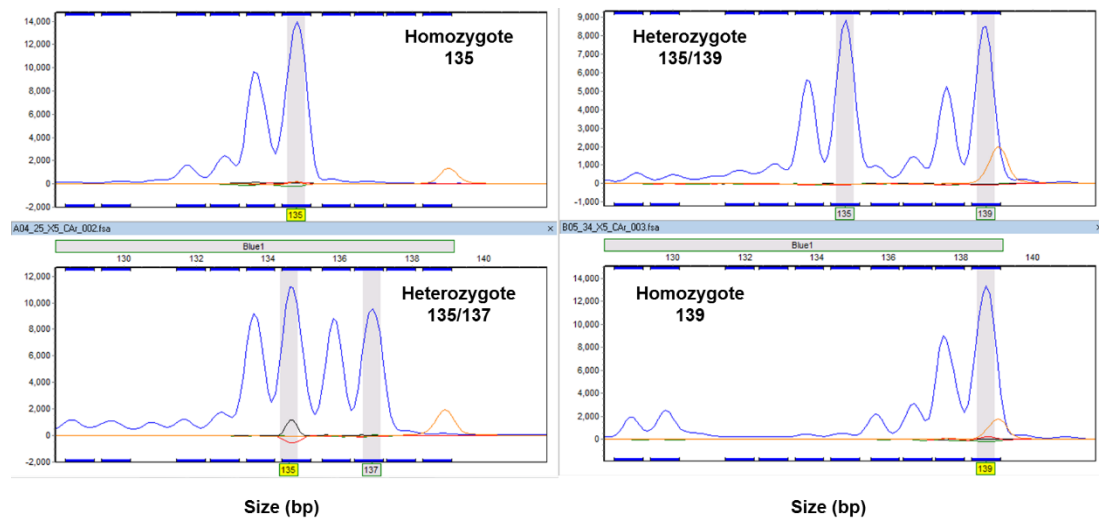


Figure 3-12: Electropherogram of allele pattern generated by the GeneMarker software. This diagram exhibits the allele image pattern for the CA repeats showing 4 different alleles identified in cases and controls. The blue peaks represent the Allelic peaks and the stutter peaks. The peak calls are indicated in rectangular boxes below the graphs. The light grey shadows are derived from the size standard, which indicate the positions for different sizes (the dark blue cutting lines above the graphs).

Table 3-3: Distribution of the microsatellite repeats of *OPTN* in controls and cases.

Microsatellite genotype	Controls	Cases
135	6	7
135/137	1	2
135/139	6	13
139/139	0	4

### 3.4 Discussion

As it has been described before, PDB has a strong genetic component. So far, *SQSTM1* is the only gene known to be mutated in PDB and mutations of this gene were found to be associated with more severe and extensive disease and a higher incidence of certain complications. PDB patients with *SQSTM1* mutations have earlier age at diagnosis and greater number of affected bones compared to non-carriers (Visconti et al., 2010). Over the past few years, progress in understanding many complex diseases has accelerated since the development of GWAS. These studies have successfully identified thousands of disease-associated loci waiting for further functional studies to confirm their association. Recently, GWAS have identified 7 new candidate genes for PDB (Albagha et al., 2011a, 2010). One of these candidate genes is the *OPTN*. The rs1561570 within *OPTN* discovered by the GWAS was replicated in different populations.

The results presented in this chapter confirmed the association between *OPTN* rs1561570 and total disease severity score in *SQSTM1* negative patients. Carriers of the risk allele "T" had a higher disease severity score compared to non-carriers. The analysis also showed that age but not gender was a significant predictor of total disease severity score, which is expected since PDB is a late onset disease. The relationship between *OPTN* rs1561570 alleles and measures of quality of life as depicted by SF36 questionnaire has also been assessed. A trend for reduced SF36 physical summary scores was found in patients carrying the rs1561570 risk allele compared to those who did not, but the relationship was not statistically significant. The relationship with the SF36 bodily pain summary score was also not significant. This study was done three years ago and presented in European Calcified Tissue Society (ECTS 2010) annual meeting (Appendix 3).

A recent study by Albagha *et al.* described the influence of the seven recently identified PDB-susceptibility loci by genome wide association analysis on the severity extent or complications of PDB either in *SQSTM1* negative patients or in combination

with *SQSTM1* mutations (Albagha et al., 2013). In this study, it was reported that the seven loci combined were associated with the number of affected bones and total disease severity score. When they analysed each locus individually for its relation to disease extent and severity, *OPTN* rs1561570 was significantly associated with the number of affected bones ( $p = 0.030$ ). Similarly, my results showed that the rs1561570 locus is significantly associated with the total disease severity score. Albagha *et al.* also found that the risk allele score of the identified loci in *SQSTM1* negative patients from the PRISM cohort was significantly associated with the number of affected bones and a trend for disease severity score but the differences were not significant. When they did a meta-analysis using other independent cohorts, they found a highly significant association between the risk alleles score identified by the seven GWAS loci and both the disease extent and severity. There was no significant association between allele risk score and the quality of life measures SF36. The same study also showed that the risk alleles had an additive effect when combined with *SQSTM1* mutations and the study was able to identify three groups of patients with low, medium and high levels of severity with specificity of 70% and sensitivity of 55% (Albagha et al., 2013). This illustrates that other genetic and environmental factors influence the disease extent and severity but further studies are required to identify these factors.

Mutation screening of the *OPTN* gene has been previously performed in patients with glaucoma and ALS in different populations. The results from these studies vary and the frequency of the identified polymorphisms within the optineurin gene differs from one ethnic background to another. For instance, the four main mutations identified in cases with glaucoma (E50K, M98K, R545Q and 2-pb AG insertion) have been reported to be responsible for 16.7% of the hereditary form of this disease. Moreover, *OPTN* was suggested as a candidate gene for familial and sporadic ALS in a Japanese cohort (Maruyama et al., 2010), while screening for *OPTN* mutations in different Caucasian populations including British, French and Dutch cohorts identified no disease-specific mutations in *OPTN* (Johnson et al., 2012; Millecamps et al., 2011; Sugihara et al., 2011).

In the current study, the *OPTN* gene from familial cases of PDB was screened for mutations that could affect the behaviour of this gene. Forty-three samples distributed between cases and controls were sequenced for the entire coding and non-coding exons as well as the exon-intron boundaries in order to cover the splice variants. Nine different non-coding polymorphisms have been identified with no known predicted function according to the FASTSNP tool. These polymorphisms have already been reported in the NCBI SNP database. The allele distribution of these polymorphisms in PDB cases was not statistically different from that observed in controls. This suggest that these polymorphisms are unlikely to be disease-causing.

A microsatellite has been detected in my study which is located between exon 2 and 3 and further analysis showed no significant association of this microsatellite with PDB risk. One limitation of my study is that a pathogenic mutation could have been missed due to small sample size. However, a further unpublished investigation from (Albagha *et al.*), has recently screened the *OPTN* gene in an additional 200 PDB cases and found no coding mutation in line with my findings. Collectively, these data suggest that the association with PDB is unlikely to be driven by mutations affecting the coding sequence of the *OPTN*. However, as the rs1561570 polymorphism is located in the intronic region, this polymorphism may be in linkage disequilibrium with another SNP that affect the promoter or an enhancer site, which leads to changes in the expression of this gene. Indeed, the rs1561570 was found to be a strong eQTL for *OPTN* in human monocytes (Zeller *et al.*, 2010) and in peripheral blood mononuclear cells (Westra *et al.*, 2013) suggesting that the association with PDB could be driven by changes in *OPTN* expression level. This eQTL was not detected in other cell types such as lymphoblastoid cell lines (Veyrieras *et al.*, 2008) or liver (Schadt *et al.*, 2008) suggesting that *OPTN* expression is regulated in a tissue-specific manner. Interestingly, the PDB-risk allele of rs1561570 "T" was associated with reduced *OPTN* gene expression suggesting that *OPTN* may have a negative effect on osteoclast differentiation.

In conclusion, my results are in harmony with recently published findings, which confirm the association of *OPTN* rs1561570 with disease severity. The other loci seem to have an additive effect on disease severity. The recently identified PDB-susceptibility loci by GWAS could be of clinical value in identifying *SQSTM1*-negative patients who are at increased risk of developing a severe form of PDB. These loci in combination with *SQSTM1* mutations can be used to predict severity levels of the disease but further research is required to apply these data in clinical practice. In addition, my results did not show a pathogenic variant(s) in the *OPTN* gene suggesting that the disease susceptibility could be due to regulatory polymorphisms that influence gene expression as described by the strong association between rs1561570 and *OPTN* gene expression. The risk allele "T" from this variant was associated with reduced PDB-*OPTN* gene expression, suggesting that reduced expression of *OPTN* could enhance osteoclast differentiation. This possibility is investigated in the next chapters.

**CHAPTER FOUR**

**OPTN DEPLETION IN MOUSE BMDMS  
ENHANCES OSTEOCLAST FORMATION,  
FUSION, AND SURVIVAL**



## 4 *Optn* Depletion in Mouse BMDMs Enhances Osteoclast Formation, Fusion, and Survival

### 4.1 Summary

Mutation screening of the exons and exon-intron boundaries in chapter 4 revealed no coding mutations in *OPTN*. However, the top GWAS hit rs1561570 is a strong eQTL for *OPTN* expression (rs1561570, expression  $P = 6.61 \times 10^{-62}$ ) in human monocytes (Zeller et al., 2010) and peripheral blood mononuclear cells (Westra et al., 2013). Collectively, these findings suggested that regulatory variant(s) could drive the association with PDB. Therefore, the aim of this study was to investigate the role of *OPTN* in osteoclast development by altering the *OPTN* expression using *in vitro* knockdown experiments. For this purpose, expression of *OPTN* was detected in bone marrow derived macrophages (BMDMs) and during osteoclast development after RANKL treatment. The expression of *Optn* was found to increase during osteoclast differentiation particularly after 3 days of RANKL stimulation. The effect of *Optn* depletion on osteoclast formation was subsequently studied in primary mouse bone marrow cultures. The expression of *Optn* in mouse BMDMs was knocked down using lentiviral particles expressing shRNA targeted against the *Optn* gene. Non-targeting shRNA lentiviral particles were used as a negative control and *Optn* knockdown in BMDMs was confirmed ( $> 70\%$ ) using western blot analysis. The first finding was that osteoclasts formed from *Optn*-depleted BMDMs were significantly higher and larger than those formed from non-targeted cells. *Optn*-depletion in BMDMs also found to enhance osteoclast survival and increased RANKL-induced NF $\kappa$ B activation. In conclusion, these findings suggested that optineurin has a role in osteoclast biology as a negative regulator of osteoclast formation *in vitro*. These findings were also consistent with the previously reported negative effect of *OPTN* on TNF $\alpha$  induced NF $\kappa$ B activation in immune cells (Sudhakar et al., 2009; Zhu et al., 2007).

## 4.2 Introduction

Mutation screening of the exons and exon-intron boundaries in chapter 4 revealed no coding mutations in *OPTN*. However, the top GWAS hit rs1561570 is a strong eQTL for *OPTN* expression (rs1561570, expression  $P = 6.61 \times 10^{-62}$ ) in human monocytes (Zeller et al., 2010) and peripheral blood mononuclear cells (Westra et al., 2013). Collectively, these findings suggested that regulatory variant(s) could drive the association with PDB. Therefore, the aim of this study was to investigate the role of *OPTN* in osteoclast development by altering the *OPTN* expression using *in vitro* knockdown experiments.

This chapter demonstrates firstly the *Optn* expression during osteoclast development derived from mouse macrophages. Then it describes the work done on RAW 264.7 cell line followed by the findings obtained after optineurin was knocked down in mouse BMDMs. The last part of this chapter describes the effect of *Optn* depletion on the RANKL-induced NF $\kappa$ B activation.

## 4.3 Results

### 4.3.1 Optimization of western blot assay to detect *OPTN* protein

Two different antibodies were used to detect *OPTN* expression by western blot using a positive control extracted from mouse brains in which *OPTN* is highly expressed. The first antibody was purchased from Abcam; this generated a lot of non-specific bands, a problem that took several trials to overcome. The first optimisation step involved using various dilution of the Abcam primary antibody. I have also tried replacing the non-fat milk with BSA as a blocking agent, and varying the time for membrane washing after blocking and after incubation with secondary antibodies.

Despite these optimisations, however, many non-specific bands still appeared in the membranes (Figure 4-1, A). Therefore, a second antibody was purchased from Cayman. Using the manufacturer's recommended concentration (1:200), this antibody identified the OPTN band at 74 kDa, as described by the manufacturer protocol, and generated few non-specific bands. Therefore, the Cayman antibody was used for all further experiments to detect OPTN in the western blots (Figure 4-1, B).

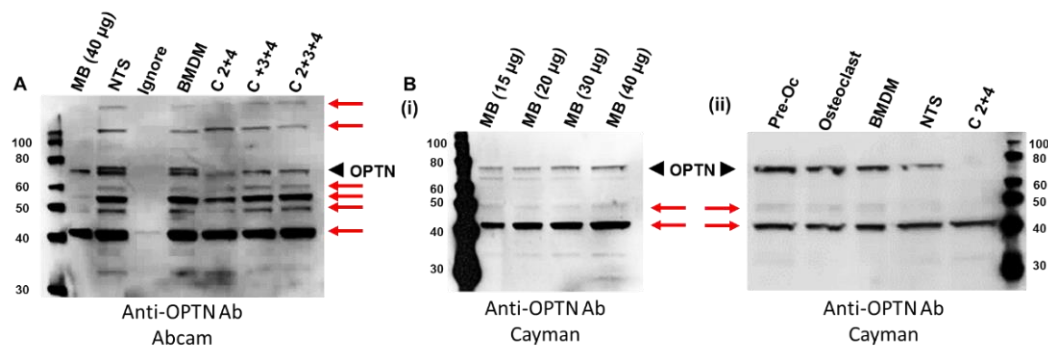


Figure 4-1: OPTN protein expression in BMDMs using Abcam and Cayman antibodies. **(A)** An example of membranes probed with Abcam anti-OPTN antibody. The membranes exhibit a lot of non-specific bands (red arrows) despite the optimisations detailed previously. The amount of total protein used for western blotting was 40 µg. **(B)** The membranes represent OPTN protein expression in BMDMs probed with Cayman antibody, **(i)** Different protein concentration of Mouse brain (MB) positive control used to determine band intensity of OPTN in western blot. **(ii)** An example of membranes probed with Cayman anti-OPTN antibody. Non-targeted shRNA (NTS), Different clones were used to determine the best clone combination for knocking down the OPTN gene in BMDMs (C 2+4, C 3+4 and C 2+3+4)

#### 4.3.2 Expression of OPTN during osteoclast development

Little is known about the expression of OPTN in osteoclasts. In this section, I investigated the expression of OPTN during osteoclast development using primary bone marrow cultures. Bone marrow cells from 3 months-old WT CD1 mice were isolated and cultured for 48 hours in the presence of M-CSF (100 ng/ml) followed by stimulation of adherent cells with RANKL (100 ng/ml) and M-CSF (25 ng/ml) for 5 days until osteoclasts were formed. Cells were lysed and protein was collected each day. OPTN, a 74-kDa protein, was detected using western blot analysis. Following

normalization to the 42-kDa  $\beta$ -actin, the expression of *Optn* was detected in BMDMs but not in total bone marrow cells. No significant difference in expression levels was found after the first day of RANKL treatment but *Optn* expression was increased by approximately 2-3 fold from day 3 onwards (Figure 4-2).

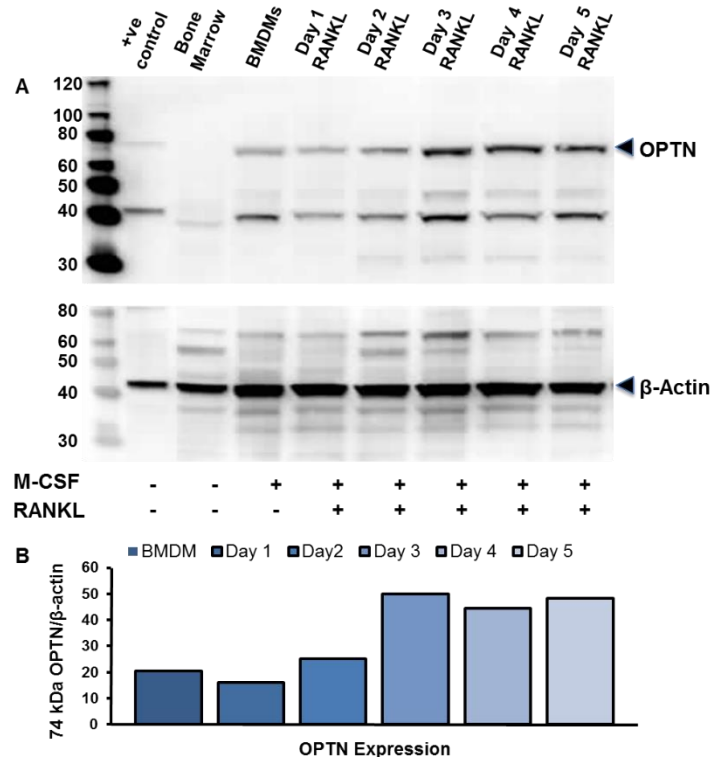


Figure 4-2: *Optn* expression during osteoclast formation. **(A)** *Optn* and  $\beta$ -actin expression from bone marrow, BMDMs and after treatment with RANKL (Day1-5). **(B)** Quantification of *Optn* expressed as a ratio of OPTN/ $\beta$ -actin. The amount of total protein used for western blotting was 40  $\mu$ g. Representative image of at least two independent experiments

### 4.3.3 Generation of lentiviral particles for *Optn* knockdown

#### 4.3.3.1 Restriction digest of lentiviral plasmid vectors

Plasmid DNA expressing shRNA targeted against *Optn* gene (or Non targeting vector) were grown from glycerol stocks and isolated as described in materials and methods section (2.2.3.3.6). Plasmid DNA were subjected to restriction enzyme

digestion and DNA sequencing in order to confirm vectors' orientation due to their tendency to recombine (Figure 4-3).

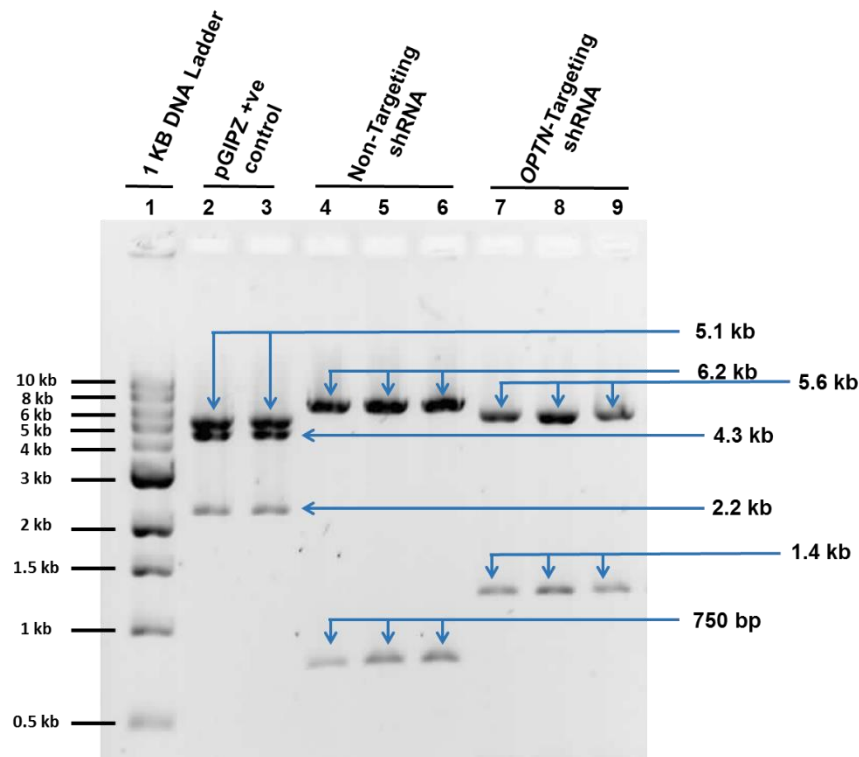


Figure 4-3: Gel electrophoresis analysis to diagnose lentiviral plasmid DNA. 10  $\mu$ l of each of the digested samples were loaded on a 1% agarose gel. Lane 1: 1 kb DNA ladder; lane 2-3: Positive control pGIPZ vector (expected bands size: 2.2, 4.3 and 5.1 kb); lane 4-6: Non-targeting shRNA vector (expected bands size: 750 bp and 6.2 kb); lane 7-9: *OPTN*-targeting vector (expected bands size: 1.4 and 5.6 kb).

#### 4.3.3.2 Optimization of puromycin selection concentration

Puromycin selection is an important step after transducing the cells because it efficiently eliminates the non-transduced cells. This process was done using BMDMs in order to generate a kill curve, which determines the minimum antibiotic concentration that kills 100% of the cell of choice in 2 days from the start of antibiotic selection. Puromycin concentration was determined according to the cell viability, which was measured using the Alamar Blue test. The kill curve revealed that 5  $\mu$ g/ml is the concentration of choice to kill the non-transduced cells in 2 days (Figure 4-4) which showed that more than 99.7% of cells were dead after 48-hour treatment.

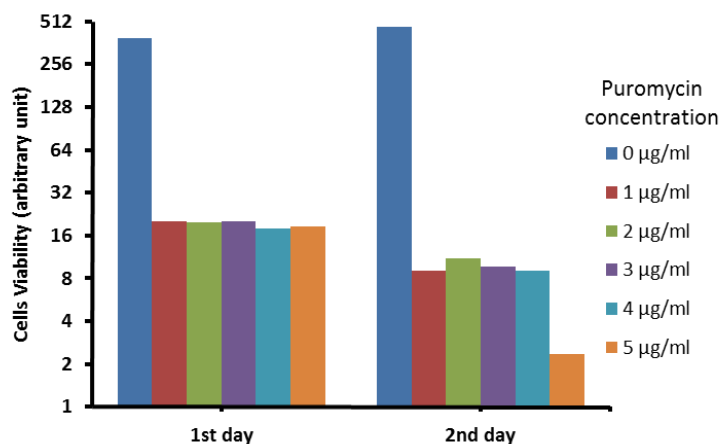


Figure 4-4: Killing curve to determine the puromycin concentration. BMDMs from CD1 mouse were seeded in 24 wells plate at  $1.5 \times 10^5$  per well for one day. Puromycin at different concentration (0-5 µg/ml) was added to the cells. The cells viability was assessed by Alamar Blue after 24 and 48 hours. Representative image of at least three independent experiments

#### 4.3.4 Effect of *Optn* depletion on RAW 264.7 cell line

RAW 264.7 is widely used in bone studies since these cells are capable of differentiating *in vitro* into osteoclasts. These cells have the further advantages of being easy to culture and relatively easy to generate stable transduced cells for genetic and regulatory manipulation (Collin-Osdoby and Osdoby, 2012). Accordingly, this cell line was chosen in order to investigate the effect of *Optn* depletion on osteoclast differentiation and the NFκB signalling pathway. Two lots of RAW 264.7 cells were used, as described below.

The first lot of these cells was provided in house and these cells expressed *Optn* to levels that can be detected in western blot (Figure 4-5). This was followed by a successful generation of stable *Optn*-depleted cell line. Briefly, four different shRNA lentiviral plasmid vectors (clones) were obtained from Sigma. These clones target different regions of the *Optn* gene sequence. Lentiviral particles were produced for each clone, as described previously (see section 2.2.3.3.6). After the lentiviral particles

were harvested, a Lenti-X GoStix from ClonTech was used to qualitatively assess their presence and concentration (Figure 4-6, D). Subsequently, RAW cells were transduced with lentivirus particles that targeted the *Optn* gene in addition to the non-targeted shRNA (negative control) and pGIPZ-expressing GFP positive control. Cells that transduced with the pGIPZ positive control were examined microscopically for the presence of TurboGFP expression (Figure 4-6, A). Puromycin was then used to select and establish a stable cell line. The survival of RAW cells after a 10-days selection with puromycin indicates that the transduction was successful (Figure 4-6, B). Knockdown efficiency was validated by qPCR and western blot (Figures 4-6, E and 4.5). The data revealed the best combination for knocking down the *OPTN* gene to be clones 2 and 4. Furthermore, *Optn* mRNA expression was found to be decreased five- to eight-folds in *Optn*-targeted cells as compared to non-targeted shRNA and untreated cells. However, these cells failed to form osteoclast-like cells when stimulated with RANKL (Figure 4-6, C).

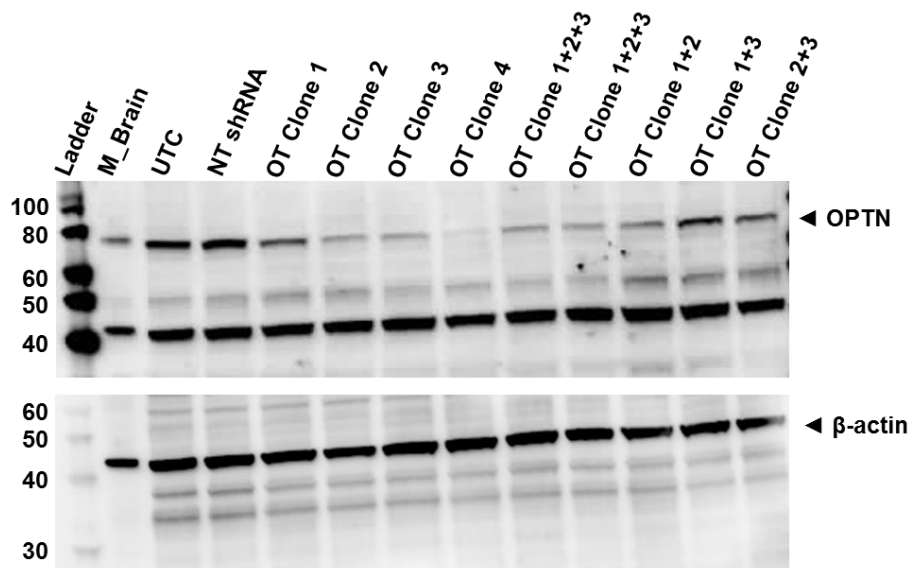


Figure 4-5: Western blot for knockdown of *Optn* in RAW 264.7 cell line. Individual and combined clones were used to determine the best clone combination for knocking down the *OPTN* gene. The total protein used for this western blot was 50 µg. untransduced cells (UTC), non-targeted (NT) cells and *OPTN*-targeted (OT).

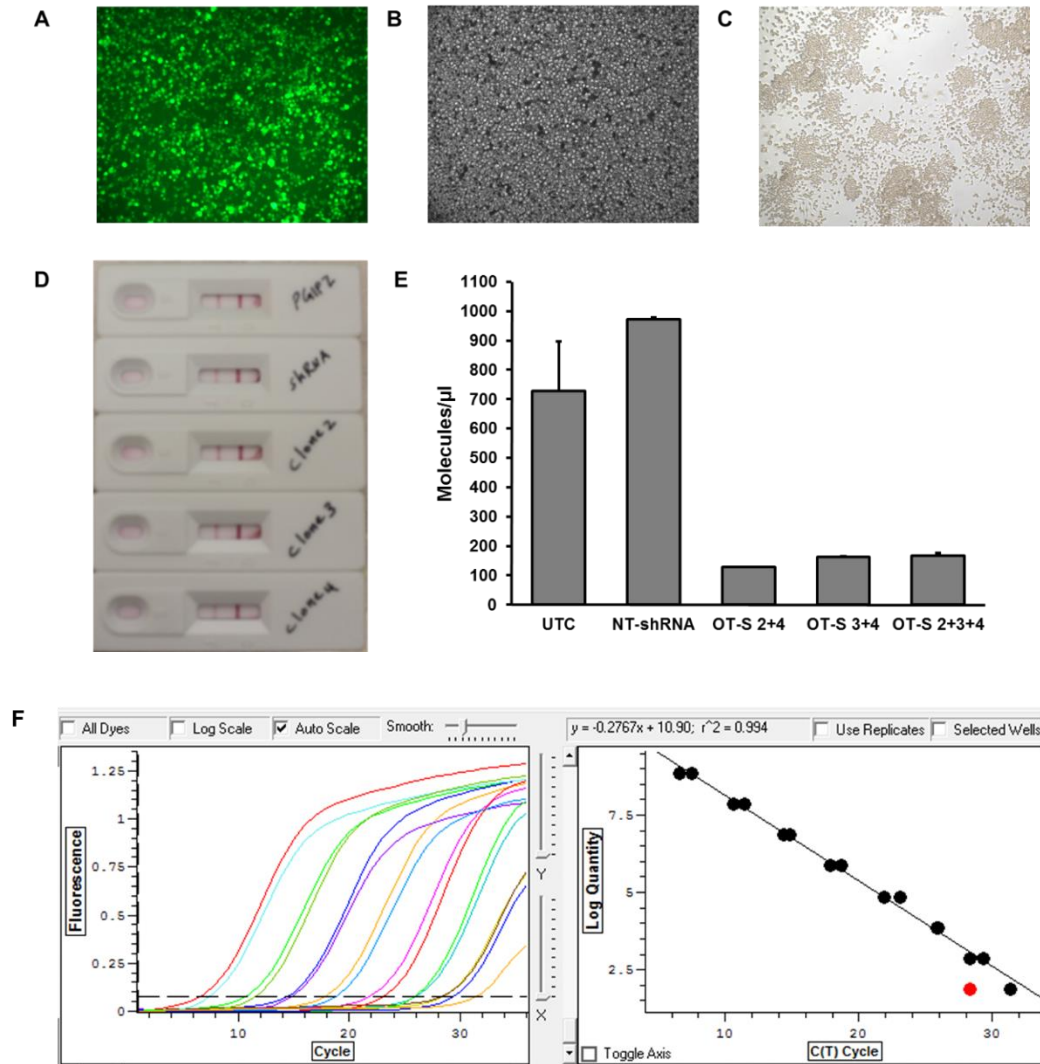


Figure 4-6: *Optn* knockdown in RAW 264.7 cells. **(A)** TurboGFP fluorescence from RAW cells 72 hours after co-transfection with pGIPZ (positive plasmid DNA) visualized at 10X magnification. **(B)** RAW cells post 10 days puromycin selection visualized at 5X magnification. **(C)** RAW cells 6 days post RANKL treatment. **(D)** Lenti-X GoStix, the letter 'C' on the strips indicates the control band and the T indicates the test band. Both bands appeared within 10 minutes according to the manufacture protocol. **(E)** mRNA expression of *Optn* of the first lot of RAW 264.7 cells. *Optn* mRNA expression was measured to assess *Optn* depletion in these cells using qPCR. The data show that *Optn* expression was successfully knocked down in *Optn*-targeted shRNA clones (OT-S 2+4, OT-S 3+4 and OT-S 2+3+4). The expression of *Optn* increased in non-targeted shRNA (NT-shRNA) cells as compared to untreated cells, probably because *Optn* expression increases in response to viral infections. The amount of total RNA used for cDNA synthesis was 2  $\mu$ g. **(F)** A standard curve was generated using a 10-fold dilution of a template amplified on MJ Research Chromo4 cycler. Each dilution was assayed in duplicate. The right picture is the amplification curves of the dilution series. On the left is the standard curve with the CT plotted against the log of the starting quantity of template for each dilution. The equation for the regression line and the  $r^2$  value are shown above the graph ( $y = -0.2767x + 10.90$ ,  $r^2 = 0.994$ ).



Due to the inability of the first lot of RAW cells to form osteoclasts, a second lot of RAW 264.7 cell line was purchased from ATCC. These cells were first checked to confirm their ability to form osteoclast upon stimulation with RANKL. Results showed that the second lot formed osteoclast-like cells in response to RANKL as expected (Figure 4-7, A). However, when *Optn* expression was assayed in these cells, results showed that they expressed very low or undetectable levels of *Optn* by western blot (Figure 4-7, B). Subsequently, these cells were stimulated with RANKL for 48-72 hours to see if *Optn* expression would increase during osteoclast formation. However, western blot analyses of protein extracts from these cells did not demonstrate apparent *Optn* bands after RANKL stimulation. Subsequently, qPCR was used in order to investigate the expression of *Optn* in these cells. Again, however, the new RAW cells were shown to have far lower levels of *Optn* than the control, which make the RAW 264.7 cells not a good model to study the effect of OPTN in bone metabolism. (Figure 4-7, C).

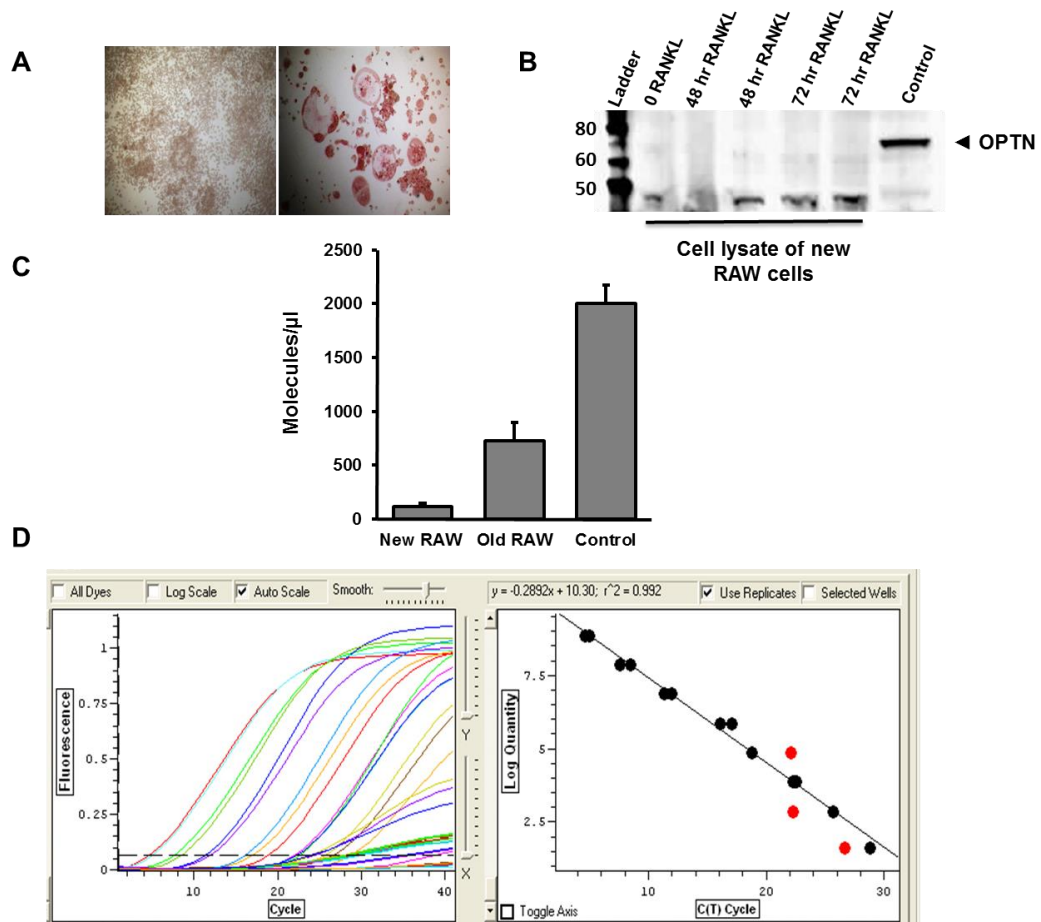


Figure 4-7: New lot of RAW 264.7 cell line . **(A)** representative pictures of RAW 264.7 cells without hRANKL (left) and the cells treated with hRANKL(100 ng/ml) until osteoclasts were formed (right). **(B)** Western Blot for new RAW 264.7 cells stimulated with hRANKL (100 ng/ml) for 48 and 72 hours. Optn band only present in the positive control extracted from the mouse brain. The total protein used for this western blot was 100  $\mu$ g. **(C)** The graph compares mRNA expression of *Optn* in the new RAW cells, old RAW cells and control. The expression of *Optn* in the new lot of RAW cells purchased from ATCC is very low compared to the positive control, which was extracted from mouse brains (MB +ve control). The amount of total RNA used for cDNA synthesis was 2  $\mu$ g. **(D)** A standard curve was generated using a 10-fold dilution of a template amplified on MJ Research Chromo4 cycler. Each dilution was assayed in duplicate. The right picture is the amplification curves of the dilution series. On the left is the standard curve with the CT plotted against the log of the starting quantity of template for each dilution. The equation for the regression line and the  $r^2$  value are shown above the graph ( $y = 0.2892x + 10.30$ ,  $r^2 = 0.992$ ).

#### 4.3.5 *Effect of Optn depletion on osteoclast differentiation from primary BMDMs*

After investigating two different clones of RAW 264 cell lines, it became clear to me that this cell line was not ideal for investigating the effect of *Optn* knock down on osteoclast differentiation. This is because the clone that formed osteoclasts upon RANKL stimulation expressed very low amount of *Optn*. So in this section I used a primary bone marrow culture which represents a better model than RAW 264 cell line to study osteoclast differentiation. However, primary cells have limited life span and are more difficult to transfect. The first step in knocking down *Optn* in BMDM was to generate enough lentiviral particles since BMDM are more difficult to transduce and they require a high MOI. The first sign of transfection efficiency was the presence of TurboGFP expression during the production of lentiviral particles (Figure 4-8, A). After harvesting and concentrating the lentiviral particles, a Lenti-X GoStix from ClonTech was used to qualitatively assess the presence and the concentration of the lentiviral particles in order to determine whether lentivirus production was within a usable range (Figure 4-8, B). The cell survival after puromycin selection is another sign for a successful transduction. At this stage after selection, the cells were transduced with lentivirus particles expressing GFP (positive control) and examined microscopically for the presence of TurboGFP expression as seen in figure (4-8, C). In addition, the cells were transduced with lentiviral particles expressing shRNA targeting *Optn* or non-targeting control. Protein was extracted from transduced BMDMs in order to assess these cells for reduction in gene activity. These tests for knockdown of *Optn* were performed for each experiment prior to investigation of the effect of *Optn* depletion on osteoclast formation and survival as described later in this chapter (Figure 4-9 and 4-12). The effect of knockdown of *Optn* during different stages of osteoclast development was also performed to make sure *Optn* knockdown persisted throughout osteoclast differentiation stages (Figure 4-8, D). Approximately 54-75% of *Optn* knockdown level was achieved in cells transduced with lentiviral particles containing shRNA-targeting *Optn* compared to non-targeting particles at different stages of osteoclast development. These results indicate that the knockdown effect persists during later stages of osteoclast development (Figure 4-8, E).

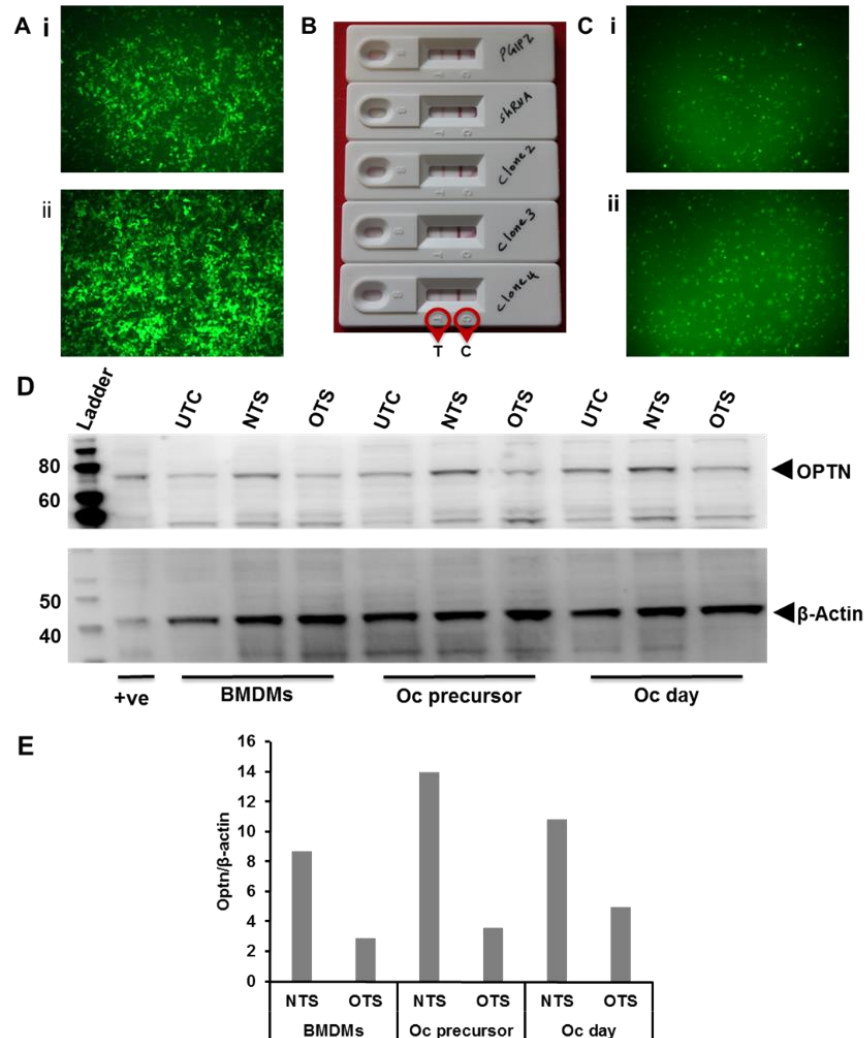


Figure 4-8: OPTN knockdown in BMDMs. **A. (i and ii)** TurboGFP fluorescence from HEK293T 24 and 48 hours respectively after co-transfection with pGIPZ (positive plasmid DNA) and Trans-Lentiviral packaging mix visualized at 10X magnification. **B.** Lenti-X GoStix, the C letter on the strips indicates the control band and the T indicates the test band. Both bands appeared within 10 minutes according to the manufacture protocol. **C. (i and ii)** TurboGFP fluorescence from BMDMs 24 and 48 hours post lentiviral transduction, visualized at 10X magnification. **D.** Western blot analysis of cell lysate shows the expression of OPTN and  $\beta$ -actin of transduced cells at day 3 post RANKL treatment (osteoclast precursors) and day 5 (osteoclast). Total protein used for this western blot was 40  $\mu$ g. (UTC: Untransfected Cells, NTS: Non-targeting shRNA, OTS: *OPTN*-targeted shRNA, OC: osteoclast). The levels of Optn expression in NTS lanes is higher than UTC lanes because the expression of Optn is induced in response to virus infection (Mankouri et al., 2010). **E.** Quantification of Optn expression at different stages of osteoclast development. Optn expression was reduced in BMDMs by 67% and at day 3 by 75% in osteoclast precursors and 54% in osteoclast which were transduced with Optn-targeting shRNA lentivirus compared with control group (cells infected with non-targeting shRNA).

#### 4.3.5.1 Effect of *Optn* depletion on osteoclast formation and fusion

Bone marrow cells from wild type CD1 mice were isolated and cultured for 48 hours in the presence of M-CSF (100 ng/ml). The adherent BMDMs were then transduced for 2 days with either lentiviral particles containing shRNA targeted against the *Optn* gene or negative control particles (non-targeting lentiviral particles that activate the RNAi pathway but do not target any mouse gene). Cell lysates of transduced cells post selection were collected and subjected to western blot analysis. *Optn* expression was successfully knocked down in BMDMs by ~ 75% in cells expressing shRNA targeting *Optn* compared with negative control (Figure 4-9).

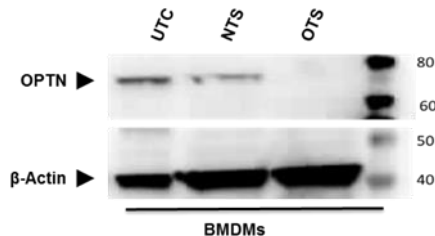


Figure 4-9: Confirmation the knockdown of *Optn*. Western blot analysis of BMDMs (untransfected cells, UTC), BMDMs infected with non-targeting shRNA (NTS) and BMDMs which were infected by lentivirus carrying shRNA targeting *Optn* (OTS). The total protein used was 50 µg.

Transduced cells post selection were plated in 96 well plates and stimulated with M-CSF (25 ng/ml) and RANKL (25 and 50 ng/ml) until osteoclasts were formed. Cells were fixed and stained for TRAcP activity as described in the methods section (2.2.3.3.5). TRAcP positive multinucleated osteoclasts (> 3 nuclei) were counted and numbers were compared to the non-targeted negative control. Large osteoclasts (> 10 nuclei) were also counted to assess the effect of *Optn* knockdown on osteoclast size. (see figure 4-10, B and C). The results revealed that knockdown of *Optn* in BMDMs significantly enhanced osteoclast differentiation as well as the formation of hypernucleated osteoclasts when compared to non-targeting controls BMDMs. The osteoclasts formed from untreated BMDMs also were counted (Figure 4-10, A). Since these cells were not subjected to lentiviral transduction and antibiotic selection, they formed more osteoclasts compared to non-targeting control. Additionally, the osteoclasts from untreated cells were formed 2-3 days earlier than the knocked down cells.

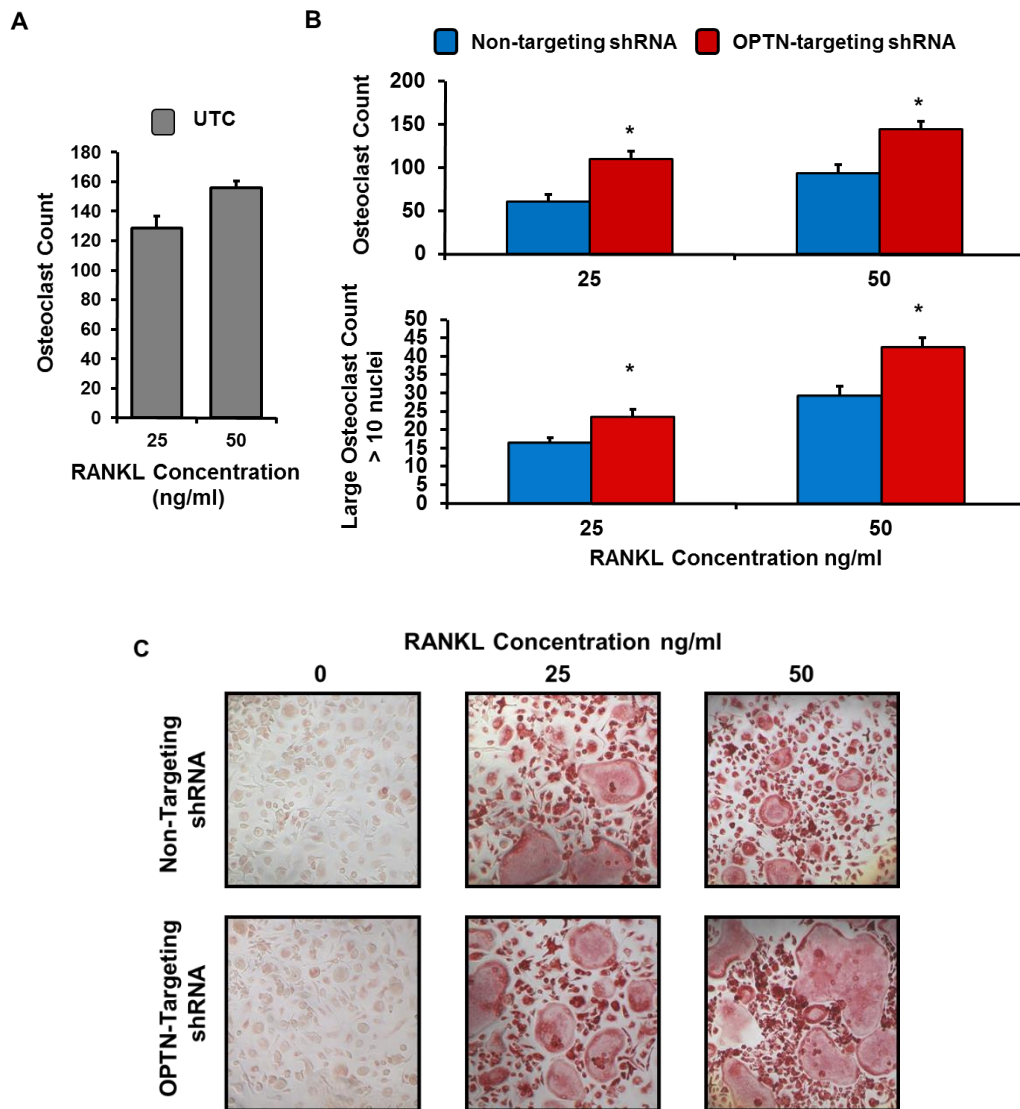


Figure 4-10: *Optn* depletion in BMDMs enhances osteoclast formation and fusion. **(A)** Numbers of multinucleated osteoclasts formed from untreated BMDMs. **(B)** Bar chart showing numbers of multinucleated osteoclasts formed in *Optn* depleted cells compared to the non-targeted negative control (values are means  $\pm$  SEM from 2 independent experiment, \*  $P < 0.05$ ). **(C)** Representative pictures of TRAcP positive multinucleated osteoclasts from *Optn* depleted cells and the non-targeted cells magnified at 10X.

#### 4.3.5.2 Effect of *Optn* depletion on osteoclast survival

For osteoclast survival experiment, one plate was fixed and TRAcP stained when osteoclasts were formed (0 hour). RANKL was withdrawn from the culture media and plates were fixed and stained with TRAcP at different time points post RANKL withdrawal (12, 24, 48 and 72 hours). Results showed that osteoclast formed from *Optn*-depleted BMDMs had higher survival 12 hours post RANKL withdrawal

compared to non-targeting control cells (see figure 4-11). Osteoclast number at the other time points is also higher in *Optn*-depleted cells but this was not significant.

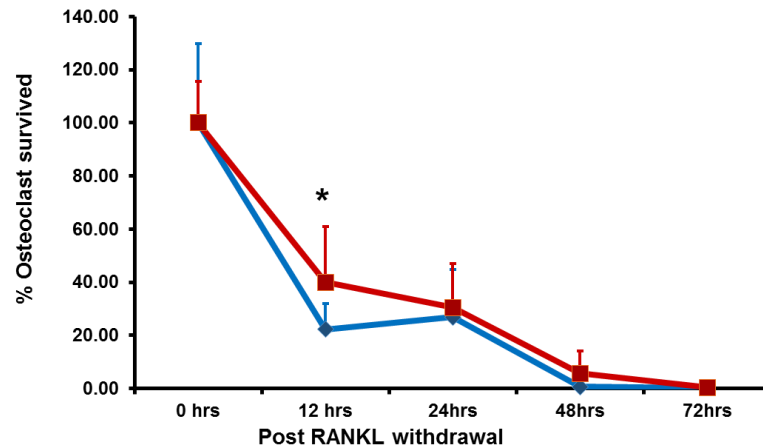


Figure 4-11: Osteoclast survival post RANKL withdrawal. Osteoclast survival was 44.1% higher in *Optn*-depleted cells after 12 hours post RANKL withdrawal compared to non-depleted cells. Osteoclast numbers at other time points were also higher in *Optn* depleted cells but this was not significant (values are means  $\pm$  SD from one experiment, \*  $P < 0.05$ ).

#### 4.3.5.3 Effect of *Optn* depletion on NF $\kappa$ B signaling pathway

BMDMs were transfected with the lentiviral particles expressing shRNA targeted against the *Optn* gene for two days. Following antibiotic selection with Puromycin (5  $\mu$ g/ml), *Optn* knockdown was confirmed in BMDMs (Figure 4-12). The cells were then transduced using lentiviral NF $\kappa$ B luciferase reporter for a further two days. The cells were then seeded in 96-well plates and stimulated with RANKL and M-CSF. Luciferase activity was measured with a SteadyGlo-luciferase reporter assay system at the basal level and following RANKL stimulation (Figure 4-13). Results showed that the NF $\kappa$ B activity was increased significantly in the *Optn*-depleted cells at the basal level and 72 hours after stimulation with RANKL compared to non-depleted cells. At day 5 post RANKL, the increase in NF $\kappa$ B activity was not significant.

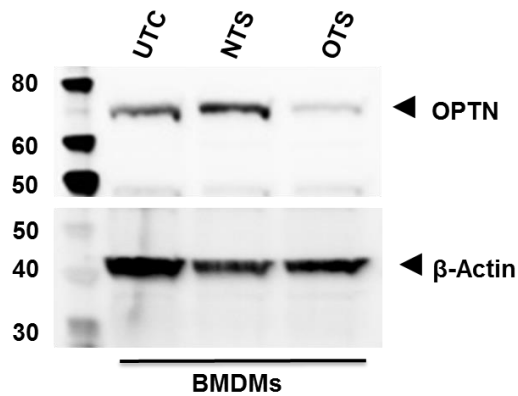


Figure 4-12: Confirmation of *Optn* knockdown by Western blot analysis of BMDMs (untransfected cells, UTC), BMDMs infected with non-targeting shRNA (NTS) and BMDMs which were infected by lentivirus carrying shRNA targeting *Optn* (OTS). The total protein used was 50  $\mu$ g.

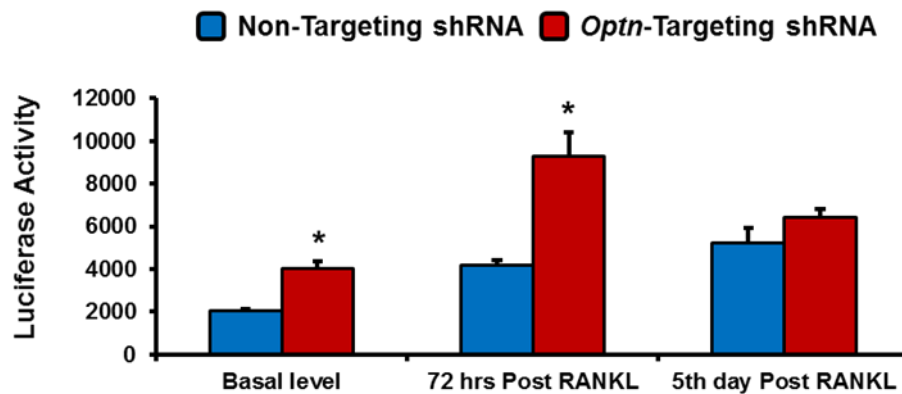


Figure 4-13: NF $\kappa$ B Activation is increased in *Optn*-depleted cells during osteoclast formation. *Optn*-depleted BMDMs were transduced with lentiviral particles expressing NF $\kappa$ B luciferase reporter and luciferase activity measured with a SteadyGlo-luciferase reporter assay system at the basal level and following RANKL stimulation (100 ng/ml) at 72 hours and 5<sup>th</sup> day (values are means  $\pm$  SEM, \*\*  $P \leq 0.01$ ). Representative image of at least two independent experiments



#### 4.4 Discussion

The role of OPTN in PDB and bone metabolism is unknown but it could be predicted from the literature. It has been reported that OPTN has a regulatory role in NF $\kappa$ B signalling and vesicular trafficking pathways, both of which have been implicated in osteoclast biology (Park et al., 2010; Sudhakar et al., 2009). Furthermore, several studies point to the role of OPTN during viral infection (Mankouri et al., 2010). The viral infection was suggested as an environmental factor that may exacerbate PDB (Mills and Singer, 1976a). Also OPTN was found to have a role in autophagy (Korac et al., 2013; Wild et al., 2011), a recent mechanism implicated in PDB (L. Hocking et al., 2010). Collectively, these findings suggest that OPTN may have an important role in bone metabolism and the development of PDB. This chapter demonstrates that *Optn* was expressed in BMDMs and its expression was increased during osteoclast development. In addition, *Optn* depleted cells in mouse BMDMs enhanced osteoclast formation, survival and increased RANKL-induced NF $\kappa$ B activation.

The expression of *Optn* in BMDMs was assessed using western blot. *Optn* was detected in BMDMs but its expression in total bone marrow cells was very low suggesting that OPTN may have important role in BMDM lineage cells. The detection of *Optn* in BMDMs post M-CSF treatment revealed its role in earlier stages of osteoclast precursors' formation. The expression of *Optn* during osteoclast differentiation was investigated after stimulating BMDMs with M-CSF and RANKL. The expression of *Optn* remained steady during the first two days of osteoclast development but a considerable increase in expression was noticeable from day three onwards until osteoclasts were formed. This suggest that OPTN may exerts its effect during later stages of osteoclast development.

The macrophage-like cells RAW 264.7 are used extensively in the literature to study the osteoclast signalling pathway. These cells exhibit classic osteoclast signalling and form osteoclast like cells in response to RANKL treatment without the need for the M-CSF (Collin-Osdoby and Osdoby, 2012) . Originally RAW 264.7 cells were chosen to study the osteoclast signalling pathway after generation of stable

transcend cells. However, the initial cell line did not form osteoclasts after RANKL treatment and the second did not express detectable levels of *Optn*. Interestingly, these findings suggest that *OPTN* may act as a negative regulator to osteoclast formation but further investigations are required, for instance, a microarray assay could be performed on the two clones of RAW 264.7 cells in order to investigate the expression state of a large number of osteoclastogenic genes or to overexpress the *Optn* in RAW cells which formed osteoclasts. Indeed, overexpression of *Optn* in RAW 264.7 cells that did not express detectable levels of *Optn* carried out later by our group exhibited a marked reduction in the number and size of multinucleated TRAcP positive cells observed upon stimulation with RANKL (Obaid et al., 2015) (Figure 4-14).

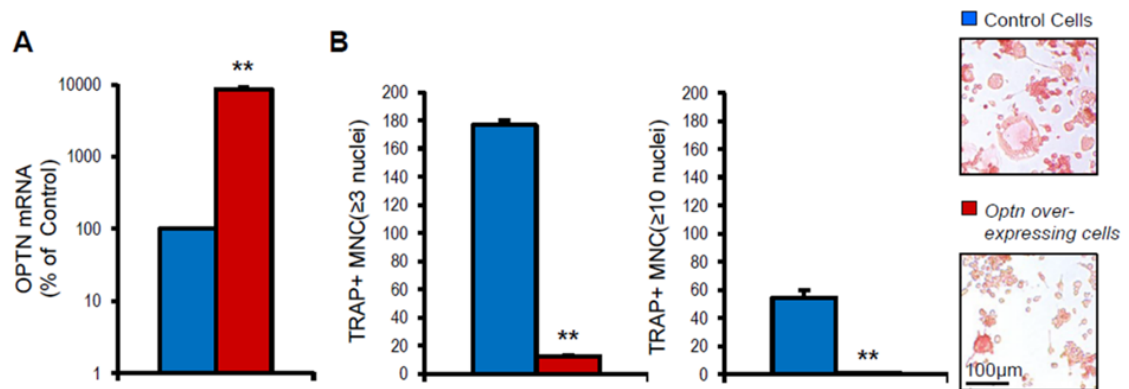


Figure 4-14: Reduced formation of TRAcP positive multinucleated cells in *Optn* overexpressing RAW 264.7 cells. (A) A representative diagram illustrates the *Optn* mRNA expression measured by qRT-PCR in control cells (blue bar) compared to overexpressing *Optn* cells. (B) This diagram shows that the number and size of TRAcP positive multinucleated cells are significantly reduced in RAW cells overexpressing *Optn* compared to control cells. Adapted from (Obaid et al., 2015). \*  $P < 0.01$

Next, mouse primary BMDMs were explored as a model for osteoclast differentiation because they represent a better model to study osteoclast function and also due to high level of *OPTN* expression. *Optn* was knocked down in BMDMs obtained from WT mice using lentiviral particles expressing shRNA targeted against the *Optn* gene. Non-targeting shRNA lentiviral particles were also used as a negative control. Approximately 75% *Optn* knockdown level was achieved in transduced

BMDMs. Data yielded from this experiment showed that the numbers of osteoclasts formed from *Optn*-depleted BMDMs were significantly higher than those formed from non-targeted cells. Similarly, large osteoclasts (>10 nuclei) were significantly higher in *Optn*-depleted BMDMs compared to negative control. Data also showed that the *Optn* depletion in BMDMs increased the osteoclast survival by 45% after 12 hours of RANKL withdrawal in knock down cells compared to control. The numbers of osteoclast survived at other time points were also high in *Optn*-depleted cells but this was not significant. These data suggest that *Optn* acts as a negative regulator of osteoclast differentiation. In order to investigate the molecular mechanism by which *Optn* inhibits osteoclast differentiation, I investigated the effect of *Optn* depletion on RANKL-induced NF $\kappa$ B activation which was assessed using lentiviral NF $\kappa$ B luciferase reporter assay. The activity of the NF $\kappa$ B was higher in *Optn* knockdown cells compared to negative control particularly on the third day post RANKL treatment. These data suggest that *Optn* exerts its negative regulatory effect at least in part by inhibiting RANKL-induced NF $\kappa$ B signaling.

NF $\kappa$ B is a crucial signalling pathway in osteoclast biology. Inhibition of NF $\kappa$ B pathway was shown to inhibit osteoclast formation and thus the resorption (Abu-Amer, 2013). The data presented in this chapter suggested that the depletion of *Optn* might enhance the activation of NF $\kappa$ B signalling, which in turn mediates RANKL-induced osteoclastogenesis. My study agrees with previous experiments in cell lines used to discover the role of OPTN in glaucoma and ALS. In one study, OPTN was found to inhibit TNF $\alpha$ -induced NF $\kappa$ B activity in Hek 293 cells and when *OPTN* is knocked down, NF $\kappa$ B activity was enhanced compared to controls (Zhu et al., 2007). In the same study, OPTN was found to interact with ubiquitinated receptor interacting protein (RIP) after the stimulation of HeLa cells with TNF $\alpha$  and authors suggested that this interaction may compete with IKK $\gamma$  (NEMO) binding for polyubiquitinated RIP because OPTN has a UBD similar to that present in NEMO. Moreover, the interaction of OPTN with polyubiquitinated RIP was not cell-type dependant as they obtained the same results when they used the mouse embryonic fibroblasts (Zhu et al., 2007). Another study found that NF $\kappa$ B binding site was recognized in *OPTN* promoter

(Sudhakar et al., 2009). This study also showed that the *OPTN* promoter became active in HeLa and A549 cells upon treatment of cells with TNF $\alpha$ . In addition, they reported that the promoter activity was inhibited and the basal promoter activity was reduced post TNF $\alpha$  treatment when they introduced a mutation at the NF $\kappa$ B site. Moreover, they suggested that *OPTN* promoter was regulated by I $\kappa$ B-NF $\kappa$ B pathway since overexpression of I $\kappa$ B $\alpha$  leads to the inhibition of promoter activity. When they overexpressed *OPTN* in these cells, the TNF $\alpha$ -induced NF $\kappa$ B activity was inhibited while the basal activity was not affected. On the other hand, *OPTN* depletion using shRNA resulted in upregulation of both basal and TNF $\alpha$ -induced NF $\kappa$ B activity (Sudhakar et al., 2009). Similarly, the NF $\kappa$ B activity was increased in a recent study when *OPTN* was knocked down in neuron cells, which enhanced the neuronal cell death and *OPTN* overexpression counteracted the toxic effect of *OPTN* depletion in these cells (Shen et al., 2011).

In other studies *OPTN* has been found to interact with two deubiquitinating enzymes, CYLD and A20, which are induced by NF $\kappa$ B and provide a negative feedback loop to regulate the NF $\kappa$ B activity (Harhaj and Dixit, 2010). Interestingly, these two enzymes are binding-partner to *OPTN* (Chalasani et al., 2008; Nagabhushana et al., 2011). CYLD was found to suppress the NF $\kappa$ B activation by removing the K63-linked polyubiquitin chains from TRAF2, and TRAF6 (Massoumi, 2010). CYLD depletion in macrophages was found to enhance osteoclastogenesis and animal lacking *Cyld* develop osteoporosis (Jin et al., 2008). Studies of A20 showed that this enzyme removes K63-linked polyubiquitin chains and then degrades RIP1, which in turn inhibits NF $\kappa$ B activity. Similar to CYLD, A20 deficiency in macrophages accelerates osteoclastogenesis and A20 knockout mice develop severe erosive polyarthritis due to increased serum levels of circulating inflammatory cytokines and prolonged NF $\kappa$ B activity in macrophages (Matmati et al., 2011).

In the knock down experiment, I have used multiple controls to make sure the findings are attributable to *Optn* depletion and not due to other confounding factors. The untreated cells control was used to make sure the cells formed osteoclast after

treatment with M-CSF and RANKL as expected. The non-targeting control shRNA was used as a control for the activation of the RNAi pathway and also to control for antibiotic selection. A positive control in the form of GFP was used to make sure the cells were successfully transduced with the lentiviral particles. The utilisation of an empty vector control would have been favourable to act as a control for lentiviral transfection. This was not used in my experiment due to the limited number of primary cells obtained from an individual mouse. Transduction of primary macrophage cells was very difficult and required large number of cells and a large amount of lentiviral particles. The experiments were performed as three independent replicates and both NTC and OPTN-targeted cells were treated with the same lentiviral particles with the only difference being the shRNA sequence that targets the OPTN gene. Additionally, the fact that overexpression of OPTN inhibits osteoclast formation confirms that the findings presented in this chapter are due to OPTN knock down.

The promoter-reporter assays are widely used since they are sensitive, reproducible and useful technique for investigating endpoint pathway regulation assays. Using an internal control reporter (Renilla luciferase) beside the test reporter (Firefly luciferase) would have been useful for normalizing the data in order to reduce variability between treatments. However, it is important to note that, primary cells have a limited lifespan in culture and are susceptible to the toxic effects of multiple transfection. Although the luciferase reporter assay that has been used in this study lacks this internal control, cells were subjected to antibiotic selection to ensure that surviving cells have retained the expression plasmid. Equal number of viable cells were then re-plated followed by addition of equal amount of lentiviral NF $\kappa$ B luciferase reporter particles. By doing so, the starting cell number is adjusted which minimize the variability between samples. In addition, a positive control, pGIPZ, was used to microscopically examine the transfection efficiency through the green fluorescent protein (GFP) expression.

The luciferase reporter assays are not sensitive to detect the early stages of NF $\kappa$ B activation; further investigations are required for this purpose. This is because the reporter genes, which in this case is the luciferase gene, are placed under the control of a basal promoter element (TATA box) joined to tandem repeats of NF $\kappa$ B

Transcriptional Response Element (TRE). Thus, the expression level of the reporter gene might be affected by transcription factors other than NF $\kappa$ B. In addition, the enzymatic activity of luciferase also could be influenced by interferences with downstream transduction machinery. Therefore, in order to monitor the early stage of NF $\kappa$ B activation, the kinetics of I $\kappa$ B degradation and re-synthesis can be estimated using western blot analysis, electrophoretic mobility shift assay (EMSA) or chromatin immunoprecipitation assay (ChIP) (Jin and Ralston, 2012; Renard et al., 2001).

In conclusion, this chapter reports that *Optn* is expressed in BMDMs and during osteoclast development. Furthermore, *Optn* depletion promotes osteoclast differentiation, fusion and survival possibly by activating NF $\kappa$ B signalling pathway in response to RANKL. The findings from this study identified a novel role of OPTN in osteoclast development in response to RANKL stimulation. However, the work described in this chapter is based on an *in vitro* model and further studies using an *in vivo* model will be required to confirm this effect (see chapter 5).

**CHAPTER FIVE**

**THE EFFECT OF LOSS OF FUNCTION  
MUTATION IN OPTN ON OSTEOCLAST AND  
OSTEOBLAST DIFFERENTIATION**

## 5 The Effect of Loss of Function Mutation in *Optn* on Osteoclast and Osteoblast Differentiation

### 5.1 Summary

The aim of this chapter was to investigate the role of *Optn* in bone turnover using a mouse model (*Optn*<sup>D477N/D477N</sup>), which harbours a D477N point mutation in the polyubiquitin binding domain of the *Optn* gene. This loss of function mutation encodes a defective protein that is unable to bind K63 polyubiquitin chain (Gleason et al., 2011).

In agreement with the previous *Optn* depletion data discussed in chapter 4, the number of multinucleated osteoclasts (>3 nuclei) formed from mutant bone marrow cells was significantly higher (239±17) than that of multinucleated osteoclasts formed from WT (195±22;  $P<0.001$ ) *in vitro*. Additionally, the number of large osteoclasts (>10 nuclei) was significantly higher in mutant cells compared to WT cells. Furthermore, following RANKL stimulation, the NFκB activity based on luciferase reporter assay was greater in *Optn*<sup>D477N</sup> mutant cells than in WT cells. The data also showed that *Optn* was expressed in all stages of osteoblasts and no significant difference was observed in the expression at different stages of osteoblast differentiation from WT and mutant mice. Similarly, the bone nodule formation by osteoblasts from knock-in mice showed no significant difference when compared to WT.

It can thus be concluded that the results of the *in vitro* work obtained from *Optn* knockdown experiments and those from the *Optn*<sup>D477N/D477N</sup> knock-in model are consistent. The data also suggested for the first time that optineurin acts as a negative regulators of osteoclast differentiation. This may partly explain optineurin's role in PDB susceptibility but further *in vivo* studies will be required to examine the skeletal phenotype of *Optn*<sup>D477N/D477N</sup> mice (chapter 6).



## 5.2 Introduction

Data from the previous chapter showed that *Optn* was expressed during osteoclast formation and its expression significantly increased during later stages of osteoclast development. In addition, *Optn*-depletion in macrophages derived from mouse bone marrow enhanced osteoclast formation, fusion and survival, whilst also increasing RANKL-induced NF $\kappa$ B activation. Although the knockdown approach using lentiviral vector-mediated expression of shRNA is recommended particularly when cells are difficult to transfect, it has a number of limitations. First of all, it is a time-consuming experiment, because BMDMs require a large dosage of virus (MOI) to be transduced. Furthermore, the experiment also involves subjecting BMDMs to additional interventions, such as use of Polybrene during transduction and Puromycin for selection.

Therefore, the aim of this chapter is to investigate if loss of function mutation in *Optn* affects osteoclast differentiation *in vivo* using *Optn*<sup>D477N/D477N</sup> mouse and compare the results with the *in vitro* findings obtained from the *Optn* knockdown experiment. The *Optn*<sup>D477N/D477N</sup> mouse model was generated by introducing a point mutation with Asp-477 of the polyubiquitin-binding domain mutated to Asn in exon 12 of the *Optn* gene. The D477N mutation abrogated the interaction of *Optn* with K63 polyubiquitin-binding chains (Gleason et al., 2011). This loss of function mutation is equivalent to the OPTN (D474N) human mutant, which also causes a defective binding to polyubiquitin. In this study, the D477N polyubiquitin binding-defective mutant was found to significantly reduce the lipopolysaccharide-induced TBK1 activity, which in turn led to the reduction of phosphorylation of IRF3 and the production of IFN $\beta$  (Gleason et al., 2011)

In previous studies, the enzyme CYLD in macrophages was described as a negative regulator of RANK signalling via its deubiquitinase activity (Jin et al., 2008). It has been found that CYLD downregulated the NF $\kappa$ B activity through the inhibition of

TRAF6 ubiquitination and was recruited to TRAF6 by its interaction with p62. In addition, CYLD was identified as an OPTN-interacting protein (Nagabhushana et al., 2011) while OPTN was suggested to be involved as a negative regulator in the NFκB signalling pathway (Akizuki et al., 2013; Nagabhushana et al., 2011; Zhu et al., 2007). However, it is still unclear through what mechanism OPTN acts as a regulatory factor in the NFκB signalling pathway in bone cells. In addition, *OPTN* was recently demonstrated to be a candidate gene of PDB (Albagha et al., 2010).. The role of *Optn* in osteoblasts of WT and mutant mice is also investigated in this chapter, as is the interaction of *Cyld* with *Optn* in order to explain, to a certain extent, the role of optineurin in RANKL-inducing osteoclastogenesis and NFκB signalling pathway.

### 5.3 Results

#### 5.3.1 Effect of *Optn*<sup>D477N</sup> mutation on osteoclast formation in *Optn*<sup>D477N/D477N</sup> mice

As discussed in chapter 4, *Optn* knockdown in BMDMs enhanced osteoclast number and size as compared with non-targeting controls. Therefore, the effect of *Optn*<sup>D477N</sup> mutation on osteoclast differentiation *in vitro* was investigated using BMDMs from *Optn*<sup>D477N/D477N</sup> mice. Bone marrow cells from WT and *Optn*<sup>D477N/D477N</sup> mice were isolated and cultured in the presence of M-CSF and RANKL until osteoclasts were formed. TRAcP positive multinucleated osteoclasts (> 3 nuclei) and large osteoclasts (> 10 nuclei) were counted and numbers were compared to the WT control (Figure 5-1).

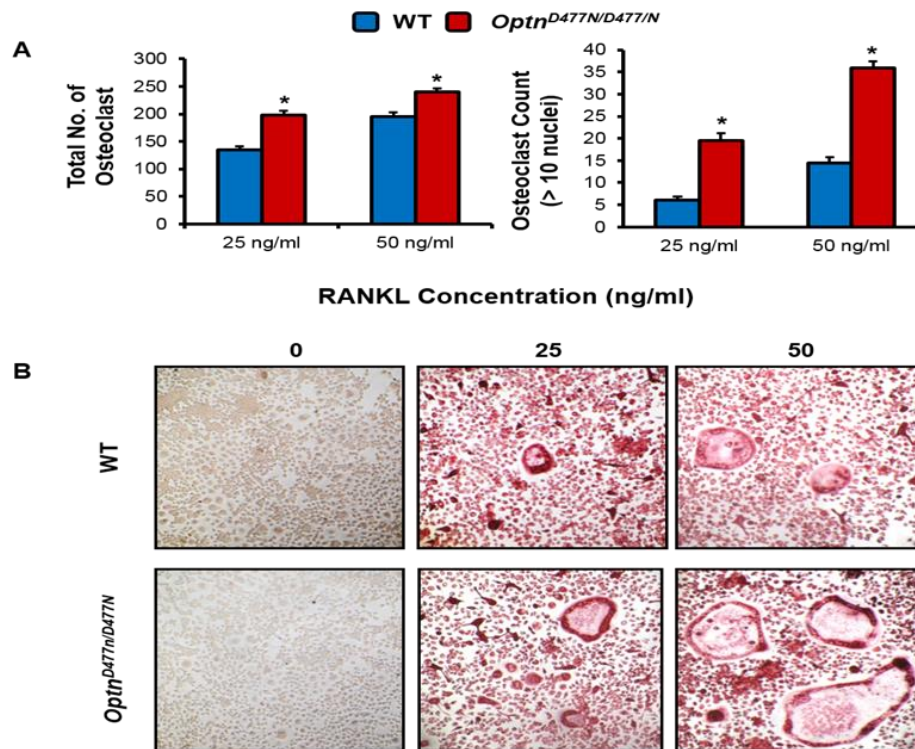


Figure 5-1: Osteoclast formation and fusion are enhanced in *Optn*<sup>D477N/D477N</sup> mouse BMDMs. **(A)** Multinucleated osteoclasts formed from *Optn*<sup>D477N/D477N</sup> were higher and larger compared to WT mice (values are means  $\pm$  SEM from 3 independent experiments, \*  $P < 0.05$ ). **(B)** Representative pictures of TRAcP positive multinucleated osteoclasts from WT and *Optn*<sup>D477N</sup> mutant cells magnified at 10X.

The results revealed that osteoclast formation and number of hypernucleated cells were significantly promoted by the *Optn*<sup>D477N</sup> mutation, replicating exactly the phenotype observed in the *Optn* knockdown experiment.

### 5.3.2 Expression of *Optn* during osteoclast (OC) development in Wild Type (WT) and *Optn*<sup>D477N/D477N</sup> mice

Compared to cultures of BMDMs from WT, cultures of BMDMs from *Optn*<sup>D477N/D477N</sup> presented more and larger osteoclasts. Therefore, *Optn* expression during osteoclast differentiation was evaluated in BMDMs under basal conditions and post-stimulation with M-CSF and RANKL in order to compare the expression pattern of *Optn* in both WT and *Optn*<sup>D477N/D477N</sup> mice. Bone marrow cells were extracted from WT BL6 and *Optn*<sup>D477N/D477N</sup> mice and cultured for 2 days in the presence of M-CSF (100 ng/ml). The adherent BMDMs were then stimulated with RANKL (100 ng/ml) and low M-CSF (25 ng/ml) until osteoclasts were formed. Western blot was used to analyse *Optn* expression in all lysates. The bands were quantitatively measured and showed that the expression of *Optn* was increased during osteoclast formation in both WT and *Optn*<sup>D477N/D477N</sup> mice, although the expression of the mutant protein was higher than that of WT (Figure 5-2).

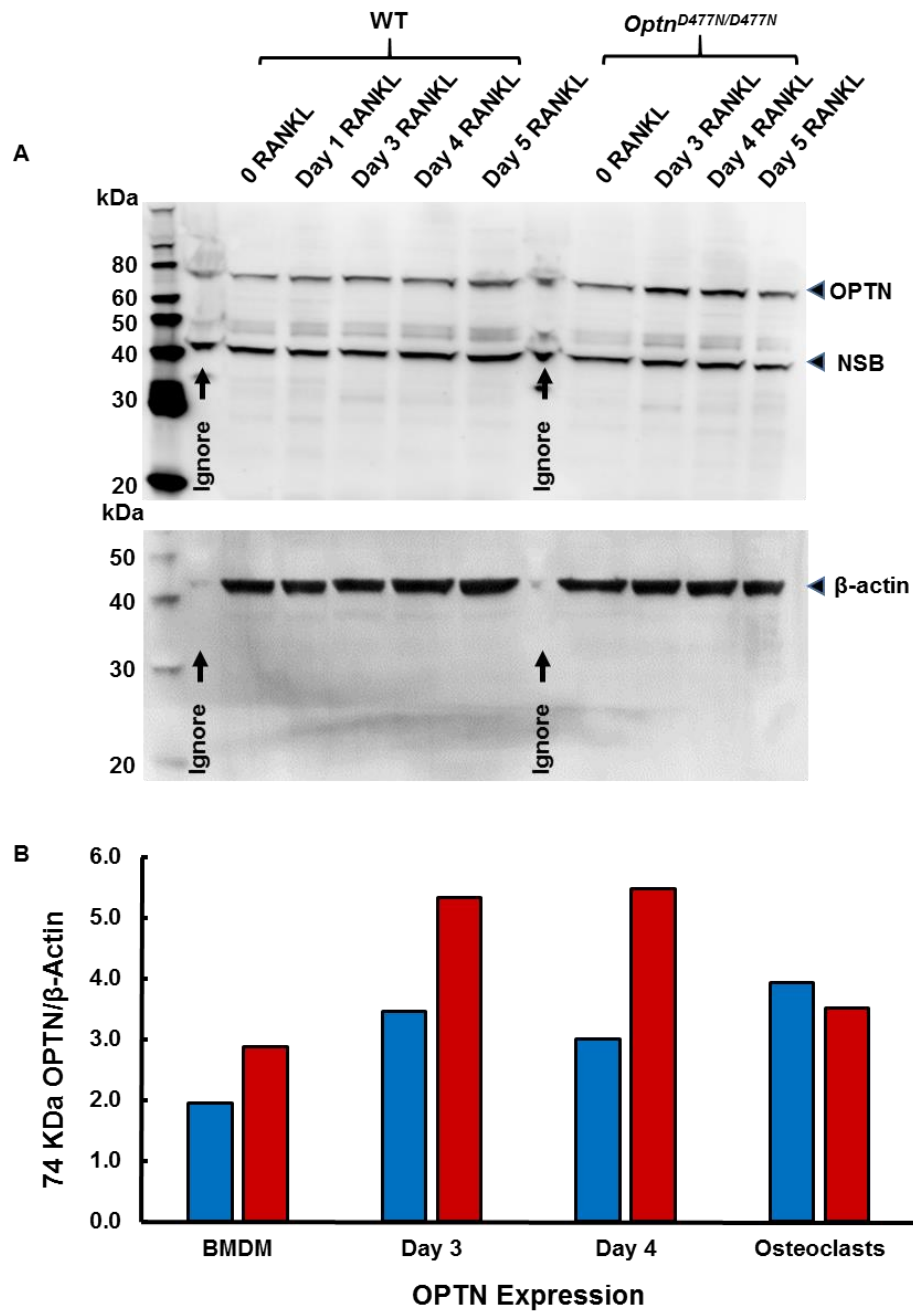


Figure 5-2: *Optn* Expression of WT and *Optn*<sup>D477N/D477N</sup> mice during osteoclast formation. **(A)** Protein lysates were extracted from different stages of osteoclast development from WT and *Optn*<sup>D477N/D477N</sup> and the total protein used was 40  $\mu$ g. The blot was exposed to *Optn* and  $\beta$ -actin antibodies. The bands were quantitatively measured and showed that expression of *Optn* was increased during osteoclast formation in both WT and *Optn*<sup>D477N/D477N</sup> mice. The expression of *Optn* was higher in *Optn*<sup>D477N/D477N</sup> mice compared to WT in BMDMs and post-RANKL stimulation. **(B)** Quantification of OPTN expression as a ratio of OPTN/ $\beta$ -actin. Representative image of at least two independent experiments.

### 5.3.3 Effect of *OPTN*<sup>D477N</sup> mutation on NFκB signalling pathway

An investigation was conducted on the extent to which the *Optn*<sup>D477N</sup> mutation modulated NFκB activation in response to RANKL. This was prompted by the fact that NFκB has been implicated in osteoclast formation, function and activity (Iotsova et al., 1997; Khosla, 2001), and the findings from chapter 4 which showed knockdown of *Optn* enhanced RANKL-induced NFκB signalling pathway. NFκB activity was first investigated by comparing kinetics of pIkBα degradation and re-synthesis in RANKL-treated WT and *Optn*<sup>D477N</sup> BMDMs. The results revealed no significant differences in NF-κB activity at the BMDM stage of osteoclast differentiation (Figure 5-3).

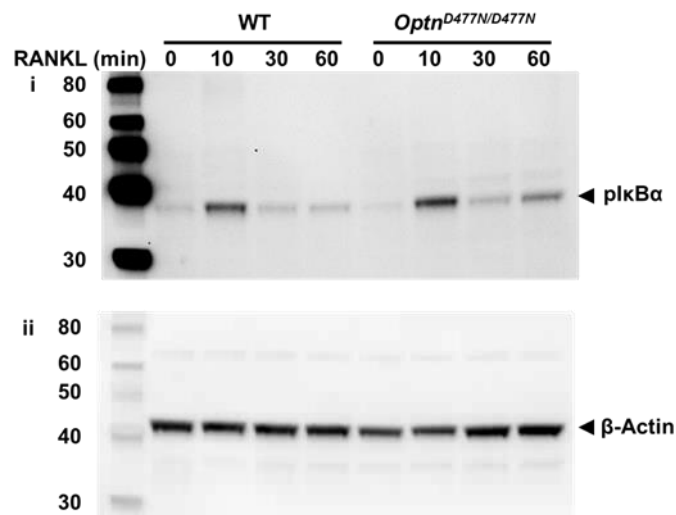


Figure 5-3: BMDMs from *Optn*<sup>D477N/D477N</sup> mice have unimpaired NFκB responses. BMDMs from WT or mutant mice were serum-starved for 1 h and stimulated with RANKL (100 ng/ml). Cells were lysed at the indicated times and immunoblotted for pIkBα (i) to assess NFκB activation and β-actin (ii) as a loading control. The amount of total protein used for western blotting was 50 µg.

Since *Optn* is upregulated during osteoclast differentiation, it is possible that the effect of *Optn* on RANKL-induced NFκB signalling is specific to osteoclast precursors. To investigate this possibility, lentiviral NFκB luciferase reporter was used to assess RANKL-induced NFκB activation during osteoclast differentiation. Adherent BMDMs of WT and *Optn*<sup>D477N/D477N</sup> mouse were transduced with lentiviral NFκB luciferase reporter for two days. The cells were selected using Puromycin (5 µg/ml) for 48 hours then detached and plated in 96 wells for 24 hours. The luciferase

activity was measured with a SteadyGlo-luciferase reporter assay system at the basal level and following RANKL stimulation (100 ng/ml). The data showed that, during osteoclast differentiation, the NF $\kappa$ B luciferase activity of *Optn*<sup>D477N/D477N</sup> cultures was higher than that of WT cultures, with a maximal effect at 2 to 3 days. This confirmed the role of *Optn* as a negative regulator of RANKL-induced NF $\kappa$ B activation (Figure 5-4).

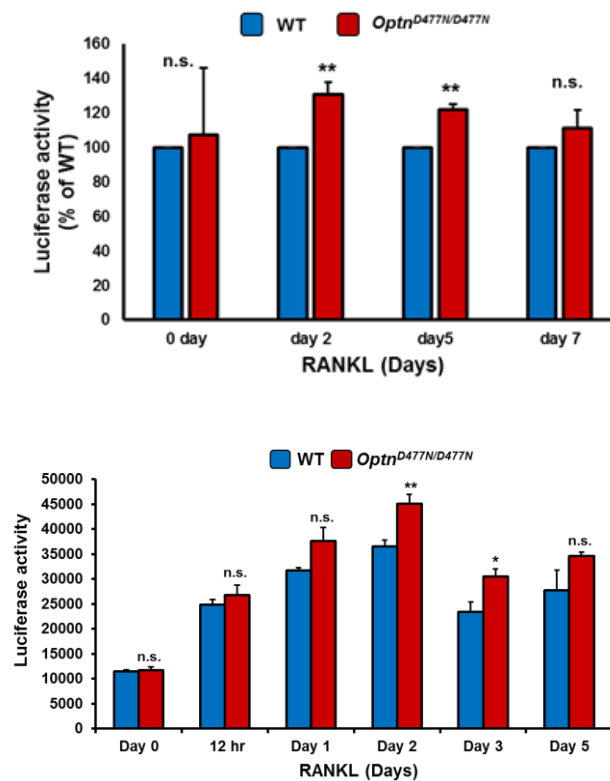


Figure 5-4: NF $\kappa$ B activity is higher in *Optn*<sup>D477N/D477N</sup> mouse BMDMs. BMDMs from WT and *Optn*<sup>D477N/D477N</sup> mice were transduced with lentiviral NF $\kappa$ B luciferase reporter to quantitatively assess NF $\kappa$ B activation at different stages of osteoclast development. NF $\kappa$ B activity was measured with a SteadyGlo-luciferase reporter assay system at the basal level and following RANKL stimulation (100 ng/ml) at different days and when osteoclasts were formed (Day 7). The upper graph represents values of three independent experiments presented as % of WT. The lower graph represents values obtained from one experiment. Values are means  $\pm$  SEM, \*  $P < 0.05$ , \*\*  $P < 0.01$ .

#### 5.3.4 *Optn* interaction with the negative regulator of NF $\kappa$ B signalling pathway; the *Cyld* enzyme

The OPTN-binding partner CYLD has been implicated as a negative regulator of RANKL-induced NF $\kappa$ B activation in BMDMs from *Cyld* null mice (Jin et al. 2008). A previous study has reported the C-terminal region of OPTN interacted with CYLD and that OPTN was required for CYLD-dependent inhibition of TNF $\alpha$ -induced NF $\kappa$ B activation (Nagabhushana et al., 2011), but its role in RANKL-induced NF $\kappa$ B activation remains unknown. Therefore, immunoprecipitation of Optn obtained from WT and *Optn*<sup>D477N/D477N</sup> mice were used to investigate the interaction with Cyld in response to RANKL. Results showed that, compared to WT cells, mutant cells displayed higher Optn expression. On this basis, Optn-bound Cyld was corrected for Optn expression level. This analysis revealed that mutant *Optn*<sup>D477N</sup> protein had reduced binding to Cyld compared to WT Optn protein in BMDMs as well as osteoclasts (P < 0.05; Figure 5-5).



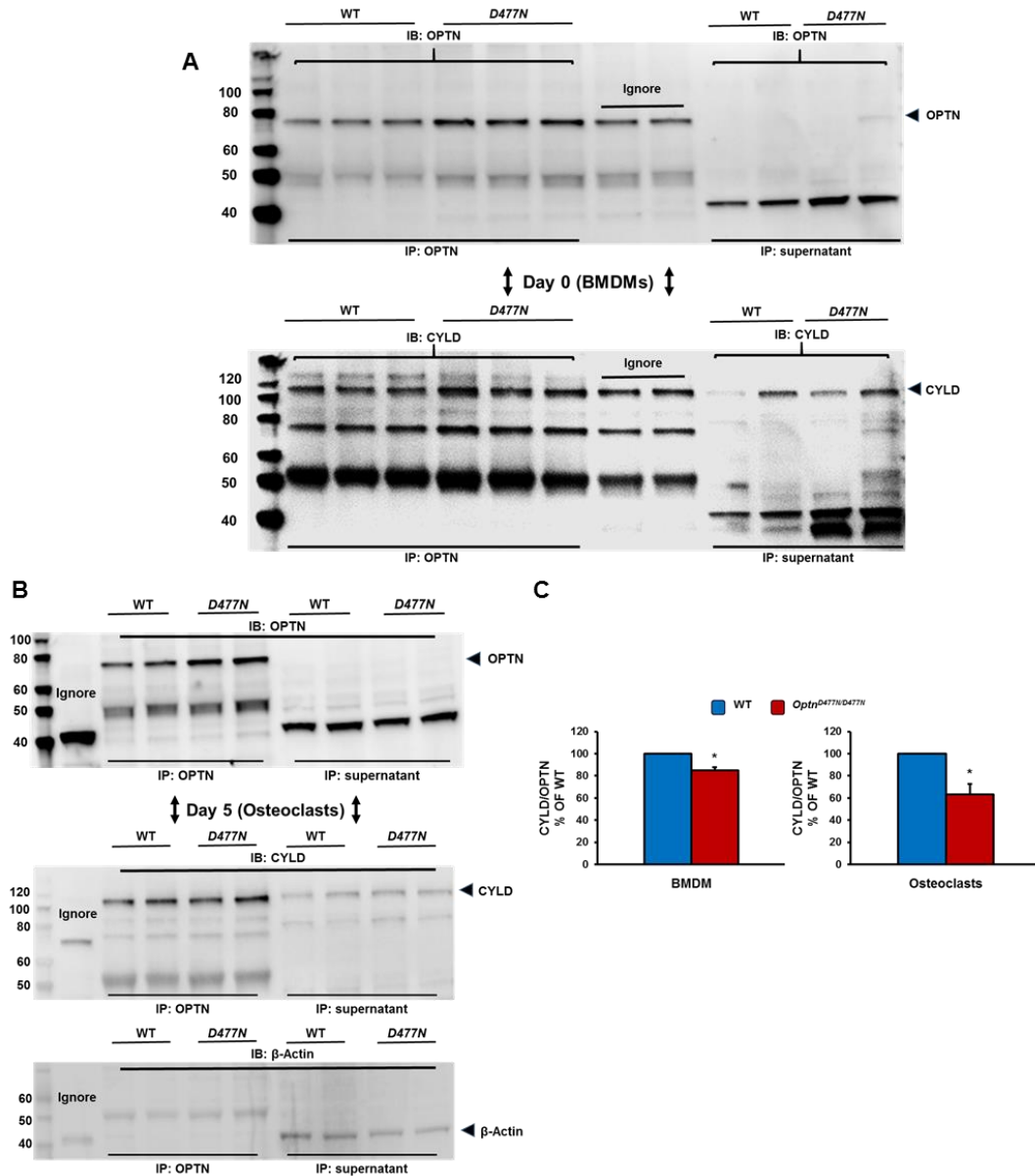


Figure 5-5: Optn interacts with Cyld. **(A)** and **(B)**, Optn was immunoprecipitated (IP) from 50  $\mu$ g of cell extract protein using 4  $\mu$ g of sheep anti-mouse OPTN antibody (s308c), and the presence of Optn and Cyld in the immunoprecipitates was analyzed by immunoblotting (IB) probed with Optn and Cyld rabbit primary antibodies. **(A)** A representative image shows the expression of Optn and Cyld in cell extract from BMDMs obtained from WT and D477N mutant mice before stimulation with RANKL (Day 0). Supernatants from wash steps were also analyzed in the same membrane to assess the immunoprecipitation specificity and ensure the target protein was not being lost in any other fractions. **(B)** Similar to the top panel (A), but cell lysates were extracted from osteoclasts (Day 5). This membrane was also blotted for  $\beta$ -actin as loading control. **(C)** The bands were quantified and the ratio of Cyld to Optn indicates lower interaction of Cyld to Optn in mutant mice compared to WT (\*  $P < 0.05$ ). Results for A-C are representative of at least three independent experiments.

### 5.3.5 *OPTN* expression during osteoblast differentiation

To investigate the effect of *Optn*<sup>D477N</sup> on osteoblast differentiation, calvaria from WT and *Optn*<sup>D477N/D477N</sup> mice were extracted and treated with osteoblast-inducing reagents. Assessment of Optn protein expression at different stages of osteoblast differentiation revealed that it had a similar level in both knock-in and WT mice, suggesting that osteoblastogenesis is unaffected by mutant *Optn* (Figure 5-6).

The effect of mutant *Optn* on bone nodule formation was investigated by undertaking bone nodule formulation by osteoblasts *in vitro*. The data obtained from this test showed no significant difference between the WT and mutant mice (Figure 5-7).

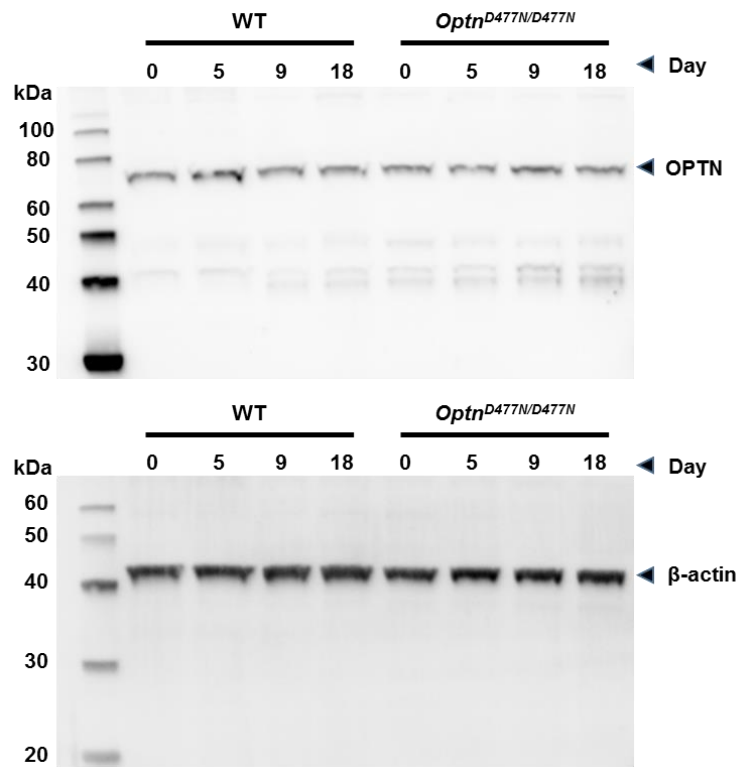


Figure 5-6: Calvaria from *Optn*<sup>D477N/D477N</sup> and WT mice were seeded into 12-well plates at 100×10<sup>3</sup> cells per well. Protein lysates were extracted before adding the osteoblast-inducing reagent and after the treatment with 3 mM β-glycerol phosphate and 50 μg/ml L-ascorbic acid at day 5, 9 and 18. Representative image of at least two independent experiments

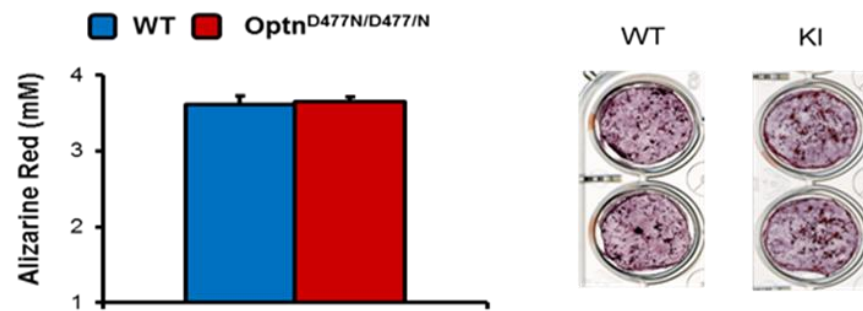


Figure 5-7: Bone nodule formation in *Optn*<sup>D477N/D477N</sup> and WT mice. Primary osteoblasts were cultured in osteogenic media for 21 days then the plates were fixed in 70% cold ethanol, and the mineralized nodules were visualized by alizarin red staining. Bone nodule formation was quantitated by destaining the cultures for 24 hours in cetylpyridinium chloride and measuring absorbance of the extracted stain by spectrophotometry. The values were normalized to cell number as determined by the Alamar blue assay. Results are presented as mean  $\pm$  SEM of two individual experiments.

## 5.4 Discussion

Bone homeostasis is a tightly regulated process controlled mainly by two processes, namely, bone resorption and bone formation. Pathological conditions, such as osteoporosis and osteopetrosis, are the result of imbalance between these two processes (Ralston, 2013a). PDB is characterised by focal abnormalities of increased bone resorption and disorganized bone formation (Ralston and Albagha, 2013). Previous chapters have shown that *Optn*-depletion in mouse BMDMs enhanced osteoclast formation, fusion and survival whilst also enhancing NFκB activation *in vitro*. In view of this, the aim of this chapter was to investigate *in vitro* the effect of *Optn* mutation on osteoclasts and osteoblasts from *Optn*<sup>D477N/D477N</sup> mice compared to WT.

In agreement with the *in vitro* findings from data of *Optn* knockdown experiment (chapter 4), *Optn* was induced at later stages of osteoclast formation after stimulation with RANKL in both WT and knock-in mice. However, the increase of *Optn* expression during these stages being in favour of *Optn*<sup>D477N/D477N</sup> mice. This was consistent with the findings of previous studies, which indicated that the expression of mutant *Optn* was higher than WT in multiple tissues (Gleason et al., 2011). What is more, compared to WT, *Optn*<sup>D477N/D477N</sup> mice also exhibited significantly greater formation and fusion of multinucleated osteoclasts. Another similar finding was that NFκB activity measured by luciferase reporter assay was significantly higher in *Optn*<sup>D477N/D477N</sup> than WT during osteoclast development. Collectively, these findings suggest a role of OPTN in osteoclast biology, role which likely takes the form of regulation of the RANK signalling pathway.

The deubiquitinase enzyme CYLD is a binding partner to OPTN and is known for its role in cleavage of k63-linked polyubiquitin chain from its target proteins, preventing NFκB activation (Massoumi, 2010). Therefore, *Optn* was immunoprecipitated and blotted for Cyld in order to confirm the interaction of *Optn* with Cyld in BMDMs before and after stimulation with RANKL. Results showed that after correction of Cyld expression to *Optn*, more interaction was found in WT

compared to knock-in mice, and this could explain at least in part the increase of NFκB activity in cells from mutant mice at different stages of osteoclast development due to the inability of the mutant *Optn* to optimally bind the *Cyld*, preventing the latter from exerting its deubiquitinating effect. Furthermore, analysis immunoprecipitation supernatants and washes indicated that Optn immunoprecipitates with most Cyld and small fraction of Cyld remained did not interact with Optn. This indicates that Optn might exert its effect in response to RANKL stimulation through interaction with Cyld. Another study has suggested that OPTN acts as an adaptor protein that mediates the interaction of CYLD with ubiquitinated RIP after stimulating HeLa cells with TNFα. This interaction negatively regulated the NFκB activity and NFκB activity was enhanced in *OPTN*-depleted cells (Nagabhushana et al., 2011). According to the IP results presented in this chapter, OPTN could mediate the interaction of CYLD to TRAF6 and thus inhibit osteoclastogenesis. Consequently, the impaired binding of mutant *Optn*<sup>D477N</sup> to polyubiquitin may affect the deubiquitinating effect of Cyld, which in turn enhances RANKL-induced NFκB activation resulting in enhanced osteoclastogenesis in *Optn*<sup>D477N/D477N</sup> mice. However, the IP experiment used in this study did not include a negative control (e.g. IgG), which is essential for detecting non-specific binding to the IP antibody or protein A/G, thus having an adverse impact on the detection of the immunoprecipitated target. However, the antibody used in this study was obtained from the Philip Cohen group, which was confirmed to specifically bind Optn in an IP experiment which included an IgG (see figure 3 from (Gleason et al., 2011)). In addition, immunoprecipitation supernatants and washes for each tested sample were used to make sure the immunoprecipitation was specific for Optn and Optn was not being lost in any other fractions. Another control used in this experiment was probing the protein of interest (Optn) with known binding protein (Cyld), both proteins having been detected.

It has been reported that putative NFκB elements exist in OPTN promotor and the enhancement of NFκB activity mediates the expression of OPTN (Sudhakar et al., 2009). This also could explain why Optn expression is higher in mutant mice compared to WT.

In order to investigate the role of OPTN in osteoblasts, cell lysates from calvarial osteoblast at different stages indicated, both before and after adding the Vitamin C, that *Optn* was expressed during osteoblast formation but there was no significant difference in the expression between these stages. Furthermore, there was no obvious difference between the *Optn* expressions in WT compared to the *Optn*<sup>D477N/D477N</sup> mice. To further investigate the effect of mutant *Optn* from the knock-in mice compared to WT on osteoblast differentiation and function *in vitro*, mineralization assay has been used to evaluate the calcium deposition in cell cultures. Results obtained from the quantification of the Alizarin Red stain concentration from WT and *Optn*<sup>D477N/D477N</sup> mice revealed no difference between the two genotypes. These results suggest that *Optn* has no direct role in promoting osteoblast function *in vitro*.

Coupling signals between osteoclasts and osteoblasts represent a complex mechanism that is necessary for balanced remodelling. Thus, the co-culture assay was used to investigate *in vitro* the communication between osteoblasts and osteoclasts and to determine the cell type affected in transgenic mice. This assay was conducted by generating mature osteoclasts from bone marrow precursors that were cultured with osteoblasts stimulated with 1, 25-(OH)<sub>2</sub> vitamin D3 and PGE2 (Itzstein and van 't Hof, 2012). Several trials were carried out to optimize the experiment conditions. However, aside from the time limitations imposed on completion of a doctoral degree, the breeding of mutant litters also posed some difficulties. The necessity to match mutant pups with WT was another challenging factor. Therefore, this experiment was scheduled to be completed at a future date. However, the co-culture experiment was undertaken by our researcher's group, observing that osteoblast cultures derived from D477N mutant mice were less capable to support osteoclast differentiation than those osteoblast cultures derived from WT (Obaid et al., 2015). Furthermore, the expression of the two pro-osteoclastogenic cytokines, RANKL and IL-6, was found to be significantly reduced in mutant osteoblasts when compared to WT osteoblasts. On the other hand, osteoclast precursor cells derived from *Optn*<sup>D477N</sup> mutant mice showed enhanced sensitivity to osteoblast stimulation. Interestingly, this finding was consistent with my previous data (section 5.3.1), where BMDMs derived from

*Optn*<sup>D477N/D477N</sup> mice formed osteoclasts of greater number and size *in vitro* when stimulated with RANKL. Collectively, these findings suggest that the D477N mutation leads to the formation of osteoclast precursor cells with enhanced sensitivity to osteoblast stimulation, which probably compensate for the reduced ability of mutant osteoblasts to support osteoclast differentiation (Obaid et al., 2015).

As discussed in chapter 4, previous studies using overexpression in cell lines and neuronal cells showed that OPTN is a negative regulator of NFκB activity in response to LPS and TNFα (Akizuki et al., 2013; Nagabhushana et al., 2011). The Dundee group who generated the mouse model used in this study found that the polyubiquitin-binding defective *Optn*<sup>D477N/D477N</sup> did not impair the LPS-induced NFκB activation in BMDMs. Instead, they found that this mutation reduced the TBK1 activity, phosphorylation of IRF3 and the production of IFNβ in BMDMs from knock-in mice compared to WT (Gleason et al., 2011). Similarly, Munitic et al. recently confirmed that *Optn* was dispensable for NFκB activity in BMDMs in response to LPS or TNFα stimulation based on the *Optn*<sup>470T</sup> mouse model, in which the entire ubiquitin-binding and C-terminal were deleted (Munitic et al., 2013). In line with these findings, the present study demonstrated that, at the BMDM stage, there was no difference between WT and mutant cells with regard to NFκB activity in response to RANKL stimulation as assessed by kinetics of pIκBα. However, the inhibitory effect of OPTN on NFκB activity was only significant during later stages of osteoclast differentiation when its expression level was increased. This could partially explain why studies based on overexpression of OPTN in cell lines showed an inhibitory effect of NFκB activation induced by LPS or TNFα. Differences in study design could also explain these findings. The first difference is that other studies examined BMDMs in response to stimulants other than RANKL, such as LPS and TNFα (Gleason et al., 2011; Munitic et al., 2013). It has been reported in the literature that OPTN-binding partner CYLD was expressed in BMDMs and the expression was induced at a later stage during osteoclast development, while the expression of CYLD did not change in response to other inducers, such as LPS and TNFα (Jin et al., 2008). Similarly, OPTN was induced at a later stage in osteoclast development, as presented previously in this study.

Therefore, OPTN could behave differently in different cell types and in response to different stimulation. Another difference between the present study and previous ones is that the measurement of NF $\kappa$ B activity in BMDMs and during osteoclast development was undertaken in this study with the luciferase reporter assay, which measures both the canonical and non-canonical pathways of NF $\kappa$ B activity; by contrast, earlier studies conducted measurements of the NF $\kappa$ B subunits at a certain time after stimulation with specific inducers in BMDMs, and only the canonical pathway was measured (Gleason et al., 2011; Munitic et al., 2013). These two studies also indicated the involvement of OPTN in the production of IFN $\beta$  through regulation of TBK1. Interestingly, IFN $\beta$  has been shown to inhibit osteoclast proliferation by interfering with the expression of c-Fos and mice lacking the IFN $\beta$  receptor have been observed to exhibit an increased osteoclast number and osteopenia (Takayanagi et al., 2002a). Indeed, recent work conducted by my group showed that OPTN might exert an inhibitory role on osteoclast differentiation by modulating the IFN $\beta$  signaling pathway (Obaid et al., 2015). They found that the production of IFN $\beta$  was significantly lower in mutant cells compared to those observed in WT. Furthermore, the expression of c-Fos was found higher in *Optn*<sup>D477N/D477N</sup> mice during later stages of osteoclast differentiation compared to that observed in WT.

Regardless of the nature of OPTN involvement in NK $\kappa$ B, several OPTN-binding partners have been identified as negative regulators of osteoclastogenesis. As discussed in chapter 6, *CYLD* knockout mice displayed several abnormalities in bone phenotype due to increased osteoclastogenesis (Jin et al., 2008). In addition, *in vitro* findings obtained from the BMDMs of these mice showed an increase in osteoclast number and size. They also reported that *CYLD* regulated the AP-1 and NF $\kappa$ B canonical and non-canonical pathways in preosteoclasts and the activity of these signalling pathways was enhanced in *Cyld*-deficient mice. Furthermore, they found that *CYLD* was coprecipitated in the same complex with TRAF6 and negatively regulated TRAF6 ubiquitination. Interestingly, p62/SQSTM1, which is involved in Paget's disease, was also found to interact with *CYLD* and promoted the TRAF6/*CYLD* interaction (Jin et al., 2008). Similarly, the other OPTN-binding



partner, A20, showed abnormal bone phenotype in A20<sup>-/-</sup> mice and the *in vitro* studies of macrophages from these mice showed sustained degradation of NFκB inhibitor IκBα, which indicated an increase in NFκB activation (Matmati et al., 2011). In addition, culturing of blood leukocytes from A20 knockout mice, as opposed to WT mice, revealed a significant increase in osteoclastogenesis in response to RANKL. Another example of a negative regulator of osteoclastogenesis is TANK, for which *in vitro* results from TANK-deficient mice revealed results similar to the findings presented here (Maruyama et al., 2012). In this study, TANK expression was induced in BMDMs during osteoclast development. In addition, osteoclast number and size were increased in *TANK* knockout mice in response to RANKL compared to WT, accompanied by enhanced NFκB activation. Furthermore, TANK was expressed during osteoblast differentiation and *TANK*<sup>-/-</sup> osteoblasts showed enhanced bone nodule formation by comparison to WT osteoblasts. It has been reported that TANK regulates the interaction between canonical IKKs (IKKα and IKKβ) and the IKK-related kinases (TBK1/IKKε) and this interaction is abolished in TANK-deficient mice, preventing IKK-related kinases from negatively regulating the canonical IKKs (Clark et al., 2011). Intriguingly, IKK-related kinases were found in a complex of adaptor proteins including TANK, OPTN, NAP1 and SINTBAD (Mankouri et al., 2010). Therefore, it would be of great interest to know whether *Optn*<sup>D477N/D477N</sup> will affect this complex and, consequently, the canonical IKKs enhancing the NFκB activity through this pathway as well as whether RANKL causes a reduction in TBK1 activity in these knock-in mice.

To conclude, the data presented in this chapter revealed that *Optn*<sup>D477N/D477N</sup> promoted osteoclastogenesis. This was accompanied by increased NFκB activity, especially during later stages of preosteoclasts with maximal effect at 2 to 4 days, suggesting that *Optn* has a greater inhibitory effect on osteoclast differentiation when its expression level is increased. *Optn* was also expressed in osteoblasts and this expression did not change at different stages of osteoblast development. From this, it could be implied that osteoblast function is not directly affected by *Optn*<sup>D477N/D477N</sup>.

**CHAPTER SIX**

**THE D477N MUTATION IN *OPTN* LEADS TO  
INCREASED BONE TURNOVER AND  
ENHANCED OSTEOCLAST FORMATION IN  
*OPTN*<sup>D477N/D477N</sup> MICE**

## 6 The D477N Mutation In *Optn* Leads To Increased Bone Turnover And Enhanced Osteoclast Formation In *Optn*<sup>D477N/D477N</sup> Mice

### 6.1 Summary

In chapter 4, it has been demonstrated that osteoclast formation *in vitro* was significantly promoted by *Optn* depletion, with the number of hypernucleated osteoclasts being considerably high. The comparison of cultures of BMDMs from *Optn*<sup>D477N/D477N</sup> and WT undertaken in chapter 5 produced similar results. The aim of this chapter was to investigate the skeletal phenotype of *Optn*<sup>D477N/D477N</sup> knock-in mouse model, which harbours a D477N point mutation in the polyubiquitin-binding domain of the *Optn*. The skeletal phenotype of *Optn* mutant mice and matched WT animals was assessed using bone histomorphometry and  $\mu$ CT. Histomorphometric analysis of bone sections of 4-month-old mice showed evidence of increased bone turnover in *Optn* mutant mice. Furthermore, bone resorption parameters were higher in *Optn* mutant mice compared to WT animals. Similarly, bone formation parameters were also higher in mutant mice compared to WT.  $\mu$ CT analysis of 4, 8 and 14 month old mice revealed no significant differences in bone morphology between WT and mutant mice. Bone turnover markers were also assessed and the bone formation marker (P1NP) was found to be significantly higher in mutant mice compared to WT, while the bone resorption marker (CTX) from mutant mice was not significantly different from WT.

In conclusion, data showed that *Optn* plays a role in regulating bone turnover *in vivo* by directly influencing osteoclast differentiation and formation. This may partly explain the role of OPTN in PDB susceptibility but further studies are advised to assess the role of OPTN in PDB cases and further explore its role in osteoclast signalling.

## 6.2 Introduction

The results obtained in chapters 4 and 5 confirmed the involvement of *Optn* in osteoclast development. Furthermore, *in vitro* findings from *Optn* knockdown and mutant *Optn* from the knock-in mice showed increased osteoclast formation, fusion and increased RANKL-induced NFκB activation. However, *in vitro* studies have limited value because they are carried out on isolated cells outside the whole organism, while complex or multifactorial disorders, such as skeletal diseases, are associated with the effects of multiple genes in combination with environmental factors. Therefore, the aim of this part of the study is to investigate the effect of *Optn* on bone phenotype using the *Optn*<sup>D477N/D477N</sup> knock-in mouse model compared to WT. Cellular and structural variables at the tibial metaphyses of these mice were measured by histomorphometric and μCT analysis. Bone histomorphometry is an essential technique for the assessment of cellular and structural variables on histological sections. The main advantage of this technique is that, by contrast to serum and urine biochemical markers, it is sensitive enough to be used in the assessment of the rate of bone formation or resorption (Allen and Burr, 2014b).

The μCT system is also an essential laboratory tool for assessing skeletal structure and density, whilst also providing accurate micro architectural measurements. Furthermore, μCT offers high-resolution images for *ex vivo* samples by generating a series of projection images within the pixel size range 1-30μm. Reconstruction of these images allows sufficient resolution to differentiating regions rich in trabecular bone from those containing just cortical bone. In addition, μCT has the capability to perform *in vivo* μCT measures on small animals. The advantage of μCT over histology is that μCT offers a 3D assessment of the entire region, while the histological procedure provides information on a single section and assumes the data obtained are applied to the entire bone. However, studies showed that the data obtained from the 2D histological analysis strongly correlated with data obtained from the 3D μCT analysis (Allen and Krohn, 2014). The Skyscan 1172 system was used to undertake

the  $\mu$ CT analysis. The left tibia from both sexes of WT and *Optn*<sup>D477N/D477N</sup> mice of different ages (4, 8 and 14 months) were scanned at a 5 $\mu$ m resolution, and trabecular and cortical bone parameters were measured with CTAn software.

## 6.3 Results

### 6.3.1 Bone histomorphometry of *Optn*<sup>D477N/D477N</sup> mice

For histomorphometric analysis, the samples were embedded in methyl methacrylate and serial longitudinal sections (5  $\mu$ m) at 3 different levels which were cut and stained to perform TRAcP, osteoid and calcein double-labelling. TRAcP staining counterstained with aniline blue was carried out to visualize osteoclasts. Von Kossa staining with Van Gieson counterstain was used to perform osteoid analysis. Calcein double-labelling was conducted to measure bone formation using aniline blue without phosphotungstic acid. Histomorphometric analysis was performed using software developed in-house, as described in section 2.2.4.5.

### 6.3.2 The D477N mutation in *Optn* increased bone resorption parameter in *Optn*<sup>D477N/D477N</sup> mice

To address the effect of mutant *Optn*<sup>D477N</sup> on osteoclast differentiation and formation *in vivo*, sectioned samples were stained for TRAcP in order to investigate the number of osteoclasts in the mutant mice compared to WT. Results indicated that the osteoclast numbers (*Oc.N/BS*), osteoclast surfaces (*Oc.S/BS*) and the mean of osteoclasts size were significantly increased in *Optn*<sup>D477N/D477N</sup> mice (Figures 6-1 and 6-2).

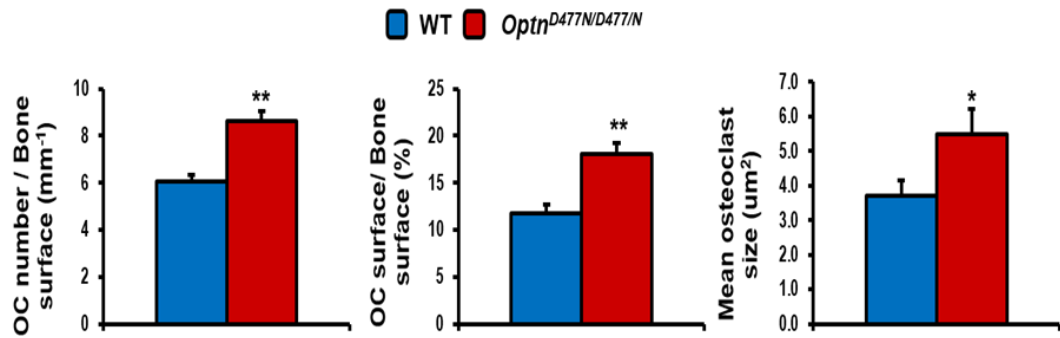


Figure 6-1: TRAcP analysis of histological sections of WT and *Optn*<sup>D477N/D477N</sup> mice. TRAcP+ multinucleated osteoclasts were significantly numerous and larger in *Optn*<sup>D477N/D477N</sup> mice compared to WT. Values are means ± sem (error bars) from 7-8 mice per group. Number of sections from each mouse (n=3) \* P < 0.05, \*\* P < 0.01

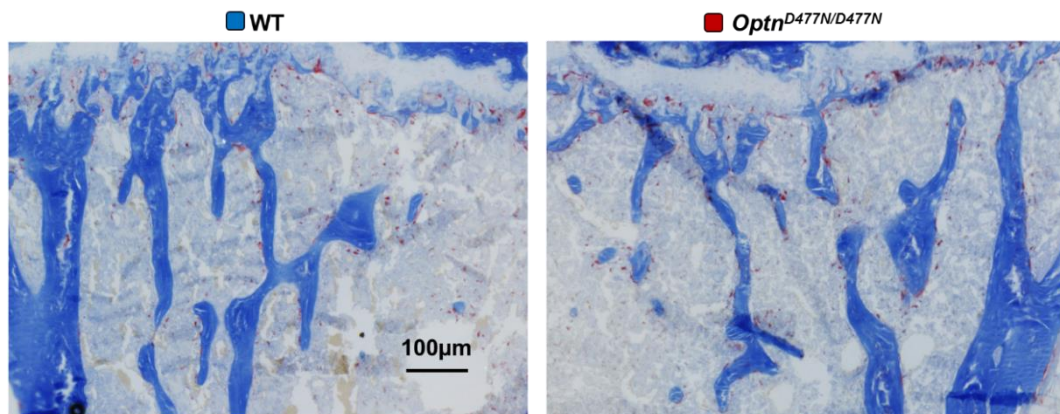


Figure 6-2: Representative images of the metaphyseal portion of tibias from WT and *Optn*<sup>D477N/D477N</sup> mice.

### 6.3.3 Bone formation parameters in *Optn*<sup>D477N/D477N</sup> compared to WT

The assessment of the bone formation process is undertaken through osteoid analysis, which examines the amounts of mineralised and non-mineralised bone. For the purpose of this osteoid analysis, sectioned samples were stained with Von Kossa staining with Van Gieson counterstain. *Optn*<sup>D477N/D477N</sup> mice exhibited increased values of osteoid surface (*Os.S/BS*) and osteoid volume (*Os.V/BV*) compared with WT mice (Figures 6-3 and 6-4).

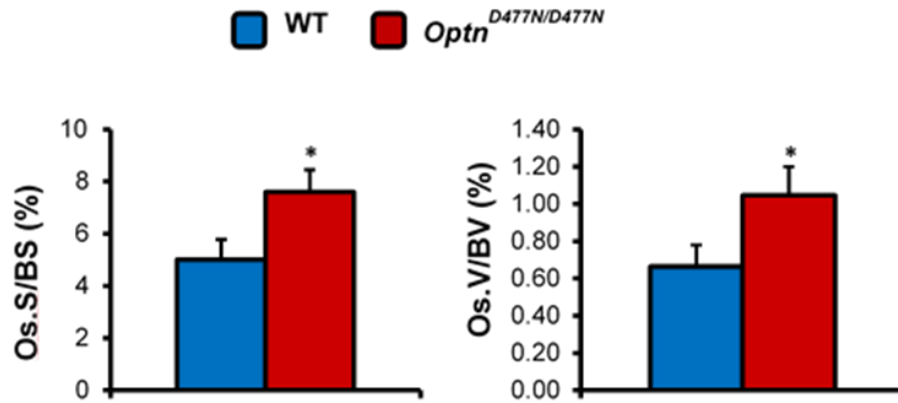


Figure 6-3: Osteoid analysis revealed higher bone formation in 4-month-old mutant mice compared to WT in terms of osteoid surface (Os.S/BS) and osteoid volume (OV/BV). Values are means  $\pm$  sem (error bars) from 7-8 mice per group. \*  $P < 0.05$

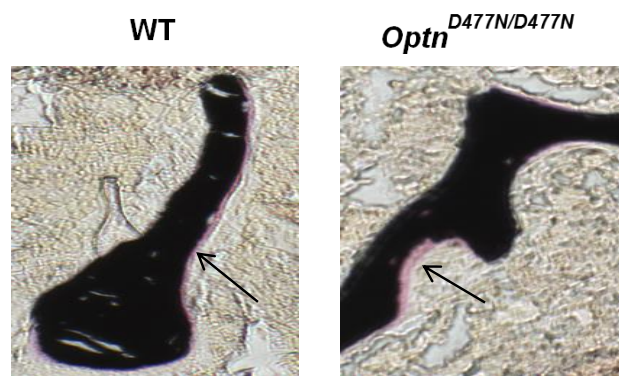


Figure 6-4: Von Kossa's staining revealed higher deposits of osteoid in *Optn*<sup>D477N/D477N</sup> compared to WT. The mineralized tissue is stained black and osteoid is stained pink. The arrow indicates the osteoid deposition.

#### 6.3.4 Analysis of dynamic bone formation indices in *Optn*<sup>D477N/D477N</sup> mice

Calcein labelling allows the calculation of newly formed bone within a given time period through the assessment of fluorochrome labels. The mice were given two intraperitoneal injections with calcein three days apart before being culled after 48 hours. Histological sections were prepared using aniline blue without phosphotungstic acid. Histomorphometry was performed using software developed in-house. Analysis

of calcein labelling revealed that the mineral apposition rate (MAR) and the label width were significantly higher in *Optn*<sup>D477N/D477N</sup> mice compared to WT. Furthermore, although by comparison to WT mice, *Optn*<sup>D477N/D477N</sup> mice exhibited a trend towards higher bone formation per bone surface (BFR/BS), this was of borderline significance (Figures 6-5, 6-6 and 6-7).

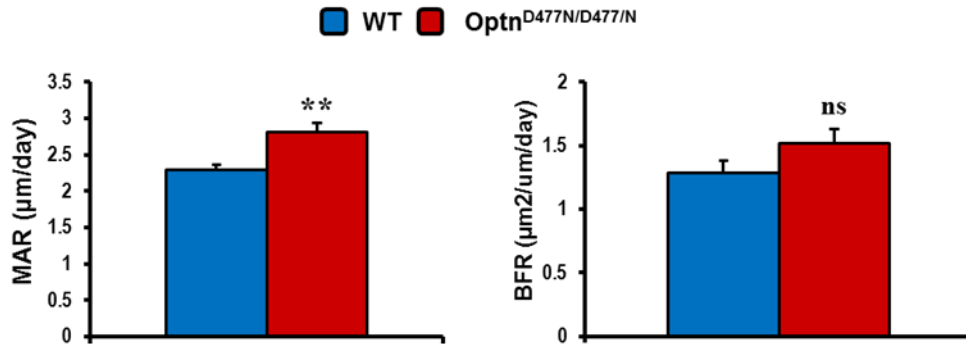


Figure 6-5: Effects of *Optn* mutation on mineral bone formation. Four-month-old male mice were labelled with calcein, and dynamic indices of bone formation were quantified in metaphyseal trabeculae of the tibia based on calcein administration of control and *Optn*<sup>D477N/D477N</sup>. Number of animals analysed (n=8) and number of sections from each animal (s=3). (BFR/BV) Bone formation rate/bone volume. (MAR) Mineral apposition rate. \*\*  $P < 0.01$ , Error bars represent SEM. ns, not significant

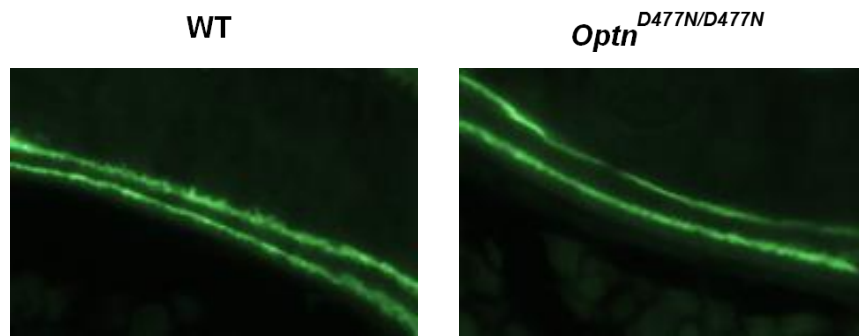


Figure 6-6: Visualization of bone formation by fluorescence microscopy after calcein double-labeling of proximal tibial metaphyses of WT and *Optn*<sup>D477N/D477N</sup> mice. The distance between the two green labels represents the amount of bone formed during the period of first and second calcein injection.



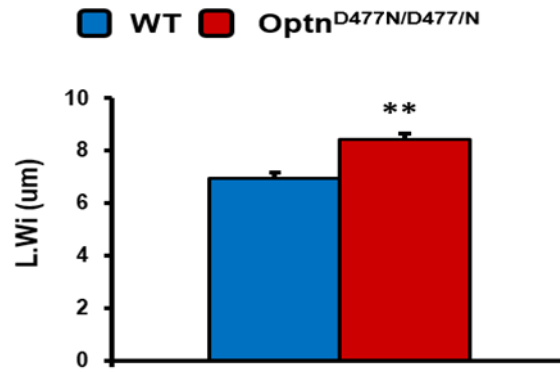


Figure 6-7: Labelling width parameter measured by histomorphometric analysis of WT and *Optn*<sup>D477N/D477N</sup> mice. \*\*  $P < 0.005$ , Error bars represent SEM.

### 6.3.5 Analysis of serum bone turnover markers in *Optn*<sup>D477N/D477N</sup> mice

A comparison of P1NP and CTX serum levels in *Optn*<sup>D477N/D477N</sup> and WT was conducted at four months. The difference between genotypes was statistically significant for P1NP in both genders but CTX differences were insignificant. These data demonstrate that knock-in mice undergo more extensive bone formation (Table 6-1).

Table 6-1: Biochemical Markers of Bone Turnover in *Optn*<sup>D477N/D477N</sup> and WT Mice

Mice		P1NP (ng/ml)	P value	CTX (ng/ml)	P value
Male	WT (n = 8)	5.4 ± 1.2	0.01	24.7 ± 3.61	0.34
	<i>Optn</i> <sup>D477N/D477N</sup> (n = 8)	6.3 ± 1.4		27.1 ± 8.74	
Female	WT (n = 3)	4.8 ± 0.59	0.04	28.4 ± 2.5	0.47
	<i>Optn</i> <sup>D477N/D477N</sup> (n = 3)	5.7 ± 0.17		28.6 ± 2.2	

### 6.3.6 $\mu$ CT analysis showed no significant difference in bone structure between the WT and mutant mice

$\mu$ CT analysis was performed using an *ex vivo* Skyscan 1172 system. The left tibia of 4-month-old WT and *Optn*<sup>D477N/D477N</sup> mice was scanned at a resolution of 5 $\mu$ m. The Skyscan NRecon package was used to reconstruct the images produces. The measurement of trabecular bone parameters was undertaken with the Skyscan CTAn software (Figures 6-8 and 6-9). Since PDB is a late onset disease, another  $\mu$ CT analysis was performed to measure the bone structure of the left tibia of 8-month-old mice with the purpose of identifying PDB-like bone lesions (Figure 6-10). Similarly, the bone structure of both tibias of 14-month-old male mice was measured with  $\mu$ CT analysis to determine whether the more advanced age caused the development of PDB-like lesions (Figure 6-11).

Cortical bone microarchitectures of the tibia isolated from 4 month (male) and 8 month (both sexes) old mice were also assessed by using  $\mu$ CT (Figure 6-12 and 6-13). The results revealed no significant difference between WT compared to knock-in mice at different ages.

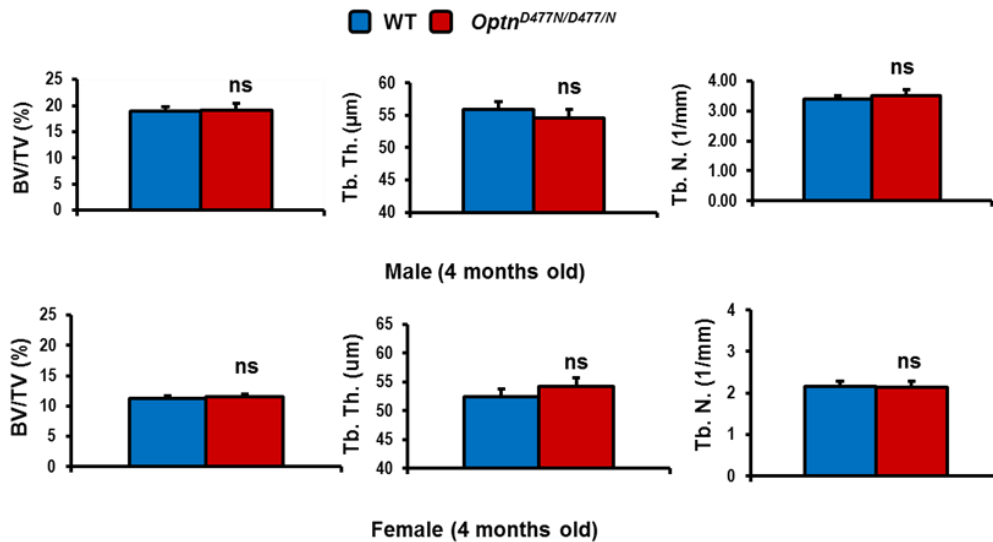


Figure 6-8:  $\mu$ CT analysis revealed no significant differences in bone morphology between WT (n = 8) and *Optn*<sup>D477N/D477N</sup> mice (n = 8) of both sexes at the age of 4 months in terms of bone volume/tissue volume (BV/TV), trabecular number (Tb. N.) and trabecular thickness (Tb. Th.). Error bars represent SEM. ns, not significant

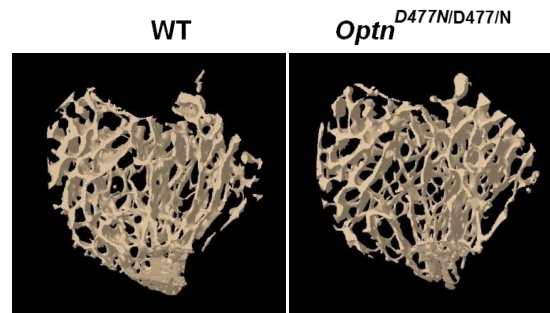


Figure 6-9: Axial  $\mu$ -CT images of distal tibial metaphyses from 4-month-old male mice.

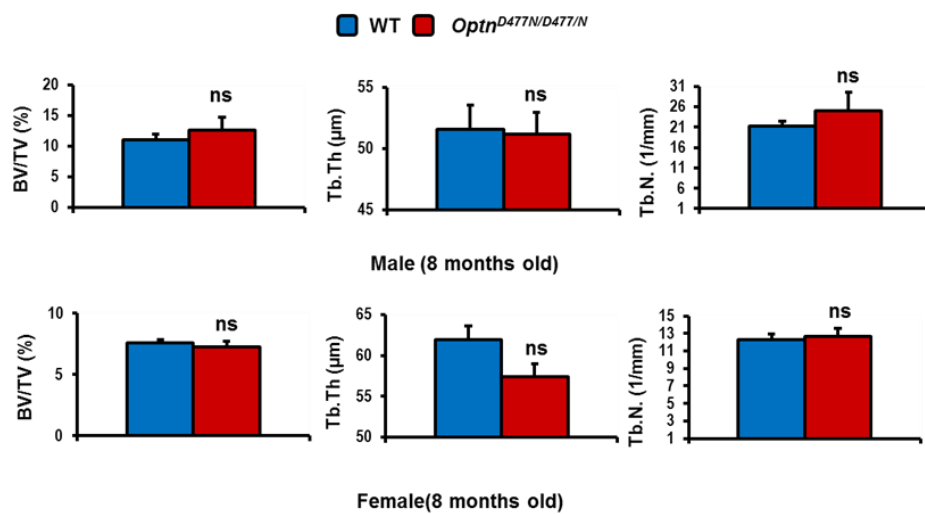


Figure 6-10:  $\mu$ CT analysis revealed no significant differences in bone morphology between WT ( $n = 5$ ) and *Optn*<sup>D477N/D477N</sup> mice ( $n = 4$ ) of both sexes at the age of 8 months in terms of bone volume/tissue volume (BV/TV), trabecular number (Tb. N.) and trabecular thickness (Tb. Th.). Error bars represent SEM.

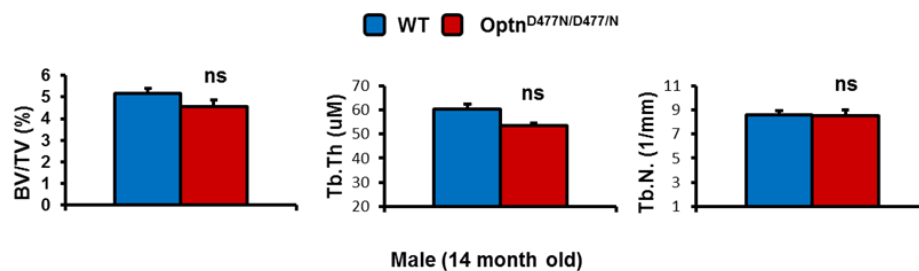


Figure 6-11:  $\mu$ CT analysis showed no significant differences in bone morphology of 14-month-old WT ( $n = 4$ ) and *Optn*<sup>D477N/D477N</sup> male mice ( $n = 5$ ) in terms of bone volume/tissue volume (BV/TV), trabecular number (Tb. N.) and trabecular thickness (Tb. Th.). Error bars represent SEM.



Figure 6-12:  $\mu$ CT analysis showed no significant differences in bone morphology of 4-month-old WT (n = 6) and *Optn*<sup>D477N/D477N</sup> male mice (n = 8) in terms of cortical thickness (Cortical Th). Error bars represent SEM.

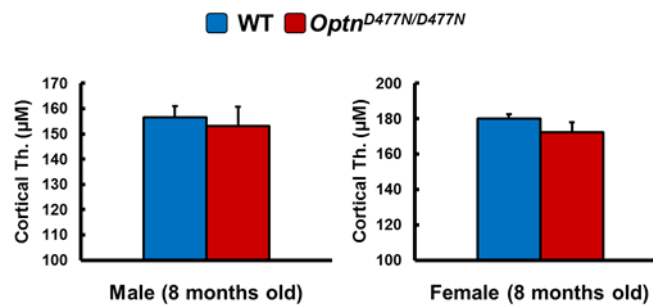


Figure 6-13:  $\mu$ CT analysis revealed no significant differences in bone morphology between WT (n = 5) and *Optn*<sup>D477N/D477N</sup> mice (n = 5) of both sexes at the age of 8 months in terms of cortical thickness (Cortical Th). Error bars represent SEM.

### 6.3.7 Analysis of PDB-like bone lesions in *Optn*<sup>D477N/D477N</sup> mice

A Skyscan 1076 system was used to undertake  $\mu$ CT analysis with the purpose of determining the connection between aging in mice *in vivo* and the development of PDB-like lesions. Live mice of WT (n=48) and *Optn*<sup>D477N/D477N</sup> (n=52) were followed for up to 18 months of age to examine whether they developed PDB-like lesions. These mice were scanned *in vivo* at various ages and at certain age (4, 8, 12, 15-18 months) of their development, group of these animals with their matched controls were being culled and bones were extracted and scanned using the *ex vivo* Skyscan scanner 1172 system. Extracted bones were then subjected to histological analysis as described in material and methods section 2.2.4.5. According to the findings of previous studies, p62 P394L mice older than one year were more likely to develop PDB-like lesions (Daroszewska et al., 2011). In order to determine whether similar PDB-like lesions

would be developed by *Optn*<sup>D477N/D477N</sup> mice, the development of such lesions was investigated at different ages (Table 6-2). Among the screened mice, only one mutant female mouse aged 15 months developed a single unilateral osteolytic PDB-like lesion affecting the left femur (Figure 6-14).

Table 6-2: Number of *in vivo* mice scanned by Skyscan  $\mu$ CT 1076 for bone lesions.

Age group	8-9 months		12 months		15-18 months	
Genotype	WT	D477N	WT	D477N	WT	D477N
Males (n)	7	11	8	12	2	6
Females (n)	13	7	12	13	6	3
Total (n)	20	18	20	25	8	9
Male with lesion (n)	0	0	0	0	0	0
Female with lesion (n)	0	0	0	0	0	1
Total with lesion (n)	0	0	0	0	0	1

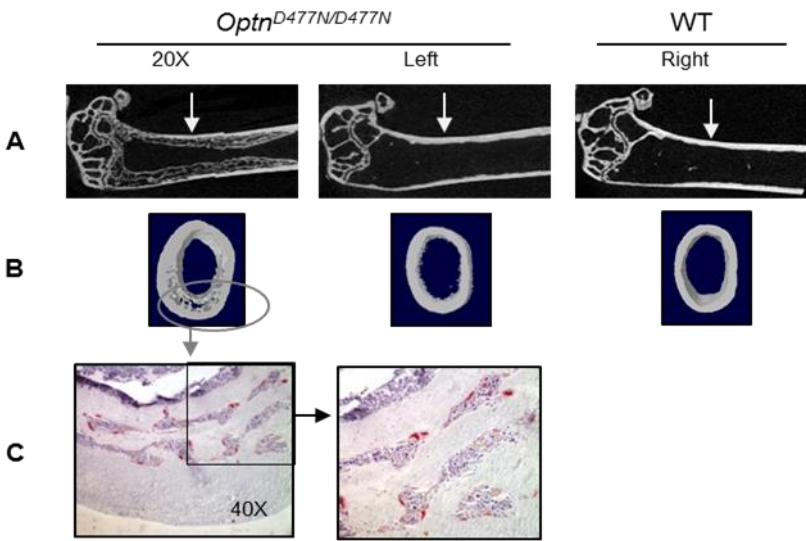


Figure 6-14: Femur of 15-month-old *Optn*<sup>D477N/D477N</sup> mouse showed PDB-like lesion. **(A)**  $\mu$ CT analysis with 3D reconstruction of the femur of WT and mutant mouse. **(B)** Cross-section from the femur of WT and *Optn*<sup>D477N/D477N</sup> mouse shows that the osteolytic bone lesion is located within the cortex of the mutant mouse **(C)** Histological analysis of the affected region shows enhanced osteoclastogenesis in *Optn*<sup>D477N/D477N</sup> mouse.

## 6.4 Discussion

The results presented in this chapter showed that mice carrying the D477N mutation in *Optn* develop several histological parameters different from WT. Consistent with the *in vitro* findings (chapter 5), metaphyseal osteoclast numbers, surfaces and sizes were augmented in *Optn*<sup>D477N/D477N</sup> knock-in mice compared to WT. However, the bone resorption marker CTX was not statistically significant between the two genotypes. This result could be due to the limitation of measuring the CTX marker as it is affected by diurnal variation and food intake (Seibel, 2005). It was not possible to control for the time and season of serum sample collection. Osteoid analysis revealed a significant difference in the bone formation process between both genotypes. In concordance with osteoid analysis, MAR, which represents the osteoblast vigour at the individual BMU level, was significantly higher in *Optn*<sup>D477N/D477N</sup> knock-in mice compared to WT. Although mutant mice exhibited a higher bone formation rate per bone surface (BFR/BS) than WT mice, this was of borderline statistical significance ( $P = 0.08$ ). Furthermore, the bone formation marker PINP was also significantly higher in knock-in mice compared to WT. An *ex vivo*  $\mu$ CT scanner was applied to mice of different ages (4, 8 and 14 months) of both genotypes to screen their cortical and trabecular bone microarchitectures. The  $\mu$ CT analysis revealed no significant differences in bone morphology between WT and *Optn*<sup>D477N/D477N</sup>. Live animals of WT (n=48) and *Optn*<sup>D477N/D477N</sup> (n=52) were also scanned using *in vivo* Skyscan scanner to determine whether aging caused the development of PDB-like lesions. Only one mouse out of 52 mutant mice developed (aged 4 months or older) a single unilateral PDB-like lesion suggesting that, in most cases, the *Optn*<sup>D477N</sup> mutation is not sufficient to develop PDB-like phenotype. In addition, these data also suggest that *Optn* has no direct effect on osteoblast activity and the enhanced bone formation *in vivo* occurs as a coupling mechanism to compensate for the elevation in bone resorption, as is thought to occur in PDB (Singer et al., 2006). The underlying mechanism is not known but it could be due to other coupling factors that control the osteoclast-osteoblast crosstalk (Sims and Martin, 2014). Indeed, the researcher's group conducted further investigations on the

expression level of the two pro-osteoclastogenic cytokines, RANKL and IL-6, in osteoblast cultures. They found the expression level of these cytokines was significantly lower in osteoblast culture derived from *Optn*<sup>D477N/D477N</sup> mice compared to WT (Obaid et al., 2015). These data suggest that the coupling mechanism between osteoblasts and osteoclasts is under the influence of the *Optn*<sup>D477N</sup> mutation.

Previous study of the OPTN-binding partner CYLD showed that *Cyld*<sup>-/-</sup> mice exhibited significant differences in trabecular analysis compared to WT in terms of bone volume (BV/TV), trabecular number (Tb.N) and trabecular thickness (Tb.Th) (Jin et al., 2008). The cortical thickness in these knockout mice was also low compared to the WT but the proportion of bone (BV/TV) was the same in WT and *Cyld*<sup>-/-</sup>. Serum osteocalcin was measured as an indicator of osteoblast activity and results showed no significant difference between the two genotypes in terms of osteocalcin concentration. These data led the authors to suggest that the defect was not in the osteoblast function. In addition to these findings, they observed that *Cyld*<sup>-/-</sup> mice exhibited osteoclast abnormalities in terms of increased number and size of osteoclasts compared to WT (Jin et al., 2008).

Another OPTN-binding partner which has been involved in the negative feedback regulation of the NFκB pathway is A20. Osteoclastogenesis was promoted in A20-deficient mice, which also developed a bone phenotype resembling rheumatoid arthritis (Matmati et al., 2011). TANK has been reported to be a negative regulator for RANKL-induced osteoclastogenesis. *Tank*<sup>-/-</sup> mice exhibited severe trabecular bone loss accompanied with increased osteoclast number. These mice also had significantly enhanced bone formation, which explained the increase in cortical bone mineral density (Maruyama et al., 2012). The similarities uncovered between these animal models and the *Optn*<sup>D477N/D477N</sup> knock-in mice support the role of OPTN in bone biology.

## Conclusion

The findings of this chapter have shown for the first time that OPTN plays a role in regulating bone turnover and suggest a direct effect of OPTN on osteoclast function. The *Optn*<sup>D477N/D477N</sup> mutation leads to increased bone resorption and formation parameters compared to WT. Only one mutant animal developed a PDB-like lesion indicating that the *Optn*<sup>D477N</sup> mutation is not sufficient to cause PDB, which suggests that other triggers contribute to the development of PDB in these mice.



## **CHAPTER SEVEN**

### **DISCUSSION AND CONCLUSIONS**

## 7 Discussion and conclusions

Research on PDB has increased in recent years and findings about the incidence pathogenicity of this disease have opened new prospects for future studies to analyse the underlying causes of the disease. PDB is a common late-onset skeletal disorder characterised by focal areas of abnormal bone remodelling. Although the aetiology of PDB is still relatively poorly understood, it is commonly accepted that both environmental and genetic factors contribute to the development of the disease. PDB has a strong genetic component and several susceptibility loci, which have been identified by linkage studies to cause a predisposition to developing PDB, but so far only one causal gene has been identified. This gene is *SQSTM1* and mutations affecting it are known to cause the high penetrance form of PDB (Laurin, 2002). However, mutations in this gene occur in about 40% of familial cases and 10% of sporadic cases, indicating that other PDB-predisposing genes still need to be identified (Ralston and Albagha, 2011). Before conducting this study, GWAS in PDB identified new susceptibility genes for PDB including variants at *CSF1*, *TNFRSF11A*, *OPTN*, *TM7SF4*, *PML*, *NUP205* and *RIN3* loci. These loci were confirmed to be associated with PDB in various European populations (Albagha et al., 2011b, 2010; Chung et al., 2010a). However, as the majority of GWAS findings are statistical signals, further investigation needs to take place to confirm the impact of these genetic variants in PDB. Therefore, the aim of this study is to investigate the role *OPTN* in bone biology and PDB.

*OPTN* was the gene of interest in this study based on multiple criteria. First of all, the highest association signal to the 10p13 locus is tagged by rs1561570, which is located within *OPTN* gene ( $P = 4.37 \times 10^{-38}$ , risk allele OR = 1.67) (Albagha et al., 2011b). Interestingly, the locus 10p13 was previously linked to PDB and has been considered the major locus for PDB in British families. However, the causative gene has not been identified despite positional cloning efforts (Lucas et al., 2007). Secondly, recent studies have shown that the *OPTN* locus rs1561570 is a strong eQTL in human monocytes (Zeller et al., 2010) and in peripheral blood mononuclear cells (Westra et

al., 2013) with decreased level of *OPTN* expression in carriers of the risk allele (T). The third factor is the role of *OPTN* can be predicted from the current literature. It was reported that *OPTN* has a regulatory role in NF $\kappa$ B signalling and vesicular trafficking pathways, both of which have been implicated in osteoclast biology (Nagabhushana et al., 2011; Park et al., 2010; Zhu et al., 2007). Furthermore, several studies point to the role of *OPTN* during viral infection (Journo et al., 2009; Mankouri et al., 2010). It was suggested as an environmental factor that may exacerbate PDB. Also, *OPTN* was found to have a role in autophagy, a recent mechanism implicated in PDB (Korac et al., 2013; Wild et al., 2011). Collectively, these criteria strongly point to the role of *OPTN* in bone biology.

At the beginning of this study, *OPTN* was investigated for the relationship between the genetic variant rs1561570 and disease severity in PDB patients without *SQSTM1* mutations. There was a significant association between *OPTN* rs1561570 and total disease severity score, so that patients who are carriers of allele “T” had more severe disease compared to non-carriers. Also, the data revealed a trend for reduced SF36 physical summary score among carriers of *OPTN* rs1561570 risk allele compared to non-carriers. These findings were first reported in the ECTS 2010 annual meeting (Appendix 3). Recently, my supervisor confirmed the association between the risk alleles identified by the GWAS that predispose to PDB and the severity and extent of the disease, either alone or in combination with *SQSTM1* mutations (Albagha et al., 2013). In this study, when each locus was analysed individually for its susceptibility to PDB, *OPTN* rs1561570 showed a significant correlation with the number of bones affected. The number of affected bones is a measure of the extent and severity of the disease, and this finding, in general, is consistent with the results previously reported in chapter 3 and confirms the association of *OPTN* with PDB extent and severity. This finding could be of clinical value in identifying those at risk of developing PDB, especially cases without *SQSTM1* mutations.

The *OPTN* rs1561570 locus is one of the highest association signals in different populations, but it is located in the intronic region (Albagha et al., 2010). Therefore, *OPTN* was screened in 43 samples obtained from 10p13-linked familial cases and

controls by direct DNA sequencing covering the coding regions as well as the exon-intron boundaries. My results identified common polymorphisms, which were previously reported in public databases. Several studies conducted on various Caucasian populations, including the British, also screened *OPTN* from ALS cases. As with the findings of this research, these studies did not identify a significant *OPTN* mutation that can be considered a pathogenic mutation in coding regions and the exon-intron boundaries (Johnson et al., 2012; Millecamps et al., 2011; Sugihara et al., 2011). However, although rs1561570 polymorphism is located in the intronic region, this locus is still a crucial finding for many reasons. First, it was reported in different populations. The second reason is that rs1561570 is a strong eQTL in human monocytes and peripheral blood mononuclear cells (Westra et al., 2013; Zeller et al., 2010) with reduced expression of *OPTN* in carriers of PDB-predisposing (T) allele. This suggests that the association with PDB is driven by a regulatory variant(s) that alter the *OPTN* expression level. Therefore, this study examines the effect of reduced expression of *OPTN* on osteoclast differentiation.

Since PDB is considered a disease of osteoclast differentiation and function, expression of *OPTN* was assessed first during osteoclast development. Intriguingly, the level of *Optn* was low in BMDMs and for the first two days after RANKL treatment. However, expression increased two to three-folds in preosteoclasts and when osteoclasts are formed. This higher induction of *Optn* expression during later stages of osteoclast development may indicate to its role at later stages of osteoclastogenesis. In order to examine the effect of *Optn* depletion in osteoclasts, *Optn* was successfully knocked down in BMDMs using lentiviral shRNA, which was confirmed by western blot. Compared with BMDMs transduced with lentivirus carrying negative control shRNA, osteoclast numbers and sizes of *Optn*-depleted BMDMs increased significantly, according to TRAcP staining. These findings correspond with results obtained from the *Optn*<sup>D477N/D477N</sup> knock-in mice, where TRAcP positive osteoclasts from these mice were also significantly higher in number and size compared to WT. These are the characteristics of osteoclasts from PDB. As with these data, metaphyseal osteoclast number, surface and size from histological

sections were significantly higher in *Optn*<sup>D477N/D477N</sup> knock-in mice compared to WT. However, the difference of bone resorption marker CTX between the mutant and WT mice was not statistically significant. This result could be explained by the possibility of this marker being impacted by food intake and diurnal variation, which were not possible to correct for during sample collection (Seibel, 2005). In addition to the previous findings, *Optn*-depletion after withdrawal of RANKL in BMDMs enhanced osteoclast survival compared to non-depleted cells. Furthermore, overexpression of OPTN in RAW 264.7 cells leads to significant reduction in the number and size of osteoclast like cells after being stimulated with RANKL (Obaid et al., 2015). Taken together, these findings suggest a novel role for OPTN in bone metabolism by acting as a negative regulator of osteoclast differentiation.

As observed in the *in vivo* analysis of histological samples, osteoid analysis and MAR were significantly higher in *Optn*<sup>D477N/D477N</sup> knock-in mice compared to WT, suggesting enhanced bone formation. The  $\mu$ CT analysis of 4, 8 and 14 month-old mice showed no significant variations in bone morphology between WT and mutant mice. On the other hand, the serum level of the bone formation marker PINP was significantly higher in knock-in mice compared to WT. The data also showed that *Optn* is expressed at different stages during osteoblast development without significant difference in the expression between these stages. In addition, the mineralised nodule formation stained with Alizarin red and quantitative analysis of solubilised Alizarin red staining showed no significant difference between WT and *Optn*<sup>D477N/D477N</sup> knock-in mice osteoblasts. Coupling events between bone formation and resorption are crucial for bone maintenance (Sims and Martin, 2014). The co-culture analysis carried out later by our group, showed that osteoblast cultures derived from D477N mutant mice had reduced capacity to support osteoclast differentiation than those osteoblast cultures derived from WT (Obaid et al., 2015). Furthermore, the analysis found the expression of two proosteoclastogenic cytokines including RANKL and IL-6 were significantly reduced in mutant osteoblasts compared with WT osteoblasts. These findings demonstrate that enhanced bone formation observed *in vivo* may occur as a

coupling mechanism due to enhanced bone resorption which is similar to the situation observed in PDB (Singer et al., 2006).

NFκB is a crucial signalling pathway that regulates osteoclast formation, function, and survival (Abu-Amer, 2013). Interestingly, OPTN has been implicated in NFκB signalling in previous studies (Nagabhushana et al., 2011; Zhu et al., 2007). In order to determine whether OPTN has the potential to affect the NFκB pathway, a SteadyGlo-luciferase reporter assay system was used at the basal level and following RANKL stimulation to assess the NFκB activity in *Optn*-depleted BMDMs as well as in cells obtained from the D477N knock-in mice. The NFκB activity was increased in *Optn*-depleted cell during osteoclast development. Similarly, the NFκB activity was increased in cells obtained from *Optn*<sup>D477N/D477N</sup> mice compared to WT. On the other hand, there was no difference between BMDMs from *Optn*<sup>D477N/D477N</sup> mice and WT when measuring the IκBα phosphorylation induced by RANKL. This finding reflects the absence of difference in RANKL-induced NFκB activation in BMDMs. Similar results have been reported in several previous studies where there is no difference in the NFκB activation in BMDMs in response to different cytokines other than RANKL (Gleason et al., 2011; Munitic et al., 2013). Interestingly, a study of *Cyld* knock out mice also showed that the level of *Cyld* was low in BMDMs and no abnormalities of RANKL-induced NFκB activation were detected. After BMDMs being stimulated with RANKL, the NFκB activation was enhanced and the level of *Cyld* was also increased during osteoclast differentiation (Jin et al., 2008). These findings are consistent with the data presented in this study, where the expression of *Optn* was low in BMDMs and no significant difference was detected in RANKL-induced NFκB activation. When BMDMs were stimulated with RANKL, the NFκB activity was enhanced and *Optn* expression was increased as osteoclast differentiation proceeds. These data suggest that OPTN effect on RANKL-induced activation depends on cells type and on its expression level.

OPTN is a binding-partner of CYLD, which was found to interact with SQSTM1 in macrophages and together deubiquitinate TRAF6 causing inhibition of NFκB

signalling (Jin et al., 2008). Since the *Optn*<sup>D477N</sup> mutation is located in the region that binds Cyld, Optn was immunoprecipitated from BMDMs lysates before and after stimulation with RANKL and immunoblotted for Optn and Cyld. The findings show that Optn physically interacts with Cyld and the interaction was less pronounced in *Optn* mutant mice. This suggests that mutation of *Optn* causes an increase in the NFκB activity at least in part by impairing the CYLD from deubiquinating TRAF6.

## 7.1 Suggested mechanisms of OPTN effect on osteoclastogenesis

The main objective of this research is to confirm the implication of *OPTN* in bone biology and PDB. The findings of previous research indicate that *OPTN* is involved in NFκB pathway in immune cells, bacterial and viral infection and autophagy. Another recent report shows that silencing of *OPTN* in neuroblastoma cell line enhances the TNFα-mediated NFκB activation that results in increased apoptosis (Shen et al., 2011). In contrast, recent research into macrophages show that *OPTN* is dispensable for NFκB pathway but rather is involved in IRF3 (Gleason et al., 2011; Munitic et al., 2013). Despite its importance in these previous studies, the involvement of *OPTN* in RANKL signalling has not been investigated. Regardless of whether *OPTN* is directly involved in NFκB pathway or not, the findings of this study show that *OPTN* may have a negative feedback regulation on RANKL-induced osteoclastogenesis. Based on the findings, and in addition to previous studies of *OPTN* and its binding partners, the following suggestions could explain the role of *OPTN* in pre-osteoclasts downstream the RANK signalling pathway.

### 7.1.1 Suggested role of *OPTN* through deubiquitinating enzymes for regulating RANKL-induced NFκB activity

The data presented in this study yielded evidence for the implication of *OPTN* in bone metabolism but the mechanisms by which *OPTN* regulates bone turnover are complex and appear to involve several signalling pathways. A review of previous research on macrophages shows that *OPTN*-binding partners including CYLD and A20 are negative regulators of the RANK-signalling pathway and both have been

shown to be negative regulators of NF $\kappa$ B activity (Jin et al., 2008; Matmati et al., 2011). Therefore, OPTN could mediate the downregulation of NF $\kappa$ B activity by interacting with these deubiquitinating enzymes. In light of this, OPTN was reported to inhibit the TNF $\alpha$ -induced NF $\kappa$ B activity by recruiting deubiquitinating enzyme CYLD to interact with the RIP (Nagabhushana et al., 2011). In this study, Optn binding with Cyld has been confirmed in response to RANKL stimulation. Interestingly, CYLD has been shown to regulate the RANK-induced osteoclastogenesis. In a previous study, *Cyld* knockout mice developed osteoporosis-like phenotype as a result of increased osteoclast differentiation (Jin et al., 2008). In addition, *Cyld*-deficient BMDMs from these mice are hypersensitive to RANKL signalling and form more osteoclasts compared to WT upon stimulation with RANKL, and CYLD requires the SQSTM1/p62 to interact with TRAF6 (Figure 7-1).

Similarly, the other deubiquitination enzyme A20 has been shown to downregulate the NF $\kappa$ B signaling at the level of TRAF6 and myeloid-specific deletion of A20 in mice triggers an autoimmune disease resembling rheumatoid arthritis. BMDMs lacking A20 exhibit enhanced NF $\kappa$ B activation and promote osteoclastogenesis in these mice (Matmati et al., 2011), however, further investigation is needed to prove the interaction with A20 in response to RANKL stimulation.



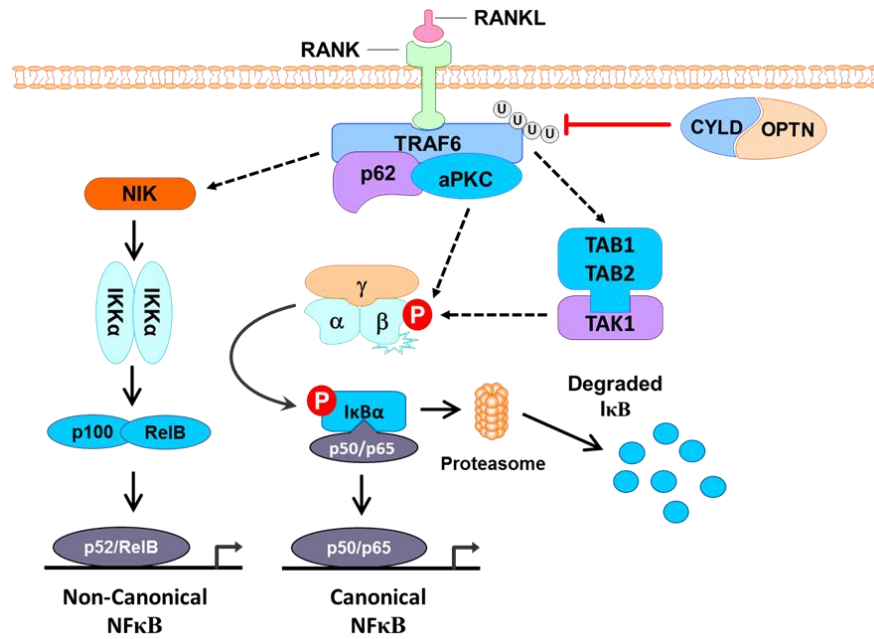


Figure 7-1: Suggested negative regulation of RANKL-induced NF $\kappa$ B signaling by OPTN. TRAF6 becomes ubiquitinated and thus activated when RANKL binds to its receptor RANK, which may then stimulate canonical NF $\kappa$ B activity either through phosphorylation of TAK1 or aPKC. This in turn leads to phosphorylation and activation of IKK $\beta$ , and subsequent degradation of the NF $\kappa$ B inhibitor subunit I $\kappa$ B $\alpha$  by proteasome. Liberated p50/p65 complex then translocates to the nucleus and induces transcription. RANK-RANKL signalling also stimulates the non-canonical NF $\kappa$ B pathway by stimulating the NF $\kappa$ B inducing kinase (NIK), which activates IKK $\alpha$  homodimers and thereby phosphorylation of p100. Subsequently, p100 cleaved to generate an active p52 product, which translocates to the nucleus along with RelB to induce transcription. CYLD is a deubiquitinating enzyme that negatively regulates NF $\kappa$ B by removing polyubiquitin chains from several proteins including TRAF6. CYLD is a binding partner to OPTN, which may also negatively regulate the RANKL-induced osteoclastogenesis through the interaction with CYLD.

### 7.1.2 Suggested role of OPTN through TBK1/IKK $\epsilon$

Studies on BMDMs showed that the expression of TBK1/IKK $\epsilon$  increased early in osteoclast differentiation in response to RANKL. Furthermore, TBK1/IKK $\epsilon$  was reported to interact with TANK and TRAF2, which in turn activate the NF $\kappa$ B upstream of IKK $\alpha$ /IKK $\beta$ . Additionally, TBK1/IKK $\epsilon$  is reported to activate the NF $\kappa$ B through direct phosphorylation of p65 (Morton et al., 2008; Sun et al., 2013). These findings suggest a role for TBK1/IKK $\epsilon$  in osteoclastogenesis. OPTN is a binding partner for TBK1 and the role of OPTN in TBK1/IKK $\epsilon$ -NF $\kappa$ B signalling pathway remains to be clarified.

### 7.1.3 Suggested role of *OPTN* through *IFN $\beta$* signalling

Another suggestion is that *OPTN* may regulate bone turnover through the regulation of *IFN $\beta$* . Previous studies showed that LPS-mediated activation of *NF $\kappa$ B* and *NF $\kappa$ B* dependent gene transcription was not impaired in *Optn*<sup>D477N/D477N</sup> when compared to WT (Gleason et al., 2011). The studies also reported diminished levels of *TBK1* and *IFN $\beta$*  in BMDMs of *Optn*<sup>D477N/D477N</sup> mice, suggesting that *OPTN* through its UBD binds *TBK1* via *TLR3/4* stimulation, enhances phosphorylation of *IRF3*. This leads to increased production of *IFN $\beta$* . These findings were reproduced in a recent study using another mouse model *Optn*<sup>470T</sup> (Munitic et al., 2013). Another study showed that *IFN $\beta$*  receptor knockout mice have increased osteoclast numbers and osteopenia (Takayanagi et al., 2002b). In addition, it has been shown that *RANKL* stimulates *IFN $\beta$*  production in osteoclast precursor cells, which in turn inhibits the osteoclast differentiation by interfering with the expression of *c-Fos* (Takayanagi et al., 2002a). However, the induction of *IFN $\beta$*  mRNA by *RANKL* was not abolished from *IRF-3/IRF-9*<sup>-/-</sup> mice, which means the induction of *IFN $\beta$*  was not dependent on *IRF3* (Takayanagi et al., 2002b) and therefore *IFN $\beta$*  gene induction mechanism differs from that induced by viruses. A possible explanation of how *OPTN* could regulate *IFN $\beta$*  is through the *STAT1* pathway. *STAT1* has been identified as an essential prerequisite for *IFN $\beta$*  expression and *STAT1* deficiency also prevented *RANKL*-induced *IFN $\beta$*  expression (Ha et al., 2008). Interestingly, *IFN $\gamma$* , which exerts its effects through *STAT1* and *IRF-1* and suppresses osteoclastogenesis by degrading *TRAF6*, which results in inhibition of the *RANKL*-induced osteoclastogenesis, has been shown to stimulate the induction of *OPTN* through the *IRF-1* promoter found in the first intron of *OPTN* (Sudhakar et al., 2013; Takayanagi et al., 2000). Collectively, these findings suggest that *OPTN* could enhance the *IFN $\beta$*  production in response to *RANKL* in BMDMs through the regulation of interferon system (*IFN- $\gamma$ -STAT1*) and independently to *IRF-3/IRF-9* pathway, which is caused by viral infection. Consequently, a defect in UBD of *OPTN* as in *Optn*<sup>D477N/D477N</sup> can lead to a fall in production of *IFN $\beta$*  and thereby enhance the osteoclast formation due to increased level of *c-Fos*. Further analysis will be required to confirm this hypothesis (Figure 7-

2). Recent findings by Albagha lab demonstrated that the expression level of IFN $\beta$  induced by RANKL was significantly lower in *Optn*<sup>D477N/D477N</sup> mutant cells compared to those observed in WT. At the same time, they found the expression of c-Fos during later stages of osteoclast differentiation was higher in mutant cells compared to WT (Obaid et al., 2015). These findings indicate that *Optn*<sup>D477N</sup> mutation enhanced the osteoclast formation *in vitro* by reducing IFN $\beta$  expression, which in turn affects the expression level of c-Fos. These results partially confirmed the previous suggestion for the possibility of OPTN to regulate osteoclast differentiation through its implication in interferon signalling pathway.

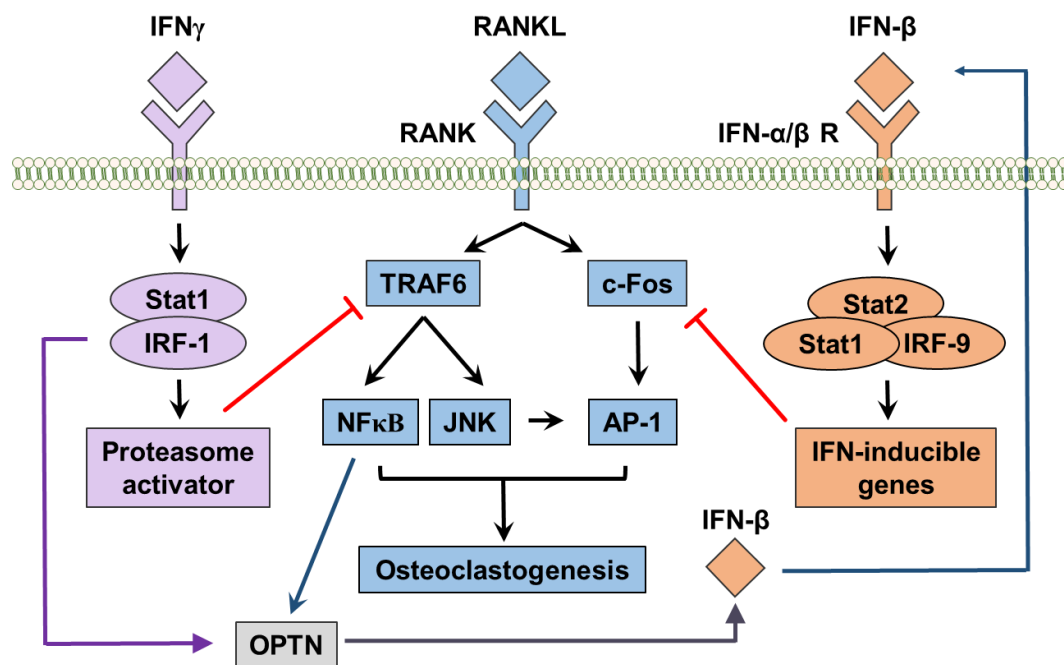


Figure 7-2: Suggested crosstalk between OPTN, RANKL and interferon system in regulation of osteoclast differentiation. During inflammatory condition, IFN $\gamma$  induces the ubiquitin-proteasome system, which exerts its inhibitory effect on RANKL signaling through STAT1 by the downregulation of TRAF6 expression. IFN $\gamma$  also stimulates the induction of OPTN through the IRF-1. OPTN expression also enhanced in response to RANKL-induced NF $\kappa$ B activity since a putative NF $\kappa$ B binding site has been reported in OPTN promoter. Increased expression of OPTN in turn enhances the induction of IFN $\beta$ , which regulates the RANKL signaling by inhibiting the expression of c-Fos.

#### 7.1.4 Suggested role of OPTN in MVNP mouse model for PDB

OPTN has also been implicated in viral infections (Journo et al., 2009; Mankouri et al., 2010), which have been suggested as one of the etiological factors for PDB because of the presence of nuclear inclusion bodies in Pagetic osteoclasts (Mills and Singer, 1976b). In MVNP mouse model, which is suggested as a model of Paget's disease, TBK1 plays a crucial role in mediating the impact of MVNP on osteoclast differentiation and formation. Moreover, TBK1/IKK $\epsilon$  have a role in innate immunity and when activated, TBK1/IKK $\epsilon$  phosphorylate the IRF3, which in turn activate the production of IFN $\beta$  (Sun et al., 2013). In view of this, the binding of OPTN to the polyubiquitin chain has recently been identified as essential for optimal activation of TBK1 and defective mutant in the polyubiquitin-binding of OPTN as in the *Optn*<sup>D477N/D477N</sup> model or insufficiency of *Optn* expression as in *Optn*<sup>470T</sup> model result in reduced activity of TBK1 and thus reduced IFN $\beta$  production (Gleason et al., 2011; Munitic et al., 2013). Therefore, OPTN may have a role in the viral etiological factor suggested for PDB. It is noteworthy that CYLD and OPTN were found complexed with TBK1/IKK $\epsilon$  and TANK, which has also been identified in innate immunity in response to viral infection as a negative regulator for antiviral signalling (Gao et al., 2011). In addition, OPTN was found in a protein complex containing TBK1 and TRAF3, which is considered an essential complex in the IFN $\beta$  signalling (Mankouri et al., 2010). Further investigation will be necessary to explore how OPTN orchestrate the RANK signalling in osteoclasts beside the viral infection (Figure 1-12, Chapter 1).

## 7.2 Future Work

The findings of this study demonstrate for the first time the implication of OPTN in bone metabolism. This suggests a number of possibilities for future research that need to be pursued to increase understanding of the role of OPTN in bone metabolism.

- Work is in progress to complete and expand the research outlined in this thesis. Another research topic would be to analyse the expression level of *OPTN* in PDB families linked to chromosome 10.
- The results discussed in this study show that in most cases *Optn*<sup>D477N</sup> alone does not cause PDB-like phenotype. Therefore, it is necessary to investigate the role of OPTN on bone metabolism using an appropriate mouse model lacking OPTN. Recently, clustered regularly interspaced short palindromic repeats (CRISPR) RNA-guided Cas9 nucleases (CRISPR/Cas9) have emerged as a new tool for precisely and effectively introducing targeted loss-of-function mutations in a broad range of species as well as cell lines and primary cells (Harrison et al., 2014). This method also allows researchers to generate multiple knockouts of different genes (Wang et al., 2013). In light of these advances, the impact of complete knockout of OPTN alone or in combination with other mutations such as SQSTM1 mutations will provide a better understanding of how these mutations are implicated in the pathogenesis of PDB. A further useful method for investigating the pathogenesis of PDB is to use the induced pluripotent stem cells (iPSC) technique (Chen, 2014). This method is capable of generating iPSC from somatic cells of affected patients. These cells can proliferate *in vitro* in large numbers and have the ability to differentiate into any cell type of the body including osteoclasts. In this way, patient-specific cells, which carry the disease-causing mutations, can be used to dissect diseases *in vitro* instead of using genetically manipulated cells. Another potential line of inquiry is to explore the implication of other candidate genes and loci, which have been identified by GWAS as potential causes of PDB including CSF1, TNFRSF11A, TM7SF4 and 2 loci 7q33 and 15q24. Interestingly, recent data obtained by our group have identified several

missense coding variants in RIN3 that may contribute to PDB (Vallet et al., 2015).

- Another area for research is to investigate the role of OPTN downstream the RANKL/RANK signalling pathway. Further signalling pathways in bone need to be investigated using DNA microarray, which measures the expression levels of large numbers of genes including, in particular, those functioning as growth factors and genes mediating osteogenesis and related cell growth, proliferation, and differentiation processes and genes involved in the development of the skeletal system and bone mineral metabolism.
- As outlined previously, autophagy is another suggested etiological factor for PDB and the role of OPTN in autophagy in bone is yet to be determined. To monitor autophagic activity, several methods are used in order to detect the number of autophagosome formed or to assess the autophagic flux (Mizushima et al., 2010). The methods used to detect the autophagosome formation require light microscopy to detect the subcellular localisation of LC3, electron microscopy to monitor endogenous LC3 and biochemical analysis to assess the LC3 processing by Western blot analysis. Several methods are also used to monitor the autophagic flux including a LC3 turnover assay that monitors degradation of LC3-II inside the autolysosome, degradation of autophagy-selective substrates such as LC3 and p62, fluorescent microscopy to detect labeled autophagosomes and their maturation into autolysosomes, measurement of long-lived protein degradation and detection of the labeled fragment generated by the degradation of labeled-LC3 inside autolysosomes (Mizushima et al., 2010). Due to the dynamic nature of autophagy and the limitations of the various methods, use of several methods is required in order to achieve accurate findings and conclusions. In addition, precaution in interpretation data acquired from *in vitro* experiments must be taken into consideration, as environmental and homeostatic conditions are different depending on how isolated cells have been treated. For example, conditions of non-resorbing osteoclasts cultured on plastic are different from resorbing osteoclasts on bone (Hocking et al., 2012).

### 7.3 General conclusions

The results reported in this thesis demonstrate for the first time that *OPTN* is implicated in bone biology. The data also showed that *OPTN* variant identified by GWAS could be of clinical value in identifying SQSTM1-negative patients and can be used to predict levels of disease severity. The data also showed that *Optn* is expressed in osteoclasts and osteoblasts and the role of *Optn* in osteoclasts is more pronounced. *OPTN* acts as a negative regulator to RANKL-induced osteoclastogenesis and this could be through the effect on NFκB activity. *OPTN* has no direct effect on osteoblasts but could enhance the osteoblast activity through its effect on osteoclasts *in vivo*. The mechanisms by which *OPTN* regulate bone turnover are complex but appear to involve: RANKL-induced NFκB activation, an interaction with *CYLD*, an interaction with interferon system and viral infection. Furthermore, the role of *OPTN* was reported in autophagy and vesicular trafficking, and this needs further clarification as they are implicated in PDB. Further analysis will be required to explore the role of *OPTN* in osteoclast signalling as the regulatory effects of this gene are cell-type specific, it responds to several types of stimulants differently and it is dependent on its expression level and its ability to bind polyubiquitin.

## References

- Abu-Amer, Y., 2013. NF- $\kappa$ B signaling and bone resorption. *Osteoporos. Int.* 24, 2377–2386.
- Akizuki, M., Yamashita, H., Uemura, K., Maruyama, H., Kawakami, H., Ito, H., Takahashi, R., 2013. Optineurin suppression causes neuronal cell death via NF- $\kappa$ B pathway. *J. Neurochem.* 126, 699–704.
- Albagha, O.M.E., Visconti, M.R., Alonso, N., Langston, A.L., Cundy, T., Dargie, R., Dunlop, M.G., Fraser, W.D., Hooper, M.J., Isaia, G., Nicholson, G.C., del Pino Montes, J., Gonzalez-Sarmiento, R., di Stefano, M., Tenesa, A., Walsh, J.P., Ralston, S.H., 2010. Genome-wide association study identifies variants at CSF1, OPTN and TNFRSF11A as genetic risk factors for Paget's disease of bone. *Nat. Genet.* 42, 520–524. doi:10.1038/ng.562
- Albagha, O.M.E., Visconti, M.R., Alonso, N., Wani, S., Goodman, K., Fraser, W.D., Gennari, L., Merlotti, D., Gianfrancesco, F., Esposito, T., Rendina, D., Di Stefano, M., Isaia, G., Brandi, M.L., Giusti, F., del Pino Montes, J., Corral-Gudino, L., Gonzalez-Sarmiento, R., Ward, L., Rea, S.L., Ratajczak, T., WALSH, J.P., Ralston, S.H., 2013. Common susceptibility alleles and SQSTM1 mutations predict disease extent and severity in a multinational study of patients with Paget's disease. *J. Bone Miner. Res.* 28, 2338–2346.
- Albagha, O.M.E., Wani, S.E., Visconti, M.R., Alonso, N., Goodman, K., Brandi, M.L., Cundy, T., Chung, P.Y.J., Dargie, R., Devogelaer, J.-P., Falchetti, A., Fraser, W.D., Gennari, L., Gianfrancesco, F., Hooper, M.J., Van Hul, W., Isaia, G., Nicholson, G.C., Nuti, R., Papapoulos, S., Montes, J. del P., Ratajczak, T., Rea, S.L., Rendina, D., Gonzalez-Sarmiento, R., Di Stefano, M., Ward, L.C., Walsh, J.P., Ralston, S.H., 2011a. Genome-wide association identifies three new susceptibility loci for Paget's disease of bone. *Nat. Genet.* 43, 685–689. doi:10.1038/ng.845
- Albagha, O.M.E., Wani, S.E., Visconti, M.R., Alonso, N., Goodman, K., Brandi, M.L., Cundy, T., Chung, P.Y.J., Dargie, R., Devogelaer, J.-P., Falchetti, A., Fraser, W.D., Gennari, L., Gianfrancesco, F., Hooper, M.J., Van Hul, W., Isaia, G., Nicholson, G.C., Nuti, R., Papapoulos, S., Montes, J. del P., Ratajczak, T., Rea, S.L., Rendina, D., Gonzalez-Sarmiento, R., Di Stefano, M., Ward, L.C., WALSH, J.P., Ralston, S.H., Consortium, G.D. of P.D. (GDPD), 2011b. Genome-wide association identifies three new susceptibility loci for Paget's disease of bone. *Nat. Publ. Gr.* 43, 685–689.
- Allen, M.R., Burr, D.B., 2014a. Bone Modeling and Remodeling, in: *Basic and Applied Bone Biology*. Elsevier, pp. 75–90. doi:10.1016/B978-0-12-416015-6.00004-6
- Allen, M.R., Burr, D.B., 2014b. Techniques in Histomorphometry, in: *Basic and Applied Bone Biology*. Elsevier, pp. 131–148. doi:10.1016/B978-0-12-416015-6.00007-1
- Allen, M.R., Krohn, K., 2014. Skeletal Imaging, in: *Basic and Applied Bone Biology*. Elsevier, pp. 93–113. doi:10.1016/B978-0-12-416015-6.00005-8
- Alvarez, L., Peris, P., Guañabens, N., Vidal, S., Ros, I., Pons, F., Filella, X., Monegal, A., Muñoz-Gomez, J., Ballesta, A.M., 2003. Serum osteoprotegerin and its ligand in Paget's disease of bone: relationship to disease activity and effect of treatment with bisphosphonates. *Arthritis Rheum.* 48, 824–8. doi:10.1002/art.10834



## BIBLIOGRAPHY

- Anborgh, P.H., Godin, C., Pampillo, M., Dhimi, G.K., Dale, L.B., Cregan, S.P., Truant, R., Ferguson, S.S.G., 2005. Inhibition of Metabotropic Glutamate Receptor Signaling by the Huntingtin-binding Protein Optineurin. *J. Biol. Chem.* 280, 34840–34848.
- Ayala-Lugo, R., Pawar, H., Reed, D., Lichter, P., 2007. Variation in optineurin (OPTN) allele frequencies between and within populations. *Mol. ....*
- Badadani, M., Nalbandian, A., Watts, G.D., Vesa, J., Kitazawa, M., Su, H., Tanaja, J., Dec, E., Wallace, D.C., Mukherjee, J., Caiozzo, V., Warman, M., Kimonis, V.E., 2010. VCP Associated Inclusion Body Myopathy and Paget Disease of Bone Knock-In Mouse Model Exhibits Tissue Pathology Typical of Human Disease. *PLoS One* 5, e13183. doi:10.1371/journal.pone.0013183
- Bailey-Wilson, J.E., Wilson, A.F., 2011. Linkage Analysis in the Next-Generation Sequencing Era. *Hum. Hered.* 72, 228–236.
- Barker, D.J., Gardner, M.J., 1974. Distribution of Paget's disease in England, Wales and Scotland and a possible relationship with vitamin D deficiency in childhood. *Br. J. Prev. Soc. Med.* 28, 226–232.
- Barker, D.J.P., 1984. The epidemiology of Paget's disease of bone. *Br. Med. Bull.*
- Baslé, M.F., Fournier, J.G., Rozenblatt, S., Rebel, A., Bouteille, M., 1986. Measles virus RNA detected in Paget's disease bone tissue by in situ hybridization. *J. Gen. Virol.* 67 ( Pt 5), 907–13. doi:10.1099/0022-1317-67-5-907
- Bellido, T., Plotkin, L.I., Bruzzaniti, A., 2014. Bone Cells, in: *Basic and Applied Bone Biology*. Elsevier, pp. 27–45. doi:10.1016/B978-0-12-416015-6.00002-2
- Beyens, G., Daroszewska, A., de Freitas, F., Fransen, E., Vanhoenacker, F., Verbruggen, L., Zmierzak, H.-G., Westhovens, R., Van Offel, J., Ralston, S.H., Devogelaer, J.-P., Van Hul, W., 2007. Identification of Sex-Specific Associations Between Polymorphisms of the Osteoprotegerin Gene, TNFRSF11B, and Paget's Disease of Bone. *J. Bone Miner. Res.* 22, 1062–1071.
- Beyens, G., Van Hul, E., Van Driessche, K., Fransen, E., Devogelaer, J.P., Vanhoenacker, F., Van Offel, J., Verbruggen, L., De Clerck, L., Westhovens, R., Van Hul, W., 2004. Evaluation of the Role of the SQSTM1 Gene in Sporadic Belgian Patients with Paget's Disease. *Calcif. Tissue Int.* 75, 144–152.
- Bignell, G.R., Warren, W., Seal, S., Takahashi, M., Rapley, E., Barfoot, R., Green, H., Brown, C., Biggs, P.J., Lakhani, S.R., Jones, C., Hansen, J., Blair, E., Hofmann, B., Siebert, R., Turner, G., Evans, D.G., Schrandt-Stumpel, C., Beemer, F.A., van Den Ouweland, A., Halley, D., Delpuch, B., Cleveland, M.G., Leigh, I., Leisti, J., Rasmussen, S., 2000. Identification of the familial cylindromatosis tumour-suppressor gene. *Nat. Genet.* 25, 160–5. doi:10.1038/76006
- Birch, M.A., Taylor, W., Fraser, W.D., Ralston, S.H., Hart, C.A., Gallagher, J.A., 2009. Absence of paramyxovirus RNA in cultures of pagetic bone cells and in pagetic bone. *J. Bone Miner. Res.* 9, 11–16. doi:10.1002/jbmr.5650090103
- Bonewald, L.F., 2011. The amazing osteocyte. *J. Bone Miner. Res.* 26, 229–38. doi:10.1002/jbmr.320
- Boyce, B.F., Xing, L., 2008. Functions of RANKL/RANK/OPG in bone modeling and remodeling. *Arch. Biochem. Biophys.* 473, 139–146.

## BIBLIOGRAPHY

- Boyce, B.F., Zuscik, M.J., Xing, L., 2012. Biology of Bone and Cartilage, in: Genetics of Bone Biology and Skeletal Disease. Elsevier Inc., pp. 1–24.
- Brakspear, K.S., Mason, D.J., 2012. Glutamate signaling in bone. *Front. Endocrinol. (Lausanne)*. 3, 1–8.
- Brandwood, C.P., Hoyland, J.A., Hillarby, M.C., Berry, J.L., Davies, M., Selby, P.L., Mee, A.P., 2003. Apoptotic gene expression in Paget's disease: a possible role for Bcl-2. *J. Pathol.* 201, 504–512.
- Burr, D.B., Akkus, O., 2014. Bone Morphology and Organization, in: Basic and Applied Bone Biology. Elsevier, pp. 3–25. doi:10.1016/B978-0-12-416015-6.00001-0
- Cenci, S., Toraldo, G., Weitzmann, M.N., Roggia, C., Gao, Y., Qian, W.P., Sierra, O., Pacifici, R., 2003. Estrogen deficiency induces bone loss by increasing T cell proliferation and lifespan through IFN-gamma-induced class II transactivator. *Proc. Natl. Acad. Sci. U. S. A.* 100, 10405–10. doi:10.1073/pnas.1533207100
- Chalasani, M.L., Balasubramanian, D., Swarup, G., 2008. Focus on Molecules: Optineurin. *Exp. Eye Res.* 87, 1–2.
- Chalasani, M.L., Swarup, G., Balasubramanian, D., 2009. Optineurin and Its Mutants: Molecules Associated with Some Forms of Glaucoma. *Ophthalmic Res.* 42, 176–184.
- Chen, I.-P., 2014. The Use of Patient-Specific Induced Pluripotent Stem Cells (iPSCs) to Identify Osteoclast Defects in Rare Genetic Bone Disorders. *J. Clin. Med.* 3, 1490–1510. doi:10.3390/jcm3041490
- Cheng, S. V, Martin, G.R., Nadeau, J.H., Haines, J.L., Bucan, M., Kozak, C.A., MacDonald, M.E., Lockyer, J.L., Ledley, F.D., Woo, S.L., 1989. Synteny on mouse chromosome 5 of homologs for human DNA loci linked to the Huntington disease gene. *Genomics* 4, 419–26.
- Chi, Z.-L., Akahori, M., Obazawa, M., Minami, M., Noda, T., Nakaya, N., Tomarev, S., Kawase, K., Yamamoto, T., Noda, S., Sasaoka, M., Shimazaki, A., Takada, Y., Iwata, T., 2010. Overexpression of optineurin E50K disrupts Rab8 interaction and leads to a progressive retinal degeneration in mice. *Hum. Mol. Genet.* 19, 2606–2615.
- Chung, P.Y.J., Beyens, G., Boonen, S., Papapoulos, S., Geusens, P., Karperien, M., Vanhoenacker, F., Verbruggen, L., Fransen, E., Van Offel, J., Goemaere, S., Zmierzczak, H.-G., Westhovens, R., Devogelaer, J.-P., Van Hul, W., 2010a. The majority of the genetic risk for Paget's disease of bone is explained by genetic variants close to the CSF1, OPTN, TM7SF4, and TNFRSF11A genes. *Hum. Genet.* 128, 615–626.
- Chung, P.Y.J., Beyens, G., de Freitas, F., Boonen, S., Geusens, P., Vanhoenacker, F., Verbruggen, L., Van Offel, J., Goemaere, S., Zmierzczak, H.-G., Westhovens, R., Devogelaer, J.-P., Van Hul, W., 2011. Indications for a genetic association of a VCP polymorphism with the pathogenesis of sporadic Paget's disease of bone, but not for TNFSF11 (RANKL) and IL-6 polymorphisms. *Mol. Genet. Metab.* 103, 287–292.

## BIBLIOGRAPHY

- Chung, P.Y.J., Beyens, G., Riches, P.L., Van Wesenbeeck, L., de Freitas, F., Jennes, K., Daroszewska, A., Fransen, E., Boonen, S., Geusens, P., Vanhoenacker, F., Verbruggen, L., Van Offel, J., Goemaere, S., Zmierzczak, H.-G., Westhovens, R., Karperien, M., Papapoulos, S., Ralston, S.H., Devogelaer, J.-P., Van Hul, W., 2010b. Genetic variation in the TNFRSF11A gene encoding RANK is associated with susceptibility to Paget's disease of bone. *J. Bone Miner. Res.* 25, 2592–2605.
- Chung, P.Y.J., Beyens, G., Riches, P.L., Van Wesenbeeck, L., Jennes, K., Daroszewska, A., Boonen, S., Geusens, P., Vanhoenacker, F., Verbruggen, L., Van Offel, J., Goemaere, S., Zmierzczak, H., Westhovens, R., Karperien, M., Papapoulos, S., Ralston, S.H., Devogelaer, J.P., Van Hul, W., 2009. Genetic variation in the TNFRSF11A (RANK) gene contributes to the risk to develop sporadic Paget's disease of bone. *Bone* 44, S347–S348.
- Chung, P.Y.J., Van Hul, W., 2012. Paget's Disease of Bone: Evidence for Complex Pathogenetic Interactions. *YSARH* 41, 619–641.
- Clark, K., Takeuchi, O., Akira, S., Cohen, P., 2011. The TRAF-associated protein TANK facilitates cross-talk within the I $\kappa$ B kinase family during Toll-like receptor signaling. *Proc. Natl. Acad. Sci. U. S. A.* 108, 17093–17098.
- Collin-Osdoby, P., Osdoby, P., 2012. RANKL-mediated osteoclast formation from murine RAW 264.7 cells. *Methods Mol. Biol.* 816, 187–202.
- Conn, P.J., Pin, J.P., 1997. Pharmacology and functions of metabotropic glutamate receptors. *Annu. Rev. Pharmacol. Toxicol.* 37, 205–237.
- Coxon, F.P., Taylor, A., 2008. Vesicular trafficking in osteoclasts. *Semin. Cell Dev. Biol.* 19, 424–433.
- Crockett, J.C., Mellis, D.J., Shennan, K.I.J., Duthie, A., Greenhorn, J., Wilkinson, D.I., Ralston, S.H., Helfrich, M.H., Rogers, M.J., 2011. Signal peptide mutations in RANK prevent downstream activation of NF- $\kappa$ B. *J. Bone Miner. Res.* 26, 1926–1938.
- Cundy, T., Hegde, M., Naot, D., Chong, B., King, A., Wallace, R., Mulley, J., Love, D.R., Seidel, J., Fawcner, M., Banovic, T., Callon, K.E., Grey, A.B., Reid, I.R., Middleton-Hardie, C.A., Cornish, J., 2002. A mutation in the gene TNFRSF11B encoding osteoprotegerin causes an idiopathic hyperphosphatasia phenotype. *Hum. Mol. Genet.* 11, 2119–2127.
- Daroszewska, A., Hocking, L.J., McGuigan, F.E.A., Langdahl, B., Stone, M.D., Cundy, T., Nicholson, G.C., Fraser, W.D., Ralston, S.H., 2004. Susceptibility to Paget's Disease of Bone Is Influenced by a Common Polymorphic Variant of Osteoprotegerin. *J. Bone Miner. Res.* 19, 1506–1511.
- Daroszewska, A., van 't Hof, R.J., Rojas, J.A., Layfield, R., Landao-Basonga, E., Rose, L., Rose, K., Ralston, S.H., 2011. A point mutation in the ubiquitin-associated domain of SQSMT1 is sufficient to cause a Paget's disease-like disorder in mice. *Hum. Mol. Genet.* 20, 2734–2744.
- Davis, M.E., Gack, M.U., 2015. Ubiquitination in the antiviral immune response. *Virology* 479–480, 52–65. doi:10.1016/j.virol.2015.02.033

## BIBLIOGRAPHY

- De Valck, D., Jin, D.Y., Heyninck, K., Van de Craen, M., Contreras, R., Fiers, W., Jeang, K.T., Beyaert, R., 1999. The zinc finger protein A20 interacts with a novel anti-apoptotic protein which is cleaved by specific caspases. *Oncogene* 18, 4182–90. doi:10.1038/sj.onc.1202787
- del Toro, D., Alberch, J., Lázaro-Diéguez, F., Martín-Ibáñez, R., Xifró, X., Egea, G., Canals, J.M., 2009. Mutant huntingtin impairs post-Golgi trafficking to lysosomes by delocalizing optineurin/Rab8 complex from the Golgi apparatus. *Mol. Biol. Cell* 20, 1478–92. doi:10.1091/mbc.E08-07-0726
- Dempster, D.W., Compston, J.E., Drezner, M.K., Glorieux, F.H., Kanis, J.A., Malluche, H., Meunier, P.J., Ott, S.M., Recker, R.R., Parfitt, A.M., 2013. Standardized nomenclature, symbols, and units for bone histomorphometry: a 2012 update of the report of the ASBMR Histomorphometry Nomenclature Committee. *J. Bone Miner. Res.* 28, 2–17.
- DeSelm, C.J., Miller, B.C., Zou, W., Beatty, W.L., van Meel, E., Takahata, Y., Klumperman, J., Tooze, S.A., Teitelbaum, S.L., Virgin, H.W., 2011. Autophagy proteins regulate the secretory component of osteoclastic bone resorption. *Dev. Cell* 21, 966–974.
- Dixit, V.M., Green, S., Sarma, V., Holzman, L.B., Wolf, F.W., O'Rourke, K., Ward, P.A., Prochownik, E. V, Marks, R.M., 1990. Tumor necrosis factor- $\alpha$  induction of novel gene products in human endothelial cells including a macrophage-specific chemotaxin. *J. Biol. Chem.* 265, 2973–8.
- Donath, J., Speer, G., Poor, G., Gergely, P., Tabak, A., Lakatos, P., 2004. Vitamin D receptor, oestrogen receptor- and calcium-sensing receptor genotypes, bone mineral density and biochemical markers in Paget's disease of bone. *Rheumatology* 43, 692–695.
- Duncan, E.L., Brown, M.A., 2013. Genome-wide Association Studies, in: *Genetics of Bone Biology and Skeletal Disease*. Elsevier, pp. 93–100. doi:10.1016/B978-0-12-387829-8.00007-X
- Duplomb, L., Baud'huin, M., Charrier, C., Berreur, M., Trichet, V., Blanchard, F., Heymann, D., 2008. Interleukin-6 inhibits receptor activator of nuclear factor kappaB ligand-induced osteoclastogenesis by diverting cells into the macrophage lineage: key role of Serine727 phosphorylation of signal transducer and activator of transcription 3. *Endocrinology* 149, 3688–97. doi:10.1210/en.2007-1719
- Durán, A., Serrano, M., Leitges, M., Flores, J.M., Picard, S., Brown, J.P., Moscat, J., Diaz-Meco, M.T., 2004. The atypical PKC-interacting protein p62 is an important mediator of RANK-activated osteoclastogenesis. *Dev. Cell* 6, 303–309. doi:10.1016/S1534-5807(03)00403-9
- ENGELKE, D., NG, S., SHASTRY, B., ROEDER, R., 1980. Specific interaction of a purified transcription factor with an internal control region of 5S RNA genes. *Cell* 19, 717–728. doi:10.1016/S0092-8674(80)80048-1
- Gao, J., Ohtsubo, M., Hotta, Y., Minoshima, S., 2014. Oligomerization of optineurin and its oxidative stress- or E50K mutation-driven covalent cross-linking: possible relationship with glaucoma pathology. *PLoS One* 9, e101206. doi:10.1371/journal.pone.0101206
- Gao, L., Coope, H., Grant, S., Ma, A., Ley, S.C., Harhaj, E.W., 2011. ABIN1 protein cooperates with TAX1BP1 and A20 proteins to inhibit antiviral signaling. *J. Biol. Chem.* 286, 36592–36602.

## BIBLIOGRAPHY

- Gao, Y., Grassi, F., Ryan, M.R., Terauchi, M., Page, K., Yang, X., Weitzmann, M.N., Pacifici, R., 2007. IFN-gamma stimulates osteoclast formation and bone loss in vivo via antigen-driven T cell activation. *J. Clin. Invest.* 117, 122–32. doi:10.1172/JCI30074
- Gaspar, T.M., 1979. Paget's disease in a treadle machine operator. *Br. Med. J.* 1, 1217–1218.
- Girard, J.-P., Baekkevold, E.S., Feliu, J., Brandtzaeg, P., Amalric, F., 1999. Molecular cloning and functional analysis of SUT-1, a sulfate transporter from human high endothelial venules. *Proc. Natl. Acad. Sci.* 96, 12772–12777. doi:10.1073/pnas.96.22.12772
- Gleason, C.E., Ordureau, A., Gourlay, R., Arthur, J.S.C., Cohen, P., 2011. Polyubiquitin binding to optineurin is required for optimal activation of TANK-binding kinase 1 and production of interferon  $\beta$ . *J. Biol. Chem.* 286, 35663–35674.
- Good, D.A., Busfield, F., Fletcher, B.H., Lovelock, P.K., Duffy, D.L., Kesting, J.B., Andersen, J., Shaw, J.T.E., 2004. Identification of SQSTM1 mutations in familial Paget's disease in Australian pedigrees. *Bone* 35, 277–282.
- Gordon, M.T., Anderson, D.C., Sharpe, P.T., 1991. Canine distemper virus localised in bone cells of patients with Paget's disease. *Bone* 12, 195–201.
- Gordon, M.T., Mee, A.P., Anderson, D.C., Sharpe, P.T., 1992. Canine distemper virus transcripts sequenced from pagetic bone. *Bone Miner.* 19, 159–74.
- Guerrini, M.M., Sobacchi, C., Cassani, B., Abinun, M., Kilic, S.S., Pangrazio, A., Moratto, D., Mazzolari, E., Clayton-Smith, J., Orchard, P., Coxon, F.P., Helfrich, M.H., Crockett, J.C., Mellis, D., Vellodi, A., Tezcan, I., Notarangelo, L.D., Rogers, M.J., Vezzoni, P., Villa, A., Frattini, A., 2008. Human osteoclast-poor osteopetrosis with hypogammaglobulinemia due to TNFRSF11A (RANK) mutations. *Am. J. Hum. Genet.* 83, 64–76. doi:10.1016/j.ajhg.2008.06.015
- Ha, H., Lee, J.H., Kim, H.N., Kwak, H.B., Kim, H.M., Lee, S.E., Rhee, J.H., Kim, H.H., Lee, Z.H., 2008. Stimulation by TLR5 Modulates Osteoclast Differentiation through STAT1/IFN-. *J. Immunol.* 180, 1382–1389.
- Harhaj, E.W., Dixit, V.M., 2010. Deubiquitinases in the regulation of NF- $\kappa$ B signaling. *Nat. Publ. Gr.* 21, 22–39.
- Harhaj, E.W., Sun, S.-C., 1999. IKK Serves as a Docking Subunit of the I B Kinase (IKK) and Mediates Interaction of IKK with the Human T-cell Leukemia Virus Tax Protein. *J. Biol. Chem.* 274, 22911–22914. doi:10.1074/jbc.274.33.22911
- Harrison, M.M., Jenkins, B. V., Connor-giles, K.M.O., Wildonger, J., 2014. A CRISPR view of development. *Genes Dev.* 28, 1859–1872. doi:10.1101/gad.248252.114.Freely
- Harvey, L., Gray, T., Beneton, M.N., Douglas, D.L., Kanis, J.A., Russell, R.G., 1982. Ultrastructural features of the osteoclasts from Paget's disease of bone in relation to a viral aetiology. *J. Clin. Pathol.* 35, 771–779.
- Hasson, T., Mooseker, M.S., 1994. Porcine myosin-VI: characterization of a new mammalian unconventional myosin. *J. Cell Biol.* 127, 425–40. doi:10.1083/jcb.127.2.425
- Hattula, K., Peränen, J., 2000. FIP-2, a coiled-coil protein, links Huntingtin to Rab8 and modulates cellular morphogenesis. *Curr. Biol.* 10, 1603–1606.

## BIBLIOGRAPHY

- Hauge, X.Y., Litt, M., 1993. A study of the origin of “shadow bands” seen when typing dinucleotide repeat polymorphisms by the PCR. *Hum. Mol. Genet.* 2, 411–5.
- Hayman, A.R., Cox, T.M., 2003. Tartrate-resistant acid phosphatase knockout mice. *J. Bone Miner. Res.* 18, 1905–7. doi:10.1359/jbmr.2003.18.10.1905
- Hayman, A.R., Macary, P., Lehner, P.J., Cox, T.M., 2001. Tartrate-resistant acid phosphatase (Acp 5): identification in diverse human tissues and dendritic cells. *J. Histochem. Cytochem.* 49, 675–84.
- Hiruma, Y., Kurihara, N., Subler, M.A., Zhou, H., Boykin, C.S., Zhang, H., Ishizuka, S., Dempster, D.W., Roodman, G.D., Windle, J.J., 2008. A SQSTM1/p62 mutation linked to Paget’s disease increases the osteoclastogenic potential of the bone microenvironment. *Hum. Mol. Genet.* 17, 3708–3719.
- Hocking, L., Azzam, E., Greenhorn, J., Helfrich, M., Coxon, F., 2010. Autophagy and Paget’s disease of bone. *Bone* 46, S63.
- Hocking, L.J., Herbert, C.A., Nicholls, R.K., Williams, F., 2001. Genomewide Search in Familial Paget Disease of Bone Shows Evidence of Genetic Heterogeneity with Candidate Loci on Chromosomes 2q36, 10p13, and 5q35. ... *Hum. Genet.*
- Hocking, L.J., Mellis, D.J., McCabe, P.S., Helfrich, M.H., Rogers, M.J., 2010. Functional interaction between sequestosome-1/p62 and autophagy-linked FYVE-containing protein WDFY3 in human osteoclasts. *Biochem. Biophys. Res. Commun.* 402, 543–8. doi:10.1016/j.bbrc.2010.10.076
- Hocking, L.J., Whitehouse, C., Helfrich, M.H., 2012. Autophagy: A new player in skeletal maintenance? *J. Bone Miner. Res.* 27, 1439–1447.
- Hoyland, J., Sharpe, P.T., 1994. Upregulation of c-fos protooncogene expression in pagetic osteoclasts. *J. Bone Miner. Res.* 9, 1191–4. doi:10.1002/jbmr.5650090808
- Hoyland, J.A., Freemont, A.J., Sharpe, P.T., 1994. Interleukin-6, IL-6 receptor, and IL-6 nuclear factor gene expression in Paget’s disease. *J. Bone Miner. Res.* 9, 75–80. doi:10.1002/jbmr.5650090111
- Hsu, H., Huang, J., Shu, H.-B., Baichwal, V., Goeddel, D. V., 1996. TNF-Dependent Recruitment of the Protein Kinase RIP to the TNF Receptor-1 Signaling Complex. *Immunity* 4, 387–396. doi:10.1016/S1074-7613(00)80252-6
- Hu, H., Brittain, G.C., Chang, J.-H., Puebla-Osorio, N., Jin, J., Zal, A., Xiao, Y., Cheng, X., Chang, M., Fu, Y.-X., Zal, T., Zhu, C., Sun, S.-C., 2013. OTUD7B controls non-canonical NF- $\kappa$ B activation through deubiquitination of TRAF3. *Nature* 494, 371–4. doi:10.1038/nature11831
- Hu, H.M., O’Rourke, K., Boguski, M.S., Dixit, V.M., 1994. A novel RING finger protein interacts with the cytoplasmic domain of CD40. *J. Biol. Chem.* 269, 30069–72.
- Hughes, A.E., Ralston, S.H., Marken, J., Bell, C., MacPherson, H., Wallace, R.G.H., van Hul, W., Whyte, M.P., Nakatsuka, K., Hovy, L., Anderson, D.M., 2000. Mutations in TNFRSF11A, affecting the signal peptide of RANK, cause familial expansile osteolysis. *Nat. Genet.* 24, 45–48. doi:10.1038/71667
- Hughes, A.E., Shearman, A.M., Weber, J.L., Barr, R.J., Wallace, R.G.H., Osterberg, P.H., Nevin, N.C., Mollan, R.A.B., 1994. Genetic linkage of familial expansile osteolysis to chromosome 18q. *Hum. Mol. Genet.* 3, 359–361.

## BIBLIOGRAPHY

- Iotsova, V., Caamaño, J., Loy, J., Yang, Y., Lewin, A., Bravo, R., 1997. Osteopetrosis in mice lacking NF- $\kappa$ B1 and NF- $\kappa$ B2. *Nat. Med.* 3, 1285–1289. doi:10.1038/nm1197-1285
- Ito, H., Fujita, K., Nakamura, M., Wate, R., Kaneko, S., Sasaki, S., Yamane, K., Suzuki, N., Aoki, M., Shibata, N., Togashi, S., Kawata, A., Mochizuki, Y., Mizutani, T., Maruyama, H., Hirano, A., Takahashi, R., Kawakami, H., Kusaka, H., 2011. Optineurin is co-localized with FUS in basophilic inclusions of ALS with FUS mutation and in basophilic inclusion body disease. *Acta Neuropathol.* 121, 555–557.
- Itzstein, C., van 't Hof, R.J., 2012. Osteoclast Formation in Mouse Co-cultures, in: *Methods in Molecular Biology*. Humana Press, Totowa, NJ, pp. 177–186. doi:10.1007/978-1-61779-415-5\_12
- Jin, H., Ralston, S.H., 2012. *Bone Research Protocols* 816. doi:10.1007/978-1-61779-415-5
- Jin, W., Chang, M., Paul, E.M., Babu, G., Lee, A.J., Reiley, W., Wright, A., Zhang, M., You, J., Sun, S.-C., 2008. Deubiquitinating enzyme CYLD negatively regulates RANK signaling and osteoclastogenesis in mice. *J. Clin. Invest.* 118, 1858–1866.
- Johnson, L., Miller, J.W., Gkazi, A.S., Vance, C., Topp, S.D., Newhouse, S.J., Al-Chalabi, A., Smith, B.N., Shaw, C.E., 2012. Screening for OPTN mutations in a cohort of British amyotrophic lateral sclerosis patients. *Neurobiol. Aging* 33, 2948.e15–2948.e17. doi:10.1016/j.neurobiolaging.2012.06.023
- Journo, C., Filipe, J., About, F., Chevalier, S.A., Afonso, P. V., Brady, J.N., Flynn, D., Tangy, F., Israel, A., Vidalain, P.-O., Mahieux, R., Weil, R., 2009. NRP/Optineurin Cooperates with TAX1BP1 to Potentiate the Activation of NF- $\kappa$ B by Human T-Lymphotropic Virus Type 1 Tax Protein. *PLoS Pathog* 5, e1000521.
- Kabeya, Y., Mizushima, N., Ueno, T., Yamamoto, A., Kirisako, T., Noda, T., Kominami, E., Ohsumi, Y., Yoshimori, T., 2000. LC3, a mammalian homologue of yeast Apg8p, is localized in autophagosome membranes after processing. *EMBO J.* 19, 5720–8. doi:10.1093/emboj/19.21.5720
- Kachaner, D., Génin, P., Laplantine, E., Weil, R., 2012. Toward an integrative view of Optineurin functions. *Cell Cycle* 11, 2808–2818.
- Khosla, S., 2001. Minireview: the OPG/RANKL/RANK system. *Endocrinology* 142, 5050–5. doi:10.1210/endo.142.12.8536
- Kitsios, G.D., Zintzaras, E., 2009. Genome-wide association studies: hypothesis-“free” or “engaged”? *Transl. Res.* 154, 161–164.
- Komatsu, M., Waguri, S., Koike, M., Sou, Y.-S., Ueno, T., Hara, T., Mizushima, N., Iwata, J.-I., Ezaki, J., Murata, S., Hamazaki, J., Nishito, Y., Iemura, S.-I., Natsume, T., Yanagawa, T., Uwayama, J., Warabi, E., Yoshida, H., Ishii, T., Kobayashi, A., Yamamoto, M., Yue, Z., Uchiyama, Y., Kominami, E., Tanaka, K., 2007. Homeostatic levels of p62 control cytoplasmic inclusion body formation in autophagy-deficient mice. *Cell* 131, 1149–1163.
- Kong, Y.Y., Yoshida, H., Sarosi, I., Tan, H.L., Timms, E., Capparelli, C., Morony, S., Oliveira-dos-Santos, A.J., Van, G., Itie, A., Khoo, W., Wakeham, A., Dunstan, C.R., Lacey, D.L., Mak, T.W., Boyle, W.J., Penninger, J.M., 1999. OPGL is a key regulator of osteoclastogenesis, lymphocyte development and lymph-node organogenesis. *Nature* 397, 315–23. doi:10.1038/16852

## BIBLIOGRAPHY

- Korac, J., Schaeffer, V., Kovacevic, I., Clement, A.M., Jungblut, B., Behl, C., Terzic, J., Dikic, I., 2013. Ubiquitin-independent function of optineurin in autophagic clearance of protein aggregates. *J. Cell Sci.* 126, 580–592.
- Kotake, S., Nanke, Y., Mogi, M., Kawamoto, M., Furuya, T., Yago, T., Kobashigawa, T., Togari, A., Kamatani, N., 2005. IFN-gamma-producing human T cells directly induce osteoclastogenesis from human monocytes via the expression of RANKL. *Eur. J. Immunol.* 35, 3353–63. doi:10.1002/eji.200526141
- Kroeber, M., Ohlmann, A., Russell, P., Tamm, E.R., 2006. Transgenic studies on the role of optineurin in the mouse eye. *Exp. Eye Res.* 82, 1075–1085.
- Kular, J., Tickner, J., Chim, S.M., Xu, J., 2012. An overview of the regulation of bone remodelling at the cellular level. *Clin. Biochem.* 45, 863–873.
- Kurihara, N., Hiruma, Y., Yamana, K., Michou, L., Rousseau, C., Morissette, J., Galson, D.L., Teramachi, J., Zhou, H., Dempster, D.W., Windle, J.J., Brown, J.P., Roodman, G.D., 2011. Contributions of the Measles Virus Nucleocapsid Gene and the SQSTM1/p62P392L Mutation to Paget's Disease. *Cell Metab.* 13, 23–34.
- Kurihara, N., Hiruma, Y., Zhou, H., Subler, M.A., Dempster, D.W., Singer, F.R., Reddy, S. V., Gruber, H.E., Windle, J.J., Roodman, G.D., 2007. Mutation of the sequestosome 1 (p62) gene increases osteoclastogenesis but does not induce Paget disease. *J. Clin. Invest.* 117, 133–142.
- Kurihara, N., Reddy, S. V., Araki, N., Ishizuka, S., Ozono, K., Cornish, J., Cundy, T., Singer, F.R., Roodman, G.D., 2004. Role of TAFII-17, a VDR Binding Protein, in the Increased Osteoclast Formation in Paget's Disease. *J. Bone Miner. Res.* 19, 1154–1164.
- Langston, A.L., Campbell, M.K., Fraser, W.D., MacLennan, G.S., Selby, P.L., Ralston, S.H., 2009. Randomized trial of intensive bisphosphonate treatment versus symptomatic management in paget's disease of bone. *J. Bone Miner. Res.* 25, 20–31.
- Laurin, N., 2002. Recurrent Mutation of the Gene Encoding sequestosome 1 (SQSTM1/p62) in Paget Disease of Bone. *Am. J. Hum. Genet.* 70, 1582–1588.
- Laurin, N., Brown, J.P., Lemaingue, A., Duchesne, A., 2001. Paget Disease of Bone: Mapping of Two Loci at 5q35-qter and 5q31. *Am. J. ....*
- Lee, J.H., Rho, S.B., Chun, T., 2005. GABAA receptor-associated protein (GABARAP) induces apoptosis by interacting with DEAD (Asp-Glu-Ala-Asp/His) box polypeptide 47 (DDX 47). *Biotechnol. Lett.* 27, 623–8. doi:10.1007/s10529-005-3628-2
- LEVER, J.H., 2002. Paget's disease of bone in Lancashire and arsenic pesticide in cotton mill wastewater: a speculative hypothesis. *Bone* 31, 434–436.
- Li, R.F., Chen, G., Ren, J.G., Zhang, W., Wu, Z.X., Liu, B., Zhao, Y., Zhao, Y.F., 2014. The Adaptor Protein p62 Is Involved in RANKL-induced Autophagy and Osteoclastogenesis. *J. Histochem. Cytochem.*
- Ling, L., Goeddel, D. V., 2000. T6BP, a TRAF6-interacting protein involved in IL-1 signaling. *Proc. Natl. Acad. Sci. U. S. A.* 97, 9567–72. doi:10.1073/pnas.170279097



## BIBLIOGRAPHY

- Lucas, G.J.A., Mehta, S.G., Hocking, L.J., Stewart, T.L., Cundy, T., Nicholson, G.C., WALSH, J.P., Fraser, W.D., Watts, G.D.J., Ralston, S.H., Kimonis, V.E., 2006. Evaluation of the role of Valosin-containing protein in the pathogenesis of familial and sporadic Paget's disease of bone. *Bone* 38, 280–285.
- Lucas, G.J.A., Riches, P.L., Hocking, L.J., Cundy, T., Nicholson, G.C., WALSH, J.P., Ralston, S.H., 2007. Identification of a Major Locus for Paget's Disease on Chromosome 10p13 in Families of British Descent. *J. Bone Miner. Res.* 23, 58–63.
- Madyastha, P.R., Yang, S., Ries, W.L., Key, L.L., 2000. IFN-gamma enhances osteoclast generation in cultures of peripheral blood from osteopetrotic patients and normalizes superoxide production. *J. Interferon Cytokine Res.* 20, 645–52.  
doi:10.1089/107999000414826
- Mankouri, J., Fragkoudis, R., Richards, K.H., Wetherill, L.F., Harris, M., Kohl, A., Elliott, R.M., Macdonald, A., 2010. Optineurin Negatively Regulates the Induction of IFN $\beta$  in Response to RNA Virus Infection. *PLoS Pathog* 6, e1000778.
- Mann, S.S., Hammarback, J.A., 1994. Molecular characterization of light chain 3. A microtubule binding subunit of MAP1A and MAP1B. *J. Biol. Chem.* 269, 11492–7.
- Martini, G., Gennari, L., Merlotti, D., Salvadori, S., Franci, M.B., Campagna, S., Avanzati, A., De Paola, V., Valleggi, F., Nuti, R., 2007. Serum OPG and RANKL levels before and after intravenous bisphosphonate treatment in Paget's disease of bone. *Bone* 40, 457–63. doi:10.1016/j.bone.2006.08.003
- Maruyama, H., Morino, H., Ito, H., Izumi, Y., Kato, H., Watanabe, Y., Kinoshita, Y., Kamada, M., Nodera, H., Suzuki, H., Komure, O., Matsuura, S., Kobatake, K., Morimoto, N., Abe, K., Suzuki, N., Aoki, M., Kawata, A., Hirai, T., Kato, T., Ogasawara, K., Hirano, A., Takumi, T., Kusaka, H., Hagiwara, K., Kaji, R., Kawakami, H., 2010. Mutations of optineurin in amyotrophic lateral sclerosis. *Nature* 465, 223–226. doi:10.1038/nature08971
- Maruyama, K., Kawagoe, T., Kondo, T., Akira, S., Takeuchi, O., 2012. TRAF Family Member-associated NF- $\kappa$ B Activator (TANK) Is a Negative Regulator of Osteoclastogenesis and Bone Formation. *J. Biol. Chem.* 287, 29114–29124.
- Massoumi, R., 2010. Ubiquitin chain cleavage: CYLD at work. *Trends Biochem. Sci.* 35, 392–399. doi:10.1016/j.tibs.2010.02.007
- Masu, M., Tanabe, Y., Tsuchida, K., Shigemoto, R., Nakanishi, S., 1991. Sequence and expression of a metabotropic glutamate receptor. *Nature* 349, 760–765.  
doi:10.1038/349760a0
- Matmati, M., Jacques, P., Maelfait, J., Verheugen, E., Kool, M., Sze, M., Geboes, L., Louagie, E., Guire, C.M., Vereecke, L., Chu, Y., Boon, L., Staelens, S., Matthys, P., Lambrecht, B.N., Schmidt-Supprian, M., Pasparakis, M., Elewaut, D., Beyaert, R., van Loo, G., 2011. A20 (TNFAIP3) deficiency in myeloid cells triggers erosive polyarthritis resembling rheumatoid arthritis. *Nat. Genet.* 43, 908–912.  
doi:10.1038/ng.874
- Matsuzawa, A., Tseng, P.-H., Vallabhapurapu, S., Luo, J.-L., Zhang, W., Wang, H., Vignali, D.A.A., Gallagher, E., Karin, M., 2008. Essential cytoplasmic translocation of a cytokine receptor-assembled signaling complex. *Science* 321, 663–8.  
doi:10.1126/science.1157340

## BIBLIOGRAPHY

- Matthews, B.G., Naot, D., Bava, U., Callon, K.E., Pitto, R.P., McCowan, S.A., Wattie, D., Cundy, T., Cornish, J., Reid, I.R., 2009. Absence of Somatic SQSTM1 Mutations in Paget's Disease of Bone. *J. Clin. Endocrinol. Metab.* 94, 691–694.
- Mays, S., 2010. Archaeological skeletons support a northwest European origin for Paget's disease of bone. *J. Bone Miner. Res.* 25, 1839–1841.
- McCarthy, M.I., Abecasis, G.R., Cardon, L.R., Goldstein, D.B., Little, J., Ioannidis, J.P.A., Hirschhorn, J.N., 2008. Genome-wide association studies for complex traits: consensus, uncertainty and challenges. *Nat. Rev. Genet.* 9, 356–369.
- Mee, A.P., Dixon, J.A., Hoyland, J.A., Davies, M., Selby, P.L., Mawer, E.B., 1998. Detection of canine distemper virus in 100% of Paget's disease samples by in situ reverse transcriptase-polymerase chain reaction. *Bone* 23, 171–5.
- Mee, A.P., May, C., Bennett, D., Sharpe, P.T., 1995. Generation of multinucleated osteoclast-like cells from canine bone marrow: Effects of canine distemper virus. *Bone* 17, 47–55.
- Mellis, D.J., Itzstein, C., Helfrich, M.H., Crockett, J.C., 2011. The skeleton: a multi-functional complex organ. The role of key signalling pathways in osteoclast differentiation and in bone resorption. *J. Endocrinol.* 211, 131–143.
- Menaa, C., Barsony, J., Reddy, S. V, Cornish, J., Cundy, T., Roodman, G.D., 2000a. 1, 25-Dihydroxyvitamin D3 Hypersensitivity of Osteoclast Precursors from Patients with Paget's Disease. *J. Bone Miner. Res.* 15, 228–236.
- Menaa, C., Reddy, S. V, Kurihara, N., Maeda, H., Anderson, D., Cundy, T., Cornish, J., Singer, F.R., Bruder, J.M., Roodman, G.D., 2000b. Enhanced RANK ligand expression and responsivity of bone marrow cells in Paget's disease of bone. *J. Clin. Invest.* 105, 1833–1838.
- Menaa, C., Reddy, S. V, Kurihara, N., Maeda, H., Anderson, D., Cundy, T., Cornish, J., Singer, F.R., Bruder, J.M., Roodman, G.D., 2000. Enhanced RANK ligand expression and responsivity of bone marrow cells in Paget's disease of bone. *J. Clin. Invest.* 105, 1833–8. doi:10.1172/JCI9133
- Meng Bao, C. Le, Y.L., E., S.K., M., Liu, Y., Choolani, M., K.Y., J., 2013. Advances in Bone Tissue Engineering, in: *Regenerative Medicine and Tissue Engineering*. InTech. doi:10.5772/55916
- Merchant, A., Smielewska, M., Patel, N., Akunowicz, J.D., Saria, E.A., Delaney, J.D., Leach, R.J., Seton, M., Hansen, M.F., 2009. Somatic Mutations in SQSTM1 Detected in Affected Tissues From Patients With Sporadic Paget's Disease of Bone. *J. Bone Miner. Res.* 24, 484–494.
- Merlotti, D., Gennari, L., Galli, B., Martini, G., Calabrò, A., De Paola, V., Ceccarelli, E., Nardi, P., Avanzati, A., Nuti, R., 2005. Characteristics and Familial Aggregation of Paget's Disease of Bone in Italy. *J. Bone Miner. Res.* 20, 1356–1364.
- Mersman, D.P., Du, H.-N., Fingerman, I.M., South, P.F., Briggs, S.D., 2009. Polyubiquitination of the demethylase Jhd2 controls histone methylation and gene expression. *Genes Dev.* 23, 951–62. doi:10.1101/gad.1769209

## BIBLIOGRAPHY

- Michou, L., Chamoux, E., Couture, J., Morissette, J., Brown, J.P., Roux, S., 2010. Gene expression profile in osteoclasts from patients with Paget's disease of bone. *Bone* 46, 598–603.
- Middleton-Hardie, C., Zhu, Q., Cundy, H., Lin, J., Callon, K., Tong, P.C., Xu, J., Grey, A., Cornish, J., Naot, D., 2005. Deletion of Aspartate 182 in OPG Causes Juvenile Paget' Disease by Impairing Both Protein Secretion and Binding to RANKL. *J. Bone Miner. Res.* 21, 438–445.
- Millecamps, S., Boillée, S., Chabrol, E., Camu, W., Cazeneuve, C., Salachas, F., Pradat, P.-F., Danel-Brunaud, V., Vandenberghe, N., Corcia, P., Le Forestier, N., Lacomblez, L., Bruneteau, G., Seilhean, D., Brice, A., Feingold, J., Meininger, V., LeGuern, E., 2011. Screening of OPTN in French familial amyotrophic lateral sclerosis. *Neurobiol. Aging* 32, 557.e11–557.e13. doi:10.1016/j.neurobiolaging.2010.11.005
- Mills, B.G., Frausto, A., Singer, F.R., Ohsaki, Y., Demulder, A., Roodman, G.D., 1994. Multinucleated cells formed in vitro from Paget's bone marrow express viral antigens. *Bone* 15, 443–8.
- Mills, B.G., Singer, F.R., 1976a. Nuclear inclusions in Paget's disease of bone. *Science* 194, 201–202. doi:10.1126/science.959849
- Mills, B.G., Singer, F.R., 1976b. Nuclear inclusions in Paget's disease of bone. *Science* (80-. ). 194, 201–202.
- Mills, B.G., Singer, F.R., Weiner, L.P., Holst, P.A., 1981. Immunohistological demonstration of respiratory syncytial virus antigens in Paget disease of bone. *Proc. Natl. Acad. Sci. U. S. A.* 78, 1209–13.
- Mizushima, N., Yoshimori, T., Levine, B., 2010. Methods in Mammalian Autophagy Research. *Cell* 140, 313–326.
- Montero, A., Okada, Y., Tomita, M., Ito, M., Tsurukami, H., Nakamura, T., Doetschman, T., Coffin, J.D., Hurley, M.M., 2000. Disruption of the fibroblast growth factor-2 gene results in decreased bone mass and bone formation. *J. Clin. Invest.* 105, 1085–93. doi:10.1172/JCI8641
- Moreland, R.J., Dresser, M.E., Rodgers, J.S., 2000. Identification of a transcription factor IIIA-interacting protein. *Nucleic acids ...* 1–8.
- Morton, S., Hesson, L., Pegg, M., Cohen, P., 2008. Enhanced binding of TBK1 by an optineurin mutant that causes a familial form of primary open angle glaucoma. *FEBS Lett.* 582, 997–1002.
- Mossetti, G., Rendina, D., De Filippo, G., Viceconti, R., Di Domenico, G., Cioffi, M., Postiglione, L., Nunziata, V., 2005. Interleukin-6 and osteoprotegerin systems in Paget's disease of bone: relationship to risedronate treatment. *Bone* 36, 549–54. doi:10.1016/j.bone.2004.11.004
- Müller, U., Steinhoff, U., Reis, L.F., Hemmi, S., Pavlovic, J., Zinkernagel, R.M., Aguet, M., 1994. Functional role of type I and type II interferons in antiviral defense. *Science* (80-. ). 264, 1918–1921.

## BIBLIOGRAPHY

- Munitic, I., Giardino Torchia, M.L., Meena, N.P., Zhu, G., Li, C.C., Ashwell, J.D., 2013. Optineurin Insufficiency Impairs IRF3 but Not NF- $\kappa$ B Activation in Immune Cells. *J. Immunol.*
- Nagabhushana, A., Bansal, M., Swarup, G., 2011. Optineurin Is Required for CYLD-Dependent Inhibition of TNF $\alpha$ -Induced NF- $\kappa$ B Activation. *PLoS One* 6, e17477.
- Nagabhushana, A., Chalasani, M.L., Jain, N., Radha, V., Rangaraj, N., Balasubramanian, D., Swarup, G., 2010. Regulation of endocytic trafficking of transferrin receptor by optineurin and its impairment by a glaucoma-associated mutant. *BMC Cell Biol.* 11, 4.
- Nagy, Z.B., Gergely Péter, J., Donáth, J., Borgulya, G., Csanád, M., Poór, G., 2007. Gene Expression Profiling in Paget's Disease of Bone: Upregulation of Interferon Signaling Pathways in Pagetic Monocytes and Lymphocytes. *J. Bone Miner. Res.* 23, 253–259.
- Nakatsuka, K., Nishizawa, Y., Ralston, S.H., 2003. Phenotypic Characterization of Early Onset Paget's Disease of Bone Caused by a 27-bp Duplication in the TNFRSF11A Gene. *J. Bone Miner. Res.* 18, 1381–1385.
- Naot, D., Bava, U., Matthews, B., Callon, K.E., Gamble, G.D., Black, M., Song, S., Pitto, R.P., Cundy, T., Cornish, J., Reid, I.R., 2006. Differential Gene Expression in Cultured Osteoblasts and Bone Marrow Stromal Cells From Patients With Paget's Disease of Bone. *J. Bone Miner. Res.* 22, 298–309.
- Neale, S.D., Schulze, E., Smith, R., Athanasou, N.A., 2002. The influence of serum cytokines and growth factors on osteoclast formation in Paget's disease. *Qjm* 95, 233–240.
- Nica, A.C., Dermitzakis, E.T., 2013. Expression quantitative trait loci: present and future. *Philos. Trans. R. Soc. Lond. B. Biol. Sci.* 368, 20120362. doi:10.1098/rstb.2012.0362
- Nimmo, E.R., Sanders, P.G., Padua, R.A., Hughes, D., Williamson, R., Johnson, K.J., 1991. The MEL gene: a new member of the RAB/YPT class of RAS-related genes. *Oncogene* 6, 1347–51.
- Obaid, R., Wani, S.E., Azfer, A., Hurd, T., Jones, R., Cohen, P., Ralston, S.H., Albagha, O.M.E., 2015. Optineurin Negatively Regulates Osteoclast Differentiation by Modulating NF- $\kappa$ B and Interferon Signaling: Implications for Paget's Disease. *Cell Rep.* doi:10.1016/j.celrep.2015.09.071
- Oganesyan, G., Saha, S.K., Guo, B., He, J.Q., Shahangian, A., Zarnegar, B., Perry, A., Cheng, G., 2005. Critical role of TRAF3 in the Toll-like receptor-dependent and -independent antiviral response. *Nature* 439, 208–211.
- Onal, M., Piemontese, M., Xiong, J., Wang, Y., Han, L., Ye, S., Komatsu, M., Selig, M., Weinstein, R.S., Zhao, H., Jilka, R.L., Almeida, M., Manolagas, S.C., O'Brien, C.A., 2013. Suppression of Autophagy in Osteocytes Mimics Skeletal Aging. *J. Biol. Chem.* 288, 17432–17440.
- Ooi, C.G., Walsh, C.A., Gallagher, J.A., Fraser, W.D., 2000. Absence of measles virus and canine distemper virus transcripts in long-term bone marrow cultures from patients with Paget's disease of bone. *Bone* 27, 417–21.
- Paget, J., 1877. On a Form of Chronic Inflammation of Bones (Osteitis Deformans). *Med. Chir. Trans.* 60, 37–64.9.

## BIBLIOGRAPHY

- Palmqvist, P., Persson, E., Conaway, H.H., Lerner, U.H., 2002. IL-6, leukemia inhibitory factor, and oncostatin M stimulate bone resorption and regulate the expression of receptor activator of NF-kappa B ligand, osteoprotegerin, and receptor activator of NF-kappa B in mouse calvariae. *J. Immunol.* 169, 3353–62.
- Pang, M., Martinez, A.F., Jacobs, J., Balkan, W., Troen, B.R., 2005. RANK ligand and interferon gamma differentially regulate cathepsin gene expression in pre-osteoclastic cells. *Biochem. Biophys. Res. Commun.* 328, 756–63. doi:10.1016/j.bbrc.2004.12.005
- Pangrazio, A., Cassani, B., Guerrini, M.M., Crockett, J.C., Marrella, V., Zammataro, L., Strina, D., Schulz, A., Schlack, C., Kornak, U., Mellis, D.J., Duthie, A., Helfrich, M.H., Durandy, A., Moshous, D., Vellodi, A., Chiesa, R., Veys, P., Lo Iacono, N., Vezzoni, P., Fischer, A., Villa, A., Sobacchi, C., 2012. RANK-dependent autosomal recessive osteopetrosis: characterization of five new cases with novel mutations. *J. Bone Miner. Res.* 27, 342–51. doi:10.1002/jbmr.559
- Park, B., Ying, H., Shen, X., Park, J.-S., Qiu, Y., Shyam, R., Yue, B.Y.J.T., 2010. Impairment of Protein Trafficking upon Overexpression and Mutation of Optineurin. *PLoS One* 5, e11547.
- Park, B.C., Shen, X., Samaraweera, M., Yue, B., 2006. Studies of Optineurin, a Glaucoma Gene: Golgi Fragmentation and Cell Death from Overexpression of Wild-Type and Mutant Optineurin in Two Ocular Cell Types. *Am. J. ....*
- Peränen, J., Auvinen, P., Virta, H., Wepf, R., Simons, K., 1996. Rab8 promotes polarized membrane transport through reorganization of actin and microtubules in fibroblasts. *J. Cell Biol.* 135, 153–67.
- Plotkin, L., Bivi, N., 2013. Local Regulation of Bone Cell Function, in: *Basic and Applied Bone Biology*. Elsevier Inc., pp. 47–74.
- Post, T.M., Cremers, S.C.L.M., Kerbusch, T., Danhof, M., 2010. Bone physiology, disease and treatment: towards disease system analysis in osteoporosis. *Clin. Pharmacokinet.* 49, 89–118.
- Rajasekaran, R., Sudandiradoss, C., Doss, C.G.P., Sethumadhavan, R., 2007. Identification and in silico analysis of functional SNPs of the BRCA1 gene. *Genomics* 90, 447–452.
- Ralston, S.H., 2013a. Bone structure and metabolism. *Medicine (Baltimore)*. 41, 581–585.
- Ralston, S.H., 2013b. Paget's Disease of Bone. *N. Engl. J. Med.* 368, 644–650.
- Ralston, S.H., 2008. Pathogenesis of Paget's disease of bone. *Bone* 1–7.
- Ralston, S.H., Afzal, M.A., Helfrich, M.H., Fraser, W.D., Gallagher, J.A., Mee, A., Rima, B., 2007. Multicenter blinded analysis of RT-PCR detection methods for paramyxoviruses in relation to Paget's disease of bone. *J. Bone Miner. Res.* 22, 569–577.
- Ralston, S.H., Albagha, O.M.E., 2013. Genetics of Paget's Disease of Bone, in: *Genetics of Bone Biology and Skeletal Disease*. Elsevier, pp. 295–308. doi:10.1016/B978-0-12-387829-8.00019-6
- Ralston, S.H., Albagha, O.M.E., 2011. Genetic determinants of Paget's disease of bone. *Ann. N. Y. Acad. Sci.* 1240, 53–60.

## BIBLIOGRAPHY

- Ralston, S.H., HOEY, S.A., GALLACHER, S.J., ADAMSON, B.B., BOYLE, I.T., 1994. CYTOKINE AND GROWTH FACTOR EXPRESSION IN PAGET'S DISEASE: ANALYSIS BY REVERSE-TRANSCRIPT/PCR. *Rheumatology* 33, 620–625.
- Ralston, S.H., Langston, A.L., Reid, I.R., 2008. Pathogenesis and management of Paget's disease of bone. *Lancet* 372, 155–163.
- Rea, S.L., Walsh, J.P., Layfield, R., Ratajczak, T., Xu, J., 2013. New Insights Into the Role of Sequestosome 1/p62 Mutant Proteins in the Pathogenesis of Paget's Disease of Bone. *Endocr. Rev.* 34, 501–524.
- Reddy, S. V, Kurihara, N., Menaa, C., Landucci, G., Forthal, D., Koop, B.A., Windle, J.J., Roodman, G.D., 2001. Osteoclasts formed by measles virus-infected osteoclast precursors from hCD46 transgenic mice express characteristics of pagetic osteoclasts. *Endocrinology* 142, 2898–2905.
- Reddy, S. V, Menaa, C., Singer, F.R., Cundy, T., Cornish, J., Whyte, M.P., Roodman, G.D., 1999. Measles virus nucleocapsid transcript expression is not restricted to the osteoclast lineage in patients with Paget's disease of bone. *Exp. Hematol.* 27, 1528–32.
- Renard, P., Ernest, I., Houbion, a, Art, M., Le Calvez, H., Raes, M., Remacle, J., 2001. Development of a sensitive multi-well colorimetric assay for active NFκB. *Nucleic Acids Res.* 29, E21. doi:10.1093/nar/29.4.e21
- Rezaie, T., 2002. Adult-Onset Primary Open-Angle Glaucoma Caused by Mutations in Optineurin. *Science* (80-. ). 295, 1077–1079.
- Rezaie, T., Child, A., Hitchings, R., Brice, G., Miller, L., Coca-Prados, M., Héon, E., Krupin, T., Ritch, R., Kreutzer, D., 2002. Adult-onset primary open-angle glaucoma caused by mutations in optineurin. *Science* (80-. ). 295, 1077–1079.
- Richards, K.H., Macdonald, A., 2011. Putting the brakes on the anti-viral response: negative regulators of type I interferon (IFN) production. *Microbes Infect.* 1–12.
- Rock, R.S., Rice, S.E., Wells, A.L., Purcell, T.J., Spudich, J.A., Sweeney, H.L., 2001. Myosin VI is a processive motor with a large step size. *Proc. Natl. Acad. Sci. U. S. A.* 98, 13655–9. doi:10.1073/pnas.191512398
- Rogov, V. V, Suzuki, H., Fiskin, E., Wild, P., Kniss, A., Rozenknop, A., Kato, R., Kawasaki, M., McEwan, D.G., Löhr, F., Güntert, P., Dikic, I., Wakatsuki, S., Dötsch, V., 2013. Structural basis for phosphorylation-triggered autophagic clearance of Salmonella. *Biochem J* 454, 459–466. doi:10.1042/BJ20121907
- Romano, C., Yang, W.-L., O'Malley, K.L., 1996. Metabotropic Glutamate Receptor 5 Is a Disulfide-linked Dimer. *J. Biol. Chem.* 271, 28612–28616. doi:10.1074/jbc.271.45.28612
- Roodman, G.D., Kurihara, N., Ohsaki, Y., Kukita, A., Hosking, D., Demulder, A., Smith, J.F., Singer, F.R., 1992. Interleukin 6. A potential autocrine/paracrine factor in Paget's disease of bone. *J. Clin. Invest.* 89, 46–52. doi:10.1172/JCI115584
- Ruddle, N.H., Li, C.B., Horne, W.C., Santiago, P., Troiano, N., Jay, G., Horowitz, M., Baron, R., 1993. Mice transgenic for HTLV-I LTR-tax exhibit tax expression in bone, skeletal alterations, and high bone turnover. *Virology* 197, 196–204.

## BIBLIOGRAPHY

- Sahlender, D.A., Roberts, R.C., Arden, S.D., Spudich, G., Taylor, M.J., Luzio, J.P., Kendrick-Jones, J., Buss, F., 2005. Optineurin links myosin VI to the Golgi complex and is involved in Golgi organization and exocytosis. *J. Cell Biol.* 169, 285.
- Sato, K., Satoh, T., Shizume, K., Yamakawa, Y., Ono, Y., Demura, H., Akatsu, T., Takahashi, N., Suda, T., 1992. Prolonged decrease of serum calcium concentration by murine gamma-interferon in hypercalcemic, human tumor (EC-GI)-bearing nude mice. *Cancer Res.* 52, 444–9.
- Schadt, E.E., Molony, C., Chudin, E., Hao, K., Yang, X., Lum, P.Y., Kasarskis, A., Zhang, B., Wang, S., Suver, C., Zhu, J., Millstein, J., Sieberts, S., Lamb, J., GuhaThakurta, D., Derry, J., Storey, J.D., Avila-Campillo, I., Kruger, M.J., Johnson, J.M., Rohl, C.A., van Nas, A., Mehrabian, M., Drake, T.A., Lusk, A.J., Smith, R.C., Guengerich, F.P., Strom, S.C., Schuetz, E., Rushmore, T.H., Ulrich, R., 2008. Mapping the genetic architecture of gene expression in human liver. *PLoS Biol.* 6, e107. doi:10.1371/journal.pbio.0060107
- Schafer, A.L., Mumm, S., El-Sayed, I., McAlister, W.H., Horvai, A.E., Tom, A.M., Hsiao, E.C., Schaefer, F. V, Collins, M.T., Anderson, M.S., Whyte, M.P., Shoback, D.M., 2014. Panostotic expansile bone disease with massive jaw tumor formation and a novel mutation in the signal peptide of RANK. *J. Bone Miner. Res.* 29, 911–21. doi:10.1002/jbmr.2094
- Schwamborn, K., Weil, R., Courtois, G., Whiteside, S.T., Israël, A., 2000. Phorbol Esters and Cytokines Regulate the Expression of the NEMO-related Protein, a Molecule Involved in a NF- $\kappa$ B-independent Pathway. *J. Biol. Chem.* 275, 22780–22789.
- Seibel, M.J., 2005. Biochemical markers of bone turnover: part I: biochemistry and variability. *Clin. Biochem. Rev.* 26, 97–122.
- Shaid, S., Brandts, C.H., Serve, H., Dikic, I., 2012. Ubiquitination and selective autophagy. *Cell Death Differ.* 20, 21–30.
- Shembade, N., Harhaj, E.W., 2010. Role of post-translational modifications of HTLV-1 Tax in NF- $\kappa$ B activation. *World J. Biol. Chem.* 1, 13–20.
- Shembade, N., Ma, A., Harhaj, E.W., 2010. Inhibition of NF- $\kappa$ B Signaling by A20 Through Disruption of Ubiquitin Enzyme Complexes. *Science (80-. ).* 327, 1135–1139.
- Shen, X., Ying, H., Qiu, Y., Park, J.-S., Shyam, R., Chi, Z.-L., Iwata, T., Yue, B.Y.J.T., 2011. Processing of optineurin in neuronal cells. *J. Biol. Chem.* 286, 3618–3629.
- Sims, N.A., Martin, T. thinsp J., 2014. Coupling the activities of bone formation and resorption: a multitude of signals within the basic multicellular unit. *Bonekey Rep.* 3, 1–10.
- Singer, F.R., Mills, B.G., Gruber, H.E., Windle, J.J., Roodman, G.D., 2006. Ultrastructure of Bone Cells in Paget's Disease of Bone. *J. Bone Miner. Res.* 21, P51–P54.
- Siris, E.S., 1994. Epidemiological aspects of Paget's disease: family history and relationship to other medical conditions. *YSARH* 23, 222–225.
- Siris, E.S., Ottman, R., Flaster, E., Kelsey, J.L., 1991. Familial aggregation of Paget's disease of bone. *J. Bone Miner. Res.* 6, 495–500. doi:10.1002/jbmr.5650060511

## BIBLIOGRAPHY

- Sofaer, J.A., Holloway, S.M., Emery, A.E., 1983. A family study of Paget's disease of bone. *J. Epidemiol. Community Heal.* 37, 226–231.
- Solomon, L.R., 1979. Billiard-player's fingers: an unusual case of Paget's disease of bone. *Br. Med. J.* 1, 931.
- Stanger, B.Z., Leder, P., Lee, T.-H., Kim, E., Seed, B., 1995. RIP: A novel protein containing a death domain that interacts with Fas/APO-1 (CD95) in yeast and causes cell death. *Cell* 81, 513–523. doi:10.1016/0092-8674(95)90072-1
- Sudhakar, C., Nagabhushana, A., Jain, N., Swarup, G., 2009. NF- $\kappa$ B Mediates Tumor Necrosis Factor  $\alpha$ -Induced Expression of Optineurin, a Negative Regulator of NF- $\kappa$ B. *PLoS One* 4, e5114.
- Sudhakar, C., Vaibhava, V., Swarup, G., 2013. IRF-1-binding site in the first intron mediates interferon-gamma-induced optineurin promoter activation. *Biochem. Biophys. Res. Commun.* 437, 179–184.
- Sugihara, K., Maruyama, H., Kamada, M., Morino, H., Kawakami, H., 2011. Screening for OPTN mutations in amyotrophic lateral sclerosis in a mainly Caucasian population. *Neurobiol. Aging* 32, 1923.e9–1923.e10. doi:10.1016/j.neurobiolaging.2011.03.024
- Sun, Q., Sammut, B., Wang, F.-M., Kurihara, N., Windle, J.J., Roodman, G.D., Galson, D.L., 2013. TBK1 Mediates Critical Effects of Measles Virus Nucleocapsid Protein (MVNP) on Pagetic Osteoclast Formation. *J. Bone Miner. Res.* 29, 90–102.
- Sundaram, K., Senn, J., Yuvaraj, S., Rao, D.S., Reddy, S. V., 2009. FGF-2 Stimulation of RANK Ligand Expression in Paget's Disease of Bone. *Mol. Endocrinol.* 23, 1445–1454.
- Sutherland, R., Delia, D., Schneider, C., Newman, R., Kemshead, J., Greaves, M., 1981. Ubiquitous cell-surface glycoprotein on tumor cells is proliferation-associated receptor for transferrin. *Proc. Natl. Acad. Sci. U. S. A.* 78, 4515–9.
- Takayanagi, H., Kim, S., Matsuo, K., Suzuki, H., Suzuki, T., Sato, K., Yokochi, T., Oda, H., Nakamura, K., Ida, N., Wagner, E.F., Taniguchi, T., 2002a. RANKL maintains bone homeostasis through c-Fos-dependent induction of interferon-beta. *Nature* 416, 744–749.
- Takayanagi, H., Kim, S., Taniguchi, T., 2002b. Signaling crosstalk between RANKL and interferons in osteoclast differentiation. *Arthritis Res.* 4, S227. doi:10.1186/ar581
- Takayanagi, H., Ogasawara, K., Hida, S., Chiba, T., Murata, S., Sato, K., Takaoka, a, Yokochi, T., Oda, H., Tanaka, K., Nakamura, K., Taniguchi, T., 2000. T-cell-mediated regulation of osteoclastogenesis by signalling cross-talk between RANKL and IFN-gamma. *Nature* 408, 600–605. doi:10.1038/35046102
- Tamura, T., Udagawa, N., Takahashi, N., Miyaura, C., Tanaka, S., Yamada, Y., Koishihara, Y., Ohsugi, Y., Kumaki, K., Taga, T., 1993. Soluble interleukin-6 receptor triggers osteoclast formation by interleukin 6. *Proc. Natl. Acad. Sci. U. S. A.* 90, 11924–8.
- Taylor, A., Mules, E.H., Seabra, M.C., Helfrich, M.H., Rogers, M.J., Coxon, F.P., 2011. Impaired prenylation of Rab GTPases in the gunmetal mouse causes defects in bone cell function. *Small GTPases* 2, 131–142. doi:10.4161/sgtp.2.3.16488



## BIBLIOGRAPHY

- Teramachi, J., Zhou, H., Subler, M.A., Kitagawa, Y., Galson, D.L., Dempster, D.W., Windle, J.J., Kurihara, N., Roodman, G.D., 2014. Increased IL-6 expression in osteoclasts is necessary but not sufficient for the development of Paget's disease of bone. *J. Bone Miner. Res.* 29, 1456–65. doi:10.1002/jbmr.2158
- The Huntington's Disease Collaborative Research Group, 1993. A novel gene containing a trinucleotide repeat that is expanded and unstable on Huntington's disease chromosomes. The Huntington's Disease Collaborative Research Group. *Cell* 72, 971–83.
- Tojima, Y., Fujimoto, A., Delhase, M., Chen, Y., Hatakeyama, S., Nakayama, K., Kaneko, Y., Nimura, Y., Motoyama, N., Ikeda, K., Karin, M., Nakanishi, M., 2000. NAK is an IkappaB kinase-activating kinase. *Nature* 404, 778–82. doi:10.1038/35008109
- Trompouki, E., Hatzivassiliou, E., Tschritzis, T., Farmer, H., Ashworth, A., Mosialos, G., 2003. CYLD is a deubiquitinating enzyme that negatively regulates NF- $\kappa$ B activation by TNFR family members. *Nature* 424, 793–796. doi:10.1038/nature01803
- Turnpenny, P., Ellard, S., 2007. Emery's Elements of Medical Genetics, 13th Editi. ed. Elsevier.
- Uranishi, H., 2001. Involvement of the Pro-oncoprotein TLS (Translocated in Liposarcoma) in Nuclear Factor-kappa B p65-mediated Transcription as a Coactivator. *J. Biol. Chem.* 276, 13395–13401.
- Vaibhava, V., Nagabhushana, A., Chalasani, M.L.S., Sudhakar, C., Kumari, A., Swarup, G., 2012. Optineurin mediates a negative regulation of Rab8 by the GTPase-activating protein TBC1D17. *J. Cell Sci.* 125, 5026–39. doi:10.1242/jcs.102327
- Vallet, M., Ralston, S.H., 2015. Biology and Treatment of Paget's Disease of Bone. *J. Cell. Biochem.* 11, n/a–n/a. doi:10.1002/jcb.25291
- Vallet, M., Soares, D.C., Wani, S., Sophocleous, A., Warner, J., Salter, D.M., Ralston, S.H., Albagha, O.M.E., 2015. Targeted sequencing of the Paget's disease associated 14q32 locus identifies several missense coding variants in RIN3 that predispose to Paget's disease of bone. *Hum. Mol. Genet.* 24, 3286–3295. doi:10.1093/hmg/ddv068
- van 't Hof, R.J., 2011. Analysis of Bone Architecture in Rodents Using Microcomputed Tomography BT - (null), in: *Methods in Molecular Biology*. Humana Press, Totowa, NJ, pp. 461–476.
- van't Hof, R.J., Ralston, S.H., 1997. Cytokine-induced nitric oxide inhibits bone resorption by inducing apoptosis of osteoclast progenitors and suppressing osteoclast activity. *J. Bone Miner. Res.* 12, 1797–804. doi:10.1359/jbmr.1997.12.11.1797
- Vermeire, K., Heremans, H., Vandeputte, M., Huang, S., Billiau, A., Matthys, P., 1997. Accelerated collagen-induced arthritis in IFN-gamma receptor-deficient mice. *J. Immunol.* 158, 5507–13.
- Veyrieras, J.-B., Kudaravalli, S., Kim, S.Y., Dermitzakis, E.T., Gilad, Y., Stephens, M., Pritchard, J.K., 2008. High-resolution mapping of expression-QTLs yields insight into human gene regulation. *PLoS Genet.* 4, e1000214. doi:10.1371/journal.pgen.1000214
- Visconti, M.R., Langston, A.L., Alonso, N., Goodman, K., Selby, P.L., Fraser, W.D., Ralston, S.H., 2010. Mutations of SQSTM1 are associated with severity and clinical outcome in paget disease of bone. *J. Bone Miner. Res.* 25, 2368–2373.

## BIBLIOGRAPHY

- Wang, H., Bedford, F.K., Brandon, N.J., Moss, S.J., Olsen, R.W., 1999. GABA(A)-receptor-associated protein links GABA(A) receptors and the cytoskeleton. *Nature* 397, 69–72. doi:10.1038/16264
- Wang, H., Yang, H., Shivalila, C.S., Dawlaty, M.M., Cheng, A.W., Zhang, F., Jaenisch, R., 2013. One-step generation of mice carrying mutations in multiple genes by CRISPR/cas-mediated genome engineering. *Cell* 153, 910–918. doi:10.1016/j.cell.2013.04.025
- Ward, L.D., Kellis, M., 2012. Interpreting noncoding genetic variation in complex traits and human disease. *Nat. Publ. Gr.* 30, 1095–1106.
- Ware John E, J., Gandek, B., 1998. Overview of the SF-36 Health Survey and the International Quality of Life Assessment (IQOLA) Project. *J. Clin. Epidemiol.* 51, 903–912.
- Watts, G.D.J., Wymer, J., Kovach, M.J., Mehta, S.G., Mumm, S., Darvish, D., Pestronk, A., Whyte, M.P., Kimonis, V.E., 2004. Inclusion body myopathy associated with Paget disease of bone and frontotemporal dementia is caused by mutant valosin-containing protein. *Nat. Genet.* 36, 377–381. doi:10.1038/ng1332
- Westra, H.-J., Peters, M.J., Esko, T., Yaghootkar, H., Schurmann, C., Kettunen, J., Christiansen, M.W., Fairfax, B.P., Schramm, K., Powell, J.E., Zhernakova, A., Zhernakova, D. V, Veldink, J.H., Van den Berg, L.H., Karjalainen, J., Withoff, S., Uitterlinden, A.G., Hofman, A., Rivadeneira, F., Hoen, P.A.C. 't, Reinmaa, E., Fischer, K., Nelis, M., Milani, L., Melzer, D., Ferrucci, L., Singleton, A.B., Hernandez, D.G., Nalls, M.A., Homuth, G., Nauck, M., Radke, D., Völker, U., Perola, M., Salomaa, V., Brody, J., Suchy-Dicey, A., Gharib, S.A., Enquobahrie, D.A., Lumley, T., Montgomery, G.W., Makino, S., Prokisch, H., Herder, C., Roden, M., Grallert, H., Meitinger, T., Strauch, K., Li, Y., Jansen, R.C., Visscher, P.M., Knight, J.C., Psaty, B.M., Ripatti, S., Teumer, A., Frayling, T.M., Metspalu, A., van Meurs, J.B.J., Franke, L., 2013. Systematic identification of trans eQTLs as putative drivers of known disease associations. *Nat. Genet.* 45, 1238–1243.
- Whyte, M.P., Mills, B.G., Reinus, W.R., Podgornik, M.N., Roodman, G.D., Gannon, F.H., Eddy, M.C., McAlister, W.H., 2000. Expansile skeletal hyperphosphatasia: a new familial metabolic bone disease. *J. Bone Miner. Res.* 15, 2330–2344.
- Whyte, M.P., Obrecht, S.E., Finnegan, P.M., Jones, J.L., Podgornik, M.N., McAlister, W.H., Mumm, S., 2002. Osteoprotegerin Deficiency and Juvenile Paget's Disease. *N. Engl. J. Med.* 347, 175–184. doi:10.1056/NEJMoa013096
- Whyte, M.P., Tau, C., McAlister, W.H., Zhang, X., Novack, D. V, Preliasco, V., Santini-Araujo, E., Mumm, S., 2014. Juvenile Paget's disease with heterozygous duplication within TNFRSF11A encoding RANK. *Bone* 68, 153–161. doi:10.1016/j.bone.2014.07.019
- Wild, P., Farhan, H., McEwan, D.G., Wagner, S., Rogov, V. V, Brady, N.R., Richter, B., Korac, J., Waidmann, O., Choudhary, C., Dotsch, V., Bumann, D., Dikic, I., 2011. Phosphorylation of the Autophagy Receptor Optineurin Restricts Salmonella Growth. *Science* (80-. ). 333, 228–233.

## BIBLIOGRAPHY

- WUYTS, W., Van Wesenbeeck, L., Morales-Piga, A., Ralston, S., Hocking, L., Vanhoenacker, F., Westhovens, R., Verbruggen, L., Anderson, D., Hughes, A., 2001. Evaluation of the role of RANK and OPG genes in Paget's disease of bone. *Bone* 28, 104–107.
- Xavier, R.J., Rioux, J.D., 2008. Genome wide association studies, a new window into immune mediated diseases. *Nat. Rev. Immunol.* 8, 631–643.
- Y., A., Valds-Flores, M., Orozco, L., Velquez-Cruz, R., 2013. Molecular Aspects of Bone Remodeling, in: *Topics in Osteoporosis*. InTech. doi:10.5772/54905
- Yamashita, S., Kimura, E., Tawara, N., Sakaguchi, H., Nakama, T., Maeda, Y., Hirano, T., Uchino, M., Ando, Y., 2013. Optineurin is potentially associated with TDP-43 and involved in the pathogenesis of inclusion body myositis. *Neuropathol. Appl. Neurobiol.* 39, 406–416.
- Yamashita, T., 2012. New roles of osteoblasts involved in osteoclast differentiation. *World J. Orthop.* 3, 175.
- Yasuda, H., Shima, N., Nakagawa, N., Yamaguchi, K., Kinosaki, M., Mochizuki, S., Tomoyasu, A., Yano, K., Goto, M., Murakami, A., Tsuda, E., Morinaga, T., Higashio, K., Udagawa, N., Takahashi, N., Suda, T., 1998. Osteoclast differentiation factor is a ligand for osteoprotegerin/osteoclastogenesis-inhibitory factor and is identical to TRANCE/RANKL. *Proc. Natl. Acad. Sci. U. S. A.* 95, 3597–602.
- Ying, H., Shen, X., Park, B., Yue, B.Y.J.T., 2010. Posttranslational modifications, localization, and protein interactions of optineurin, the product of a glaucoma gene. *PLoS One* 5, e9168.
- Yuan, H.Y., Chiou, J.J., Tseng, W.H., Liu, C.H., Liu, C.K., Lin, Y.J., Wang, H.H., Yao, A., Chen, Y.T., Hsu, C.N., 2006. FASTSNP: an always up-to-date and extendable service for SNP function analysis and prioritization. *Nucleic Acids Res.* 34, W635–W641.
- Zeller, T., Wild, P., Szymczak, S., Rotival, M., Schillert, A., Castagne, R., Maouche, S., Germain, M., Lackner, K., Rossmann, H., Eleftheriadis, M., Sinning, C.R., Schnabel, R.B., Lubos, E., Mennerich, D., Rust, W., Perret, C., Proust, C., Nicaud, V., Loscalzo, J., Hübner, N., Tregouet, D., Münzel, T., Ziegler, A., Tiret, L., Blankenberg, S., Cambien, F., 2010. Genetics and Beyond – The Transcriptome of Human Monocytes and Disease Susceptibility. *PLoS One* 5, e10693.
- Zhu, G., Wu, C.-J., Zhao, Y., Ashwell, J.D., 2007. Optineurin Negatively Regulates TNF $\alpha$ -Induced NF- $\kappa$ B Activation by Competing with NEMO for Ubiquitinated RIP. *Curr. Biol.* 17, 1438–1443.
- Zuccato, C., Cattaneo, E., 2014. Neurotrophic Factors. doi:10.1007/978-3-642-45106-5

## APPENDICES

### Appendix 1: Materials, Apparatus and software

Materials and reagents	Supplier
1 ml pasteur pipette	Fisher Scientific, Leicestershire, UK
1.5 ml eppendorf tubes with cap	Greiner Bio-One Inc, Gloucestershire, UK
2-methoxyethyl acetate (MEA)	Sigma Aldrich, Dorset, UK
2-Propanol	Sigma Aldrich, Dorset, UK
Acetic Acid Glacial	Sigma Aldrich, Dorset, UK
Agarose	Bioline
alamarBlue™ reagent	Invitrogen, Paisley, UK
Alizarin Red S	Sigma Aldrich, Dorset, UK
Amersham Hybond™-P	GE Healthcare Life Sciences, Buckinghamshire, UK
Aniline Blue	Sigma Aldrich, Dorset, UK
Bicinchoninic acid (BCA) protein assay	Sigma Aldrich, Dorset, UK
Bovine serum albumin	Sigma Aldrich, Dorset, UK
Calcein	Sigma Aldrich, Dorset, UK
Centrifuge tubes (15 and 50 ml)	Fisher Scientific, Leicestershire, UK
Cetylpyridinium chloride	Sigma Aldrich, Dorset, UK
Chloroform	Sigma Aldrich, Dorset, UK
Cignal Lenti NFB reporter	SA Biosciences
Collagenase (type 1A)	Sigma Aldrich, Dorset, UK
Copper (II)-sulfate	Sigma Aldrich, Dorset, UK
Cover slips	Scientific Laboratory supplies Ltd, Hessle, UK
Criterion™ XT pre-cast gels (12% Bis-Tris)	Bio-Rad Laboratories, Hertfordshire, UK
CTX serum assay (RatLaps™ EIA)	Immunodiagnostic Systems Ltd. (IDS), Boldon Colliery, UK
CYLD mAb Rabbit/IgG	Cell signalling
DEPC Treated Water	Invitrogen, Paisley, UK
DL-Dithiothreitol (DTT)	Sigma Aldrich, Dorset, UK
DMSO	Sigma Aldrich, Dorset, UK
DNA Ladder 1kb	New England Biolabs, Hitchin, Hertfordshire, UK
DPX mounting medium	Sigma Aldrich, Dorset, UK
DTT	Invitrogen, Paisley, UK
Dulbecco's Modified Eagle Medium	Fisher Scientific, Leicestershire, UK
Dulbecco's Modified Eagle Medium + high glucose	Fisher Scientific, Leicestershire, UK
EDTA	Sigma Aldrich, Dorset, UK
Electrophoresis power supply	Anachem, Bedfordshire, UK
Embedding baskets	Leica Microsystems, Milton Keynes, UK
Embedding molds	Custom-made by the University workshop
Embedding rings	Leica Microsystems, Milton Keynes, UK
Ethanol Absolute	Fisher Scientific, Leicestershire, UK
Extra thick blot papers	Bio-Rad Laboratories, Hertfordshire, UK
Fast Red	Sigma Aldrich, Dorset, UK
Fetal calf serum (FCS)	Hyclone
Filter Paper	Fisher Scientific, Leicestershire, UK
Filter Tips Axygen	Thistle Scientific, Glasgow, UK
Fuchsin Acid	Taab Lab, Berkshire, UK
GenElute Mammalian Total RNA kit	Sigma Aldrich, Dorset, UK
Glycine	BDH Laboratory Supplies, Poole, Dorset, UK
Hanks buffer (HBSS)	Sigma Aldrich, Dorset, UK

## APPENDICES

HiPure Plasmid Midiprep Kit	Invitrogen, Paisley, UK
HistoResin Mounting Medium (solution and powder)	Leica Microsystems, Milton Keynes, UK
Hydrochloric acid	BDH Laboratory Supplies, Poole, Dorset, UK
Hydroquinone	Sigma Aldrich, Dorset, UK
Isopropanol	Sigma Aldrich, Dorset, UK
Kaleidoscope	Bio-Rad Laboratories, Hertfordshire, UK
Kisol foil	Taab Lab, Berkshire, UK
Knife 16cm long tungsten carbide tipped profile D	Leica Microsystems, Milton Keynes, UK
Knife Holder NZ	Leica Microsystems, Milton Keynes, UK
Lenti-X Concentrator	ClonTech
Lenti-X GoStix	ClonTech
L-Glutamine	Invitrogen, Paisley, UK
Low molecular weight DNA ladder	New England Biolabs, Hitchin, Hertfordshire, UK
Magic Marker	Invitrogen, Paisley, UK
Magnesium chloride	Sigma Aldrich, Dorset, UK
M-CSF	Prospec Tech
Methanol	Fisher Scientific, Leicestershire, UK
Methyl Methacrylate	Sigma Aldrich, Dorset, UK
Microtubes (0.5, 1.5, 2 ml)	Sarstedt Ltd, Leicester, UK
Minimum Essential Medium ( $\alpha$ MEM)	Sigma Aldrich, Dorset, UK
Mission mouse Optn shRNA pLKO.1-puro clones	Sigma Aldrich, Dorset, UK
N,N-Dimethylformamide	Fisher Scientific, Leicestershire, UK
N,N-dimethyl-p-toluidine	Leica Microsystems, Milton Keynes, UK
Napthol-AS-BI-phosphate	Sigma Aldrich, Dorset, UK
Needles (19, 21 and 25G)	Fisher Scientific, Leicestershire, UK
Neubauer Haemocytometer	Hawksley, Lancing, UK
Nitrile gloves	Fisher Scientific, Leicestershire, UK
Optineurin pAb Rabbit/IgG	Abcam
Optineurin pAb Rabbit/IgG	Cayman
Paraformaldehyde	Taab Lab, Berkshire, UK
Pararosanilin	Sigma Aldrich, Dorset, UK
PBS tablets	Invitrogen, Paisley, UK
PCR lid strip	Fisher Scientific, Leicestershire, UK
PCR microplate 96 well and lids	Fisher Scientific, Leicestershire, UK
PCR microtubes	Fisher Scientific, Leicestershire, UK
PCR primers	Invitrogen, Paisley, UK
Penicillin/Streptomycin	Invitrogen, Paisley, UK
Petri Dishes	Becton Dickinson, Berkshire, UK
Phospho-I $\kappa$ B $\alpha$ mAb Rabbit/IgG	Cell Signalling
Phosphotungstic acid	Sigma Aldrich, Dorset, UK
Picric acid	Sigma Aldrich, Dorset, UK
PINP serum assay (Rat/Mouse PINP EIA)	Immunodiagnostic Systems Ltd. (IDS), Boldon Colliery, UK
Pipette tips (all sizes)	Starlab, Milton Keynes, UK
Polysciences Silane coated microscope slides	Park Scientific Ltd., Northampton, UK
Protein G- agarose	Calbiochem
Puromycin	GIBCO
QIAprep Spin Miniprep Kit	Qiagen
QIAquick PCR Purification Kit	Qiagen (UK), West Sussex, UK

## APPENDICES

qScript™ cDNA SuperMix	Quanta BioSciences
Quant-iT RiboGreen RAN	Invitrogen, Paisley, UK
Rabbit Anti-Actin (AA20-33) IgG	Sigma Aldrich, Dorset, UK
RANKL human recombinant	Gift from Dr. Patrick Mollat (Proskelia SASU)
RipoPure-Blood Kit	Ambion
RNase-free water	Invitrogen, Paisley, UK
Scalpel, disposable	VWR International LTD, Leicestershire, UK
SensiFast Probe No-ROX kit	Bioline
Silver nitrate	Sigma Aldrich, Dorset, UK
Slide press cover slips	Taab Lab, Berkshire, UK
Sodium acetate anhydrous	Sigma Aldrich, Dorset, UK
Sodium barbiturate	BDH Laboratory Supplies, Poole, Dorset, UK
Sodium chloride	Sigma Aldrich, Dorset, UK
Sodium dodecyl sulphate (SDS)	Bio-Rad Laboratories, Hertfordshire, UK
Sodium hydroxide	VWR International LTD, Leicestershire, UK
Sodium phosphate	Sigma Aldrich, Dorset, UK
Sodium tartrate dibasic dihydrate	Sigma Aldrich, Dorset, UK
Sodium tetraborate	BDH Laboratory Supplies, Poole, Dorset, UK
Steady Glo Luciferase Assay	Promega
Steel Knife 16cm	Leica Microsystems, Milton Keynes, UK
Sterile filter (0.45µm)	Sartorius Mechatronics UK Ltd., Epsom Surrey, UK
Stripettes (5, 10, 25 and 50 ml)	Sarstedt Ltd, Leicester, UK
SuperSignal West Dura Extended Duration Substrate	Fisher Scientific, Leicestershire, UK
Syngene BIO imaging system	Syngene BIO imaging
Syringes (all sizes)	Becton Dickinson, Berkshire, UK
<i>Taq</i> DNA Polymerase	Invitrogen, Paisley, UK
TBE buffer 10X	Invitrogen, Paisley, UK
Tissue culture 75cm <sup>2</sup> flasks	Fisher Scientific, Leicestershire, UK
Tissue culture microplates (6, 12, 24, 48 and 96-well plates)	Fisher Scientific, Leicestershire, UK
Toluidine Blue	Sigma Aldrich, Dorset, UK
Trans-lenti Viral Packaging Mix and reagents	Thermo scientific Open Biosystem
Tris	Bio-Rad Laboratories, Hertfordshire, UK
Tris-EDTA buffer	Sigma Aldrich, Dorset, UK
Trypsin/EDTA	Sigma Aldrich, Dorset, UK
Tween-20	Bio-Rad Laboratories, Hertfordshire, UK
UPL probes	Roche Diagnostics Ltd., East Sussex, UK
UV 96 well plates for plate reader	Fisher Scientific, Leicestershire, UK
Van Gieson stain	TAAP
Vitamin C (Ascorbic acid)	Sigma Aldrich
XT-MOPS	Bio-Rad Laboratories, Hertfordshire, UK
Xylene	Sigma Aldrich, Dorset, UK
β-glycerophosphate	Sigma Aldrich, Dorset, UK

## APPENDICES

<b>Software used in this thesis</b>	<b>Supplier</b>
Aphelion Image Analysis tool kit	ADCIS, Hérouville-Saint-Clair, France
Bio-Tek Gen5™ plate reader software	Fisher Scientific, Leicestershire, UK
Chromas Pro	Technelysium
GeneMarker software	Softgenetics
ImageJ	U. S. National Institutes of Health Bethesda, MA-US
Minitab 16	Minitab LTD
Opticon Monitor analysis software version 3	Genetic Research Instrumentation Ltd (GRI), Essex, UK
QCapture Pro software	Media Cybernetics UK, Berkshire, UK
Skyscan 1172 MicroCT software	SKYSCAN, Kontich, Belgium
Skyscan CTAn analysis software	SKYSCAN, Kontich, Belgium
Skyscan CTVol software	SKYSCAN, Kontich, Belgium
Skyscan NRecon reconstruction system	SKYSCAN, Kontich, Belgium
Syngene GeneSnap software	Fisher Scientific, Leicestershire, UK
Syngene GeneTool software	Fisher Scientific, Leicestershire, UK

## APPENDICES

<b>Apparatus used in this thesis</b>	<b>Supplier</b>
AA Hoefer protein transfer apparatus	Fisher Scientific, Leicestershire, UK
Automatic tissue processor	Leica Microsystems, Milton Keynes, UK
Axiomager A1 upright research microscope	µCarl Zeiss Ltd., Hertfordshire, UK
Axiovert 200 inverted research Microcope	Carl Zeiss Ltd., Hertfordshire, UK
Axiovert inverted microscope 40 CFL	Carl Zeiss Ltd., Hertfordshire, UK
Balancer Fisherbrand	Fisher Scientific, Leicestershire, UK
Bench-top Eppendorf centrifuge	Fisher Scientific, Leicestershire, UK
Bio-Tek Synergy HT plate reader	Fisher Scientific, Leicestershire, UK
Class II microbiological safety cabinet	Biomart
CO <sub>2</sub> Incubators Cell 240	Heraeus
Electrophoresis tanks	Fisher Scientific, Leicestershire, UK
Grant OLS 200 water bath	Thistle Scientific, Glasgow, UK
Heat Block	Grant
Hotplate/stirrer	Thistle Scientific, Glasgow, UK
Ice Maker	Scotsman AF 103
MJ Research Chromo 4 Real Time PCR thermocycler	Genetic Research Instrumentation Ltd (GRI), Essex, UK
MJ Research Tetrad Thermal cycler	Genetic Research Instrumentation Ltd (GRI), Essex, UK
Nitchipet and Gilson Pipettes (2, 10, 100, 200 and 1000µl)	Thistle Scientific, Glasgow, UK
NuAir Class II Biological safety cabinet	TripleRed Ltd., Buckinghamshire, UK
PowerPac basic <sup>TM</sup>	Bio-Rad Laboratories, Hertfordshire, UK
Refrigerated centrifuges	Sigma
Rockin Table	Biometra
Rotary Microtome	Leica Microsystems, Milton Keynes, UK
Rotary tool	Dremel UK, Uxbridge, UK
SkyScan 1172 X-ray Microtomography system	SKYSCAN, Kontich, Belgium
SkyScan 1176 in-vivo µCT	SKYSCAN, Kontich, Belgium
Syngene GeneGenius Gel Bio-Imaging system	Fisher Scientific, Leicestershire, UK
SynSyngene GeneGnome Bio-Imaging system for chemiluminescence	Fisher Scientific, Leicestershire, UK
Tube Rotator	Stuart
Vortex	Thistle Scientific, Glasgow, UK
Water Bath	Grant



## Appendix 2: Solutions and Recipes

### Appendix 2.1 Solutions for TRAcP staining

#### Naphthol-AS-BI-phosphate

10 mg/ml Naphthol-AS-BI-phosphate in Dimethylformamide

#### Veronal buffer

1.17 g sodium acetate anhydrous and 2.94g sodium barbiturate both dissolved in 100 ml of dH<sub>2</sub>O

#### Acetate buffer

0.82 g sodium acetate anhydrous dissolved in 100 ml of dH<sub>2</sub>O and pH adjusted to 5.2 with 0.6 ml glacial acetic acid made up to 100 ml with dH<sub>2</sub>O

#### Pararosanilin

1 g Pararosanilin dissolved in 20 ml of dH<sub>2</sub>O and 5 ml of 5M HCl added to it  
The solution was heated carefully whilst stirring and filtered after cooling.

#### TRAcP Staining Solution

The TRAcP staining solution was freshly prepared by mixing solution A and B as outlined below.

#### Solution A

150 ml of Naphthol-AS-BI-phosphate  
750 ml of Veronal buffer  
900 ml Acetate buffer  
900 ml Acetate buffer with 100 mM Sodium Tartate

#### Solution B

120 ml of Pararosanilin  
120 ml of Sodium Nitrate (4% w/v)

## **Appendix 2.2: Solutions for Histology**

### **Infiltrating solution**

89 g MMA, 10 g Dibutyl phthalate, 1 g Perkadox 16, and 0.01 g Novoscave for 100 g of infiltration solution

### **TRAcP stain with Aniline Blue counterstain**

#### **TRAcP solution**

70 mg Naphthol AS-TR Phosphate, 250 µl N-N Dimethyl formamide, 50 ml 0.2M Sodium Acetate Buffer pH5.2, 155 mg Sodium Tartrate dehydrate and 70 Fast Red Salt TR For 50 ml of TRAcP solution.

#### **Aniline Blue counterstain**

0.166 g Aniline Blue, 3 g for Phosphotungstic Acid and 500 ml dH2O

### **VON KOSSA with Van Gieson Counterstain**

#### **Working solutions**

1% aqueous silver nitrate,  
0.5 % hydroquinone

#### **Van Gieson Counterstain:**

50 ml Saturated Aqueous picric acid, 1% Aqueous acid fuchsine (9 ml) and 50 ml dH2O.

### **Aniline Blue without Phosphotungstic Acid for Calcein labelling**

0.1 g Aniline Blue and 150 ml dH2O

## **Appendix 2.3: 2X LB broth (low salt) media preparation**

10 g/l Enzymatic Digest of Casein, 10 g/l Yeast Extract, 10 g/l Peptone and 5 g/l Sodium Chloride with a final pH:  $7.3 \pm 0.2$  at 25°C.

**Appendix 2.4: Solutions for Western Blot**

**Electrophoresis running buffer**

50 ml of XT-MOPS (20X) in 1000 ml of dH<sub>2</sub>O

**Samples loading protein buffer (5X stock)**

5.2 ml of 1M Tris-HCl pH adjusted to 6.8, 1 g of DL-Dithiothreitol (DTT), 3 g SDS, 6.5 ml glycerol and 130 l of 10% (w/v) Bromophenol Blue.

**Transfer buffer**

3.63 g of Tris, 14.4g of Glycine, 200 ml of Methanol and 3.75 ml of 10% (w/v) SDS made up to 1000 ml with dH<sub>2</sub>O.

**TBS**

1 M of Tris and 1 M Tris-HCl. pH adjusted to 7.9 prior to addition of 3 M Sodium Chloride. Stored at room temperature.


**TBST**

0.1% (v/v) Tween-20 in TBS.

**Stripping buffer**

1 mM DTT, 2% (w/v) SDS and 62.5 mM Tris-HCl (pH 6.7).

## Appendix 3: Abstracts and Publications



## Genetic variants in the Optineurin gene are associated with disease severity in Paget's disease of bone.

Rami A. Obaid<sup>1</sup>, W.D. Fraser<sup>2</sup>, P.L. Selby<sup>3</sup>, S.H. Ralston<sup>1</sup>, O.M. Albagha<sup>1</sup>.

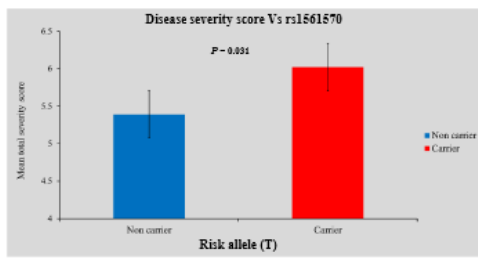
<sup>1</sup>Institute of Genetics and Molecular Medicine, University of Edinburgh, Edinburgh, UK; <sup>2</sup>Department of Clinical Chemistry, Royal Liverpool University Hospital, Liverpool; <sup>3</sup>Department of Medicine, University of Manchester, Manchester, United Kingdom

### Introduction

Paget's disease of bone (PDB) is a common metabolic bone disease that affects about 2% of individuals over the age of 55 in the UK. The disease is characterised by focal areas of increased bone resorption, coupled to increased and disorganised bone formation. Genetic factors are important in PDB and between 15% - 40% of individuals have an affected first degree relative[1]. Mutations in *SQSTM1* (the only gene known to cause PDB with mutations affecting its ubiquitin associated domain) found in about 10% of sporadic cases and 40% of familial PDB cases [2], suggesting that other genes still remain to be identified. A recent genome-wide association study (GWAS) has revealed new susceptibility loci contributing to PDB. One of these loci is related to a novel candidate gene for PDB and showed a significant association observed with rs1561570 on 10p13 within the optineurin *OPTN* gene ( $P = 6.09 \times 10^{-13}$ , OR = 0.65 (0.58-0.73) Fig1. Interestingly, this region previously identified by linkage study. The role of this gene is unknown in bone metabolism but it has a role in NFkB signalling and/or vesicular trafficking, which have been described in relation to bone metabolism [3].

### Results

***OPTN* rs1561570 is associated with total disease severity score**



Analysis of variance using generalised linear model ANOVA showed a significant association between the rs1561570 and total severity score among carrier ( $6.02 \pm 0.11$ ) compared to non-carrier ( $5.39 \pm 0.11$ ) of risk allele. The analysis also showed the *P* values are significant for age (0.005) but not for gender (0.622). This is expected as PDB is a late onset disease in either gender.

### Objective

The aim of the study was to investigate the relationship between the genetic variant rs1561570 (found by the GWAS) in the *OPTN* gene and the disease severity in 635 PDB patients without *SQSTM1* mutations.

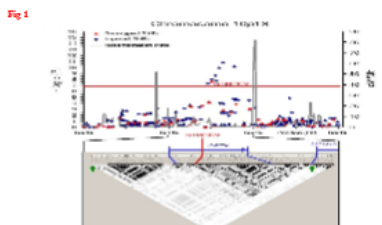
### Methods

- The analysed data was obtained from several studies conducted on participants who took part in the PRISM study.

Cases Number	Gender		Risk Allele	
	Male	Female	Non-Carrier	Carrier
635	344	291	77	558

- PDB severity was assessed as previously described (Visconti JMBR, 2010). It was devised based on several clinical features including: number of affected bones, clinical evidence for bone deformity, the presence of bone pain, bone fractures, requirements of orthopaedic surgery and the use of hearing aid for deafness. Patient's occupation and milk consumption also have been taken into the consideration during the study. Health related quality of life was assessed by the SF-36 questionnaire.
- We used one way analysis of variance (one way ANOVA) to analyse the association between rs1561570 and each individual parameter. Subsequently, generalised linear model ANOVA was used to analyse the significant association between the rs1561570 variant and the total disease severity of PDB adjusted for age and gender.

### The Association of *OPTN* variant with PDB risk

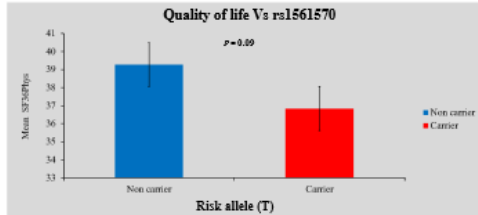


Association and LD plots of regions showing genome-wide significant association with PDB located on 10p13.

Chr	SNP	Discovery		Replication		Combined	
		<i>P</i> <sub>a</sub>	OR (95%CI)	<i>P</i> <sub>a</sub>	OR (95%CI)	<i>P</i> <sub>a</sub>	OR (95%CI)
10	rs1561570	$1.11 \times 10^{-8}$	0.64 (0.56-0.74)	$1.59 \times 10^{-5}$	0.67 (0.56-0.80)	$6.09 \times 10^{-13}$	0.65 (0.58-0.73)

GWAS was performed in individuals with PDB cases without *SQSTM1* mutations and three candidate loci have been identified in the first phase of the study. These loci then replicated in an independent set of samples.

### The association of *OPTN* rs1561570 with patients' physical activity



Using analysis of variance ANOVA to determine the association between Quality of life and rs1561570 indicate that there is a trend for reduced quality in patients who carried the risk allele ( $36.8 \pm 1.41$ ) compared to those who did not ( $39.3 \pm 0.5$ ).

### Conclusions


- The association between *OPTN* rs1561570 and total disease severity score is significant so that carrier of the risk allele "T" had a higher severity score compared to non-carrier.
- There is also a trend for reduced quality of life among carrier of the risk allele compared to those who did not.
- These findings could be of clinical value to identify *SQSTM1* negative patients who are at increase risk of developing severe form of PDB.

### References

[1] Obaid RA, et al. Pathogenesis of Paget's disease of bone. Bone 2008;43(1):145-152.  
[2] Selby PL, et al. Association of the gene encoding SQSTM1 with Paget's disease of bone. Ann Rheum Dis 2011; 70: 1191-1195.  
[3] Obaid RA, et al. Association of the gene encoding SQSTM1 with Paget's disease of bone. Ann Rheum Dis 2011; 70: 1191-1195.  
[4] Obaid RA, et al. Association of the gene encoding SQSTM1 with Paget's disease of bone. Ann Rheum Dis 2011; 70: 1191-1195.

### Acknowledgements

I would like to acknowledge the advice and guidance of Dr. Omar Albagha and the Ministry of Higher Education of Saudi Arabia for their financial support.



Presented at the ECTS 10th 2014 Joint Meeting Meeting, Athens, Greece, May 7-11, 2015. r.a.a.obaid@ed.ac.uk

## Optineurin Negatively Regulates Osteoclast Formation *in vitro*

Rami A. Obaid, S. Wani, S. H. Ralston, O.M.E. Albagha.

Molecular Medicine Centre, University of Edinburgh, Crewe Road South, Edinburgh EH4 2XU



### Introduction

Our recent genome wide association studies have identified variants in the *OPTN* gene that predispose to Paget's disease of bone (PDB)[1,2], a disease characterized by focal areas of increased bone turnover leading to symptoms like bone pain, deformity osteoarthritis and fracture. Variants within *OPTN* were significantly associated with the risk of PDB in many populations (rs1561570; OR = 1.67;  $P = 4.4 \times 10^{-11}$ ) suggesting that *OPTN* is a novel gene for the regulation of bone metabolism. *OPTN* encodes a ubiquitously expressed cytoplasmic protein called optineurin. Mutations in *OPTN* have been linked to glaucoma and recently to amyotrophic lateral sclerosis (ALS) [3] but the role of optineurin in PDB and bone metabolism is yet unknown. Current evidence suggests that optineurin plays a regulatory role in the NF- $\kappa$ B signaling pathway; an essential pathway in osteoclast biology. When optineurin is down regulated, the TNF- $\alpha$ -induced NF- $\kappa$ B activation is markedly enhanced, suggesting a negative regulatory role of optineurin in NF- $\kappa$ B signaling pathway[4]. However, the mechanism of how optineurin acts as a regulatory factor in the NF- $\kappa$ B signaling is still unclear. It could be related to its NEMO-like domain that competes with NEMO (NF- $\kappa$ B essential modulator) to bind with PolyUb RIP (receptor interacting protein), which is necessary for NF- $\kappa$ B activation[5]. Studies have also shown that optineurin plays a role in the vesicular trafficking and autophagy pathways which have been implicated in osteoclast biology[6,7]. Collectively, these findings suggest that optineurin may have an important role in bone metabolism and the development of PDB.

### Objective

The aim of this study was to investigate the role of optineurin in osteoclast development using *in vitro* knock-down experiments.

### Methods

- 1) Expression of *OPTN* during osteoclast development: Bone marrow cells from wild type CD1 mice were isolated and cultured for 48 hours in the presence of M-CSF (100ng/ml) followed by stimulation of adherent cells with RANKL (100ng/ml) and M-CSF (25ng/ml) for 5 days until osteoclasts were formed. *OPTN* expression was determined using western blot analysis.
- 2) Effect of *OPTN* depletion on osteoclast formation: Bone marrow cells from wild type CD1 mice were isolated and cultured for 48 hours in the presence of M-CSF (100ng/ml). The adherent bone marrow derived macrophages (BMDMs) were then transduced with either lentiviral particles containing shRNA targeted against the *OPTN* gene or negative control particles (non-targeting lentiviral particles that activate the RNAi pathway but do not target any mouse gene). Transduced cells were selected for 48hrs using Puromycin (5 $\mu$ g/ml) in order to reduce background expression from untransduced cells. We used western blot to confirm the knock down of *OPTN* in these cells. *OPTN*-depleted BMDMs were then plated in 96 well plates and stimulated with M-CSF (25ng/ml) and RANKL (25 and 50ng/ml) until osteoclasts were formed. TRAP positive multinucleated osteoclasts (> 3 nuclei) were counted and numbers were compared to the non-targeted negative control.
- 3) Effect of *OPTN* depletion on NF- $\kappa$ B signaling pathway: BMDMs were transfected with the lentiviral particles expressing shRNA targeted against the *OPTN* gene for two days. Transduced cells were selected for 48hrs using Puromycin (5 $\mu$ g/ml) followed by transduction with lentiviral NF- $\kappa$ B luciferase reporter for further two days. The cells were then plated in 96 wells for 24hrs, luciferase activity measured with a SteadyGlo-luciferase reporter assay system at the basal level and following RANKL stimulation (100ng/ml) at 24 and 72 hrs.

### Results

#### 1. Optineurin Expression is Increased During Osteoclast Formation

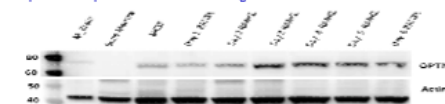


Figure 1. *OPTN* Expression during osteoclast formation. Expression of *OPTN* was detected in BMDMs but not in total bone marrow cells. No significant changes in *OPTN* expression were observed during the first two days of osteoclast development. However the expression of *OPTN* significantly increased from day 3 until osteoclasts were formed suggesting that *OPTN* could play a role during later stages of osteoclast formation.

#### 2. Confirmation of *OPTN* Knock-Down in Mouse Bone Marrow Derived Macrophages

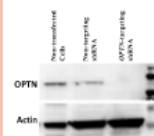


Figure 2. Confirmation of *OPTN* knock-down. Western blot analysis of cell lysates from non-transfected, non-targeting shRNA transfected, and *OPTN*-targeting shRNA transfected cells. Approximately 80% *OPTN* knock-down level was achieved in cells transfected with lentiviral particles containing shRNA targeting *OPTN* compared to non-targeting particles.

#### 3. *OPTN* Knock-Down Enhances Osteoclast Formation in Mouse BMDMs

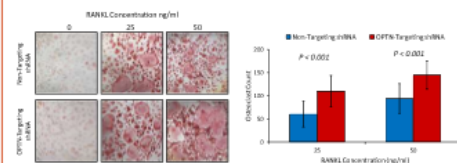


Figure 3. *OPTN* Knock-down enhances osteoclast formation. *OPTN*-depleted mouse bone marrow derived macrophages (BMDMs) formed higher number of osteoclasts compared to non-depleted cells when stimulated with M-CSF and RANKL.

#### 4. *OPTN* Knock-Down Increases Basal NF- $\kappa$ B Activation in Mouse BMDMs

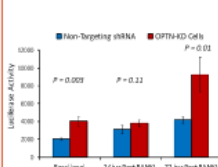


Figure 4. NF- $\kappa$ B Activation is increased in *OPTN* depleted cells during osteoclast formation. The NF- $\kappa$ B activity is increased significantly in the *OPTN* depleted cells at the basal level and 72 hrs after stimulation with RANKL compared to non-depleted cells. At 24hrs post RANKL, the increase in NF- $\kappa$ B activity was not significant.

### Conclusions

- *OPTN* is expressed during osteoclast formation and its expression significantly increased during later stages of osteoclast development.
- *OPTN*-depletion in mouse bone marrow derived macrophages enhanced osteoclast formation and increased basal and RANKL-induced NF- $\kappa$ B activation.
- Our data suggest that *OPTN* negatively regulates osteoclast formation through inhibition of NF- $\kappa$ B signaling pathway but further studies will be required to investigate the underlying mechanism.

### References

1. Albagha, O.M.E. et al. Genome-wide association identifies three new susceptibility loci for Paget's disease of bone. *Nature Publishing Group* 43, 685–689 (2011).
2. Albagha, O. et al. Genome-wide association study identifies variants at CSF1, OPTN and TNFRSF11A as genetic risk factors for Paget's disease of bone. *Nature Genetics* 42, 520–524 (2010).
3. Maruyama, H. et al. Mutations of optineurin in amyotrophic lateral sclerosis. *Nature* 465, 223 (2010).
4. Zhu, G., Wu, C.-L., Zhao, Y. & Ashwell, J.D. Optineurin Negatively Regulates TNF- $\alpha$ -Induced NF- $\kappa$ B Activation by Competing with NEMO for Ubiquitinated RIP. *Current Biology* 17, 1438–1443 (2007).
5. Nagabhashana, A., Bansal, M. & Suresh, G. Optineurin Is Required for CYLD-Dependent Inhibition of TNF- $\alpha$ -Induced NF- $\kappa$ B Activation. *PLoS One* 6, e17477 (2011).
6. Hortobágyi, T. et al. Optineurin inclusions occur in a minority of TDP-43 positive ALS and FTLD-TDP cases and are rarely observed in other neurodegenerative disorders. *Acta Neuropathol* 121, 519–527 (2011).
7. Widi, P. et al. Phosphorylation of the Autophagy Receptor Optineurin Restricts Salmonella Growth. *Science* 333, 228–233 (2011).

### Acknowledgements

I would like to acknowledge the advice and guidance of Dr. Omar Albagha, Dr. Sachin Wani and the Ministry of Higher Education of Saudi Arabia for their financial support.



## Depletion of the autophagy adaptor *OPTN* leads to increased osteoclast formation, fusion and survival as well as increased NF- $\kappa$ B activation *in vitro*

Rami A. Obaid, S. Wani, S. H. Ralston, O.M.E. Albagha.

Molecular Medicine Centre, University of Edinburgh, Crewe Road South, Edinburgh EH4 2XU



### Introduction

Our recent genome wide association studies have identified variants in the *OPTN* gene that predispose to Paget's disease of bone (PDB) [1,2], a disease characterized by focal areas of increased bone turnover leading to symptoms like bone pain, deformity osteoarthritis and fracture. Variants within *OPTN* were significantly associated with the risk of PDB in many populations (rs1561570; OR = 1.67; P =  $4.4 \times 10^{-10}$ ) suggesting that *OPTN* is a novel gene for the regulation of bone metabolism. *OPTN* encodes a ubiquitously expressed cytoplasmic protein called optineurin. Mutations in *OPTN* have been linked to glaucoma and recently to amyotrophic lateral sclerosis (ALS) [3] but the role of optineurin in PDB and bone metabolism is yet unknown. Current evidence suggests that optineurin plays a regulatory role in the NF- $\kappa$ B signaling pathway; an essential pathway in osteoclast biology. When optineurin is down regulated, the TNF- $\alpha$ -induced NF- $\kappa$ B activation is markedly enhanced, suggesting a negative regulatory role of optineurin in NF- $\kappa$ B signaling pathway [4]. However, the mechanism of how optineurin acts as a regulatory factor in the NF- $\kappa$ B signaling is still unclear. It could be related to its NEMO-like domain that competes with NEMO (NF- $\kappa$ B essential modulator) to bind with PolyUB RIP (receptor interacting protein), which is necessary for NF- $\kappa$ B activation [5]. Studies have also shown that optineurin plays a role in the vesicular trafficking and autophagy pathways which have been implicated in osteoclast biology [6,7]. Collectively, these findings suggest that optineurin may have an important role in bone metabolism and the development of PDB.

### Objective

The aim of this study was to investigate the role of optineurin in osteoclast development using *in vitro* knock-down experiments.

### Methods

- 1) Expression of *OPTN* during osteoclast development:** Bone marrow cells from wild type CD1 mice were isolated and cultured for 48 hours in the presence of M-CSF (100ng/ml) followed by stimulation of adherent cells with RANKL (100ng/ml) and M-CSF (25ng/ml) for 5 days until osteoclasts were formed. *OPTN* expression was determined using western blot analysis.
- 2) Effect of *OPTN* depletion on osteoclast formation, fusion and survival:** Bone marrow cells from wild type CD1 mice were isolated and cultured for 48 hours in the presence of M-CSF (100ng/ml). The adherent bone marrow derived macrophages (BMDMs) were then transfected with either lentiviral particles containing shRNA targeted against the *OPTN* gene or negative control particles (non-targeting lentiviral particles that activate the RNAi pathway but do not target any mouse gene). After selection with Puromycin (5 $\mu$ g/ml), cells were then plated in 96 well plates and stimulated with M-CSF (25ng/ml) and RANKL (25 and 50ng/ml) until osteoclasts were formed. TRAP positive multinucleated osteoclasts (> 3 nuclei) were counted and numbers were compared to the non-targeted negative control. For the osteoclast survival one plate is fixed and TRAP stained at the stage where osteoclasts are formed. RANKL was then removed from the culture media and plates were fixed and stained with TRAP at different time points post RANKL withdrawal (12hrs, 24hrs, 48hrs and 72hrs).
- 3) Effect of *OPTN* depletion on NF- $\kappa$ B signaling pathway:** BMDMs were transfected with the lentiviral particles expressing shRNA targeted against the *OPTN* gene for two days. Transfected cells were selected for 48hrs using Puromycin (5 $\mu$ g/ml) followed by transduction with lentiviral NF- $\kappa$ B luciferase reporter for further two days. The cells were then plated in 96 wells for 24hrs, luciferase activity measured with a SteadyGo-luciferase reporter assay system at the basal level and following RANKL stimulation (100ng/ml) at 24 and 72 hrs.
- 4) Expression of *OPTN* during osteoblast development:** Primary osteoblasts were isolated from the calvarial bones of 3 day old mice and cultured in standard  $\alpha$ MEM until confluent. Osteoblasts were then detached and seeded and cells were treated with 50 $\mu$ g/ml Vit C and 3mM betaglycerophosphate ( $\beta$ -GP). Expression of *OPTN* was assessed at different time points using western blot.

### Results

#### 1. Optineurin Expression is Increased During Osteoclast Formation

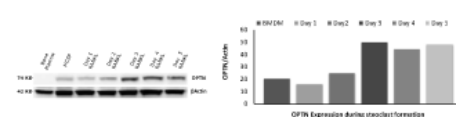


**Figure 1. *OPTN* Expression during osteoclast formation.** Expression of *OPTN* was detected in BMDMs but not in total bone marrow cells. No significant changes in *OPTN* expression were observed during the first two days of osteoclast development. However the expression of *OPTN* significantly increased from day 3 until osteoclasts were formed suggesting that *OPTN* could play a role during later stages of osteoclast formation.

#### 2. *OPTN* Knock-Down Enhances Osteoclast Formation in Mouse BMDMs

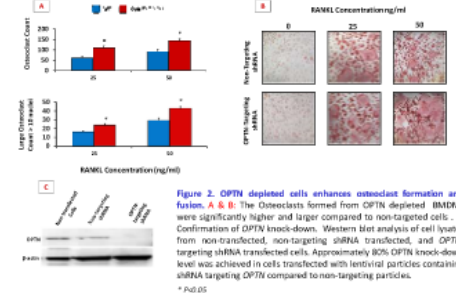


**Figure 2. *OPTN* depleted cells enhances osteoclast formation and fusion.** A & B: The Osteoclasts formed from *OPTN* depleted BMDMs were significantly higher and larger compared to non-targeted cells. C: Confirmation of *OPTN* knock-down. Western blot analysis of cell lysates from non-transfected, non-targeting shRNA transfected, and *OPTN*-targeting shRNA transfected cells. Approximately 80% *OPTN* knock-down level was achieved in cells transfected with lentiviral particles containing shRNA targeting *OPTN* compared to non-targeting particles.

#### 3. *OPTN* depletion enhances osteoclast survival

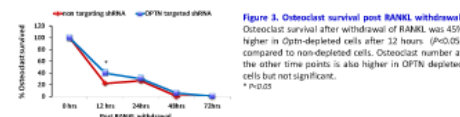


**Figure 3. Osteoclast survival post RANKL withdrawal.** Osteoclast survival after withdrawal of RANKL was 45% higher in *Optn*-depleted cells after 12 hours (P<0.05) compared to non-depleted cells. Osteoclast number at the other time points is also higher in *OPTN* depleted cells but not significant.

#### 4. *OPTN* Knock-Down Increases Basal NF- $\kappa$ B Activation in Mouse BMDMs

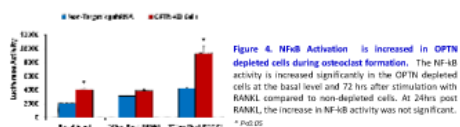


**Figure 4. NF- $\kappa$ B Activation is increased in *OPTN* depleted cells during osteoclast formation.** The NF- $\kappa$ B activity is increased significantly in the *OPTN* depleted cells at the basal level and 72 hrs after stimulation with RANKL compared to non-depleted cells. At 24hrs post RANKL, the increase in NF- $\kappa$ B activity was not significant.

#### 5. The role of *OPTN* in osteoblast formation

**Figure 5. *OPTN* is expressed during osteoblast mineralization assay.** Western blot analysis of cell lysates from osteoblast before and after adding the Vit C. Indicates that *OPTN* is expressed during osteoblast formation but further studies will be required to investigate if *OPTN* play a role in osteoblast formation.

### Conclusions

- *OPTN* is expressed during osteoclast formation and its expression significantly increased during later stages of osteoclast development.
- *OPTN*-depletion in mouse bone marrow derived macrophages enhanced osteoclast formation, fusion and survival and increased basal and RANKL-induced NF- $\kappa$ B activation.

### References

1. Albagha, O.M.E. et al. Genome-wide association identifies three new susceptibility loci for Paget's disease of bone. *Nature Genetics* 45, 580-589 (2013).
2. Albagha, O.M.E. et al. Genome-wide association study identifies variants at CSF1, *OPTN* and TNFRSF11A as genetic risk factors for Paget's disease of bone. *Nature Genetics* 45, 520-524 (2013).
3. Mancaioni, M. et al. Mutations of optineurin in amyotrophic lateral sclerosis. *Nature* 465, 223 (2010).
4. Zhu, G., Wu, C.-J., Zhao, Y. & Ashwell, J.D. Optineurin Negatively Regulates TNF- $\alpha$ -Induced NF- $\kappa$ B Activation by Competing with NEMO for Ubiquitinated RIP. *Current Biology* 17, 1438-1443 (2007).
5. Nishitohhara, A., Samal, M. & Senoo, G. Optineurin Is Required for CytD-Dependent Inhibition of TNF- $\alpha$ -Induced NF- $\kappa$ B Activation. *PLoS ONE* e17477 (2012).
6. Horstshagen, T. et al. Optineurin Inducers occur in a minority of TDP-43 positive ALS and FTLD-TDP cases and are rarely observed in other neurodegenerative disorders. *Acta Neuropathol* 122, 529-527 (2012).
7. Wink, T. et al. Phosphorylation of the Autophagy Receptor Optineurin Restricts Salmonella Growth. *Science* 333, 228-233 (2012).

### Acknowledgements

I would like to acknowledge the advice and guidance of Antonia Sophocleous and Rob van't Hof and Arthritis Research UK and the Ministry of Higher Education of Saudi Arabia for their financial support.



Please cite this article in press as: Obaid et al., Optineurin Negatively Regulates Osteoclast Differentiation by Modulating NF- $\kappa$ B and Interferon Signaling: Implications for Paget's Disease, Cell Reports (2015), <http://dx.doi.org/10.1016/j.celrep.2015.09.071>

## Cell Reports Report

OPEN  
ACCESS  
CellPress

# Optineurin Negatively Regulates Osteoclast Differentiation by Modulating NF- $\kappa$ B and Interferon Signaling: Implications for Paget's Disease

Rami Obaid,<sup>1,4</sup> Sachin E. Wani,<sup>1,4</sup> Asim Azfer,<sup>1</sup> Toby Hurd,<sup>2</sup> Ruth Jones,<sup>3</sup> Philip Cohen,<sup>3</sup> Stuart H. Ralston,<sup>1</sup> and Omar M.E. Albagha<sup>1,4</sup>\*

<sup>1</sup>Centre for Genomic and Experimental Medicine, Institute of Genetics and Molecular Medicine, University of Edinburgh, Edinburgh EH4 2XU, UK

<sup>2</sup>Medical Research Council Human Genetic Unit, Institute of Genetics and Molecular Medicine, University of Edinburgh, Edinburgh EH4 2XU, UK

<sup>3</sup>Medical Research Council Protein Phosphorylation and Ubiquitylation Unit, The Sir James Black Centre, University of Dundee, Dundee DD1 5HE, UK

<sup>4</sup>Co-first author

\*Correspondence: [omar.albagha@ed.ac.uk](mailto:omar.albagha@ed.ac.uk)

<http://dx.doi.org/10.1016/j.celrep.2015.09.071>

This is an open access article under the CC BY-NC-ND license (<http://creativecommons.org/licenses/by-nc-nd/4.0/>).

## SUMMARY

Paget's disease of bone (PDB) is a common disease characterized by osteoclast activation that leads to various skeletal complications. Susceptibility to PDB is mediated by a common variant at the optineurin (*Optn*) locus, which is associated with reduced levels of mRNA. However, it is unclear how this leads to the development of PDB. Here, we show that *OPTN* acts as a negative regulator of osteoclast differentiation in vitro and that mice with a loss-of-function mutation in *Optn* have increased osteoclast activity and bone turnover. Osteoclasts derived from *Optn* mutant mice have an increase in NF- $\kappa$ B activation and a reduction in interferon beta expression in response to RANKL when compared to wild-type mice. These studies identify *OPTN* as a regulator of bone resorption and are consistent with a model whereby genetically determined reductions in *OPTN* expression predispose to PDB by enhancing osteoclast differentiation.

## INTRODUCTION

Paget's disease of bone (PDB) is a common skeletal disorder characterized by osteoclast activation, which provokes increased but disorganized bone turnover, leading to pathological fractures, bone deformity, and bone pain. The disease has a strong genetic component, but the genes responsible have not been fully characterized. The most important predisposing gene is *SQSTM1*, which is mutated in ~10% of patients with the disease. The *SQSTM1* causal mutations increase osteoclastogenesis by enhancing receptor activator of nuclear factor kappa B (NF- $\kappa$ B) (RANK) signaling in osteoclasts and their precursors (Cavey et al., 2006; Daroszewska et al., 2011; Hiruma

et al., 2008). Linkage studies in families (Lucas et al., 2008) coupled with genome-wide association studies (GWAS) (Albagha et al., 2010, 2011) have identified a strong susceptibility locus for PDB at the *OPTN* locus on chromosome 10p13. The *OPTN* gene encodes optineurin, a ubiquitously expressed cytoplasmic protein involved in many cellular processes including regulation of (NF- $\kappa$ B) signaling (Zhu et al., 2007), autophagy, and innate immunity (Wild et al., 2011), but the role of optineurin in bone metabolism is unknown. Here, we investigated the role of *OPTN* in regulating bone turnover and evaluated the molecular mechanisms by which variants at the *OPTN* locus predispose to PDB.

## RESULTS AND DISCUSSION

### Reduced Expression of *OPTN* Predisposes to PDB

In order to identify disease-causing mutations in the *OPTN* locus, we conducted mutation screening of the coding exons of *OPTN* in 200 PDB patients, but results showed no mutations in the protein-coding region (data not shown). However, the top GWAS hit (rs1561570) was found to be a strong expression quantitative trait locus (eQTL) in human monocytes (Zeller et al., 2010) and in peripheral blood mononuclear cells (Westra et al., 2013) with substantially reduced levels of *OPTN* mRNA expression in carriers of the PDB-predisposing "T" allele with an evidence of an allele-dose effect (Figure 1). These observations indicate that susceptibility to PDB is associated with reduced expression of *OPTN* and raise the possibility that *OPTN* might act as a negative regulator of osteoclast function.

### *Optn* Knockdown Enhances Osteoclast Differentiation

Here, we studied the expression of optineurin during osteoclast differentiation and investigated the effects of *Optn* knockdown in primary bone-marrow-derived macrophage (BMDM) cultures. Expression of optineurin increased considerably during osteoclast differentiation, following stimulation of the cultures with macrophage colony-stimulating factor (M-CSF) and receptor

Cell Reports 13, 1–7, November 10, 2015 ©2015 The Authors 1

CELREP 2123